DEVELOPMENT OF MICROWAVE BASED METHODS FOR RECYCLING OF OXIDE AND MIXED OXIDE NUCLEAR FUEL REJECTS

By

GITENDER SINGH
CHEM01201404017

Bhabha Atomic Research Centre, Mumbai

A thesis submitted to the
Board of Studies in Chemical Sciences
In partial fulfillment of requirements
for the Degree of
DOCTOR OF PHILOSOPHY
of
HOMI BHABHA NATIONAL INSTITUTE

August, 2019

Homi Bhabha National Institute

Recommendations of the Viva Voce Committee

As members of the Viva Voce Committee, we certify that we have read the dissertation prepared by **GITENDER SINGH** entitled **"DEVELOPMENT OF MICROWAVE BASED METHODS FOR RECYCLING OF OXIDE AND MIXED OXIDE NUCLEAR FUEL REJECTS"** and recommend that it may be accepted as fulfilling the thesis requirement for the award of Degree of Doctor of Philosophy.

Chairman – Prof. C. P. Kaushik **Date:** 7/8/2019

Guide / Convener – Prof. Pradeep Kumar **Date:** 7/8/2019

Examiner – Prof. S. Anthonysamy S. Anthonysamy **Date:** 7/8/2019.

Member 1- Prof. N. L. Misra **Date:** 07/08/2019

Member 2- Prof. S. C. Parida — **Date:** —

Member 3- Prof. R. K. Vatsa **Date:** 7/8/2019

Technology Advisor- Dr. D. K. Das **Date:** 7/8/2019

Final approval and acceptance of this thesis is contingent upon the candidate's submission of the final copies of the thesis to HBNI.

I hereby certify that I have read this thesis prepared under my direction and recommend that it may be accepted as fulfilling the thesis requirement.

Date: 7/8/2019
Place: HBNI, mumbai

Dr. Pradeep Kumar
Guide

Annexure 1

CERTIFICATION ON ACADEMIC INTEGRITY

1. I **GITENDER SINGH**, HBNI Enrolment No. **CHEM01201404017** hereby undertake that, the Thesis entitled **"DEVELOPMENT OF MICROWAVE BASED METHODS FOR RECYCLING OF OXIDE AND MIXED OXIDE NUCLEAR FUEL REJECTS"** is prepared by me and that the document reports the original work carried out by me and is free of plagiarism.
2. I am aware and undertake that if plagiarism is detected in my thesis at any stage in future, suitable penalty will be imposed as per the applicable guidelines of the Institute/ UGC.

7.8.2019

Signature of the Student
(with date)

Endorsed by the PhD Supervisor

7/8/2019

Signature (with date)

Name: Dr. Pradeep Kumar

Designation: Assistant Professor HBNI

Department/ Centre: BARC, Mumbai

Name of the CI/ OCC: BARC, Mumbai

STATEMENT BY AUTHOR

This dissertation has been submitted in partial fulfillment of requirements for an advanced degree at Homi Bhabha National Institute (HBNI) and is deposited in the Library to be made available to borrowers under rules of the HBNI.

Brief quotations from this dissertation are allowable without special permission, provided that accurate acknowledgement of source is made. Requests for permission for extended quotation from or reproduction of this manuscript in whole or in part may be granted by the Competent Authority of HBNI when in his or her judgment the proposed use of the material is in the interests of scholarship. In all other instances, however, permission must be obtained from the author.

GITENDER SINGH

DECLARATION

I, hereby declare that the investigation presented in the thesis has been carried out by me. The work is original and has not been submitted earlier as a whole or in part for a degree / diploma at this or any other Institution / University.

GITENDER SINGH

List of Publications arising from the thesis

Journals

1. "Impurity analysis and dissolution behaviour of plutonium bearing impure MOX scrap: An assessment of recycling feasibility"

   G. Singh, *Pradeep Kumar, N. D. Save, R. K. Malav, B. N. Mahanty, D. K. Das, A. K. Mishra, P. G. Behere, Mohd. Afzal and Arun Kumar*

   J Radioanal. Nucl. Chem. (2016) 309:1159–1168

2. "A novel method for stoichiometric reduction of (U_3O_8,PuO_2) and its controlled oxidation using microwave"

   G. Singh, *Pradeep Kumar, S. Aher, P. Purohit , P.M. Khot, Amrit Prakash, D.K. Das, P.G. Behere, Mohd Afzal*

   Journal of Nuclear Materials, (2016) 479: 145-151

3. "Microwave based oxidation process for recycling the off-specification (U,Pu)O_2 fuel pellets"

   G. Singh*, P.M. Khot, Pradeep Kumar, R.B. Bhatt, P.G. Behere, Mohd Afzal*

   Journal of Nuclear Materials, (2017), 484: 81-90

4. "An integrated process for recycling the ThO_2 based mixed oxide rejected nuclear fuel pellets"

   Gitender Singh, *Prashal M. Khot, Pradeep Kumar, Chetan Baghra, Raj Bhushan Bhatt, Praveen G. Behere*

   World Journal of Nuclear Science and Technology, (2017) 7: 309-330.

Conferences

1. "Low Temperature Microwave Reduction of (U_3O_8+PuO_2) Powder Prepared via Microwave Co-denitration Process and Property Evaluation for Mixed Oxide Fuel Fabrication"

   G. Singh, *R. K. Malav, A. B. Name, R. B. Bhong, S. Aher, P. Purohit, Pradeep Kumar, D. K. Das, Surendra Kumar, P. G. Behere and Mohd. Afzal* **Proceedings of Nuclear and Radiochemistry Symposium (NUCAR-2015), Feb- 2015, BARC Mumbai, pp-126-127**

2. "Impurity analysis in dirty rejected oxide generated during mixed oxide fuel fabrication"

   G. Singh, N.D. Save, R.K. Malav, Pradeep Kumar, D.K. Das, P.G. Behere and Mohd. Afzal

Proceedings of Current Trends in Analytical Chemistry CTAC, Niyamak Bhavan AERB, Anushaktinagar, Mumbai, 26-29, May, 2015 pp-129.

3. “Microwave heating Based Calcination of Uranium Oxides”

   G. Singh. *Pradeep Kumar, D. K. Das, P.G. Behere, Mohd Afzal*

   Proceedings of National Conference on "Analytical Science and Technology 2015" with theme Analytical Science for Technological Excellence and Environmental Sustainability" organised by ISAS, Kerela Chapter, Munnar on September 24-26, Page MCP-25.

4. “Glove-box adaptation and performance testing of a dynamic method based BET surface area analyser”

   G. Singh*, S. Aher, P. Purohit, A. B. Name, R. B. Bhong, R. K. Malav, A. P. Karande, Pradeep Kumar, D. B. Sathe, Anoop Kelkar, D. K. Das, R. B. Bhatt and P. G. Behere*

   13th DAE-BRNS, Nuclear and Radiochemistry Symposium, (NUCAR-2017), KIIT Bhubaneswar, Odisha, India 6-10 Feb 2017, pp 676-677.

5. Feasibility evaluation of deploying solvent extraction in microwave based integrated approach for wet recycling of impure MOX scrap

   G. Singh*, Anoop Kelkar, R. K. Malav, N. D Save, A. B. Name, R. B. Bhong, A. P. Karande, Pradeep Kumar, R. B. Bhatt and P. G. Behere*

   13th DAE-BRNS, Nuclear and Radiochemistry Symposium (NUCAR-2017), KIIT Bhubaneswar, Odisha, India 6-10 Feb 2017, pp 158-159.

Others:

1. “Development of Microwave Direct Denitration Technology for Recycling of Rejected (U,Pu)O_2 MOX Fuel”

   G. Singh, *Pradeep Kumar, S. Aher, P. Purohit, A. G Kelkar, D. K. Das, D. B. Sathe, , R. B. Bhatt, P.G. Behere*

   BARC News Letter Founders Day Special Issue, Oct 2018, pp 120-129.

GITENDER SINGH

DEDICATIONS

DEDICATED
TO
SHREE JWALAJI
MY FAMILY
&
TEACHERS

ACKNOWLEDGEMENTS

When expressed in words, feelings of gratitude are partially conveyed

At the very outset, I wish to express my deepest and sincere gratitude to my guide, Dr. Pradeep Kumar for his valuable guidance, constant encouragement and motivation extended throughout the course of work. I am thankful to him for sharing his knowledge, scientific understanding and presentation skills with me.

I am privileged to thank Shri Arun Kumar, Former Director, Nuclear Fuels Group, Mr. Mohd. Afzal, Former Head, Advanced Fuel Fabrication Facility (AFFF), Shri P. G. Behere, Former Chief Superintendent, AFFF, Sh. R. B. Bhatt, GM, FF-INRP(O) (previously named AFFF) and Dr. Amrit Prakash, Radio-Metallurgy Division (RMD) for their unstinted support and encouragement without which this work would not have been possible. Your advice has played a major role in shaping my work. I am grateful to Dr. K. B. Khan, Former Head, RMD and especially Dr. Amrit Prakash, RMD for the help extended in characterization of samples.

I would like to express my sincere regards to Dr. D. K. Das, Former Superintendent, CQCS, AFFF who has always been extremely helpful to me. I sincerely acknowledge valuable suggestions received from Shri R. B. Bhatt, GM, FF-INRP(O), Shri D. B. Sathe, AGM (TS), FF-INRP(O), Shri P. V. Suresh Varma, FF-INRP(O) throughout the course of this work.

I take this opportunity to convey special thanks to my colleagues Shri R. K. Malav, Shri A. B. Name, Shri R. B. Bhong, Shri R. K. Pandey, Shri A. P. Bhatkar and Shri A. K. Yadav for their invaluable cooperation during the experimental work.

I am grateful to my colleagues from Quality Control Sections; Dr. Anoop Kelkar, Shri Ashish Pandey, Mr. F. A. Khan, Smt. Neeta Save, Shri Chetan Baghra, Shri Nagendra Kumar for tremendously helping me in my research work.

I gratefully acknowledge the support provided by my colleagues especially Shri P. M. Khot, RMD, Shri P. Purohit, FF, Shri Sachin Aher, FF while designing the experimental setups. I would like to extend my thanks to Shri A. K. Mishra, Former Superintendent, OFS and Shri B. Surendra, OFS for providing the raw material to carry out this work.

I am thankful to Prof. B. S. Tomar, Former Director, RC&IG and Former Dean, Chemical Sciences, HBNI for helping during registration of my Ph.D. work and the keen interest in my work. I am grateful to Prof. A. K. Tyagi, Dean, Chemical Sciences, HBNI for helping me in thesis and other documents preparation matters.

It gives me immense pleasure to thank the respected and distinguished members of the doctoral committee, Dr. S. K. Mukherjee (Former Chairman), Dr. C. P. Kaushik (Chairman), Dr. S. C. Paridha, (Member), Dr. N. L. Misra (Member), Dr. R. K. Vatsa (Member), Dr. D. K. Das (Technology Advisor) and Dr. Pradeep Kumar (Guide and Convener) for their critical reviews and suggestions during the progress reviews and pre-synopsis presentation.

I cannot imagine my current position without the blessings of my teachers and will always be indebted to them.

I fall short of words in thanking and appreciating my beloved wife “Savita”, my daughter “Geet” and my son “Abhi” for gracefully bearing with the pains of negligence inflicted during the period of this work. This work would not have completed without the blessings and love of my parents and all other family members, who supported me constantly and made my work easier. Further, I cannot forget to acknowledge my uncle Dr. J.C. Negi for inspiration throughout my studies.

Finally, I express thanks to all my friends, colleagues for their supporting and generous helping attitude. I would like to take this opportunity to thank everyone, who supported me throughout this thesis.

August, 2019

GITENDER SINGH

CONTENTS

SYNOPSIS

The nuclear fuel fabrication processes have inherent limitation of generation of significant quantity of nuclear material scrap [1]. The present thesis describes the development of microwave based methods for recycling of fuel scrap or rejects generated during the industrial production of oxide and mixed oxide (MOX) fuels. The fuel rejects contain significant amount of fissile and fertile materials depending upon the composition of the fuel. India has meager nuclear resources, this necessitate the recycling of nuclear scrap. Microwave heat processing is eventually gaining increased attention of the nuclear community for variety of applications [2-10] besides other industries [11-15]. The applications of microwave have been reported for processing of nuclear fuel and waste materials, conversion or co-conversion of products in reprocessing, analysis of elements in variety of fuel and environmental samples, drying of intermediates, pyrolytic synthesis of nuclear materials etc. [2-10]. The microwave heating is fundamentally different from the conventional processes of heating. In case of microwave heating, the heat is generated within the material itself upon microwave irradiation due to interaction with its constituents (atoms, ions, molecules etc.). The microwave heating process offers several distinct advantages in comparison to conventional heat techniques such as non-contact, rapid temperature ramp-up, material selective, bulk and uniform heating [13-16]. The reverse thermal gradients, quick start and stopping ability are distinctly different.

Uranium, plutonium and thorium in the forms of metals, alloys, oxides, carbides, nitrides, cermets etc. are used as nuclear fuels in several geometric shapes of rods, pins, plates, pellets, spheres etc. In most of the commercial power reactors, oxides or mixed oxides of these elements are used as fuel owing to their superior operational properties, ease of fabrication and well established reprocessing of irradiated fuel. The most commonly employed method for the industrial production of oxide or mixed oxide fuel is powder-pellet route which starts with standard sinterable oxide powders [17]. UO_2 is obtained from ammoniumdiuranate (ADU) route whereas for PuO_2 and ThO_2 are obtained by oxalate precipitation route. In addition to powder-pellet process, several other advanced processes have been developed for fabrication of $(U_{1-y}Pu_y)O_2$, $(Th_{1-y}U_y)O_2$ and $(Th_{1-y}Pu_y)O_2$ fuels. Among these, some were specially developed for ^{233}U based fuels at BARC, considering its handling challenges due to high radiation dose [18].

Advanced Fuel Fabrication Facility (AFFF), Tarapur, BARC India is engaged in fabricating various types of oxide and mixed oxide fuels (cylindrical pellet type) for various Indian reactors. The fabrication follows the standard powder-pellet route which involves unit operations such as milling, cold compaction and sintering to get solid or annular pellets of high density (>90% TD). A significant quantum of the scrap gets produced invariably in various manufacturing operations and quality control (QC) activities (to a lesser extent). The scrap arisings comprise; ThO_2, UO_2, PuO_2 and their mixed powders, sintered pellets (major portion), chips, solution etc. The off-specification fuel pellets are produced for non-compliance of numerous physical or chemical specifications like dimensional, compositional, density, impurity content, physical defects, fissile rich agglomerates etc. These rejects can be categorized as 1) clean rejected oxide (CRO) or clean scrap and 2) dirty rejected oxide (DRO) or impure scrap, depending upon the chemical impurity content. The proportion of several types of scrap generated during $(U_{1-y}Pu_y)O_2$ fuel manufacturing is shown in **Fig. S1.**

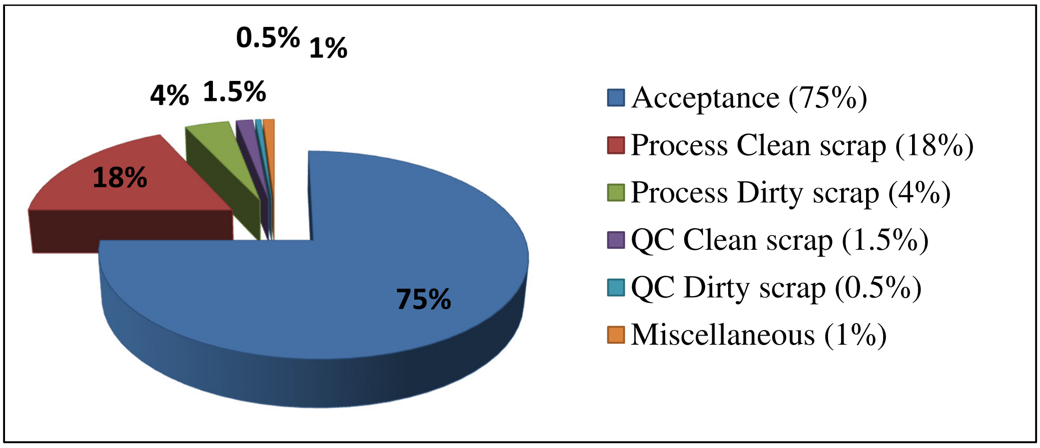

Fig. S1: Proportion of various scrap in MOX fuel fabrication by powder-pellet route

The process of 'recycling' consists of 'recovery' of scrap and 'reuse' as feed material. The practice of recycling of scrap nuclear material becomes essential for following main reasons [1, 19-20]:

1. Recovery of valuable fissile (^{235}U, Pu, ^{233}U) materials locked in the rejects.
2. Aversion of personnel exposure due to high radiation emitting decay products which build-up with time lapse. For example, ^{241}Am (γ: 60 KeV) from decay of ^{241}Pu and ^{212}Bi/ ^{208}Tl (γ: 0.7–1.8 MeV/ 2.6 MeV) from ^{232}U (ppm level) present in ^{233}U fuel.
3. Quick recycling alleviates the total fissile content (TFC) reduction in Pu due to decay of fissile ^{241}Pu into ^{241}Am. Thus, old scrap tends to loose value.
4. Recycling curtails the fuel costs and consequently the energy cost.
5. Recycling saves natural resources and fresh/ standard feed stock materials.

Recycling of nuclear fuel rejects has gained recently more attention worldwide [21-27]. The preliminary research work was carried out in small laboratory scale microwave ovens at AFFF. The encouraging results were observed, which inspired us to upscale the work on industrial level and to meet the requirements of the AFFF. Microwave processing systems of industrial capacities were designed, fabricated and installed. The recycling using microwave has indicated a tremendous potential yet to be explored [5, 7, 27]. Thus, systematic study using microwave was planned to be carried out and establish the recycling processes for these fuel rejects which shares large quantum (~25%) of the total material throughput (**Fig. S1**). The extensive experimental research work carried out was immediately implemented for recycling of large quantity of $(U_{1-y}Pu_y)O_2$ rejects on the industrial scale. Oxide/ mixed oxide fuel scrap more than 3 MT has been recycled. The detailed study has been described in the present thesis.

The present work includes microwave based recycling of both the chemically clean and impure rejects of UO_2, ThO_2, PuO_2 and their mixed oxides. The $(U_{1-y}Pu_y)O_2$ rejects were kept stored over many years that were piled-up in different MOX fuel campaigns (BWR, PFBR, FBTR or experimental fuel) at AFFF. The recycling of $(U_{1-y}Pu_y)O_2$ in the entire range of PuO_2 (y: 0-1) was studied. The study also includes the recycling of thoria based rejected fuels $(Th_{1-y}U_y)O_2$ with (y: 0-3) and $(Th_{1-y}Pu_y)O_2$ with (y <0.1) which were produced during the course of fuel development programme at AFFF for future thorium fueled reactors (AHWR, AHWR-LEU etc.) and for experimental irradiation. Depleted UO_2 was used for simulating $^{233}UO_2$ and $LEUO_2$ (unless stated) in the present study.

The most attractive application of microwave is dissolution and denitration of nuclear oxides. The microwave heating is used for the faster dissolution of difficult to dissolve sintered Pu and Th oxides/ mixed oxides. The microwave direct denitration of so obtained nitrate solution produces sinterable grade powder without forming the ‘mastic phase’; a technical lacuna in the conventional direct denitration [8-10, 28-29]. The efficient heating by microwave for calcination, oxidation, reduction or sintering etc. of nuclear material oxides constitutes another important application [30-32]. The quick material heating with high ramp rates and thermal runaways (a disadvantage) were exploited for the oxidative pulverization of UO_2 or UO_2 containing MOX matrix [2, 5, 31-32]. In view of the cutting edge advantages of microwave over conventional heating, the present study was planned to exclusively exploit microwave heating technology with the following main objectives:

1. Development of efficient methods for recycling of characteristically different MOX fuel rejects on industrial scale.
2. Development of a wet recycling method based on dissolution and direct denitration for which the main driving forces were minimal liquid waste generation and standard powder equivalent properties.
3. Development of dry recycling methods for UO_2 based rejects by microwave direct oxidation with objectives to lower the temperature and shorten the conventional

prolonged heat process cycles thereby improving the products comparatively. The main motivations are their high production rates and no liquid waste generation.

4. The methods preferably that can use 100% recycled powder for fabrication of fuel bringing out the maximum scrap recycling ratio (SRR: 1) offering several advantages to the fuel fabricators. SRR indicates the weight fraction of recycled powder added to the total weight of fuel batch fabricated.
5. To study the effects of various parameters which influence the product properties so as to tailor the characteristics of recycled powder.

The entire thesis is written in total eight chapters; their brief description is as follows:

Chapter 1: Introduction

After briefly introducing the objective of the present thesis, this chapter in the beginning gives a general introduction to microwave processing. Subsequently, the current scenario of microwave applications in the nuclear fuel cycle and processing of the nuclear materials is outlined. The thrust of nuclear power in India, the nuclear power programme and various types of fuels used in the reactors are briefed. The candidate nuclear fuels, their types and properties are discussed. The important chemical, physical and technological properties of the standard feed materials for fabrication of oxide fuels are elaborated. The overview of the methods for synthesis for sinterable grade UO_2, PuO_2, ThO_2 and their mixed oxides powders like gelation, denitration, precipitation-calcination etc. [8-10, 17, 28-29, 33-34] is presented. The powders are compared for the several synthesis routes considering the key parameters like BET surface area, particle size, morphology, flowability, sinterability and industrial maturity. The denitration/ co-denitration methods of synthesis are more elaborated due to their direct relevance to the present work. The solution chemistry of Th, U and Pu and their oxide/ mixed oxides is pertinent to the present work, hence presented in detail. The solid state oxidation and reduction behavior and compounds formed were discussed in relation to development of dry methods of recycling. The constraints, challenges in handling and working with nuclear materials are briefed upon specially emphasizing the plutonium. The long half-lives of Pu isotopes, high specific activity and long retention times in the body (>100 years) make it one of the most hazardous and radiotoxic elements to handle. To work with plutonium essentially requires its handling in negatively ventilated and high integrity glove-boxes. The powder-pellet route for fabrication of MOX fuel alongwith quality control techniques is elaborated. The radioactive waste generation in fabrication of fuels is also briefly mentioned.

The rejects or scrap produced in the fabrication of oxide/ mixed oxide nuclear fuel, causes of generation, their recycling needs and attributes of recycling methods are highlighted. The extensive literature was reviewed on the recycling of oxides/ mixed oxide scrap [21-27, 35-37]. The conventional methods of recycling for rejected UO_2, $(U_{1-y}Pu_y)O_2$, $(Th_{1-y}U_y)O_2$ fuels are based on either dry processes using comminution, oxidative pulverization (UO_2 to U_3O_8) in electrical resistance furnaces [21-27, 35-36] or wet processes involving dissolution and liquid-liquid extraction, precipitation and conversion [29, 34]. The recycling of ThO_2 and ThO_2 based MOX scrap is studied to a small extent and limited literature is available [26, 37]. The dry processes generate radioactive dust, have prolonged cycles and the powder properties are inferior to the standard feed materials. The powders from the conventional dry processing methods have low sinterability and usually mixed with standard powders. Thus, the scrap recycling ratios (SRR) are <1 (typically 0.1-0.2).

The recycling using conventional precipitation-calcination wet routes (ADU, AUC/ AUPuC, oxalate etc.) produce powder with better and consistent properties as compared to dry routes. However, the conventional wet processes of recycling have multi steps, associated liquid waste generation, low production rates and thus non-economic. Some other problems associated are higher sensitivity of the product characteristics to several process parameters, criticality, additional packaging and transport etc. The direct denitration potentially has the minimum number of process steps and parameters thus, outweigh the gelation and precipitation methods [10, 29]. The foremost advantages of the denitration process are simple steps, fast processing and little liquid waste generation that too in the treatment of the off gases. In the precipitation-calcination methods, several parameters need to be controlled such as pH, concentration of reactants and products, temperature, sequence and rate of addition etc. This is well known that the conventional thermal denitration is unable to produce sinterable UO_2 powder [28]. However, among the acceptable denitration techniques like fluidized bed denitration [38], ammonium-uranium nitrate double salt decomposition [39] and microwave direct denitration etc., the later has gained distinct merits; primary being the synthesis of sinterable UO_2 powder through bulk solution denitration without forming the hard lumps (via mastic phase) [8-10]. Thus, microwave dissolution-denitration was selected for the wet recycling of fuel rejects. The high temperature ramp rates throughout the bulk and thermal runaways in UO_2 by microwave brings out efficient oxidation and pulverization of sintered pellets so explored in dry method of recycling. An overview of the present work including problem identification, objectives, motivation behind development of novel recycling methods, recycling methodologies investigated, scope of work are described at the end of the chapter.

Chapter 2: Microwave Heating Fundamentals and Nuclear Material Processing

At the outset of the chapter, microwave frequencies under ISM band are stated. Various types of heating methods (Ohmic, induction, microwave etc.) are compared. The mechanism of microwave heating has been explained with respect to material-microwave interaction, classification of materials, dielectric properties of materials including nuclear materials.

The direct heating of materials using microwave is consequence of the oscillating electric field of microwave (~10^9 Hz), wherein the molecular dipoles (permanent, induced, instantaneous etc.) and ions oscillate back and forth or start rotating [13-16]. Due to higher penetration depths of microwaves (depending upon dielectric properties) each individual constituent molecule interacts. The phenomenon of oscillation and rotation occurs throughout the bulk, resulting in enormous molecular friction and instantaneous generation of heat. Whereas, the electrical resistance heating starts from the surface of the material and heat is transferred by conduction or convection up to core.

The microwave heating of nuclear material oxides and their aqueous nitrate solutions is promising and can be employed for various processing (dry heating, hydrothermal synthesis etc.) required in the nuclear fuel cycle. The nuclear oxides of interest (UO_2, U_3O_8, PuO_2) and their nitrates are strong absorbers of microwaves and high temperatures are achievable [40-43]. ThO_2 is room temperature microwave transparent; however, its nitrate compounds are microwave absorber making its hydrothermal processing feasible [44-47]. The working of magnetron and its characteristics are described. The adaptation and integration of indigenous microwave processing systems for nuclear material processing in glove-boxes is presented. The 'microwave effect' on the observation of enhanced mass transport and solid-state reaction rates in ceramics and accelerated reaction kinetics in the chemical processing is focused in the chapter. The measurement of temperature in the microwave fields and microwave power in application systems beside the leakage are also described. A brief description on the salient features and economics of the microwave heating is included. At the end of the chapter, the safety perspectives of the microwave and RF fields are discussed.

Chapter 3: Experimental Materials, Methods and Instruments

In the beginning of this chapter, the standard materials used for fuel fabrication, their important properties and sources are stated. The rejected fuel materials to be recycled (starting materials); sintered thoria and urania based MOX fuel pellets subjected to fuel recycling experiments are described. The preparation and sources of the chemicals and reagents employed in the present study are recorded. Subsequently, the processing equipments used in the studies are described alongwith their operation and technical specifications. The analysis methods and instruments employed are detailed alongwith photographic illustrations. As the work involves the plutonium handling, the experimental work, equipments and instruments are housed inside the glove-boxes. The instruments, methods and key parameters that were used for evaluating the suitability of the recycled powder for fuel re-fabrication as bulk density, particle size, surface area, morphology; SRR, sintered density, XRD analysis, impurity content etc. are shown and described.

Chapter 4: Development of Methods for Recycling of (U,Pu)O_2 MOX

The first half of this chapter describes the microwave dissolution and direct denitration technique based wet recycling of UO_2 and $(U_{1-y}Pu_y)O_2$. The dry recycling using microwave direct oxidation process is elaborated in the second half of the chapter.

In the wet recycling, initially the parameters (batch size, dissolvent volume, dissolution time, temperature, PuO_2 composition, crushing, oxidation, mode of heating etc.) influencing the microwave dissolution of CRO in HNO_3 were studied. After optimizing the dissolution parameters, microwave direct denitration experiments were carried out. The mechanism of microwave denitration of U, Pu nitrate solutions through formation of $(U,Pu)O_2(OH)NO_3$ up to UO_2 is elaborated. The shape of de-nitration vessel, stirring, temperature (in denitration, calcination and reduction), addition of polyvinyl alcohol (PVA) as pore former and PuO_2 composition affects the product characteristics (cake and powder bulk density, surface area, particle size etc.) and their detailed influence was examined. The optimized parameters were selected. The recycled powders were characterized. Based on the studies, the flow sheet reported by Khot et al. [27] was modified and the process was called modified MicroWave Direct Denitration (Modified-MWDD). Experimental fuel batches were fabricated using the recycled powder from Modified-MWDD and compared with the batches prepared from the standard powder and earlier reported MWDD method. The major modifications incorporated are; stirring during dissolution-concentration stage, addition of PVA, microwave based low temperature calcination-reduction and magnetic separation. The modified method improved the sintered density, fissile homogeneity, grain size and achieved SRR of 1. The applicability of the method has been discussed for recycling pure sintered UO_2, low Pu (3-4 wt%) $(U_{1-y}Pu_y)O_2$ MOX, high Pu (20-30 wt%) $(U_{1-y}Pu_y)O_2$, and $(U_{1-y}Pu_y)O$ with Pu> 35% requiring fluoride catalyzed dissolution and 100% PuO_2. The applicability of the method was extended for recycling the Quality Control (QC) generated clean scrap. The photograph of microwave denitrated product inside a glove-box is shown in **Fig. S2.** A schematic of recycling of $(U_{1-y}Pu_y)O_2$ by microwave dissolution-denitration technique is depicted in **Fig. S3**.

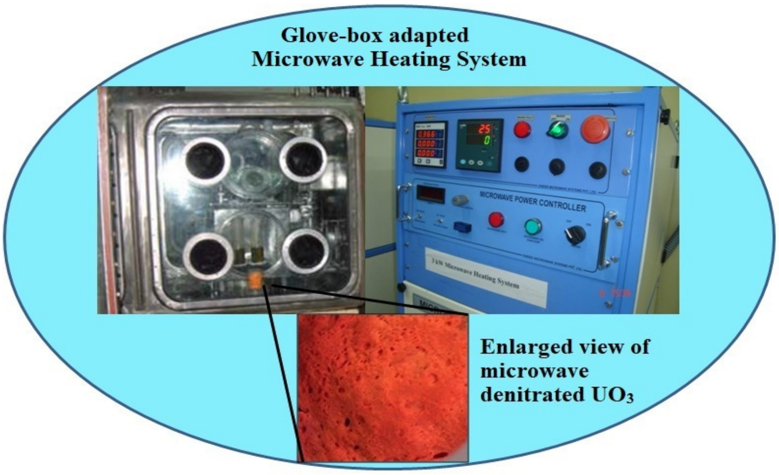

Fig. S2: Photograph of microwave denitrated UO_3 cake in a Glove-box

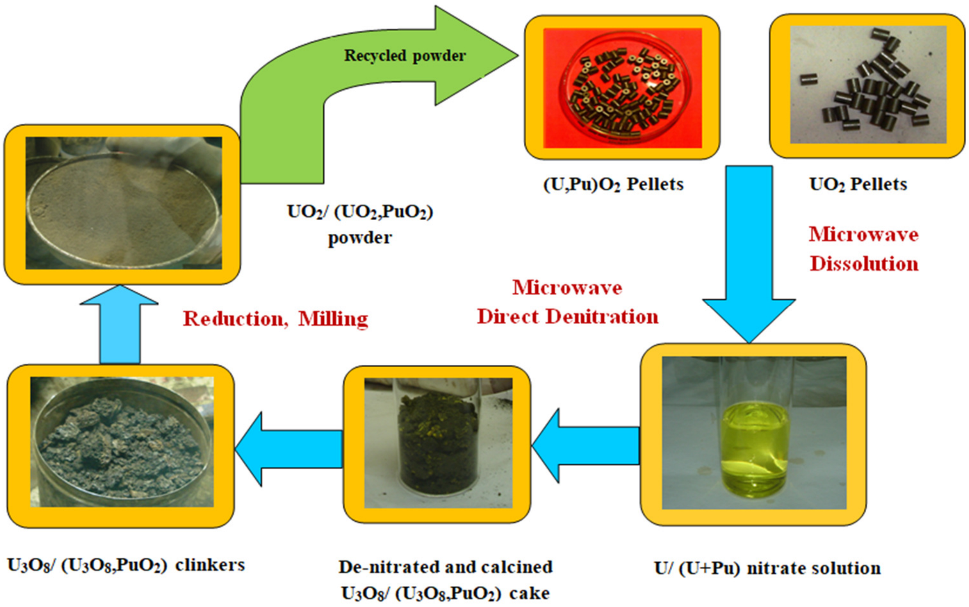

Fig. S3: Schematic of wet recycling of $(U_{1-y}Pu_y)O_2$ by microwave denitration

The development of MicroWave Direct Oxidation (MWDO) process of UO_2 and $(U_{1-y}Pu_y)O_2$ clean rejects is inspired from the observation of cracking of the pellets during microwave sintering at higher temperature ramp rates [5, 31-32]. The process consists of two distinct stages of heating using microwave as shown in **Fig. S4**. The factors affecting the oxidation process were studied systematically as mode of heating, PuO_2 composition, oxygen partial pressure, multiple oxidation cycles, initial crushing etc. (**Fig. S5**). The schematic of the MWDO dry recycling process for recycling of $(U_{1-y},Pu_y)O_2$ is shown in **Fig. S6**.

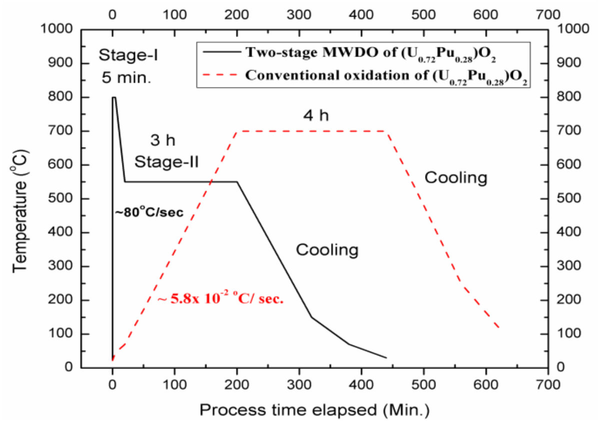

Fig. S4: Comparison of temperature profiles for two-stage MWDO and conventional oxidation

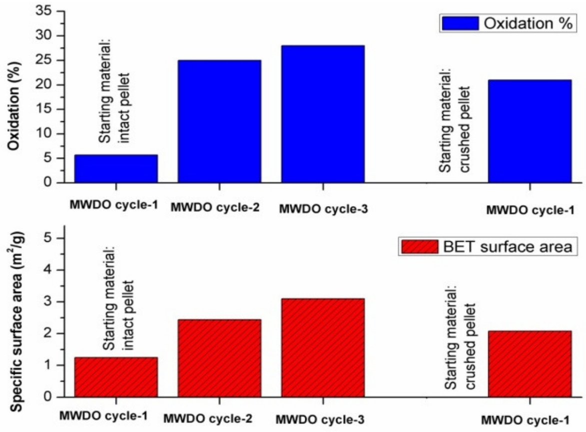

Fig. S5: Effect of physical form and multiple oxidation cycles on surface area and oxidation in 28% PuO_2 MOX

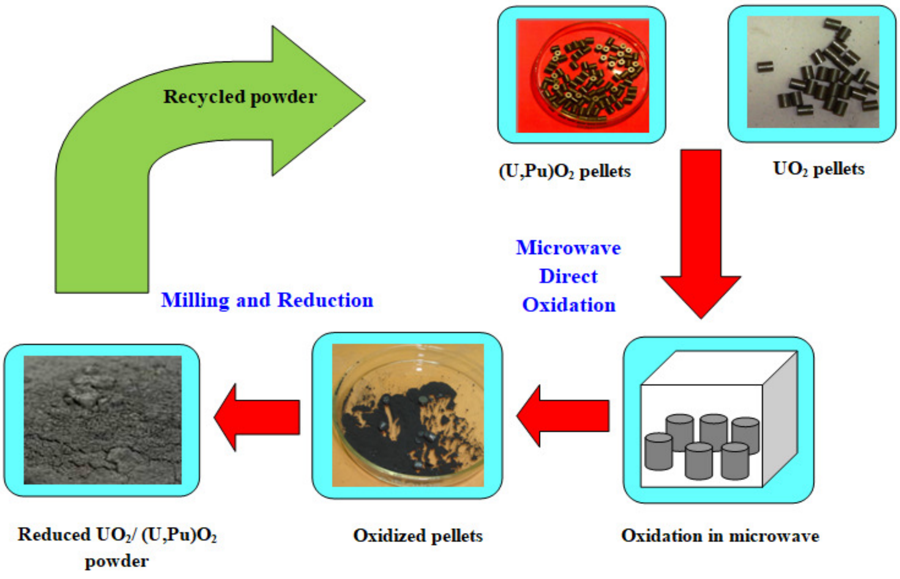

Fig. S6: Microwave Direct Oxidation process for recycling of $(U_{1-y}Pu_y)O_2$

The recycling of $(U_{1-y}Pu_y)O_2$ MOX using MWDO was discussed under three heads as UO_2, low Pu (3-4 wt%) MOX and high Pu (> 20 wt%) MOX. A comparative evaluation of the wet and dry processes developed for recycling of $(U_{1-y}Pu_y)O_2$ is made at the end.

Chapter 5: Development of Methods for Recycling of ThO_2 and ThO_2 based MOX

This chapter is dedicated for development of methods for recycling of thoria based fuel rejects. The sintered pellets under study were ThO_2, $(Th_{1-y}U_y)O_2$ ($y< 0.3$) and $(Th_{1-y}Pu_y)O_2$ ($y< 0.1$). The inabilities of the applicability of traditional oxidative methods of recycling ThO_2 are discussed in the beginning. An integrated method was developed combining three basic approaches; mechanical micronisation, oxidative pulverization (in UO_2 containing MOX) and dissolution followed by direct denitration using microwave (**Fig. S7**) for complete recycling of thoria based fuel rejects. The morphology of microwave denitrated ThO_2 (**Fig. S8**) was found to be irregular as compared to the typical platelet for oxalate derived [3]. The effect of several factors like mode of heating, HF addition, PVA addition, UO_2/ PuO_2 content on the product properties was studied. The suitability assessment of the recycled powder for re-fabrication was carried out by comparative evaluation with standard powders. **Fig. S9** shows pictorial representation of the integrated method of recycling for sintered thoria based rejects.

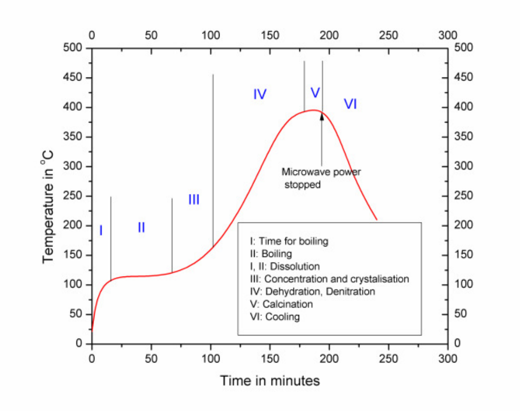

Fig. S7: Temperature profile of microwave dissolution-denitration of ThO_2

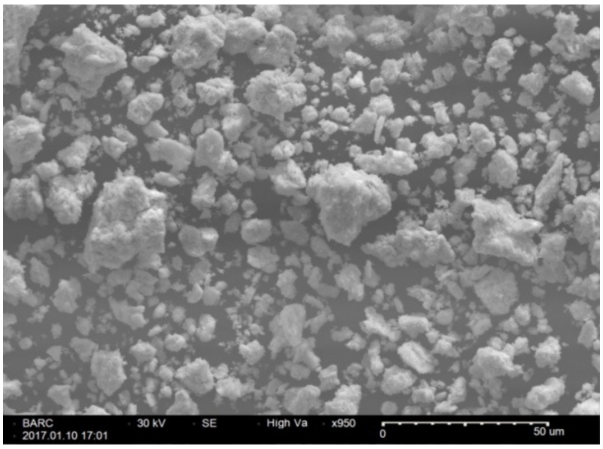

Fig. S8: SEM microphotograph of direct microwave denitrated ThO_2

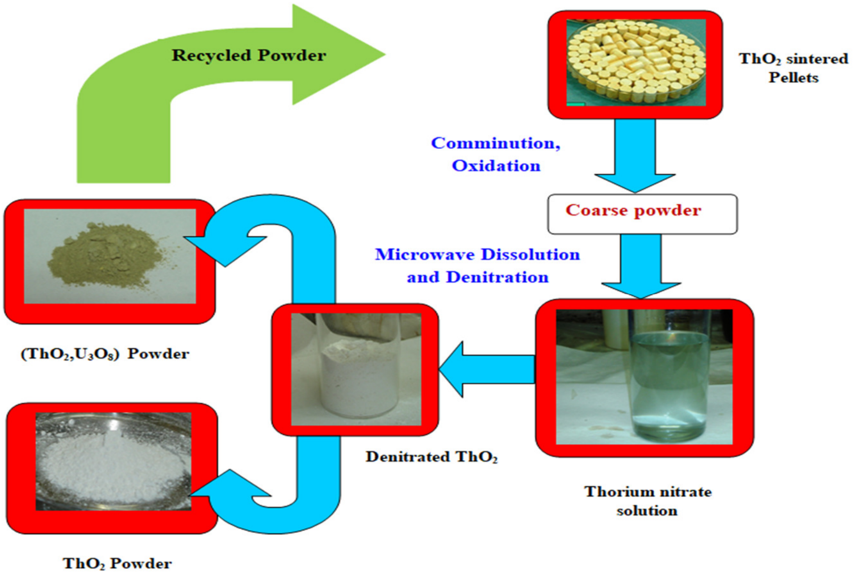

Fig. S9: Schematic of the integrated method of recycling thoria rejects

Chapter 6: Development of Methods for Recycling of Impure Oxide and Mixed Oxide Fuel Scrap Materials

This chapter presents the detailed experimental work carried out for recycling the impure fuel scrap. Initially, impurity analysis and source identification in several process and QC generated impure scrap were carried out. Both, metallic and non-metallic impurities were determined and the deviation from the acceptable value was expressed in terms of impurity factors (IFs). The dissolution behavior of scrap was studied by dissolution test (**Fig. S10**).

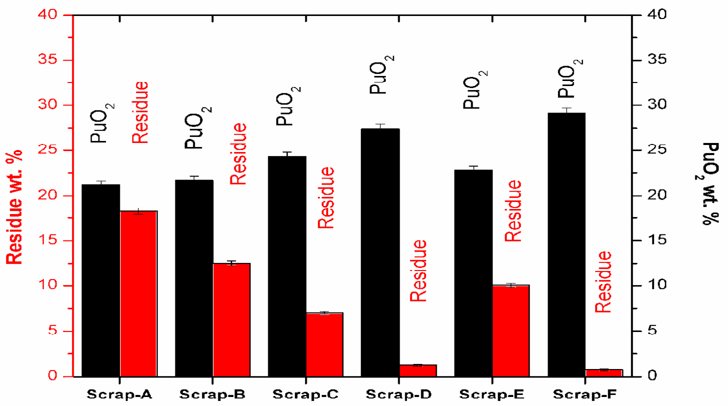

Fig. S10: Residue obtained in the dissolution test and PuO_2 in various process generated impure MOX scrap samples

Based on the impurity analysis and dissolution behavior study, the recycling methodologies have been developed. A flow sheet has been designed which involved head-end treatments to rid-off foreign items, carboneous impurities etc. The dissolution-purification (TBP extraction) route was followed for scrap having non-volatile impurities. This flow sheet has been annexed to that for clean scrap using microwave direct denitration process. A few impure scrap batches were recycled and related data are presented in the chapter. Since, quantitative dissolution is required (not for all the types of impure scrap), fluoride catalysed and solid solution formation through sintering (fluorideless) dissolutions were compared. The feasibility study on the recovery of U and Pu from the used graphite crucibles generated in the QC of the MOX fuel is described.

Chapter 7: Low Temperature Material Processing Applications Using Microwave

The low temperature processing of the feed materials (standard or recycled) is beneficial, since higher temperature deteriorates the sinterability of the powders besides energy economics. The lower temperature and faster accomplishment of solid state reactions like sintering, oxidation, reduction etc. in ceramics are result of enhanced mass transport under microwave fields [2, 48]. The microwave electric fields induce a ponderomotive driving force on constituent ions resulting enhanced mass transport in addition to thermo-chemical driving force. Thus, microwave heating could complete the processing at lower temperature. The microwave reduction was carried out at 550 ^{o}C, 3h as compared to the conventional at 700 ^{o}C, 4h. The parameters for reduction of U_3O_8 were optimized (**Fig. S11)** and applied for stoichiometric reduction of (U_3O_8,PuO_2) powder (**Fig. S12**). The novel method of reduction was further modified to achieve controlled oxidation of the reduced powder. The processed powders were characterized for bulk density, particle size, BET-SSA, O/M ratio and phase using XRD.

The calcination of several uranium oxides and mixed oxides at lower temperature with smaller processing cycle (350 °C, 1h and 550 °C, 1h) than the conventional (700 °C, 2-4h) have been studied using microwave.

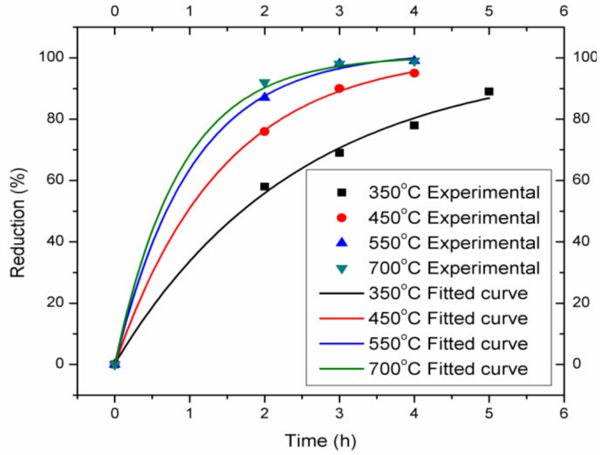

Fig. S11: Temporal variation of % reduction of U_3O_8 at different temperatures in microwave

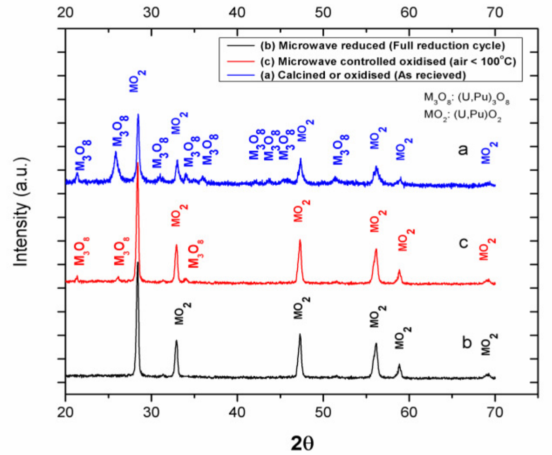

Fig. S12: XRD patterns of MWDO recycled $(U_{0.72}Pu_{0.28})O_2$ (a) Oxidized, (b) microwave reduced and (c) controlled oxidized powder

Chapter 8: Conclusive Summary and Future Scope

This chapter summarizes the major conclusions and findings of the detailed study carried out. On the basis of the systematic study, flow sheets for 100 % recycling of rejects have been developed. The recycled products and intermediates were comprehensively characterized. The recycled powder suitability for re-fabrication was demonstrated by fabrication of several experimental fuel batches initially and then implemented at the industrial scale at AFFF. In summary, the major conclusions of this thesis are as follows:

1. Development of microwave based methods for clean $(U_{1-y}Pu_y)O_2$ scrap

a. Rejected sintered $(U_{1-y}Pu_y)O_2$ with (y: 0-1) could be recycled by Modified-MWDD technique. However, the $(U_{1-y}Pu_y)O_2$ with PuO_2> 35wt% (y> 0.35) need fluoride for complete dissolution and addition of pore formers to achieve desired bulk density and surface area. The recycled powder have shown high sinterablilty (density >92% TD) and fissile homogeneity. The recycled powders have surface area > 3 m^2/g and average particle size in the range 1-4 µm. More than 3.5 MT of rejected $(U_{1-y}Pu_y)O_2$ MOX was successfully recycled by microwave denitration methods.

   - **b.** The microwave based thermo-oxidation process viz. MWDO was found to be superior to the conventional oxidation method of recycling owing to smaller processing time, higher oxidation (%) achievable and better powder properties. The multiple micronisation-oxidation cycles further enhanced the oxidation (%) and BET-SAA of recycled powder. Approximately 240 Kg of UO_2 and $(U_{1-y}Pu_y)O_2$ MOX was recycled using MWDO process.

2. **Development of microwave based methods for clean ThO_2, thoria based MOX**
   - **a.** The integrated method was successfully demonstrated for recycling of sintered ThO_2, $(Th_{1-y}U_y)O_2$ (y; 0-0.3) and $(Th_{1-y}Pu_y)O_2$ (y; 0-0.1) pellets. Nearly 40 Kg of ThO_2 based pellets were recycled via developed process.
   - **b.** The addition of PVA during denitration increased the specific surface area of the denitrated ThO_2 (> 7 m^2/g). The presence of UO_2 in ThO_2 improved the powder properties (bulk density, surface area etc.) whereas that of PuO_2 could not.
   - **c.** The microwave denitrated ThO_2 was found to have irregular morphology than standard ThO_2 having platelet.

3. **Development of methods for recycling impure MOX scrap**
   - **a.** The impure scrap contains a variety of impurities manifold higher than the allowed limits. The non-metallic impurities are associated with all types of the impure scrap studied; hence needed a head-end heat treatment. The presence of metallic impurities requires chemical purification steps for recycling.
   - **b.** The dissolution behavior of most of the $(U_{1-y}Pu_y)O_2$ impure scrap has shown large plutonium rich residues (in DT) either needing fluoride or sintering for complete dissolution. ThO_2 based impure scrap essentially needed fluoride for dissolution.

  - **c.** The compaction of (U,Pu)O_2 impure scrap into pellets and sintering at ~1600 ^oC followed by fluorideless dissolution in HNO_3 using microwave is recommended for industrial recycling.
  - **d.** The integrated flow sheet has demonstrated the complete recycling of impure scrap.

4. **Low temperature applications of microwave**
  - **a.** The calcination of various uranium oxides was demonstrated at 550 ^oC, 1h than conventional at 700 ^oC, 2-4h. The microwave calcination of UO_3 needs addition of UO_2 or U_3O_8 as microwave absorbing seed.
  - **b.** The optimum condition for stoichiometric reduction of U_3O_8 and (U_3O_8,PuO_2) using microwave was found to be 550 ^oC, 3h compared to the prolonged conventional process at 700 ^oC for 4h.
  - **c.** A quick method for getting controlled hyper-stoichiometry in the reduced powder was successfully demonstrated for improved the sinterability and passivated stabilization of $(U_{1-y}Pu_y)O_2$ powder for long term storage.

The present study reports the development of microwave based efficient wet and dry methods for recycling of various kinds of rejected MOX fuel from nuclear fuel fabrication plants and filled the potential gaps in the technology of recycling. The scale-up plans, future work directions to economize the process of nuclear fuel fabrication with regard to recycling are stated. The recycling of the fuel rejects by the developed methods which exclusively use novel microwave heating technique was implemented at AFFF, BARC. The systematic study and the characterization of intermediate/ products at each step have provided the in-depth knowledge of the process and subsequently used for tailoring the product properties. The technologically attractive features of microwave heat processing like direct material bulk heating, high temperature ramp-ups and non-contact heating make this more attractive and implementable for the nuclear material processing.

REFERENCES TO SYNOPSIS

[1] International Atomic Energy Agency (IAEA), (1999) TECDOC-1115.

[2] Y. Zhao et al. (2008) Prog. Nucl. Energy, (50): 1-6.

[3] G. Singh et al. (2011) Analytical Methods, 3: 622–627.

[4] R. K. Malav et al. (2013) J. Radioanal. Nucl. Chem., 295 (1): 425-430.

[5] G. K. Mallik et al. (2005) Int. J. Nucl. Energy Sci. Technol. 1(2/3): 184-190.

[6] N. N. Mirashi et al. (2010) Microchemical Journal, 94(1): 24-27.

[7] Y. M. Kulyako et al. (2011) Radiochemistry: 604-607.

[8] M. Koizumi et al. (1983) J. Nucl. Sci. Technol. 20 (7): 529–536.

[9] W. Bao, C. Song (1998), China Nucl. Sci. Technol. Report CNIC-01272 TSHUNE-0083.

[10] E. D. Collins (2015) in Robin Taylor (Ed.), “Reprocessing and recycling of spent nuclear fuels”, WP Publishers Elsevier: 313-323.

[11] D. E. Clark et al. (1996) Annu. Rev. Mater. Sci. 26: 299-331.

[12] D. Aggarwal (2006) Trans. Indian Ceram. Soc. 65(3): 129-144.

[13] R. R. Mishra et al. (2016) Composites: Part A (81): 78-97.

[14] W. H. Sutton (1989) Am. Ceram. Soc. Bull. 68(2): 376-386.

[15] Clark et al., (2000), Mater. Sci. Eng. A, 287: 153-158.

[16] Roger Meredith (Ed.), (1998) “Engineers handbook of Industrial microwave heating”, The Institution of Electrical Engineers, UK.

[17] International Atomic Energy Agency (IAEA), (2012) TECDOC-1686.

[18] S. K. Mukherjee et al. (2013) in D. Das and S. R. Bharadwaj (Eds.), “Thoria-based Nuclear Fuels”, Springer-Verlag, London: 205-277.

[19] E. R. Merz, C. E., Walter, G. M. Pshakin (Eds.) (1995), “Mixed Oxide Fuel (Mox) Exploitation and Destruction in Power Reactors”, Vol. 2, Springer: 177.

[20] International Atomic Energy Agency (IAEA), (2000) TECDOC-1130.

[21] Fateh Mernache et al. (2016) J. Nucl Sci. Technol. 53 (6): 790-796.

[22] R. I. Larson and J. W. Sammey (2002) United State Patent US2002/0005597A1.

[23] J. H. Yang et al. (2010) J. Nucl. Sci. Technol. 47 (6): 538-541.

[24] K.W. Kang, et al. (2008) J. Nucl. Sci. Technol. 45 (11): 1150-1154.

[25] K. K. Bae, et al. (1994) J. Nucl. Mater. 209: 274-279.

[26] S. Mishra et al. (2015) Thorium Energy Conference, ThEC15, India: 637-643.

[27] P. M. Khot et al. (2014) Nucl. Eng. Des. 270: 227–237

[28] P. A. Hass (1988), Nucl. Technol. 81(3): 393-406.

[29] E. D. Collins, (2011) “Evaluation of co-precipitation processes for the synthesis of mixed oxide fuel feedstock materials”, ORNL, Milestone Report.

[30] M. S. Ioffe (2000) “Method for preparing uranium dioxide powder” WO2000032517A1.

[31] T. Subramanian et al. (2000) Mater. Lett. (46):120-124.

[32] J. H. Yang et al. (2004) J. Nucl. Mater. (325):210-216.

[33] V. N. Vaidya, (2008), J. Sol-Gel Sci. Technol. 46(3): 369-381.

[34] M. J. Sarsfield (2015) in Robin Taylor (Ed.), “Reprocessing and recycling of spent nuclear fuels”, WP Publishers Elsevier: 325-351.

[35] I. Schwartz et al. (1979), J. Nucl. Mater. 82: 54-59.

[36] A. Vandergheynst et al. (2004)., United State Patent US6783706B1.

[37] S. Cagno et al., (2017) J. Sustain. Metall., 3 (3), 659-667.

[38] Neetu A. Baveja et al. (2012) BARC News Letter, 326: 22-29.

[39] K. Notz and P. Hass (1981) ORNL/TM-7820.

[40] C. E. Holocombe (1983) Am. Ceram. Soc. Bull. 62: 1388.

[41] P. A. Hass (1979) Am. Ceram. Soc. Bull. 58: 873.

[42] Y. Kato et al. (2004) J. Nucl. Sci. Technol. 41 (8): 857-862

[43] E. F. Strucken and L. E. McCurry, (1991) Report WSRC-MS-90-330.

[44] V. Chandramouli (1999) A Thesis submitted for award of Ph. D. to Univ. of Madras, India.

[45] B. J. F Palmer et al. (1984) Am. Ceram. Soc. Bull. 63(8): 1030-1034.

[46] G. K. Mallik (2013) BARC News Letter, 331: 26-30.

[47] I. N. Toumanov (Ed.) (2003), “Plasma and High Frequency Processes for Obtaining and Processing Materials in the Nuclear Fuel Cycle”, Nova Science Publishers Inc., New York: 192-193.

[48] John H. Booske et al. (1997), Mater. Res. Innovat. 1: 77-84.

LIST OF ABBREVIATIONS

ADU	Ammonium diurante
AFFF	Advanced Fuel Fabrication Facility
AHWR	Advanced Heavy Water Reactor
AL	Allowed Limit
ALI	Annual Limit on Intake
AMAD	Activity Median Aerodynamic Diameter
ASTM	American Society for Testing and Materials
AUC	Ammonium uranyl carbonate
AUPuC	Ammonium uranyl-plutonyl carbonate
BET-SSA	Brunauer–Emmett–Teller Specific Surface Area
BWR	Boling Water Reactor
CAP	Coated Agglomerate pelletisation
CBD	Cake Bulk Density
CRM	Certified Reference Material
CRO	Clean Rejected Oxide
DAC	Derived Air Concentration
DC-Arc-AES	Direct Current-Arc- Atomic Emission spectroscopy
DDC	Dual Directional Coupler
$DDUO_2$	Deeply depleted UO_2
DF	Decontamination Factor
DRO	Dirty Rejected Oxide
DT	Dissolution Test
EBC	Equivalent Boron Content
EDTA	Ethylenediaminetetraacetate
EMI	Electromagnetic Interference
EODT	Electro Oxidative Dissolution Technique
ERDT	Electro Reductive Dissolution Technique
FBG	Fiber Bragg Grating
FBTD	Fluidized Bed Thermal Denitration
FBTR	Fast Breeder Test Reactor

FCC	Face Centered Cubic
FCCI	Fuel Clad Chemical Interaction
GAR	Gamma Auto Radiography
GB	Glove Box
GBI	Glove-Box Indicator
GLM	Green Linear Mass
HDPE	High Density Polyethylene
HEPA filter	High Efficiency Particulate Air filter
ICNIRP	International Commission on Non-Ionizing Radiation Protection
IAEA	International Atomic Energy Agency
ICP-OES	Inductively Coupled Plasma- Optical Emission Spectroscopy
ID	Inner Diameter
IF	Impurity Factor
IGF	Inert Gas Fusion
ILW	Intermediate Level Waste
ISE	Ion Selective Electrode
ISM	Industrial, Scientific and Medical
ISO	International Organization for Standardization
LD	Laser Diffraction
LEU	Low Enriched Uranium
LLW	Low Level Waste
LOC	Limit of Concentration
LPF	Leak Path Factor
LTMC	Low Temperature Microwave Calcination
LTMR	Low Temperature Microwave Reduction
MDD	Modified Direct Denitration
MHS	Microwave Heating System
MIMAS	Micronisation and MASter process
MMTT	Microwave Moderate Temperature Treatment
MOX	Mixed Oxide
MPE	Maximum Permissible Exposure

MT	Metric Ton (1000 Kg)
MWDD	MicroWave Direct Denitration
MWDO	MicroWave Direct Oxidation
n-DD	Normal dodecane
NOx	Nitrogen oxides
NSDF	Dear Surface Disposal Facility
NWCC	Neutron Well Coincidence Counter
OD	Outer Diameter
O/M	Oxygen to Metal (Th/ U/ Pu) Ratio
OSHA	Occupational Safety and Health Administration
PBD	Powder Bulk Density
PEG	Polyethylene Glycol
PFA	Perfluoroalkoxy alkane
PFBR	Prototype Fast Breeder Reactor
PHWR	Pressurized Heavy Water Reactor
PSD	Particle Size Distribution
PTDD	Primitive Thermal Direct Denitration
PUREX	Plutonium Uanium Redox EXtraction
PVA	Polyvinyl alcohol
QC	Quality Control
RF	Radiofrequency
RSD	Relative Standard Deviation
SGMP	Sol Gel Microsphere Pelletisation
SLM	Sintered Linear Mass
SRR	Scrap Recycling Ratio
SSNTD	Solid State Nuclear Track Detection
TBP	Tri-n-butyl phosphate
TCD	Thermal Conductivity Detector
TD	Theoretical Density
TFC	Total Fissile Content
THOREX	THORium EXtraction

TOPO	Tri-n-octyl phosphine oxide
TZM alloy	Titanium Zirconium strengthened Molybdenum alloy
UNH	Uranyl nitrate hexahydrate
WG	Water Gauge
X-GAR	X-ray Gamma Auto Radiography
XRD	X-Ray Diffraction
XRF	X-Ray Fluorescence

LIST OF SYMBOLS

$(U_{1-y}Pu_y)O_{2\pm x}$	U, Pu mixed oxide, y: weight fraction of PuO_2, (1-y) is weight fraction of UO_2 and x represents oxygen non-stoichiometry
§	Section or subsection
σ	Thermal neutron absorption cross section (barn)
E^o	Standard electrode potential (volt)
Å	Angstrom (10^{-10} m)
ε^*	Complex dielectric permittivity
ε'	Relative dielectric permittivity
ε''	Dielectric loss factor
$\varepsilon' \tan\delta$	Dielectric loss product factor
$\tan\delta$	Loss tangent
K_{eff}	Effective multiplication factor
wt%	Weight percentage
Ht.	Height
Dia.	Diameter
L	Litre
µm	Micrometer (10^{-6} m)
TWh	TeraWatt hour
MeV	Mega electron volt (10^6 eV)
t_p	Powder formation time
T_c	Critical temperature for microwave absorption
$\bar{x}$	Arithmatic mean or average
s	Standard deviation
n	Number of measurement replicates
D^U	Diffusion coefficient of uranium
Z_O	Theoretical increment in O/M for 100% oxidation of an oxide
Z_R	Theoretical decrement in O/M for 100% reduction of an oxide

LIST OF FIGURES

LIST OF TABLES

Chapter 1

INTRODUCTION

Microwave heating is emerging as a powerful technique in the modern era of material processing and hazardous waste remediation [1-8]. The microwave processing applications are gaining increased interest for processing of numerous ceramics, polymers, organic/ inorganic materials and advanced composites. The processing of medical wastes, de-vulcanization of rubber, treatment of sewage sludge, treatment of chemical residues from petrochemical industry, glass processing, chemical wastes etc. are among a few examples.

Notably, the microwave heating progressively is gaining more and more attention of the nuclear community for variety of applications [8-16]. The feasibility of microwave application in the processing of nuclear materials is completely based on their microwave coupling behavior. The most important nuclear materials UO_2, U_3O_8, PuO_2 are known to show strong microwave coupling behavior. Due to their strong absorbing nature high temperature can be achieved [2, 17-19]. Water and mineral acids (HNO_3, H_2SO_4, H_3PO_4 etc.) are good microwave absorbers thus microwave processing can be effectively applied in the hydrothermal processing involving nuclear materials [1, 5, 8]. The nuclear materials which usually we come across in the fuel fabrication are in the form of their oxides and nitrates. The nitrates of U, Pu, Th and oxides can be efficiently heated in the microwave fields [8-23].

The microwave has shown tremendous potential in the processing of nuclear materials leaving the conventional methods far behind. Some remarkable applications include superior dissolution of fuel for processing and analytical applications, drying and organic material burnout, product conversion or co-conversion in several fuel cycle activities, calcination or reduction of intermediates, sintering, pyrolytic synthesis of materials, synthesis of fuel materials and recycling of nuclear fuel scrap [8-23].

The nuclear fuel fabrication processes have inherent limitation of generation of significant quantities of nuclear material scrap or rejects [24]. The fuel scrap like metals, alloys, mixed carbides, oxides, mixed oxides etc. get generated during the production of variety of nuclear fuels [25-30]. The oxide and mixed oxide (MOX) fuels find large usage in most of the commercial power reactors owing to their superior operational properties, ease of fabrication and well established reprocessing. Thus, the recycling of oxide and MOX fuel scrap is of paramount significance to the nuclear industry in the context of fuel and hence energy economics, sensible utilization of nuclear resources and long term storage issues.

Advanced Fuel Fabrication Facility (AFFF), BARC, Tarapur is involved in fabrication of MOX fuels constituting ThO_2, UO_2 and PuO_2 to meet various departmental (Department of Atomic Energy) needs. The powder-pellet route is employed for MOX fuel fabrication at AFFF. During the fuel fabrication several types of fuel scrap gets generated. The proportions of average acceptance and several types of fuel scraps are shown in **Fig. 1.1**.

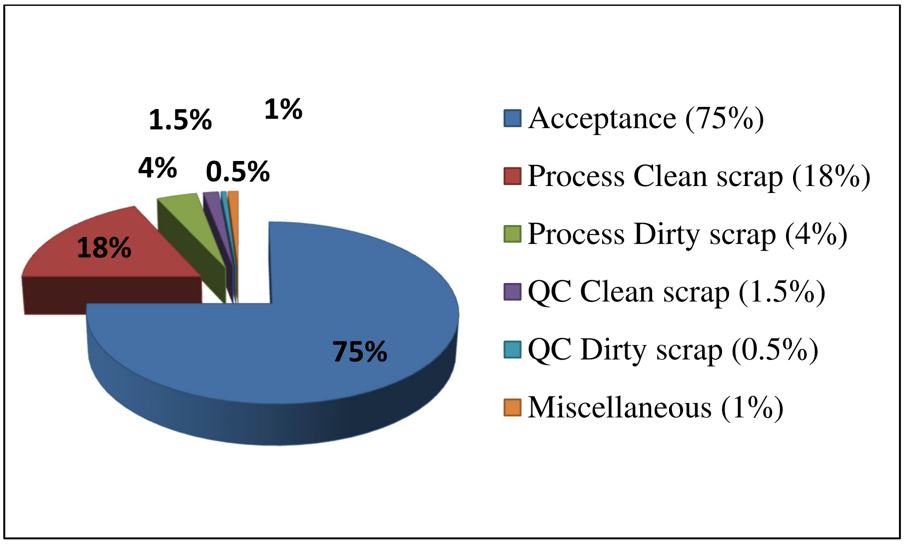

Fig. 1.1: Proportion of Various Scraps in MOX Fuel Fabrication

Considerably large quantities of oxide and MOX fuel scrap or rejects nearly 25wt% of the total material throughput are produced in various manufacturing operations and quality control (QC) activities (to a lesser extent) in the form of sintered pellets (major portion), mixed powders, chips, solution etc. The contribution to scrap mainly arises from the rejected off-specification fuel pellets due to non-compliance of numerous physical or chemical specifications like, dimensional, compositional, density, impurity content, physical defects, fissile agglomerates etc. These rejects can be categorized as 1) clean rejected oxide (CRO) or clean scrap and 2) dirty rejected oxide (DRO) or impure scrap, depending upon the chemical impurity content [31-33]. The fuel rejects contain significant amount of fissile[1] and fertile[2] materials depending upon the composition. India has meager nuclear resources [34], which necessitates the recycling of the scrap. The judicious utilization of the feedstock materials and natural resources can be accomplished by the recycling of the rejects.

Recycling consists of ‘recovery’ from scrap and ‘reuse’ for fuel fabrication. The recycling has gained recently more attention worldwide [35-44]. Although, the use of microwave in the recycling of oxide and MOX has indicated a tremendous prospective yet its potential is not fully utilized [11, 13, 44]. In view of this, the present study has been taken up. The present thesis describes the development of microwave based methods for recycling of scrap or rejects generated at AFFF during the industrial production of UO_2, ThO_2, $(U_{1-y}Pu_y)O_2$, $(Th_{1-y}U_y)O_2$ and $(Th_{1-y}Pu_y)O_2$ fuels. The recycling of sintered fuel rejects using microwave technology is a novel work. The recycling by conventional methods is very cumbersome or not viable in many cases. The extensive experimental research work is carried out using microwave technology. Based on the encouraging outcomes the recycling of large scale quantities of UO_2, $(U_{1-y}Pu_y)O_2$ rejects was successfully achieved. The methods were developed for 100% recycling of several types of characteristically different sintered $(U_{1-y},Pu_y)O_2$, $(Th_{1-y},U_y)O_2$ and $(Th_{1-y},Pu_y)O_2$ fuel rejects. The systematic study scopes the

---

[1] Fissile materials undergo nuclear fission reaction with neutrons of any energy (thermal or fast) for example ^{233}U, ^{239}Pu and ^{235}U.

[2] Fertile materials ^{232}Th and ^{238}U can be converted into fissile ^{233}U and ^{239}Pu respectively upon neutron absorption.

development of methods for recycling the chemically clean and impure scrap generated in the production and quality control activities during MOX fuel fabrication.

1.1 Introduction to Microwave Processing in the Nuclear Fuel Cycle

Microwave heating is fundamentally different from the conventional heating processes. The heat is generated within the material itself upon microwave irradiation due to interaction with the constituents (atoms, ions, molecules etc.). In the case of conventional heating methods (electrical resistance, hot plate, flame etc.) heat is supplied from external surface. The thermal effects of microwaves are the result of electromagnetic nature of microwaves and dielectric properties (dielectric permittivity, loss factor and loss tangent) of the material [45-46]. The materials are divided into three different classes according to material-microwave interaction as 1) Opaque or reflectors (metal sheets), 2) Absorbers; which absorb microwave (partially or completely) and subsequently get heated (UO_2, water, HNO_3, SiC etc.) and 3) Transparent, through which microwave transmits without interaction (Si_3N_4, glass, teflon etc.). The interaction of microwaves with the non-magnetic material is based on polarization (electronic, atomic, ionic, molecular, Maxwell-Wagner etc.), dielectric relaxation (field lagging) and ionic conduction [1-2, 47]. In the magnetic materials; hysteresis and eddy current losses are major mechanisms [1, 47]. The electric and magnetic components of microwave agitate the orientation, movement of diploes, free electrons, ions, magnetic domains etc. and are mainly responsible for energy transfer at molecular level and volumetric heat generation [1].

Microwave heating offers a number of unique advantages in comparison to conventional heating [1-5]. Microwave is non-contact, rapid, material selective, uniform and volumetric or bulk heating technique. It offers reverse thermal gradients and quick start/ stopping ability. The highly improved product yields, microstructures and properties are claimed [2]. Microwave processing of materials offers significant time saving, cost and energy efficacy in clean and environment friendly manner. Microwave has been a breakthrough in the processing of variety of radioactive and nuclear materials in the nuclear fuel cycle [7-24]. The important applications are outlined below:

1.1.1 Dissolution of Nuclear Fuel for Processing and Analytical Applications

Dissolution of the fuel is required at many stages of the nuclear fuel cycle like ore processing, fuel fabrication and spent nuclear fuel[3] reprocessing. Remarkable improvements have been demonstrated in the dissolution or acid digestion using microwave heating. Zhao et al. [48-49] carried out a comparative study on the dissolution kinetics of sintered UO_2 pellets in HNO_3. The study revealed that the dissolution ratio increases 26-46% in microwave heating in comparison to conventional heating. The microwave acid digestion study of variety of sample matrices like marine sediments [50], uranium ore [51-52] and geological samples [53] in pressure vessels is reported to be distinctly advantageous for estimation of radioactive elements and pre-treatment of ores. The quantitative dissolution of $(U_{1-y}Pu_y)O_2$ fuel samples in HNO_3 using microwave heating has been reported for analysis of bulk and trace elements [11, 54]. The microwave assisted dissolution of difficult to dissolve thoria based sintered fuel samples (powder, microspheres and pellets) in HNO_3 [9, 55-56] and in H_3PO_4 [12] is reported to be accomplished in 1-2 hrs than usual time taking (several hours) by conventional heating methods.

1.1.2 Drying and Organic Material Burnout

The moisture, organic materials and other volatile contaminants can be driven out efficiently and rapidly from the bulk materials by heating using microwave. The drying and organic material removal using microwave particularly from thick sections of materials has high efficacy where conventional drying methods are inefficient [2]. The efficient

---

[3] Spent nuclear fuel is a nuclear fuel that has been irradiated in a nuclear reactor.

demoisturisation and dewaxing in sintered UO_2 pellets have been reported [11]. Microwave heating has been found effective in drying of the thorium oxalate and in the synthesis of sinteractive thoria powder [57].

1.1.3 Product Conversion in Reprocessing Facilities

Product conversion from the purified nitrate solutions of U or (U+Pu) from reprocessing plants is an important link in the nuclear fuel cycle. The co-conversion is desired from non-proliferation viewpoint in the nuclear material safeguards. Microwave direct denitration of enriched uranyl nitrate solution into UO_2 has been reported by Bao et al. [15]. The microwave direct denitration of U,Pu nitrate solutions from Tokai reprocessing plant in Japan has demonstrated production of sinterable powder on industrial scale in batch mode and in screw type continuous denitration units [14, 16, 58-59].

1.1.4 Nuclear Waste Treatment

Microwave heating has been used in the vitrification of high level liquid waste [7, 14, 60] and for solidification of Pu contaminated waste [14, 61]. Incineration of α-active poly vinyl chloride (PVC) waste was demonstrated by microwave heating [10]. The microwave incineration of α-active combustible waste and subsequent dissolution of so obtained ash was used to recover Pu and U [11].

1.1.5 Calcination, Reduction and Sintering using Microwave Heating

Microwave can be used for calcination of ammonium diuranate (ADU), ammonium uranyl carbonate (AUC), UO_3, U_3O_8 and PuO_2. Reduction of UO_3 to UO_2 under microwave radiation to produce UO_2 with O/M ratio of 2.04 has been reported [62]. The sintering of UO_2 pellets by microwave heating has been reported long back [63-65]. The pellets were found to be cracked during sintering of green UO_2 pellets without binders or covers of microwave absorbers at 1200 °C in CO_2 [11, 66]. UO_2 pellets could be sintered up to 95% of TD using microwave heating by covering with UO_2 powder as a thermal insulation material

[67]. Subsequently, the applications of microwave heating have been progressively investigated for sintering of crack free UO_2 fuel pellets [68]. The time required for sintering of UO_2 pellets by microwave heating has been reported to be less than one hour than several hours (> 6 hrs) required by conventional sintering at 1700 °C [8].

1.1.6 Pyrolysis of Compounds and Synthesis of Fuel Materials

UO_2 has been prepared by reductive denitration of solid uranyl nitrate by hydrazine hydrate using microwave at 120 °C [69]. Synthesis of uranium oxides by microwave thermal decomposition of $[UO_2(H_2O)_2(NH_2O)_2].H_2O$, $(NH_4)_2U_2O_7$ and $UO_2(NO_3)_2.6H_2O$ showed considerably less power and time consumption relative to the process with electrical resistance furnaces [13]. Microwave assisted decomposition of ammonium uranyl nitrate produced sinterable UO_2 [70-71]. The solid solutions of urania, plutonia and thoria in any composition can be synthesized using microwave heating by several methods e.g. direct denitration [15], ammonium uranyl nitrate decomposition [70-71], solution combustion [72-75] etc. The nanocrystalline UO_2 and ThO_2 powders were synthesized by citrate gel combustion method [72] and polyvinyl alcohol (PVA) aided microwave synthesis [73].

1.2 Nuclear Power in India

1.2.1 Thrust for Nuclear Power in India

The nuclear energy is clean energy with less impact on the environment, hence favorable alternative to the fossil fuels (coal, oil, natural gas etc.). The fossil fuels are the major source for increasing the greenhouse gases in the atmosphere. Presently in India the electricity is obtained mainly from coal based thermal plants and hydro-electric power projects. The nuclear energy contributes ~3% of electricity produced and is the fourth-largest source after thermal, hydro-electric and renewable sources [76-77]. The energy demand is increasing due to industrial growth coupled with population increase. In an estimate, India will need around 3400 TWh (TeraWatt hour) of electricity annually by 2070 [78]. The estimated total potential of all renewable in India is 1229 TWh, which when completely realized will account only 36.1% of the total estimated demand. Eventually, about 100 years later, the contribution from fossil fuels will also become negligible given the rate at which these are being consumed. Hence, the only sustainable energy resource in the long run is the nuclear energy. Owing to the limited resources of naturally occurring uranium (^{235}U), the sustainability of nuclear energy depends on the availability of the man-made plutonium and ^{233}U from thorium.

1.2.2 Indian Nuclear Power Programme and the Nuclear Fuel Cycle

The Indian nuclear resources have been estimated to be 60,000 MT (Metric Ton) of uranium and about 3,60,000 MT of thorium (about 32% of the world's reserves) [77, 79]. Dr. Homi J. Bhabha envisaged the nuclear power programme in India in early years of 1950s for the effective utilization of the limited natural resources [34] which is schematically shown in **Fig. 1.2** and is based upon the closed nuclear fuel cycle.

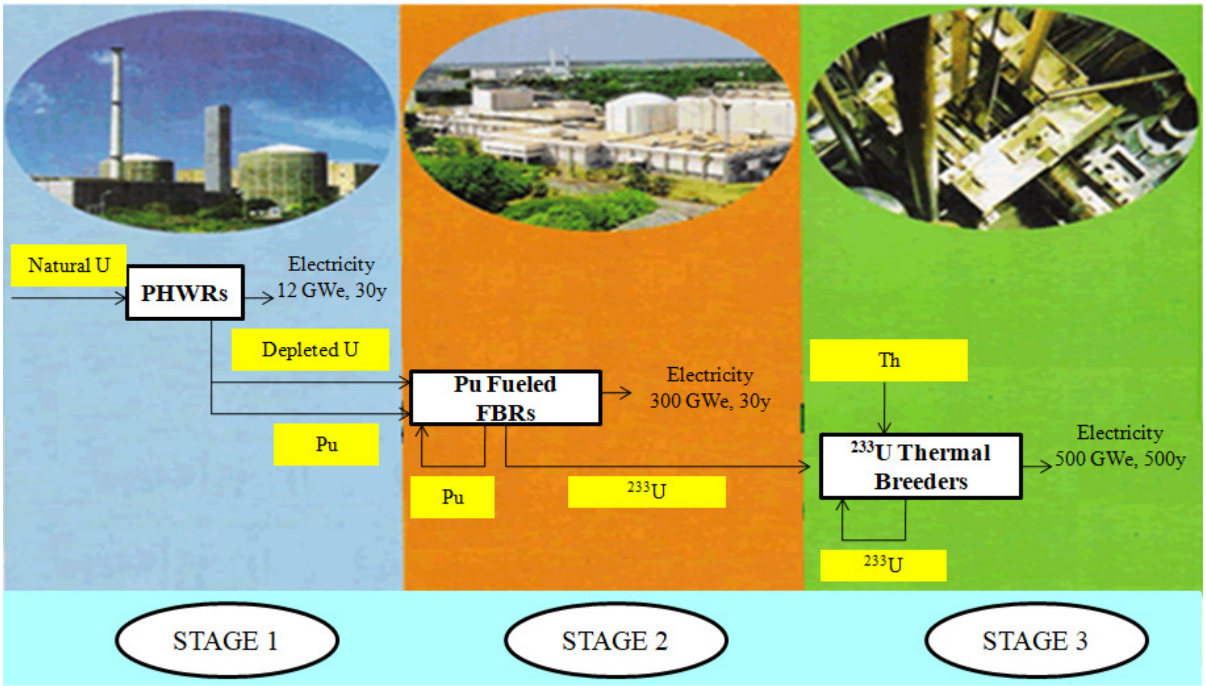

Fig. 1.2: The Three Stage Indian Nuclear Power Programme

1.2.3 Indian Nuclear Reactors and their Fuels

Several research and power reactors are in operation or in construction stage which deploy different kinds of fuels. These reactors alongwith the fuels are listed in **Table 1.1** [80-86].

Table 1.1: Fuel used in Indian Research and Power Reactors

Research Reactor	Fuel	Power Reactor	Fuel
Apsara	^{235}U (93 wt.%)-Al Alloy	BWR	Low Enriched UO_2
Cirus	Natural U Metal	PHWR	Natural UO_2
Dhruva	Natural U Metal	PFBR	$(U_{0.79}Pu_{0.21})O_2$, $(U_{0.72}Pu_{0.28})O_2$
Kamini	^{233}U (20 wt.%)-Al Alloy	AHWR	$(Th_{0.97}{}^{233}U_{0.03})O_2$, $(Th_{0.9625}{}^{233}U_{0.0375})O_2$, $(Th_{0.9675}Pu_{0.0325})O_2$
FBTR	$(U_{0.3}Pu_{0.7})C$, $(U_{0.45}Pu_{0.55})C$	AHWR-LEU	ThO_2-18, 22, 22.5 wt% LEU-UO_2 (^{235}U: 19.75 wt%)

1.3 Nuclear Fuels

1.3.1 Candidate Elements for Nuclear Fuels

The nuclear fuels are based on three candidate elements which are uranium, plutonium and thorium [87]. These are f-block elements and are initial members of actinide series.

1.3.1.1 Uranium

Uranium is the naturally occurring heaviest element. Several isotopes of uranium are known, however naturally occurring uranium consists three isotopes ^{238}U (99.274 wt%), ^{234}U (0.0056 wt%) and ^{235}U (0.7205 wt%). ^{235}U is the fissile isotope in natural uranium. A few ores of uranium are Pitchblende (U_3O_8), Coffinite [$U(SiO_4)_{1-x}(OH)_{4x}$] and Pyrochlore [$(Na_4Ca_2.U,Th)(Nb,Ta)_4O_{12}$] [87]. Indian uranium ore has 0.07% U_3O_8 which is found in Jaduguda, Turamadih etc. in Jharkhand state of India. From ore, the uranium is extracted as magnesium diuranate and sent to NFC, Hyderabad for purification and preparation of nuclear grade UO_2. Another important fissile isotope of uranium is ^{233}U. ^{233}U is produced in the thorium fueled reactors artificially from the fertile ^{232}Th. The radiological properties of uranium isotopes are listed in **Table 1.2**.

Table 1.2: Radiological Properties of Prominent Uranium Isotopes [87]

Isotope	Radiological half-life	Decay mode with energy in MeV (Branching ratio %)		Sp. Activity (Ci g^{-1})
^{232}U	71.7 year	α	5.32(68.6), 5.263(31.2)	2.147
^{233}U	1.59 ×10^{5} year	α	4.82(82.7), 4.78 (14.9)	9.64 ×10^{-3}
^{234}U	2.46 × 10^{5} year	α	4.78(72), 4.72(28)	—
^{235}U	7.04 ×10^{8} year	α	4.40(57), 4.36(18)	2.16 ×10^{-6}
^{238}U	4.47 ×10^{9} year	α	4.19(77), 4.14(23)	3.38 ×10^{-6}

1.3.1.2 Plutonium

Plutonium does not occur naturally, it is produced in nuclear reactors. Out of nearly 15 known isotopes of plutonium [88], important to the nuclear fuels are from ^{238}Pu to ^{242}Pu. ^{239}Pu and ^{241}Pu are fissile isotopes. The isotopic composition of Pu depends on the burn-up[4] of the fuel [88]. The schematic of production of various isotopes of Pu is shown in **Fig. 1.3** [89].

Separation of plutonium from spent fuels is highly technical, complicated and full of radiological hazards. Out of several processes, the Plutonium Uanium Redox EXtraction (PUREX) process has been most commonly employed for commercial production of plutonium. The radiological properties of important plutonium isotopes have been listed in **Table 1.3**.

---

[4] Burn-up is a measure of energy extracted from a nuclear fuel. It is measured both as the fraction of fuel atoms that underwent fission in % FIMA (fissions per initial metal atom) and as the energy released per unit mass of initial fuel commonly in megawatt-days/ metric ton of heavy metal (MWd/MT).

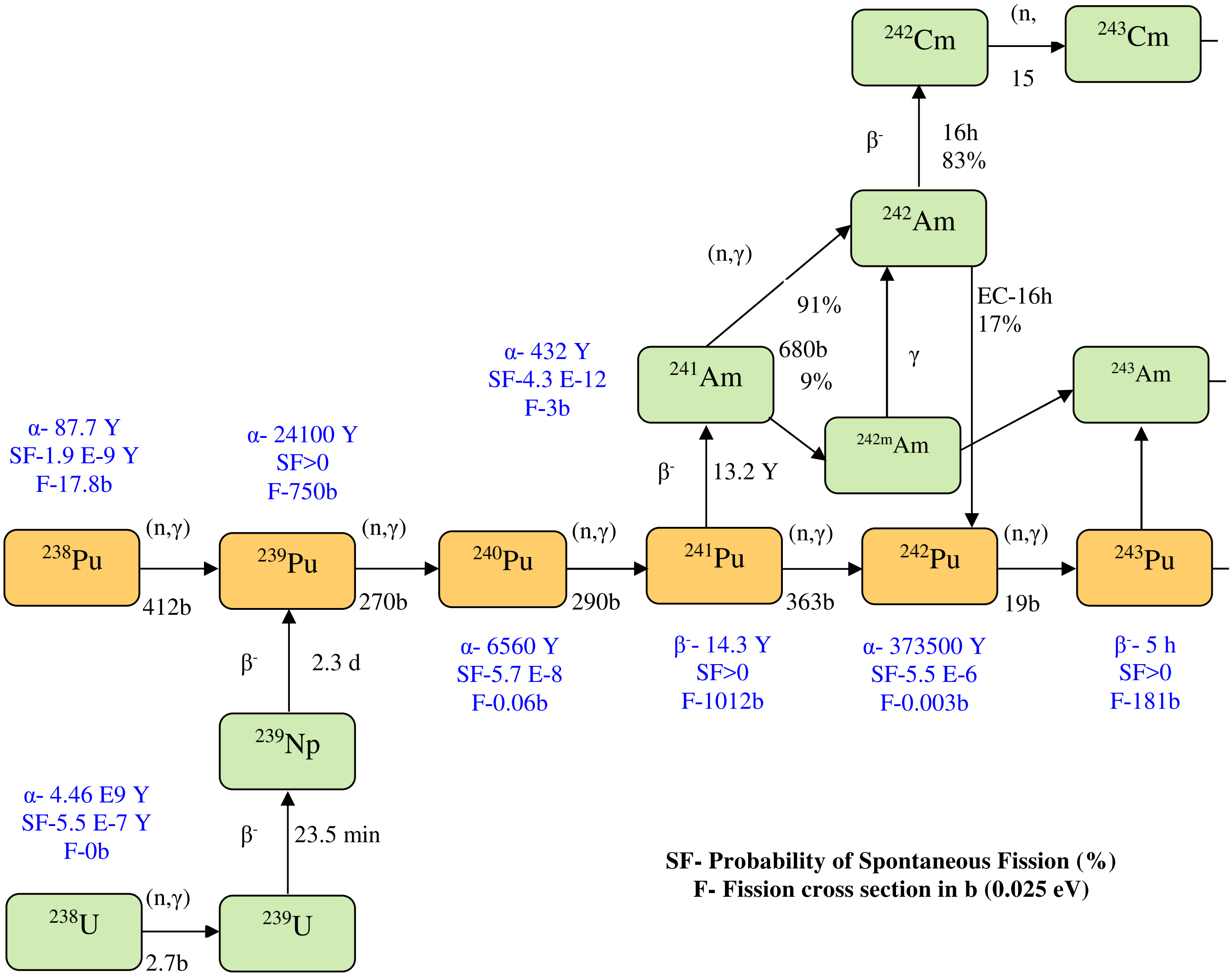

Fig. 1.3: Schematic for Production of various Isotopes of Plutonium

Table 1.3: Radiological Properties of Important Plutonium Isotopes and ^{241}Am [87-88]

Isotope	Radiological half-life	Decay mode with energy in MeV (Branching Ratio %)		Sp. Activity (Ci g^{-1})
^{238}Pu	87 year	α	5.49(70.9), 5.45(29.1)	17.4
^{239}Pu	2.44 ×10^{4} year	α	5.15(70.8), 5.14(17.1), 5.09 (12)	0.052
^{240}Pu	6537 year	α	5.16 (72.8), 5.12(27.1)	0.226
^{241}Pu	14.89 year	β^{-}	0.02	113
^{242}Pu	3.8 ×10^{5} year	α	4.89(76.5), 4.86(23.5)	0.0039
^{241}Am	433 year	α	5.48(84), 5.43(13.1)	3.13

1.3.1.3 Thorium

Thorium is widely distributed in earth's crust and is about three times as abundant as uranium [87, 90-91]. Indian Monazite; (La,Ce,Th,U)PO_4 contains nearly 8% of ThO_2 and 0.35% of U_3O_8. Thorium is mono-isotopic (^{232}Th) which is fertile and cannot directly be used as fuel. Thus, initial enrichment with a fissile material like ^{239}Pu, ^{233}U or ^{235}U is needed. The thorium fuel cycle has been much acclaimed as it generates lesser minor actinides than its uranium analogue [90]. The production of ^{233}U from ^{232}Th in reactor and associated products (^{232}U etc.) are shown in **Fig. 1.4** [92].

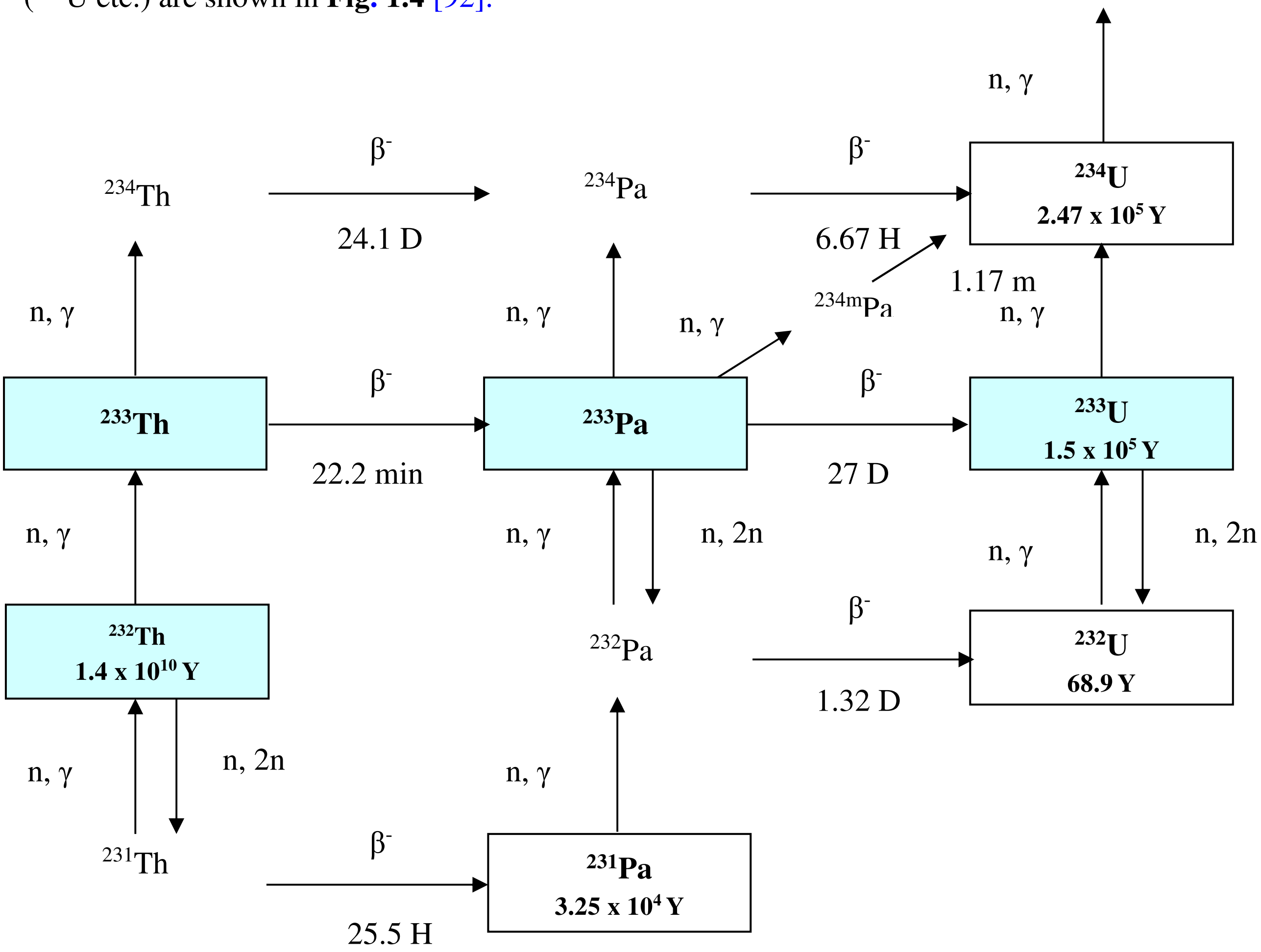

Fig. 1.4: Schematic for Production of ^{233}U from ^{232}Th and other Irradiation Products

^{233}U is reprocessed from the spent ThO_2 based fuels by THORium EXtraction (THOREX) process. The ^{233}U thus obtained from reprocessing is accompanied with trace level (ppm) of ^{232}U. The decay products of ^{232}U are ^{212}Bi and ^{208}Tl which are hard gamma emitters. Their gamma energies are 0.7–1.8 MeV and 2.6 MeV respectively. Thus, the presence of ^{232}U is of high concern in thorium fuel cycle. The decay chain of ^{232}U is depicted in **Fig. 1.5** [92].

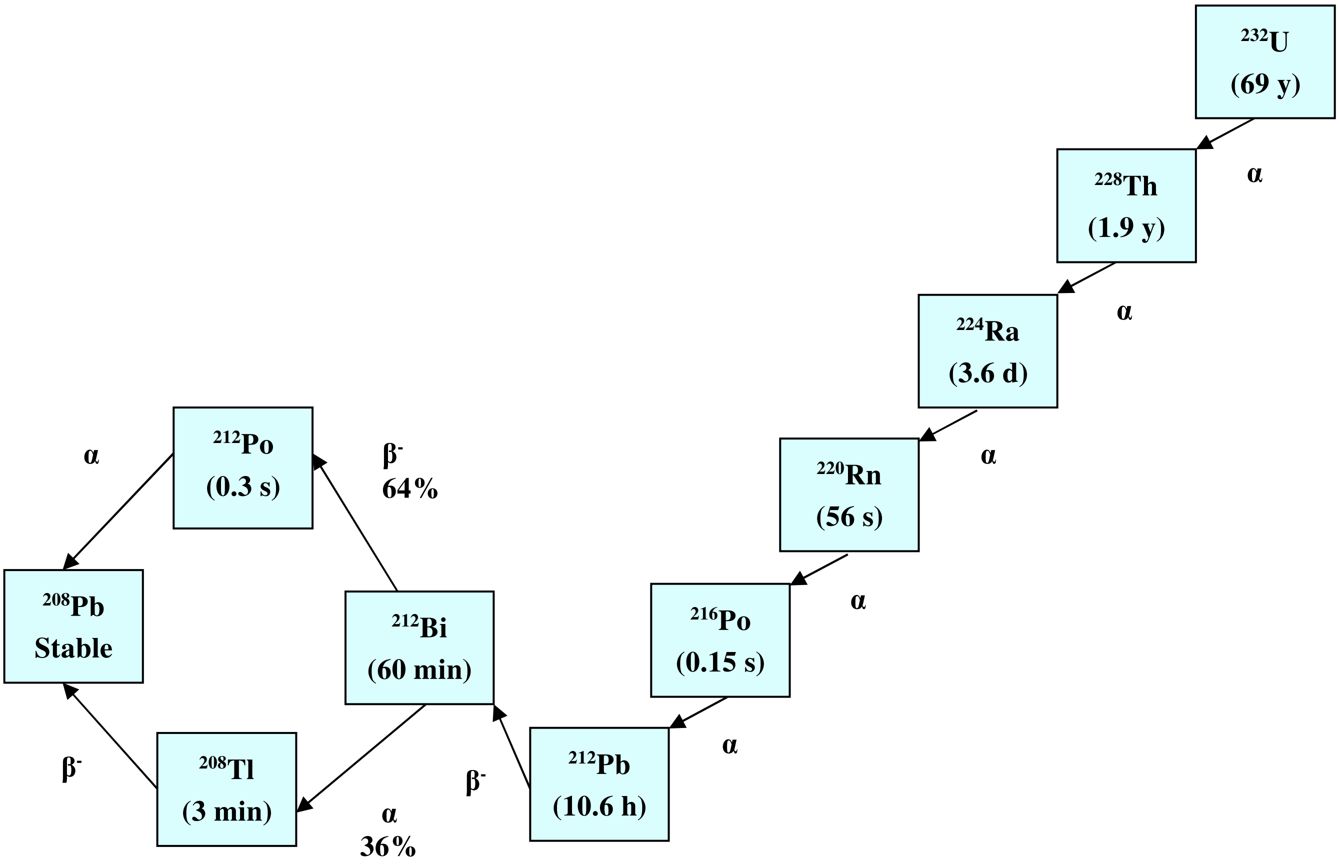

Fig. 1.5: Decay Chain of ^{232}U showing Formation of ^{212}Bi and ^{208}Tl

1.3.2 Characteristics and Types of Nuclear Fuels

U, Pu and Th are used as nuclear fuel in metal form or compound as oxides, carbides, nitrides, silicides, cermets etc. They are used in definite size, shape (pins, plates, pellets, spheres) and composition in nuclear reactors. The fuel is irradiated by neutrons and is under high pressure and temperature. The fuel is desired to sustain this complex heterogeneous environment without failing for long time to achieve high burn-ups. Thus, the ideal fuel material should have high thermal conductivity, high melting point, phase stability, resistance to radiation damage, excellent compatibility with cladding and coolant, larger heavy metal fraction, lower fraction of neutron absorbing elements, easy fabricability and ease of reprocessing [87, 93].

1.3.2.1 Metallic Fuels

Uranium and plutonium as metals possess high heavy metal fraction, density, thermal conductivity and breeding potential (in fast reactors). However, they are not suitable as fuel for power reactor as they have low melting points and undergo several phase changes with concomitant volume changes from room temperature up to their respective melting points [94]. Uranium has low melting point (1132 °C) and undergoes three phase transitions. Similarly, plutonium also owes low melting point (640 °C) and undergoes transitions through six allotropic forms up to melting. They are pyrophoric and need high purity inert gas cover for fabrication by melting-casting route [95]. They find application as nuclear fuel for research reactor. The U-Pu-Zr fuel is taken up for intensive investigations worldwide for the future fast reactors.

1.3.2.2 Oxide and Mixed Oxide (MOX) Fuels

The oxide and MOX fuels are most widely used fuels for power reactors. They possess high melting points, phase stability over a large temperature range and good compatibility with coolants/ clads. Thus, high burn-ups are achievable. Oxide and MOX fuels are easy to fabricate and their reprocessing is well established. However, they have lower thermal conductivity, density, heavy metal fraction and breeding ratio than carbide, nitride and metallic fuels [87]. The important properties of oxide fuel are listed in **Table 1.4** [96].

Table 1.4: Important Properties of Oxides Nuclear Fuel Materials

Property	**ThO_2**	**UO_2**	**PuO_2**
Crystal structure	FCC (CaF_2)	FCC (CaF_2)	FCC (CaF_2)
Lattice parameters (Å)	5.5975	5.4704	5.396
Theoretical Density (TD) (gcm^{-3})	10.00	10.96	11.46
Metal density (gcm^{-3})	8.79	9.66	10.10
Metal fraction (%)	87.89	88.15	88.19
Melting Point (^oC)	3370	2850	2350
Thermal conductivity (W/m-^oC) at 500 ^oC	6.2	4.80	4.48

1.3.2.3 Carbide and Nitride Fuels

Carbide and nitride fuels are considered as advanced fuels for fast reactors. However, fabrication of carbide and nitride fuels via powder- pellet route is more difficult than oxide fuels and involves more number of process steps. Carbide fuel is highly prone to oxidation and hydrolysis and is pyrophoric in the powder form, thereby needing a high purity inert cover gas (Ar) inside the glove-boxes [97].

1.3.3 Constraints and Challenges to Work with Nuclear Fuel Materials

Th, U and Pu are primarily α-active elements (**Table 1.2, 1.3**). However, they also emit other radiations like β, γ, X-rays and neutrons. Thorium gives higher γ doses compared to uranium due to associated decay products (^{208}Tl, ^{212}Bi). Natural uranium (Nat U) has low specific activity and high chemical toxicity. The reprocessed uranium contains fission products (^{106}Ru, ^{95}Zr, ^{95}Nb etc.) and trace uranics (^{232}U, ^{236}U, ^{237}U etc.), ^{237}Np, Pu (<0.4 ppm) etc. [98]. Uranium does not pose much external hazards, however the internal exposure is of concern and controlled by engineering methods like once through ventilation and working within the enclosures. ^{233}U is always associated with ^{232}U (few ppm >1000 ppm) whose decay products (^{208}Tl, ^{212}Bi) emit γ ~2 MeV. ^{233}U having <10 ppm ^{232}U can be handled in shielded glove-boxes whereas higher ^{232}U content require handling inside the hot cells [99].

Pu has high specific activity (^{239}Pu; 6.203×10^{-2} Cig^{-1}) and renders high γ doses (^{241}Am build-up). The high neutron doses from spontaneous fission of ^{238}Pu, ^{240}Pu and ^{242}Pu and (α,n) reactions are of concern in Pu handling. The main serious concern is the chance of criticality in handling and processing of plutonium. The long half-lives of its isotopes (^{239}Pu; 2.411×10^{4} years), high activity and long retention times in the body (>100 years) make it one of the most hazardous and radiotoxic elements to handle [100-102]. The hazard potential of plutonium especially in fine powder form raises serious safety concerns due to inhalation. Hence, plutonium handling is carried out in specially designed laboratories equipped with leak-tight glove-boxes. The leak rates < 0.05% of glove-box volume per hour at ±100 mm of water gauge provides high level of integrity [100, 103-104].

The activity concentration and intake of nuclear materials are controlled in the working environment. The annual limit of intake (ALI) and derived air concentration (DAC) of various radionuclides for Activity Median Aerodynamic Diameter (AMAD) of 5μm in different classes of absorption are listed in **Table 1.5** [105].

Table 1.5: ALI and DAC Values of Radionuclides Important to Fuel Fabrication

Radionuclide	Absorption class	ALI (Bq)	DAC (Bqm^{-3})
^{232}Th	S	1670	0.7
	M	690	0.29
^{233}U	S	3.03x 10^{4}	12.6
	M	9090	3.79
^{235}U	S	3000	1.25
	M	1.2x10^{4}	5
^{238}U	M	1.25 x10^{4}	5.21
	S	3500	1.46
^{239}Pu	M	625	0.26
	S	2400	1

S: Slow class and M: Moderate class

1.4 Production of Sinterable Powders for Oxide and MOX Fuel Fabrication

UO_2, PuO_2 and ThO_2 powders are used as feed materials for fabrication of oxide and MOX fuels. Several methods are reported for their production from respective precursors by thermal decomposition, precipitation-calcination, by denitration of aqueous solutions or solid nitrate compounds etc. The commercial production of UO_2 is carried out by ADU precipitation-calcination, AUC precipitation-calcination and peroxide precipitation-calcination routes [106]. The PuO_2 and ThO_2 powders are obtained using oxalate precipitation-calcination process [90, 106].

The feed powders are required to possess certain properties for the fabrication of oxide and MOX fuels with specified properties. These are specific surface area (SSA), particle size and its distribution, flowability, powder bulk density (PBD) etc. Over and above is the sinterability; the ability of the powder compacts to achieve densities near to theoretical density (TD) upon sintering. Therefore, important production methods are compared considering the above properties in view of oxide and MOX fuel fabrication.

1.4.1 Uranium Dioxide Powder

The production of UO_2 powder or particles is carried out mainly by four types of basic methods as a) Denitration [16], b) Precipitation-calcination [106], c) Gelation [106-107] and d) Dry routes [106]. The overview of UO_2 production from various methods is presented in **Fig. 1.6**. A comparative evaluation of the methods for production of UO_2 considering key parameters for oxide fuels is made in **Table 1.6** [15-16, 70-71, 106, 108-111].

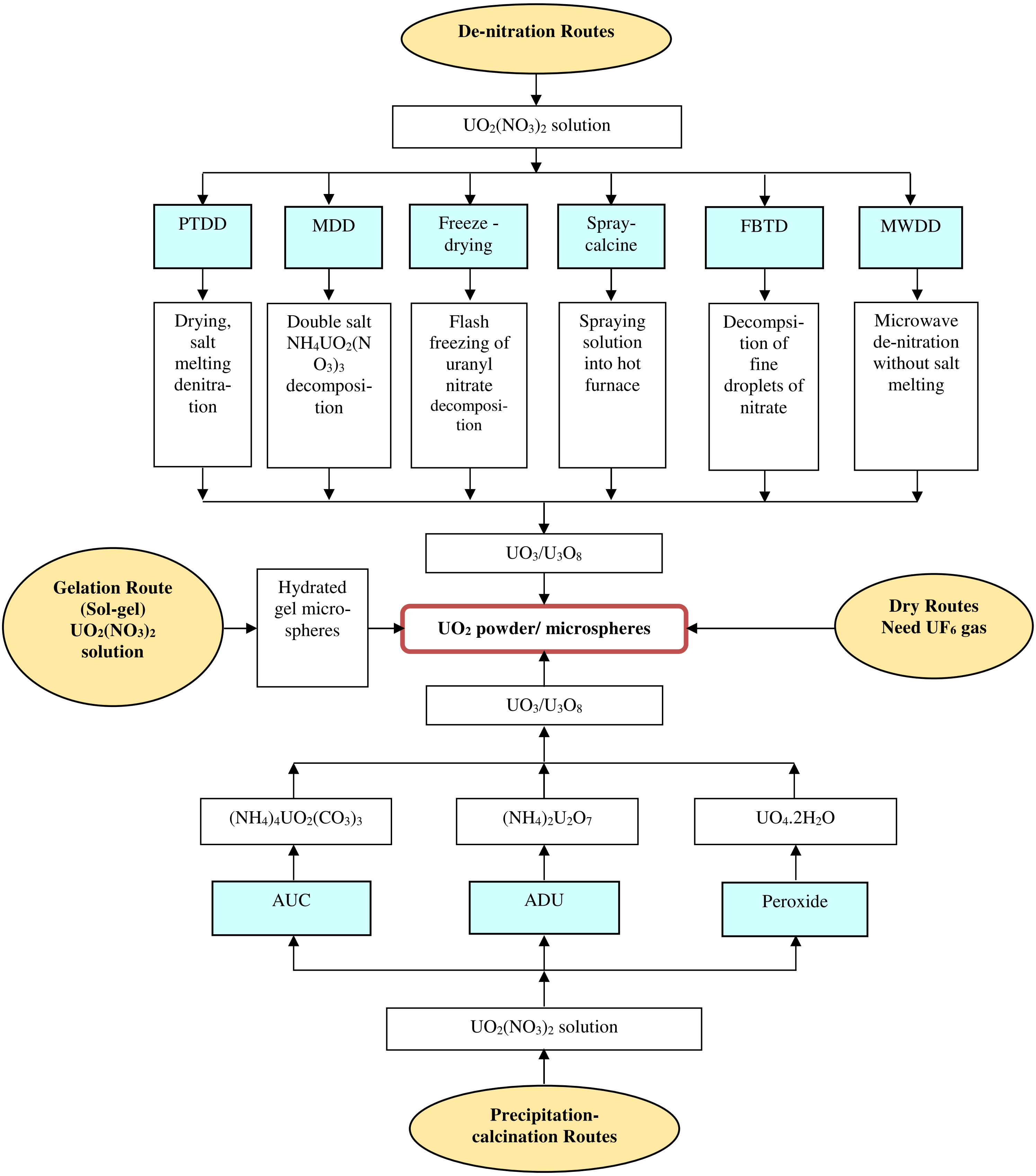

Fig. 1.6: Overview of UO_2 Production Methods for Oxide and MOX Fuel Fabrication

Table 1.6: Key Parameters for UO_2 Powder obtained from Different Routes Relevant to Oxide and MOX Fuel Fabrication

Method	SSA (m^2g^{-1})	Particle size (μm)	Flowability	Sinterabaility (% TD)	Industrial maturity
PTDD	0.5-1.6	--	No	80-85	Nil
MDD	8-12	--	No	>90	Low
FBTD	--	--	No	>90	Low
MWDD	2-8	1-6	No	>90	High
ADU	2.5–6.0	2-15	No	>90	highest
AUC	5-7	30-400	Yes	>90	highest
Sol-gel	10-20	10-1000	Yes	>90	Moderate
Dry route	2.0	< 5	No	>90	Low

1.4.2 Plutonium Dioxide Powder

PuO_2 powder is prepared by several routes of which Pu(IV) oxalate precipitation-calcination process is most commonly used. An overview of the PuO_2 synthesis from a) Pu(IV) oxalate [112-117], b) Pu(III) oxalate [112, 117], c) hydroxide precipitation [117] and d) peroxide precipitation [117] routes is depicted in **Fig. 1.7**. The comparative assessment of PuO_2 production methods assessing their suitability for MOX fuel is presented in **Table 1.7**.

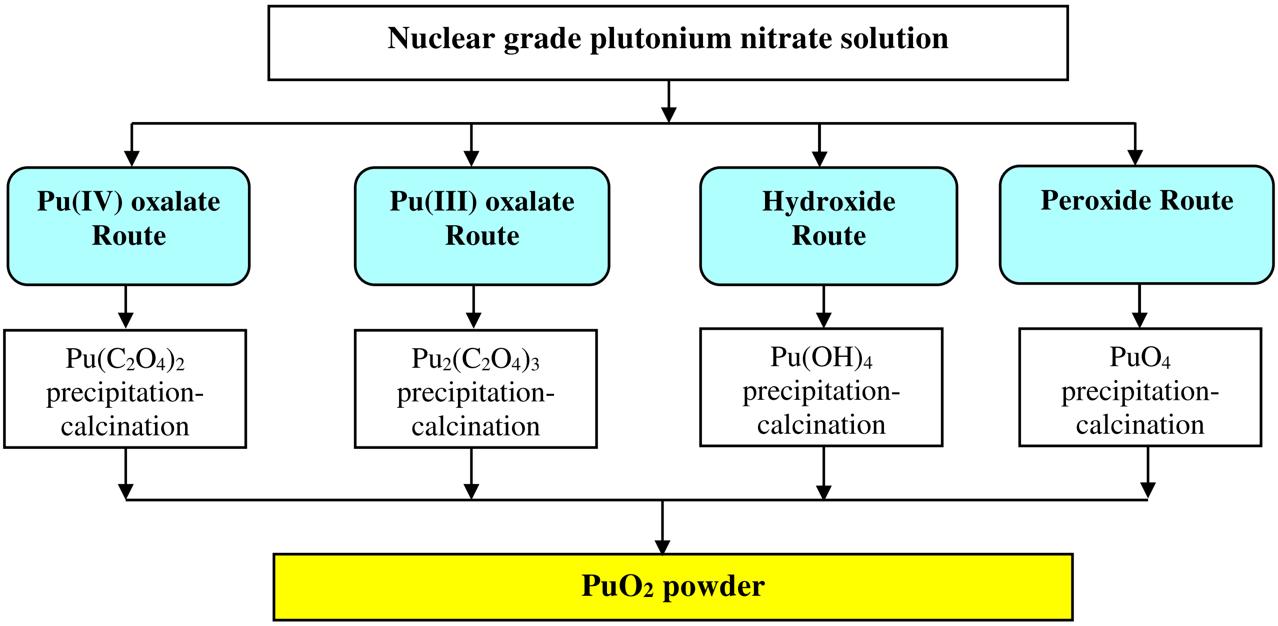

Fig. 1.7: Overview of PuO_2 Powder Production Methods for MOX Fuel Fabrication

Table 1.7: PuO_2 Powder Key Properties obtained from Different Methods Relevant for MOX Fuel Fabrication

Method	SSA (m^2g^{-1})	Particle size (µm)	Flowability	Sinterability (% TD)	Industrial maturity
Pu(IV) oxalate	10-40	1-2	No	>95%	Highest
Pu(III) oxalate	10-35	1-2	No	>95%	Moderate
Hydroxide Precipitation	--	--	No	--	Least
Peroxide Precipitation	--	--	No	--	Least

1.4.3 Thorium Dioxide Powder

Thorium dioxide is prepared by several methods. These include a) oxalate precipitation-calcination process [99, 118-120], b) Hydroxide precipitation route [99], c) Freeze-drying route [99, 118], d) Solution combustion [73, 121] and e) Thermal denitration route [118, 122]. **Fig. 1.8** gives an overview of the several methods for ThO_2 production. Various methods for ThO_2 production are compared on the basis of a few key parameters relevant to oxide or its MOX fuel fabrication in **Table 1.8**.

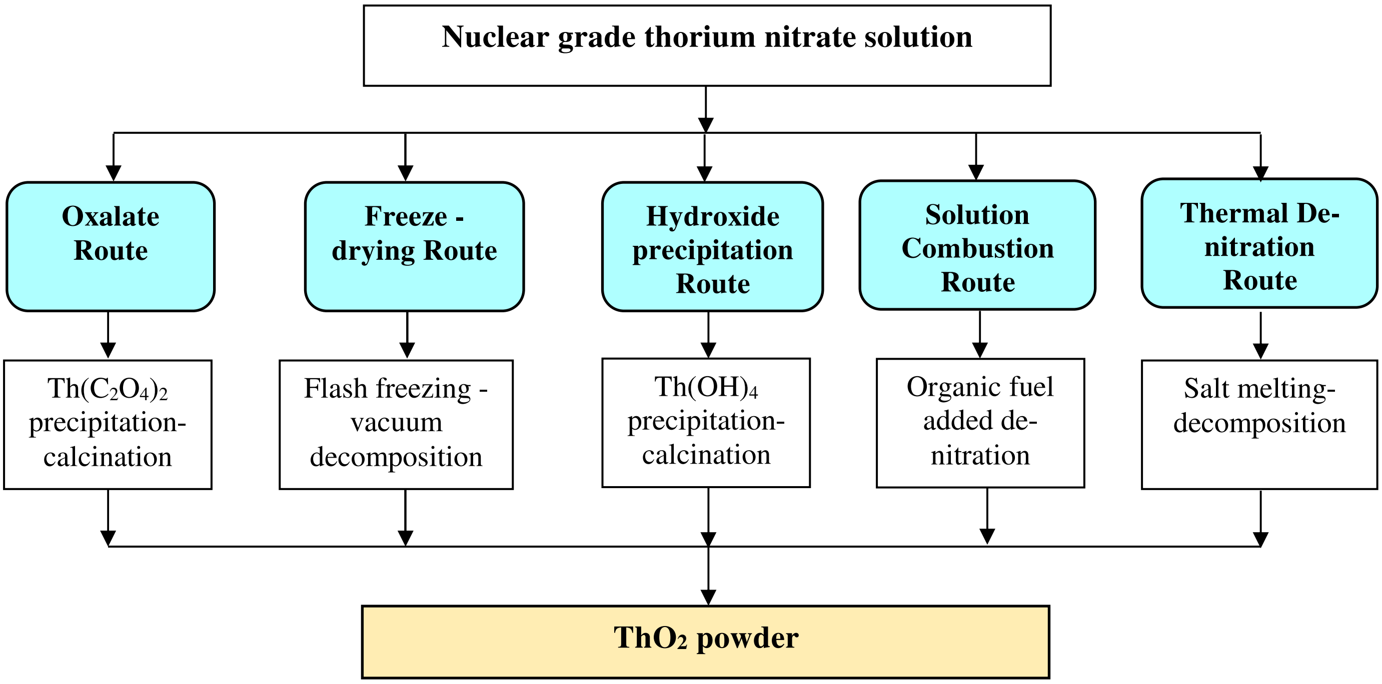

Fig. 1.8: Overview of ThO_2 Production Methods for Oxide and MOX Fuel Fabrication

Table 1.8: ThO_2 Powder Key Properties for Several Production Methods Pertaining to Oxide and MOX Fuel Fabrication

Method	SSA (m^2g^{-1})	Particle size	Flowability	Sinterability (% TD)	Industrial maturity
Oxalate Precipitation	2-10	2-5 µm	No	>92	Highest
Hydroxide Precipitation	--	--	No	--	Least
Freeze drying	--	--	No	--	Least
Solution combustion	>50	10 nm	No	~97%	Least
Thermal denitration	<1	10-70 µm	No	<90%	Least

1.4.4 Mixed Oxide Powder for MOX Fuel Fabrication

Several methods are reported and being practiced worldwide for production of mixed oxide feedstock materials for fabrication of MOX fuels. The various methods are 1) Mechanical blending [106], 2) ammonium uranyl-plutonyl carbonate (AUPuC) route [106, 123-124], 3) Hydroxide co-precipitation [124], 4) Oxalate co-precipitation [124], 5) Co-denitration routes; Modified direct denitration (MDD) [124-125], fluidized bed denitration [110], microwave direct denitration (MWDD) etc. [14-16, 124] and 6) Sol-gel method [106-107]. **Fig. 1.9** depicts an overview of the methods for mixed oxide feedstock powders.

Mechanical blending of individual powders (UO_2, PuO_2 and ThO_2) is largely used method. However, the major drawbacks of this process are dry powder handling causing radioactive dust hazard and mix blends (hence pellets) have higher compositional heterogeneity. The co-conversion (co-precipitation, co-denitration and sol-gel) methods offer excellent homogeneity and dust free processing. The co-conversion of uranium and plutonium, with no separation of free plutonium, provides a safeguard against the diversion of Pu. **Table 1.9** summarizes the key parameters of mixed oxide powder obtained from several methods.

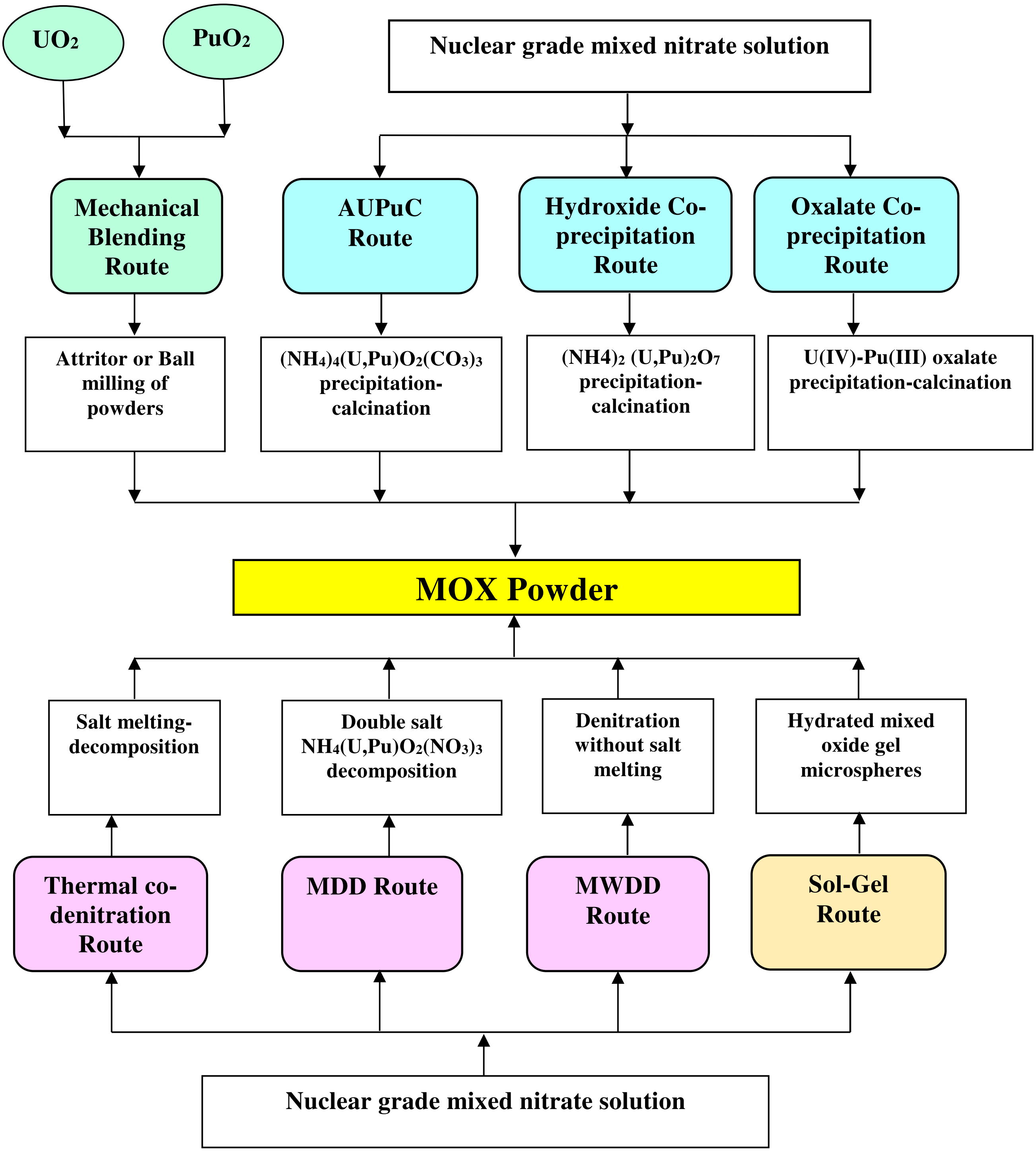

Fig. 1.9: Methods for Production of Mixed Oxide Powders for MOX Fuel Fabrication

Table 1.9: Properties of Mixed Powder via several routes for $(U_{1-y}Pu_y)O_2$ Fuel Fabrication

Method	Bulk density (gcm^{-3})	SSA (m^2g^{-1})	Particle size (µm)	Sinterability (% TD)	Industrial maturity
Blending	>1.8	# >4	# 5-15	>93%	Highest
AuPuC	>1.5	5-7	30-400	>93%	High
Oxalate	>2.0	4-24	1-40	>93%	Moderate
Denitration	1.6-2.5	0.1-1.6	40-70	~73%	Least
MDD	1.0	6-8	3-7	>90%	Moderate
MWDD	2.2	3-7	1-7	>94%	High
Sol-gel	--	10-25	300-1000	>94%	High

#: Depends upon wt. proportion, milling time and initial property value in constituents

1.4.5 Denitration based Methods for Synthesis of Oxide and MOX Feed Materials

Notably, it is always the nitrate solutions of Th, U or Pu which usually are encountered during conversion into oxides or mixed oxides either in the reprocessing plants or post purification of the concentrates in the front end of nuclear fuel cycle. This is because their nitrates have good solubility in organic solvents like alcohols, ketones, ethers, TBP etc. commonly employed for extraction/ co-extraction and readily soluble in water [126].

The nitrate solutions of U, Pu and Th can be crystallized and subsequently can be thermally decomposed into respective oxides. The thermal decomposition of metal nitrate compounds into respective oxide is called denitration. However, the conventional denitration produces a powder which is not suitable for fuel fabrication [70-71]. These powders could not produce the sintered pellets with required quality. Nevertheless, with development of understanding in the denitration technology and advent of advanced heating methods, the nuclear community has conquered this simplest method of conversion. The denitration process can be performed in a batch or in continuous mode, using a variety of techniques such as bulk denitation [127], pot denitration, fluidized bed [109-110], freeze-drying [99, 118, 128-129], spray-calcine [99, 118], rotary calciners, solution combustion [72-73] and microwave [14-15, 130-132]. Microwave denitration is distinctly advantageous among them.

1.4.5.1 Primitive Thermal Direct De-nitration

The denitration of nitrate solutions directly by heat sources is called ‘direct denitration’. The conventional denitration called Primitive Thermal Direct Denitration (PTDD) involves denitration in a resistance furnace or on hot plate. PTDD of uranyl nitrate and subsequent reduction gives UO_2 of low SSA and reactivity. The UO_2 and urania-plutonia powders from PTDD process sinter poorly compared to UO_2 from precipitation conversion processes and consequently failed to meet existing specifications for pellets [70-71, 133].

In direct denitration process, the uranyl nitrate solution concentrates by evaporation and then crystallization of $UO_2(NO_3)_2.6H_2O$ starts. Further, heating of the $UO_2(NO_3)_2.6H_2O$ crystals at 62-65 ^{o}C (melting point) brings out the melting of crystals. The solid phase in equilibrium with the melt is trihydrate as represented by Eq. (1.1):

$$UO_2(NO_3)_2.6H_2O \rightarrow UO_2(NO_3)_2.3H_2O + 3H_2O \qquad (1.1)$$

This melt is responsible for poor quality of the UO_2 powder. This melt forms a ‘mastic’ phase and results in making the material sticky. As denitration continues, the melt thickens and then forms a glassy cake, which subsequently cracks into pieces with low surface area [134]. Hard lumps appear after denitration which even after extensive milling could not improve the sinterability of the UO_2. The density of the pellets using this powder was 83-85% of TD [71].

ThO_2 can also be prepared by direct thermal decomposition of thorium nitrate starting from aqueous nitrate solution [122]. However, the powder obtained by this process is coarse and pellets of density >90 % TD cannot be obtained [118]. Palmer et al. [122] investigated another method called ‘pot denitration’ involving heating a vessel containing nitrate solution in a resistance furnace which increased the density of the sintered pellets comparatively.

1.4.5.2 Modified Direct Denitration

A major breakthrough in the direct denitration methodology appeared when the primitive denitration method was modified at ORNL [70-71]. The Modified Direct Denitration (MDD) involves addition of NH_4NO_3 into the uranyl nitrate solution and heating to prepare dry crystals of uranium-ammonium double salts. The double salt formation removed the problem of melting and subsequent formation of hard lumps. The favorable effect of the NH_4NO_3 is due to result from decomposition of $NH_4UO_2(NO_3)_3$ as a solid, whereas the $UO_2(NO_3)_2$ (without NH_4NO_3) decomposes as a molten salt. The MDD process [125] proceeds through sequence of reactions; a) dehydration at 40 ºC Eq. (1.2), b) loss of 1 mole of ammonium nitrate at 170 ºC Eq. (1.3) and c) denitration of $NH_4UO_2(NO_3)_3$ at 270 ºC Eq. (1.4) as:

$$(NH_4)_2UO_2(NO_3)_4.2H_2O \rightarrow (NH_4)_2UO_2(NO_3)_4 + 2H_2O \qquad (1.2)$$

$$(NH_4)_2UO_2(NO_3)_4 \rightarrow NH_4UO_2(NO_3)_3 + 2N_2O + 2H_2O \qquad (1.3)$$

$$NH_4UO_2(NO_3)_3 \rightarrow UO_3 + N_2O_5 + N_2O + 2H_2O \qquad (1.4)$$

1.4.5.3 Microwave Direct Denitration

Microwave denitration of uranyl nitrate solution for production of UO_2 has been investigated extensively in Japan, China and India [14-15, 130-132]. Microwave direct denitration can accomplish the denitration and the conversion process from uranyl nitrate or uranyl-plutonium nitrate solution to oxide/ mixed oxide in the same vessel without forming the mastic phase. The process involves heating of uranyl nitrate solution. Initially, water and the nitric acid evaporate thus concentrating the solution. This process of concentration leads to formation of the hydrated crystals of uranyl nitrate hexahydrate (UNH). Further heating causes the stepwise removal water of hydration. The thermal decomposition of the lower hydrated nitrates leads to denitration through intermediate products producing UO_3 finally. UO_3 is further calcined and converted to U_3O_8. UO_2 has also been prepared by reductive denitration of uranyl nitrate by hydrazine using microwave [69]. Current reprocessing and recycle fuel fabrication are based on the production of separated UO_2 and PuO_2 to fabricate MOX fuel. The separated plutonium is viewed as a safeguard concern therefore, co-denitration methods are being developed in several countries for use in future reprocessing and recycle fuel fabrication plants. The denitration of uranyl nitrate and plutonium nitrate individually are represented by Eq. (1.5) and Eq. (1.6) respectively [16, 58, 124]:

$$UO_2(NO_3)_2.6H_2O \rightarrow UO_3 + 1.86\,NO_2 + 0.14\,NO + 0.57O_2 + 6H_2O \qquad (1.5)$$

$$PuO_2(NO_3)_2.5H_2O \rightarrow PuO_2 + NO_2 + \,NO + 1.5O_2 + 5H_2O \qquad (1.6)$$

1.4.6 Comparison of Powder Production Processes at Industrial Scale

The feed powders for oxide and MOX fuel fabrication on industrial scale are mainly based upon precipitation-calcination, gelation and denitration techniques. In the precipitation processes, the precipitation conditions control the particle morphology, filterability, particle size and its distribution and morphology [112, 115]. The precipitation kinetics depends on process parameters like temperature, pH, concentration of reactants, free acidity, rate of addition, order of mixing, hydrodynamics and mixing mechanism. The gelation processes produce microspheres owing excellent flowability (**Table 1.6**) in dust free manner; however these processes suffer from large number of process steps, parameters and associated liquid waste generation.

The denitration methods on the other hand possess several advantages like lesser number of process steps, least effluent treatment, arising little secondary liquid waste (in the scrubbing of the off gases), no primary liquid waste generation contrary to precipitation or sol-gel methods, negligible material loss, simple and fast, easy automation and recyclability of HNO_3 vapors and NOx gases. Use of direct thermal denitration eliminates multiple precipitation, filtration and calcination steps and enables the use of less complicated process equipments [16]. The three types of the methods are compared in **Table 1.10**.

Table 1.10: Evaluation of Important Processes for Production of Nuclear Fuel Material

Parameter	Denitration method	Precipitation method	Gelation methods
Liquid waste Generation	Negligible	Large	Large
Liquid waste type	Secondary	Primary	Primary
Material loss	Negligible	Higher	Higher
Process steps	Lesser	More	More
Process parameters controlling the properties	Lesser	More	More
Decontamination from impurities	Nil; Pure solution required	Inherently present	Nil; Pure solution required

1.5 Manufacturing of Oxide and Mixed Oxide Nuclear Fuels

The powder-pellet route has been extensively used worldwide for manufacturing of UO_2, $(U_{1-y}Pu_y)O_2$, ThO_2, $(Th_{1-y}U_y)O_2$ and $(Th_{1-y}Pu_y)O_2$ fuel [106]. Many advanced methods have also been developed for their fabrication such as sol-gel microsphere pelletisation (SGMP) [106-107], pellet impregnation [135], coated agglomerate pelletization (CAP) [136-137], co-precipitation technique [138] and impregnated agglomerate pelletisation (IAP) process [139]. Among these, many have been specially developed for ^{233}U based fuels considering the challenges in handling of ^{233}U. However, the powder-pellet route among all has highest technical and industrial maturity [106].

1.5.1 MOX Fuel Fabrication Process at AFFF

AFFF, BARC is the only industrial scale MOX fuel plant in India and has been engaged in fabrication of several types of oxide and MOX fuels (cylindrical pellet type) for various Indian reactors. At AFFF, powder-pellet route has been adopted for MOX fuel fabrication. **Fig. 1.10** illustrates the flow sheet for MOX fuel fabrication.

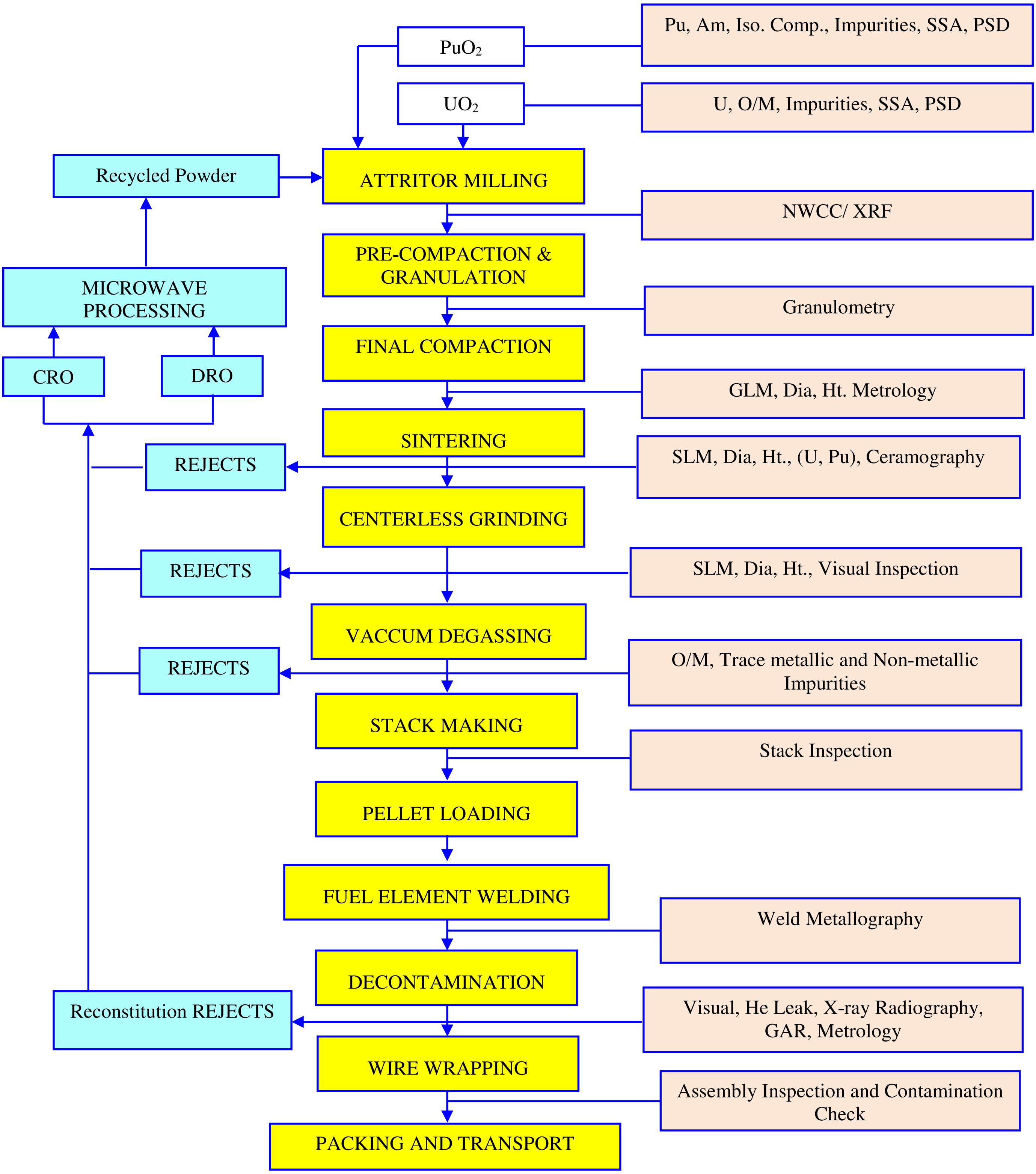

Fig. 1.10: Flow Sheet for Fabrication of MOX Fuel by Powder-Pellet Process alongwith Quality Control and Recycling Steps

NWCC: Neutron Well Coincidence Counting, XRF: X-Ray Fluorescence, Iso Comp: Isotopic Composition, SSA: Specific Surface Area, PSD: Particle Size Distribution, GLM: Green Linear Mass, SLM: Sintered Linear Mass, Dia.: Diameter, Ht.: Height, CRO: Clean Rejected Oxide, DRO: Dirty Rejected Oxide

The first step in fabrication process involves mechanical blending of the feed powders (UO_2, PuO_2, ThO_2 etc.). The attritor mill is used for achieving uniformity of the fissile content as well as a good dispersion of lubricant and binder [140]. Oleic acid (0.8-1wt%) and polyethylene glycol (1 wt%) are used as lubricant and binder respectively. The blended powder thus obtained is not free flowing and is therefore not suitable for feeding to a pellet compaction press. Hence, the powder is pre-compacted in compaction press. This is followed by granulation. The granules are obtained by crushing the low density (~30% of TD) pre-compacts in an oscillatory type granulator. The compaction of the free flowing granules (800-1200 μm) into pellets is carried out in the final compaction press and density ~55% of TD is achieved. The compact is termed as green pellet. These green pellets are then sintered in mixture of N_2+H_2 gas environment at 1650 ^{o}C under specified temperature profile.

The oversize sintered pellets are dry ground in a centreless grinding machine to control the diameter. The pellets in the correct size range are further subjected to vacuum degassing at 100 ^{o}C, 2h at 10^{-2} torr to remove the moisture. Degassed pellets are loaded in the bottom-end welded fuel elements and welded at the top-end after filling helium gas (1-2 $Kgcm^{-2}$). The fuel elements are decontaminated using ultrasonic and laser decontamination methods [141].

Numerous methods were developed for fabrication of ThO_2 based fuels in India [106, 135-139, 142]. Many campaigns for fabrication of ThO_2 based fuels were completed using the powder-pellet route for experimental irradiation and fuel development for the third stage of Indian Power Programme at AFFF [143]. The $DDUO_2$ was used to simulate $^{233}UO_2$. ThO_2 has high melting point (~3370 ^{o}C) and its sintering needs temperatures >2000 ^{o}C to obtain specified density pellets. However, with small addition of sintering aids (<500 ppm) like the pentavalent ions, Nb^{+5} as Nb_2O_5, or the divalent, Ca^{2+} as CaO and Mg^{2+} as MgO etc., high-density ThO_2 pellets can be obtained by sintering at 1200-1500 ^{o}C [99, 142-143].

1.5.2 Oxide and MOX Fuel Campaigns Accomplished at AFFF

Several campaigns were successfully completed at AFFF [144-146]. $DDUO_2$ and ThO_2 oxide fuels are manufactured for their applications like thermal insulation pellets to avoid excessive temperature exposure to the internal components of fuel pin, axial blanket for breeding purpose (in fast reactor), neutron flux flattening[5] in reactors and cold trials for fuel development programmes. The insulation and the breeding blanket pellets are kept on both the side of the MOX fuel column in the fuel element [141]. Solid $DDUO_2$ pellets are used as axial blanket for breeding plutonium in the PFBR MOX fuel element. The various types of oxide fuel pellets fabricated at AFFF are listed in **Table 1.11**.

Table 1.11: Oxide Fuel Campaigns at AFFF alongwith their Important Parameters

Parameter	**PFBR**	**BWR**	**AHWR**
Composition	$DDUO_2$	Natural UO_2	ThO_2
Pellet: Cylindrical	Solid	Solid	Solid
Pellet Ht./ Dia. ratio	1-1.4	1-1.5	0.5-1.0
Purpose	Axial blanket for breeding	Thermal insulation pellets	Fuel development programme

The $(U_{1-y}Pu_y)O_2$ MOX fuels manufacturing campaigns for Indian reactors like BWR, PHWR, hybrid core of FBTR and first core of PFBR were successfully accomplished at AFFF. The MOX fuel was used for TAPS 1&2, BWRs consequent to difficulties experienced in procuring the low enrichment uranium (LEU) fuel. Thus, $(U_{1-y}Pu_y)O_2$ MOX fuel was developed as an alternate fuel to the imported $LEUO_2$ fuel and to demonstrate the self reliance [32]. The $(U_{1-y}Pu_y)O_2$ MOX fuel for PHWR was taken up under the plutonium recycling scheme in thermal reactors [146]. The MOX fuel for FBTR was planned alongwith

---

[5] The neutron flux (neutrons/ m^2s) inside a nuclear reactor core is controlled by a combination of structural designs, neutron reflectors, neutron absorbers and control rods. Neutron flux flattening involves reducing neutrons from high flux regions which helps in uniform fuel burn-up and thus better utilization of fuel and reactors structural materials.

the driver carbide fuel to form hybrid core and the core size expansion studies [147]. Large quantities of PuO_2 (> 2 MT) and MOX (>10 MT) were handled during fabrication of the first core of $(U_{1-y}Pu_y)O_2$ MOX fuel of PFBR. **Table 1.12** lists the $(U_{1-y}Pu_y)O_2$ fuels manufactured at AFFF, fuel bundles or sub-assemblies (SA) supplied and their important specifications.

Table 1.12: Typical Data of $(U_{1-y}Pu_y)O_2$ MOX Fuel Campaigns Completed at AFFF

Parameter	**BWR-MOX**	**PHWR-MOX**	**FBTR-MOX**	**PFBR-MOX**
Composition (wt% PuO_2)	0.9, 1.55, 3.25- Nat UO_2	0.4- Nat. UO_2	44- Nat. UO_2	21, 28- $DDUO_2$
Pellet : cylindrical	Solid	Solid	Annular	Annular
Pin length (mm)	3893	493	932	2580
Density (% TD)	93-96	96±2	94±2	94±2
O/M ratio	1.98-2.015	1.98-2.015	1.98-2.00	1.96-2.00
Impurities (ppm)	≤ 2500	≤ 1500	≤ 5000	≤ 5000
Pins/ Bundle or SA	6×6	7	37	217
Total supply	12 Bundles	50 Bundles	8 SA	39,277 pins
Reactor site	TAPS 1&2, Tarapur	KAPS, Kakrapar	IGCAR, Kalpakkam	Bhavini, Kalpakkam

Fig. 1.11 shows the schematic diagram of a PFBR MOX fuel pin. The cladding material of the fuel pin is Stainless Steel D9[6] having diameter 6.6mm. The other details of the fuel are mentioned in **Table 1.12**. The fuel pin contains 1000 mm stack of $(U,Pu)O_2$ MOX annular pellets and 300 mm stack of $DDUO_2$ blanket pellets on both the sides. There is a plenum of 710 mm on the bottom end plug (30mm) side for accommodating the fission gases. A crimp (10 mm) separates the plenum and the bottom $DDUO_2$ blanket. A helical compression steel spring and spring support are put as shown in **Fig. 1.11**. A spacer wire of stainless steel D9 (Dia. 1.6mm) is wrapped helically (pitch 200 mm) around the fuel pin for effective flow of coolant and to maintain the specified pin-pin distance.

---

[6] SS D9: Titanium modified austenitic stainless steel also called alloy D9, is the current choice of material for fuel cladding and wrapper material for fast reactors.

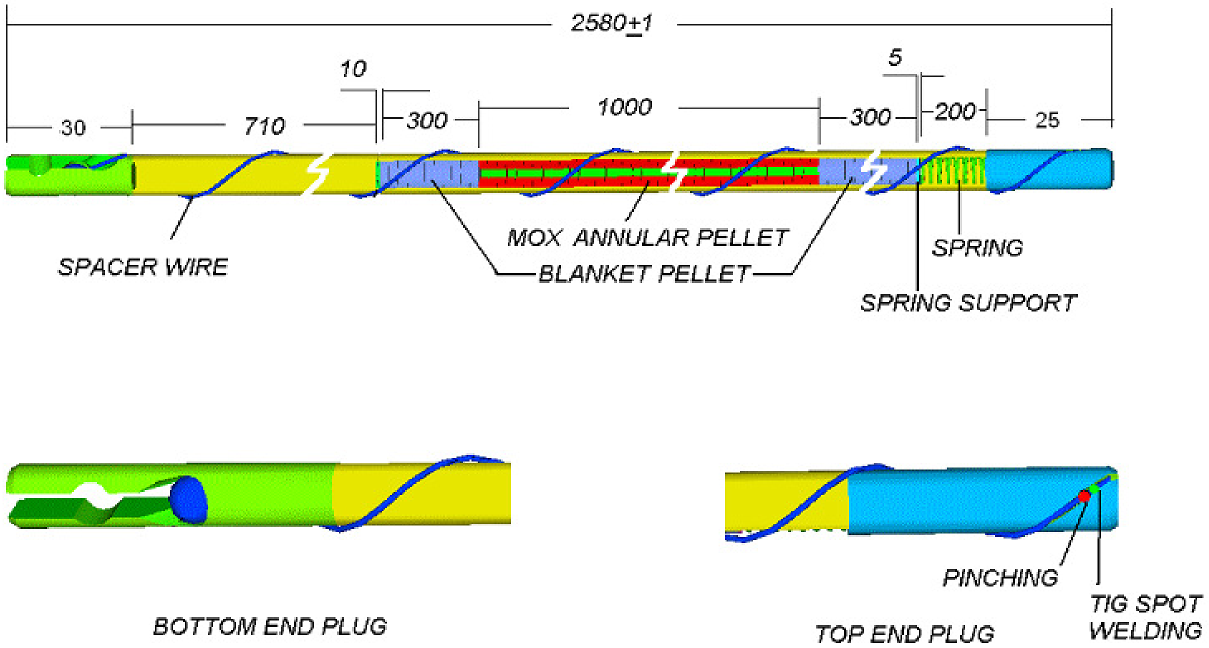

Fig. 1.11: Schematic Diagram of PFBR MOX Fuel Pin

The ThO_2 based fuels were manufactured for experimental irradiation in the research reactors or fuel development programme. **Table 1.13** lists the various campaigns for ThO_2 based fuels at AFFF and related data

Table 1.13: ThO_2 based Experimental Fuel Manufacturing at AFFF

Parameter	**Experimental fuel for AHWR**	**Experimental fuel for AHWR-LEU**	**Experimental irradiation**	**Experimental Irradiation in Dhruva**
Composition	$(Th_{0.9625}U_{0.0375})O_2$	$(Th_{0.86}U_{0.14})O_2$ $(Th_{0.7}U_{0.3})O_2$	$(Th_{0.9}U_{0.1})O_2$ ^{235}U: 1wt%	$(Th_{0.99}Pu_{0.01})O_2$ $(Th_{0.92}Pu_{0.08})O_2$
Pellet shape	Solid cylinder	Solid cylinder	Solid cylinder	Solid cylinder
Ht./Dia. ratio	0.5-1.0	0.5-1.0	0.5-1.0	0.5-1.0
Density (% TD)	90-95% TD	90-95% TD	90-95% TD	90-95% TD
O/M Ratio	2.00	2.00	2.00	1.98-2.00
Impurities (ppm)	≤ 2500	≤ 2500	≤ 2500	≤ 2500

1.5.3 Radioactive Waste Generation in Fabrication of Nuclear Fuels

Significant quantities of radioactive wastes get generated during nuclear fuel fabrication process. The wastes are mainly alpha bearing and contain long lived alpha emitters like isotopes of U, Pu and Th. Their classification into different categories is carried out for management involving segregation, selection of appropriate treatment process, storage and/ or disposal.

The solid wastes are categorized into four categories [148-149]. Out of these, Cat-IV refers to alpha bearing waste having alpha activity >4000 Bqg^{-1}. The IAEA has recommended the disposal in Near Surface Disposal Facilities (NSDF) for waste having activity < 4000 Bqg^{-1}. The Cat-IV alpha waste is sent to waste management facilities for further treatment and recovery of valuable nuclear materials.

As a conventional practice the liquid wastes are broadly classified into three categories viz. low level waste (LLW) having gross β, γ activity < 37 $MBqL^{-1}$, intermediate level waste (ILW) with gross β, γ activity in the range 37 $MBqL^{-1}$ to 37 $GBqL^{-1}$) and high level waste (HLW) with gross β, γ activity > 37 $GBqL^{-1}$ [149].

The gaseous waste which mainly comprises the ventilated air may also contain particulates of Pu, U, Th etc. To control and minimize discharge of activity through air route in conformity with the national and international regulations; series of HEPA (High Efficiency Particulate Air) filters are employed which practically retain most of the particulate radionuclides. The efficiency of a HEPA filter is minimum 99.97% for particles of size 0.3 µm. Thus, a single HEPA filter offers a very low leak path factor (LPF[7]) (3×10^{-4}) for particles of size 0.3 µm. The filter efficiency increases for particles that are smaller than 0.3 µm and larger than 0.3 µm. The replaced HEPA filters also contribute to the alpha active solid waste.

---

[7] LPF is the fraction of particles penetrating a HEPA filter with efficiency E (%) and given by $LPF = 1 - \frac{E}{100}$

1.6 Quality Control of Oxide and Mixed Oxide Nuclear Fuels at AFFF

The quality control checks are carried out on the feed materials, fuel pellets and fuel pins. The key chemical and physical quality control requirements and the methods used are described briefly in the following sections.

1.6.1 Chemical Quality Control Requirements and Methods

1.6.1.1 Heavy Metal Content

The accurate and precise determination of heavy metals (U, Pu and Th) is of utmost importance for the nuclear fuels [150]. The fuel designer specifies the upper and the lower limits of these elements for the designed operation of the reactor.

The composition of blended powders is usually determined by fast non-destructive methods. These methods being fast, give quick green signal for fabrication process to proceed further and thus serve as process control methods. The plutonium in the blended mixed oxide powder is determined by process control methods such as Neutron Well Co-incidence Counter (NWCC) and X-Ray Fluorescence (XRF) (**Fig. 1.10**) [151-153].

The precise and accurate elemental analysis of sintered fuel pellets is achieved by destructive chemical methods based on redox titrimetry. Uranium is analyzed by Davies & Gray [154] and plutonium by Drummond & Grant redox titrimetric methods [155]. The ethylenediaminetetraacetate (EDTA) complexometric titration is employed for thorium determination in thoria based fuels [150, 156-157].

1.6.1.2 Isotopic Composition

The isotopic composition [158] is needed to calculate the total fissile content (TFC) of the nuclear fuel. The TFC is arithmetic sum of the at. % or wt% of the fissile isotopes (^{235}U, ^{239}Pu, ^{241}Pu, ^{233}U). However, in case of fast reactors all the isotopes of Pu are fissionable[8] [145, 159]. Thus, equivalent ^{239}Pu (Eq. ^{239}Pu) is calculated for plutonium using Eq. (1.7).

$$Eq.Pu^{239} = Pu^{239}\,(wt\,\%) + 0.58Pu^{238}(wt\,\%) + 0.1Pu^{240}(wt\,\%) + \ 1.5Pu^{241}(wt\,\%) + 0.04Pu^{242}(wt\,\%) - 0.24\,Am^{241}(wt\,\%) \qquad (1.7)$$

The thermal ionization mass spectrometer (TIMS) is employed for measuring the isotopic composition of nuclear materials [158]. For ^{232}U and ^{238}Pu, alpha spectrometry is preferred due to their high specific alpha activity, low abundance and isobaric interference during spectrometric analysis. ^{241}Am content is also determined by alpha spectrometry [158].

1.6.1.3 Trace Metallic Impurities

The nuclear fuels should have high purity as presence of impurities even at trace level affects its performance significantly in terms of the neutron economy, physico-chemical, thermal and mechanical properties [160-166]. The metallic impurities are present in the feed materials and get further added-up from the process pick-ups during various fabrication steps [160-161, 163-166]. Elements like B, Cd and rare earths (Dy, Eu, Gd, Sm etc.) have large neutron absorption cross sections resulting in loss of neutrons. W, Mo, Ta etc. are refractory elements and cause creep resistance resulting in clad damage by mechanical interaction. Presence of light elements Ca, Na, Al etc. reduces the fuel density and decreases the fissile content. Fe, Cr, Ni etc. are generally monitored to check the process pick-up and condition of the process equipments. The overall high impurity content leads to fuel dilution. Thus, trace metallic constituents are controlled and monitored in the nuclear fuels [160-161, 163-166].

The trace metals are determined by carrier distillation DC-Arc-AES method [161]. The main advantage of the method is its usefulness for solid samples. ICP-OES is better than the DC-Arc-AES technique [161]. The several advantages include no self absorption, large linear dynamic range (4-5 orders) and high temperature (~6000 K) stability of the ICP and

---

[8] The nuclear fission in ^{232}Th, ^{238}U and ^{240}Pu is possible with sufficiently fast neutrons (> 1 MeV), they are known as fissionable nuclides.

better precision (1-2% RSD). However, ICP-OES method is a solution method where dissolution of sample and separation of major matrix elements (U, Pu, Th) is necessary as they emit rich line spectrum.

1.6.1.4 Trace Non-Metallic Impurities

The non-metallic impurities react with cladding, if gaseous cause its pressurization and rupture [162]. The carbon may react with the clad elements Zr (in zircaloy), and Cr (in stainless steel) and result in carburization by forming ZrC and $Cr_{23}C_6$ respectively causing clad embrittlement. With zirconium alloys hydriding is major concern and thus, hydrogen is critically controlled (< 1 ppm). The moisture reacts with chloride/ fluoride (Cl^-/F^-) impurities and forms respective acids, which cause corrosion of the clad. The specifications for non-metallics in feed materials and fuels are reported [162-166].

Quantitative estimation of the specified non-metallic constituents in the fuel is carried out by various techniques. Carbon is estimated by a method involving combustion forming CO_2 followed by measurement using thermal conductivity detector (TCD) or infrared detector using commercial determinators [160, 162]. Hydrogen is determined by inert gas fusion (IGF) technique employing TCD [167]. Nitrogen is measured commonly by two methods, viz., i) nitrogen determinator based on IGF technique [167] and ii) Kjeldhal distillation technique [168]. Chlorine and fluorine impurities are analysed after their pyro-hydrolytic extraction at 900 ºC under moist N_2/ Ar condition. The liberated HCl and HF are collected in the buffer solutions and estimated by respective ion selective electrodes [169].

1.6.1.5 Equivalent Boron Content (EBC)

The equivalent boron content (EBC) is used to quantify the neutron-absorbing properties of a nuclear material [170]. The net effect of neutron absorbing impurities is put together in terms boron. The boron equivalents are determined using the atomic weight of elements and the thermal neutron absorption cross sections (in barns). The boron equivalent of each impurity is added to arrive at the EBC (in ppm) using the expression Eq. (1.8)

$$EBC = \sum_{i=1}^{n} \frac{At.wt.\ of\ B}{\sigma_B} \times \frac{\sigma_{E_i}}{At.wt.\ of\ E_i} \times E_i (in\ ppm) \tag{1.8}$$

where, σ_B and σ_{E_i} are neutron absorption cross sections of boron and the impurity element E_i.

1.6.1.6 Oxygen to Metal Ratio (O/M)

The O/M is oxygen to metal ratio where O is gram atom of oxygen and M is gram atom of heavy metal (U, Pu, Th). O/M ratio is critical specification for MOX fuels and in the feed materials. Thorium has only single valance (+4) and thus, ThO_2 exists as stable stoichiometric compound. However, U exists in valancies (+4) and (+6), therefore hyper-stoichiometric compositions UO_{2+x} are found. Similarly, Pu has (+4) and (+3) valancies thus, may be found as hypo-stoichiometric PuO_{2-x}. Therefore, in the fabrication of MOX fuels, O/M ratio is strictly controlled by fabrication parameters.

A higher value of O/M ratio of the UO_2 powder gives a defective sintered product having cracks. The fuel fabrication with U_3O_8 cannot be carried out because of large density change from U_3O_8 (8.35 gcm^{-3}) to UO_2 (10.96 gcm^{-3}). The enormous amount of the oxygen release from U_3O_8 during reductive sintering makes the pellets defective. Thus, U_3O_8 is reduced to UO_{2+x} ($0< x<0.15$) for fuel fabrication.

The O/M ratio affects the thermal conductivity, melting point, number of phases etc. in the oxide and MOX fuel [171-172]. The stoichiometric $(U,Pu)O_2$ has highest thermal conductivity which decreases on both the sides of non-stoichiometry. The O/M ratio of fuel influences the extent of fuel clad or coolant chemical interaction (FCCI). ^{239}Pu fission gives larger fraction of the noble fission elements (Ru, Pd, Rh etc.) than ^{235}U. Thus, Pu based fuel are more oxidizing than UO_2 and hence O/M ratio is kept hypo-stoichiometric. There are several methods for estimation of O/M ratio [172, 173-174]. The gas equilibration thermo-gravimetry is most widely used method.

1.6.1.7 Fissile Bulk Homogeneity

Bulk homogeneity of the fissile in the host fertile matrix is essentially required to be determined. The presence of inhomogeneity may cause inpile hot spot generation, enhanced fission gas release resulting in increase of fuel pin internal pressure and consequent clad failure [175]. On the other hand the PuO_2 or plutonium rich mixed oxide agglomerates are difficult to dissolve in the reprocessing dissolvent typically 10-12M HNO_3. For $(U_{1-y}Pu_y)O_2$ bulk homogeneity is an important specified parameter which is determined by dissolution test wherein the residue is the measure of Pu inhomogeneity [176].

1.6.2 Physical Quality Control Requirements and Techniques

1.6.2.1 Bulk Density of Feed Powders

The powder density of feed material influences the compactability in the fuel fabrication [99]. Densities of powders are generally expressed as either bulk/ apparent or tap densities. The higher bulk and tap densities are indicative of poor physical properties. For UO_2 powder, the bulk density >0.625 up to 2.0 g cm^{-3} are specified [163, 177]. Sinterable PuO_2 and ThO_2 powders have bulk densities of 1-1.5 g cm^{-3} and 0.8-1.2 g cm^{-3} respectively [164, 178-179].

1.6.2.2 Powder Particle Size Distribution

The particle size distribution (PSD) of a granular aggregate or powder is a quantitative measure of the number of particles sorted according to their diameter (usually considered spherical). The PSD data of feed powders UO_2, PuO_2 and ThO_2 are used to optimize the process of fuel fabrication and to tailor the properties of product. The average particle size and median of the size distribution lies in the range 5-15 μm for ADU derived

UO_2. The PSD decides the flowability, chemical reactivity and mechanical strength of a powdered or granular aggregate. Additionally, for nuclear materials, PSD data is used to determine the respirable fraction of fine bulk powders. The PSD is governed by parameters selected for precipitation process [99, 106, 108, 118].

Although, the classical sieve analysis is still used to determine the PSD of powders, the modern methods determine the PSD in the small size range where the sieve analysis is impractical. Commonly used technique is Laser Diffraction (LD) technique [180].

1.6.2.3 Powder Specific Surface Area

The knowledge of specific surface area (SSA) of the powders alongwith other powder properties is required to optimize the fuel fabrication parameters. The SSA is one of the parameters which determine the sinterability of the powder and govern the process of sintering [108]. Typical ADU route derived UO_2 powder has SSA nearly 3.2 m^2g^{-1}. In contrary to others (UO_2, ThO_2), the SSA of PuO_2 powder is higher (typical value is 16 m^2g^{-1}) and is important from its sinterability and storage point of view. PuO_2 powder readily adsorbs water vapors from atmosphere. The adsorbed water undergoes radiolysis and forms potentially explosive H_2 gas in PuO_2 [181]. The SSA of powders is decided by the parameters selected for calcination process (temperature and time) and exponentially decreases with temperature [99, 108]. The evaluation of the SSA of a powder is based on the Brunauer–Emmett–Teller (BET) technique for inert gas (N_2) physisorption onto a solid surface at liquid nitrogen temperature and calculating the amount corresponding to monomolecular layer [182-183].

1.6.2.4 Powder Flowablity and Sinterblity

The powder flowability is an important technological parameter. Flowability is relevant for achieving uniform die filling of the compaction press in order to avoid density variation in the compacted green pellets [184]. The nuclear feed materials can be non-flowing fine powders to free flowing spherical or granular aggregates.

The sinterability of a ceramic powder is its ability to achieve density close to TD thereby forming dense mass when its green compacts are heated below its melting point in presence or absence of pressure. The sinterability test is carried out to verify the powder to pellet fabricability (cold compaction, sintering etc.) and density of pellet ≥ 94% of TD [163]. The sinterability is governed by powder SSA, PSD, O/M ratio, density, particle shape etc.

1.6.2.5 Powder Particle Morphology

An important parameter which significantly influences the compaction and sintering of green fuel compacts is particle shape or morphology of powders. The particle morphology determines the flow characteristics of the powder and packing properties affecting the green and sintered pellet densities [118]. The exterior shape of the particle depends upon the precipitation conditions. The ThO_2 and ThO_2-UO_2 powders obtained from oxalate route shows 'platelet' morphology with varying size from 2-5 μm [99]. UO_2 powder produced from ADU calcination and reduction shows 'spherical' morphology [99, 185]. The oxalate derived PuO_2 possess 'spherical' morphology [99, 186].

1.6.2.6 Density of Green and Sintered pellets

The geometrical density of green and sintered pellets is measured using diameter, height and weight [163, 165, 187]. The inner and outer diameters are measured in the annular cylindrical pellets to calculate the geometrical density. The green densities of the pellets are achieved in the range of 55-60% of TD. The sintering leads to densification above 90% of TD in the sintered pellets.

1.6.2.7 Fissile Micro-Homogeneity and Microstructure

Alpha auto-radiography of pellets using track etch technique is used to detect micro in-homogeneity of the fissile distribution in the fertile host matrix [188-189]. The α-radiograph presents distribution and the size of fissile (Pu, ^{235}U) or fissile rich agglomerate. The microstructure of sintered pellet is evaluated by optical microscopy [190] to ensure grain size of the pellet is within specified limit. The fission gas release behavior depends upon the grain size; smaller the grain size, more the fission gas release and vice versa.

1.6.2.8 Weld X-ray Radiography and X-GAR

The X-ray radiography of end-plug of nuclear fuel pins is carried out to check the physical integrity of welds [191]. The X-GAR is combination of X-ray radiography and Gamma Auto Radiography. In the X-GAR technique, the fuel pin is subjected to X-rays (from X-ray radiography machine) and image of internal components is taken on a radiographic film. Simultaneously, the gamma rays from the fuel (UO_2, PuO_2) irradiate the same radiographic film. The intensity difference in the gamma rays among MOX and $DDUO_2$ (in GAR) leads to differential exposure of the radiographic film. The radiographic film is developed using chemical etchants (developers) and analysed under an illuminator. The X-ray radiograph shows the presence/ absence of pellets, chipping of pellet and correct sequence of internal components (pellets, spring, spring support etc.) in a fuel element (**Fig. 1.11**). The GAR detects the cross mixing of pellets of different compositions, plutonium agglomerate, compositional variation in the fuel column.

1.6.3 Specifications for Feed Materials and MOX Fuels

The feed powder materials for fabrication of oxide and MOX fuels are required to satisfy several chemical and physical properties. **Table 1.14** lists important parameter specifications for nuclear grade UO_2, PuO_2 and ThO_2 powders for fabrication of oxide and MOX fuels [161-164, 177-179].

Table 1.14: Specifications for UO_2, PuO_2 and ThO_2 Powders for Fuel Fabrication

Parameter	**UO_2**	**PuO_2**	**ThO_2**
Heavy Metal (%)	≥87	≥87.5	≥87
Total impurities (ppm)	1500	5000	2500
O/M Ratio	≤2.15	2.00	2.00
EBC (ppm)	4	5.5	2.5
SSA (m^2g^{-1})	3.0-8.0	5-30	3.5-4.5
Particle size (100% pass)	425 μm mesh	140 μm mesh	150 μm mesh
Bulk density (gcm^{-3})	>0.625	1-1.5	0.8-1.2
Al, Fe (ppm)	250, 250	100, 500	100, 800
B, Eu (ppm)	0.3, 3	3, 3	1, 0.5
Cd+Dy+Gd+Sm (ppm)	20	20	3
Ca+ Mg (ppm)	200	400	500
Cr, Ni, Co, Cu (ppm)	200, 200, 100, 150	200, 100, 200, 200	5,_,1, 50
Pb, Mn, Mo, Si (ppm)	250, 250, 250,300	100, 200, 200, 200	20, 2, 20, 400
Th (ppm)	10	200	NA
U (ppm)	NA	2 wt%	10
Pu (ppm)	0.4 (Rep. U)	NA	NA
Am (wt%)	NA	0.25	NA
C, (Cl+F) (ppm)	100, 200	200, 500	200, 200

NA: Not Applicable; Rep. U: Reprocessed uranium or depleted uranium

The stringent specifications are laid down for the nuclear fuels to render their designed performance. These involve numerous chemical and physical parameters to be controlled and measured. The typical specifications of natural UO_2 fuel are listed in **Table 1.15**. The specifications for $(U_{1-y}Pu_y)O_2$ MOX fuel for a thermal and fast reactor differs significantly [161-162, 177-178]. The typical specifications of MOX fuel for thermal and a fast reactor are compared with each other (**Table 1.15**). The specifications for an experimental $(Th_{1-y}Pu_y)O_2$ MOX fuel fabricated at AFFF is also listed in **Table 1.15**.

Table 1.15: Specifications of Oxide and MOX Fuels for Thermal and Fast Reactors

Parameter	UO_2	$(U_{1-y}Pu_y)O_2$		$(Th_{1-y}Pu_y)O_2$
	PHWR	**Thermal Rx**	**Fast Rx**	**AHWR**
Heavy metal content (wt%)	≥87.5	≥87.5	≥87.5	≥87
Sintered Density (% TD)	92-96	93-96	92-96	90-95
O/M Ratio	2.00-2.015	1.98-2.02	1.96-2.00	1.98-2.00
Total gas content (cm^3g^{-1} at STP)	0.04	0.04	0.1$^{\#}$	—
Eq. Boron content (ppm)	1.5	1.5	NA	2.5
Total impurities (ppm)	1500	2500	5000	2500
Hydrogen (ppm)	1	1	3	1
Moisture (ppm)	9	9	30	9
B (ppm)	0.3	0.5	3	1
Cd (ppm)	0.2	1	23	1
Dy, Sm, Gd, Eu (ppm)	0.15	0.15		2
Cl+ F (ppm)	25	25	50	25
Residue in DT (wt%)	NA	≤ 0.1	1	NA
Grain size (μm)	5-50	5-50	5-50	5-50
Fissile agglomerate size (μm)	NA	400	100	400

NA: Not Applicable; $^{\#}$: Excluding Hydrogen; Rx: Reactor

1.7 Oxide and MOX Fuel Scrap and their Recycling Considerations

Significant quantity of nuclear material scrap gets generated during fuel fabrication processes [24]. The scrap mainly comprises of the off-specification fuel pellets which get produced invariably in the various manufacturing operations and allied QC activities. The fuel pellets get rejected at various stages of fuel fabrication process attributable to non-compliance of numerous physical or chemical specifications as specified. **Table 1.16** lists various factors responsible for rejection of fuel.

Table 1.16: Main Parameters and Causes for Rejection of Oxide and MOX Fuel

Parameter	Cause of rejection
Pellet Size	Under size (over size are ground)
Sintered Density	Lower density than specified
Fissile content	Lower or higher than the specified
Composition	Deviation from specified range
Impurity content	Higher than the specified
Physical defects	Beyond allowed limits
Fissile (Pu or U) agglomerates	Beyond specified size and location
Reconstitution of fuel elements	Cross mixing of different compositions

1.7.1 Categorization of Oxide and MOX Fuel Scrap as CRO and DRO

The scrap having acceptable impurity content is referred as CRO or clean scrap and the scrap containing impurities beyond acceptable limits as DRO or impure scrap [31-33]. The average shares of various MOX scrap generated during $(Th_{1-y}Pu_y)O_2$ fuel manufacturing by powder-pellet route at AFFF are shown in **Fig. 1.1**. Among the several types of fuel scrap, the clean scrap contributed largest (20-22 wt%) of a batch on an average. The typical batch size is 10 Kg. The impure scrap constitutes ~5 wt% of the total material throughput. The major portion of the scrap is contributed by fuel manufacturing operations in the form of rejected pellets. The QC activities also generate recyclable scrap to a lesser extent. The fuel fabrication is carried out in campaigns based on the compositions. The surplus fuel of different campaigns also needs recycling which is nearly 1wt% and shown as miscellaneous share in **Fig. 1.1**.

1.7.2 Need of Recycling Nuclear Fuel Scrap

The recycling of valuable materials is important for the nuclear industry like other industrial processes. The process of recycling consists of the recovery of rejected fuel and their reuse as feed material. The avoidance of off-specification products is the main method of increased productivity and scrap minimization. However, practically every industrial process produces more or less scrap demanding its recycling. Interestingly, the oxide and MOX fuel rejects contain significant amount of fissile and fertile materials depending upon the composition of the fuel. The judicious utilization of the feedstock materials and natural resources is accomplished by recycling these rejects. The practice of recycling becomes essential for following main reasons [24, 192-193]:

1. The valuable fissile (^{235}U, Pu, ^{233}U) materials locked in the fuel rejects are essentially need to be recovered. This has direct impact on the demand-supply balance of fuel to the operating reactors.
2. Quick recycling alleviates the TFC reduction in Pu due to fissile ^{241}Pu decay. ^{241}Pu, the fissile isotope of Pu ($T_{1/2}$; 14.2 years) decays primarily by beta emission (99.99%) into non-fissile ^{241}Am (**Fig. 1.3**). Hence, the old scrap tends to loose value.
3. The immediate recycling of Pu and ^{233}U based fuels averts personnel exposure due to high radiation emitting decay products during long term in-house storage. ^{241}Am ($T_{1/2}$; 458 years) is alpha emitter and decays to ^{237}Np with gamma emission of 60 keV energy. Thus, ^{241}Am increases progressively with ageing of Pu, rendering high radiation dose. For every 1% of ^{241}Pu, ^{241}Am build-up is 0.05% per year. Similarly, in ^{233}U based fuels, the decay products of ^{232}U viz. ^{212}Bi/ ^{208}Tl (γ: 0.7–1.8 MeV/ 2.6 MeV respectively) (**Fig. 1.5**) make heavy shielding mandatory for the handling aged ^{233}U. ^{233}U contains ^{232}U which varies from a few ppm to >500 ppm [99, 194].
4. The practice of recycling curtails the fuel costs and hence significantly improves the energy economics.
5. Recycling saves natural resources and fresh/ standard feed stock materials.

1.7.3 Factors Influencing the Recycling Practices

The recycling practices are industrial activities that are governed by multiple factors. Whether to proceed with recycling option largely depends on the characteristics and economic value of the material, nature and duration of storage. Some major factors are; 1) quantity of material, 2) technical feasibility, 3) economics, 4) waste generation and 5) available disposal options [24, 193]. For large quantum of scrap materials, the implementation of recycling options is more likely to be justified than for smaller quantities. Thus, the recycling of fuel rejects sharing large quantum ~25 wt% (**Fig. 1.1**) is justifiable.

1.7.4 Attributes of Good Recycling Methods

The selection of recycling methods is crucial. The UO_2, $(U_{1-y}Pu_y)O_2$, $(Th_{1-y}U_y)O_2$ and $(Th_{1-y}Pu_y)O_2$ fuel rejects are characteristically different, thus a single method cannot be used to all the scrap types. A good recycling method should have following attributes;

1. From time economy point of view the recycling method should be fast enough to favor enhanced production rates.
2. The process should be able to recycle 100% scrap. In other words, the recycled material should have ability to be used in the production of a batch on 100% basis.
3. It should produce the recycled material having better or equivalent properties to that of the standard materials.
4. The process should be a multiple recycling technique. In other words, the rejects produced from a batch fabricated from the n^{th} recycle could be recycled in the $(n+1)^{th}$ recycle without posing different problems.
5. The lesser number of process steps are desirable.
6. The process should generate no or minimum waste that too manageable.

1.8 Recycling of Nuclear Fuel Scrap: An Insight into Literature

A few methods have been reported in the literature on recycling of fuel scrap generated in the production of variety of nuclear fuels like metals, alloys, mixed carbides, oxides, mixed oxides etc. [25-30, 35-44]. However, the recycling of oxide and MOX fuel scrap is comparatively more studied due to their significantly large usage.

1.8.1 Recycling of Scrap UO_2

The conventional methods of recycling for rejected UO_2 fuel involve oxidative pulverization of UO_2 (into U_3O_8) in electrical resistance furnaces [35-40, 195-197]. The UO_2 scrap is first oxidized in a fluidized bed which simultaneously oxidizes and comminutes the scrap, subsequently the oxidized material (U_3O_8) is reduced back to UO_2 with improved sinterability [196]. Larson et al. [36] have demonstrated that UO_2 powder of good quality can be obtained from scrap material by low temperature oxidation (350-400 °C) followed by reduction at 800 °C. Fuel scrap resulted in the form of UO_2 grinding swarf and UO_2 sinter scrap were oxidized to U_3O_8 powder and added with fresh UO_2 to fabricate fuel in simple and economic way of recycling [197]. Dias et al. [197] showed that there is only a small influence of such scrap addition on the irradiation behavior, especially for the fission gas release. Schwartz et al. [42] have demonstrated three dry recovery routes for ceramic UO_2 waste material: (a) calcination of waste material into U_3O_8 and blending with the fresh UO_2 powder; (b) calcination to U_3O_8, then reduction to UO_2 and blending with the fresh UO_2 powder; (c) grinding the waste material into a fine powder and blending with the fresh UO_2 powder. Yang et al. [37] have reported the lower temperature (325 °C) oxidative recycling process for obtaining sinter-active U_3O_8 powder. Recycled U_3O_8 powder with a high surface area and small particle size could be obtained by lowering the oxidation temperature. The low temperature oxidized sinter-active U_3O_8 powder is effective in mitigating the density drop of the UO_2 pellets usually found when recycled U_3O_8 powder is added. The unirradiated defective UO_2 pellets stored for 10 years were recycled by technique based on oxidation (250-600 °C)-reduction (300-800 °C) [35]. It is reported that after five oxidation-reduction cycles, the specific surface area of uranium dioxide was improved >2.5 m^2g^{-1} [35]. The spallation mechanism of UO_2 unirradiated sintered pellets into U_3O_8 powder at 400°C was examined by Bae et al. [40]. Transformation of UO_2 to intermediate phases was assigned the main driving force for the pulverization. During the formation of intermediate phases at 400°C, intergranular cracks were extensively developed and these cracks caused the spallation. The formation of U_3O_8 only accelerated the pulverization. The grain size of the UO_2 pellets was found to increase after adding recycled U_3O_8 powder having controlled morphology [38]. Song et al. [26] demonstrated that ~10wt% of oxidatively recycled (at 400 °C) U_3O_8 when added to fresh UO_2 powder produced acceptable quality fuel pellets. They studied the entire range of recycled U_3O_8 (0-100%) addition to fresh UO_2 and observed that the sinter density goes down with addition of recycled U_3O_8.

Recycling of rejected sintered UO_2 pellets and scrap UO_2 powder by heating in air in microwave ovens was reported by Thornton et al. [63-64]. Kulyako et al. [39] used microwave heating for thermal oxidation of substandard UO_2 pellets in air converting into U_3O_8 and subsequently reduction to UO_2. The microwave recycled U_3O_8 and UO_2 (~10wt%) were added to fresh UO_2 powder and demonstrated their suitability for fuel fabrication.

The wet route for recycling UO_2 scrap involved dissolution in boiling HNO_3, liquid-liquid extraction, precipitation as ADU, AUC, peroxide etc. and conversion to UO_2 [24, 198]. Recycling of enriched UO_2 nuclear fuel scrap containing gadolinium oxide (~3 wt%) was carried out by dissolving the scrap in HNO_3, extracting using TBP and precipitated as ADU [199]. UO_2 powder was prepared for fuel pellet fabrication from uranium peroxide UO_4 recovered from UO_2 scraps using carbonate-hydrogen peroxide solution [200]. Recovery of uranium from (U,Gd)O_2 fuel scrap by dissolution and precipitation in carbonate media is reported [201].

1.8.2 Recycling of Scrap $(U_{1-y}Pu_y)O_2$ Mixed Oxide

Limited literature is available on the recycling of $(U_{1-y}Pu_y)O_2$ fuel scrap. The applicability of the oxidative methodology in $(U_{1-y}Pu_y)O_2$ depends upon Pu/(U+Pu) ratio. As Pu content increases the ease of oxidation decreases. The recycling of the $(U_{1-y}Pu_y)O_2$ scrap generated during the MOX fuel fabrication has been discussed by Kamath et al. [202]. A thermo-mechanical method involving oxidation and mechanical crushing for dry recycling of low Pu content scrap during MOX fuel fabrication was reported by Somayajulu et al. [203]. Around 40 wt% of the rejected $(U_{1-y}Pu_y)O_2$ pellets from Micronisation and MASter blend (MIMAS) process are recycled using a dry process involving micronisation and forced sieving of the scraps [43]. The oxidative-reductive methodology for $(U_{1-y}Pu_y)O_2$ with y~0.25 sintered rejects could utilize 20 wt. % of the recycled powder for batch fabrication [204]. Khot et al. [44] have developed a dry and a wet method for recycling the clean rejected $(U_{1-y}Pu_y)O_2$ MOX fuel pellets. They [44] reported that the thermal oxidative pulverization of the sintered $(U_{1-y}Pu_y)O_2$ rejects having high Pu content is cumbersome despite of employing multiple oxidation/ reduction steps and higher oxygen potential. Maurice et al. [30] have reported a wet recovery process for recovery of Pu from the non-irradiated $(U_{1-y}Pu_y)O_2$ MOX after dissolution in HNO_3 by forming the complete solid solution [30].

1.8.3 Recycling of Scrap ThO_2 based Fuel

Recycling of highly refractory thoria based fuel rejects is studied to a very less extent [16, 23, 41, 205]. The recycling of ThO_2 based MOX fuels is difficult as compared to UO_2 based fuels. ThO_2 having single oxidation state (+4) is a stoichiometric compound and doesn't undergo oxidation like UO_2 into U_3O_8. Similarly, the reduction of ThO_2 to lower oxides is not feasible. Therefore, the dry recycling of ThO_2 sintered pellets by oxidative or oxidative-reductive methodology is not feasible. The comminution processes, however are applicable where sintered rejected pellets are mechanically crushed and micronised. The presence of UO_2 in $(Th_{1-y}U_y)O_2$ opens an option for oxidative pulverisation of the matrix which is function of uranium content [206-207]. Further, the third alternative is available which involves the aqueous recycling by either dissolution following oxalate precipitation/ co-precipitation [118] or by direct denitration. The thoria and thoria-urania powders were successfully prepared by bulk microwave denitration from respective solutions [21-23].

A dry recycling process was reported for $(Th_{0.86}U_{0.14})O_2$ combining mechanical crushing and oxidation by Khot et al. [208]. Addition of only 30 wt% of so recycled powder to the fresh feed material could bring the specified density. Mishra et al. [41] have reported the addition of maximum 15wt% of the $(Th_{0.7}U_{0.3})O_2$ sintered rejects recycled via mechanical pulverization (crushed and attritor milled) for re-fabrication of fuel. In another method, they [41] have combined the mechanical pulverization with oxidation to bring out 100% recycling of $(Th_{0.7}U_{0.3})O_2$ sintered rejects and removed the need of fresh powder addition. Recently, an aqueous method for recycling of ThO_2 from nuclear fuel production scrap has been reported which involves its dissolution in trfiflic acid (CF_3SO_3H) [205]. So obtained thorium(IV) triflate is converted into thoria via oxalic acid precipitation and calcination. The spent triflic acid could be recycled and reused for dissolution of new batches of scrap thoria.

1.8.4 Summary of the Conventional Scrap Recycling Methods

The conventional recycling for rejected UO_2, $(U_{1-y}Pu_y)O_2$, $(Th_{1-y}U_y)O_2$ fuels is based on either dry processes using comminution (crushing and micronisation), oxidative ($UO_2 \rightarrow U_3O_8$) or oxidative-reductive ($UO_2 \leftrightarrow U_3O_8$) pulverization in conventional furnaces or wet processes involving dissolution, liquid-liquid extraction, precipitation and conversion into oxide/ mixed oxide powder [16, 24, 35-44, 198-205].

The dry processes generate radioactive dust, have prolonged cycles and the powder properties are inferior to the standard feed materials. The powders from the conventional dry processing methods have low sinterability and usually mixed with standard powders in optimized proportions usually <20 wt%, thus, SRR achieved <1 (typically 0.1-0.2). As the content of PuO_2 increases in $(U_{1-y}Pu_y)O_2$, the dry methods based on oxidative pulverization become impractical. In ThO_2 and $(Th_{1-y}Pu_y)O_2$, the oxidative method is not applicable whereas in $(Th_{1-y}U_y)O_2$, the oxidation is function of UO_2 content.

The recycling using conventional wet routes based upon precipitation-calcination (peroxide, ADU, AUPuC, oxalate etc.) produce powder with better and consistent properties than dry routes [16, 115, 124]. However, the wet processes of recycling have multi steps, associated liquid waste generation, low production rates and thus non-economic. The wet routes are promising, however are not favored due to associated liquid waste and higher sensitivity of the product characteristics to process parameters. Additional issues are criticality, low productivity, packaging and transport etc. A comparison between conventional dry and wet processes is made considering several key factors and listed in **Table 1.17**.

Table 1.17: Comparative Evaluation of Key Factors for Dry and Wet Recycling Routes

Factors	**Dry routes**	**Wet routes**
Production rate	Higher	Lower
Liquid waste generation	No	Significant
Radioactive dust generation	Yes	No
Number of process steps	Usually lesser	Usually more
Powder properties as compared to standard powder	Inferior	Equivalent or better
Sensitivity of product characteristics to the process parameters	Lower	Higher
Consistency in the powder properties	Lower	Higher

1.9 Chemistry of U, Pu and Th Relevant to Recycling of Fuel Rejects

1.9.1 Solution Chemistry of U, Pu and Th

U, Pu and Th as metal or their compounds (mostly oxides) are encountered as nuclear fuels. They show vivid solution chemistry. The wide variety of colours exhibited by actinide ions is characteristic of transition series of elements. In addition to simple hydrated ions M^{3+}, M^{4+}, they exhibit higher valent oxyions as MO_2^+ and MO_2^{2+}. The oxidation state (VII) for Pu is found in the form of ion of type MO_5^{3-} in highly alkaline solutions. Due to closeness of 7s, 6d and 5f shells, U and Pu exhibit variable oxidation states. The oxidation states of Th, U and Pu and their colors in different oxidation states are recorded in **Table 1.18** [209].

Table 1.18: Oxidation States of Thorium, Uranium, Plutonium and their Colours

Oxidation state	Th ion and color	U ions and color	Pu ions and color
(III)	---	U^{3+}: Red	Pu^{3+}: Deep blue/ Violet
(IV)	[IV] Th^{4+}: Colorless	U^{4+}: Green/ Blue	[IV], Pu^{4+}: Tan Orange
(V)	---	UO_2^+: Colorless	PuO_2^+: Pale-Pink- colorless
(VI)	---	[VI], UO_2^{++}: Yellow	PuO_2^{++}: Pink Orange
(VII)	---	---	PuO_5^{3-}: Dark red

[X] represents the most stable oxidation state

Their oxidation-reduction relationships are understood using Latimer or Reduction potential diagrams [210]. **Table 1.19** lists the standard electrode potential values of important couples for their solution chemistry [150, 210].

Table 1.19: Standard Electrode Potentials of Some Important Couples versus NHE

Redox couple	Standard Redox Potential (E^o) In volt
U(VI)/U(IV)	+ 0.332
U(IV)/U(III)	+ 0.771
Pu(VI)/Pu(IV)	+ 1.04
Pu(IV)/Pu(III)	+ 0.98
NO_3^-/ NO	+0.96
NO_3^-/NO_2^-	+0.94

1.9.1.1 Solution Chemistry of Uranium

The solution chemistry of uranium is complex [211]. The U(VI) does not exist as U^{+6} but as uranyl ion, UO_2^{2+}. U^{+6} owing to its high charge, is unstable in solutions and is immediately hydrolysed and stabilized by formation of UO_2^{2+}. This species exists not only in aqueous solutions but in solids too. U^{3+} has very strong reducing properties such that its aqueous solution evolves H_2 Eq. (1.9). The U(V) as UO_2^+, disproportionates (self oxidation-reduction) by Eq. (1.10). The U^{4+} aqueous solutions are not stable and slowly oxidize to UO_2^{2+} Eq. (1.11), thus require stablising agents like Hydrazine.

$$2U^{3+} + 2H_2O \rightarrow 2U^{4+} + H_2 + 2OH^- \qquad (1.9)$$

$$2UO_2{}^+ + 4H^+ \rightarrow UO_2{}^{2+} + U^{4+} + 2H_2O \qquad (1.10)$$

$$U^{4+} + 2H_2O \rightarrow UO_2{}^{2+} + 2H^+ + H_2 \qquad (1.11)$$

1.9.1.2 Solution Chemistry of Plutonium

Plutonium has mainly five oxidation states (**Table 1.18**). The lower oxidation states; Pu(III) and Pu(IV) are more stable in acid solution while the higher oxidation states, Pu(VI) and Pu(VII) are favored under alkaline conditions [212-213]. The co-existence of more than one oxidation states simultaneously in varying proportions is unique characteristic of plutonium. The redox potentials that couple the various Pu oxidation states are all of comparable magnitude (**Table 1.19**). Thus, they undergo self oxidation-reduction reactions. The existence of Pu in multiple oxidation states simultaneously is attributed to (i) the tendency of Pu (IV) and Pu(V) ions to disproportionate and (ii) slow kinetics of formation or breaking of Pu-O bonds [214]. The disproportionation reactions of Pu(IV) and Pu(V) in acidic solutions are shown by Eq. (1.12) and Eq. (1.13) respectively.

$$3Pu^{+4} + 2H_2O \rightarrow 2Pu^{+3} + PuO_2{}^{2+} + 4H^+ \qquad (1.12)$$

$$3\,PuO_2{}^+ + 4H^+ \rightarrow Pu^{3+} + 2PuO_2{}^{2+} + 2H_2O \qquad (1.13)$$

Pu exists in (III), (IV), (V) and (VI) in 1.5 to 16M HNO_3, whereas upon boiling all the oxidation states transform into (VI) and is called valency fixation by boiling [16, 106, 124].

1.9.1.3 Solution Chemistry of Thorium

Thorium is known to have only one oxidation state Th^{4+}(aq.) in aqueous solution. So, the oxidation-reduction reaction does not have much importance for thorium solution chemistry [215]. Th^{4+}(aq.) is colorless unlike most of the other actinide ions. Being the largest actinide tetravalent ion, Th^{4+}(aq.) is least hydrolysable among them.

1.9.2 Dissolution Behavior of U, Pu and Th Oxides

The dissolution of UO_2, PuO_2 and ThO_2 is carried out mostly in HNO_3 in the various activities of nuclear fuel cycle. In comparison to UO_2; ThO_2 and PuO_2 cannot be dissolved in HNO_3. Their varying dissolution behavior can be understood in terms of thermodynamics and redox chemistry [150, 216].

1.9.2.1 Dissolution of Uranium Oxides

UO_3 is amphoteric in nature and readily dissolves in acid or alkali. UO_2 and U_3O_8 dissolve in nitric acid or fuming perchloric acid. The dissolution reaction of UO_2 in HNO_3 is represented by Eq. (1.14). The feasibility of the dissolution is explained by negative standard Gibbs energy (ΔG_{298} = -16.9 Kcal/mole) for reaction Eq. (1.14). UO_2 is readily oxidized by HNO_3 acid as evident from the standard electrode potential values of couples U(VI)/U(IV), NO_3^-/ NO and NO_3^-/NO_2^- (**Table 1.19**) and hence, dissolution is oxidative dissolution.

$$UO_2 + 3HNO_3(aq.) \rightarrow UO_2(NO_3)_2\,(aq.) + HNO_2 + H_2O \qquad (1.14)$$

The dissolution of UO_2 has been studied in detail [216-225] and dissolution rate is found to depend upon; 1) temperature, 2) SSA of UO_2, 3) pressure, 4) Stirring speed > 400 revolutions/ min. decreases the dissolution rate, 5) The calcination temperature of the precursor producing UO_2, 6) route of fabrication of UO_2, 7) the concentration of HNO_2, 8) the mechanism for dissolution and 10) nitric acid concentration.

1.9.2.2 Dissolution of Plutonium Dioxide

The dissolution reaction of PuO_2 in HNO_3 is represented by Eq. (1.15);

$$PuO_2 + 4HNO_3(aq.) \rightarrow Pu(NO_3)_4(aq.) + 2H_2O \tag{1.15}$$

ΔG_{298} value for reaction Eq. (1.15) is +9.8 Kcal/mole and suggests the non-spontaneity of the dissolution. Further, the ΔG increases with temperature, causing dissolution of PuO_2 in HNO_3 to be more unfavorable at higher temperatures as reflected by ΔG_{373} value 15.3 Kcal/ mole. The oxidative or reductive mechanism for dissolution of PuO_2 by HNO_3 is not feasible. The E^o values of couples Pu(VI)/(IV) and Pu(IV)/(III) suggest that the HNO_3 neither oxidize Pu(IV) to (VI) nor reduce Pu(IV) to Pu(III) (**Table 1.19**).

Dissolution of even green PuO_2 in nitric acid is extremely slow and incomplete. The fluoride catalysed [226] and the electrolytic dissolution [227] of PuO_2 are commonly employed methods. Aqueous methods like dissolution with complexing agents, digestion with 40% NaOH solution, refluxing in $(NH_4)_2SO_4$-9M H_2SO_4 mixture, H_3PO_4 (200 °C), HCl-$HClO_4$ at high temperature and pressure in sealed tube are reported in literature [228-230].

In the fluoride catalysed dissolution [150, 230], the fluoride ions being more electronegative than oxygen, displaces oxygen from PuO_2, a surface reaction and forms soluble fluoride complexes $PuF_x^{(4-x)+}$. As concentration of nitrate ions is very high in the vicinity of fluoride complexes, the fluoride ligands are replaced by NO_3^-. The liberated fluoride ions are again available and process of displacement and dissociation continues. Since, fluoride acts as a catalyst; a small amount of it is sufficient. A large excess will precipitate insoluble PuF_4. The mechanism of fluoride catalysed dissolution is expressed through Eq. (1.16) to (1.18);

$$PuO_2\,(s) + F^- + 2H^+ \rightarrow PuOF^+ + H_2O \tag{1.16}$$

$$PuOF^+ + F^- + 2H^+ \rightarrow PuF_2{}^{2+} + H_2O \tag{1.17}$$

$$PuF_2{}^{2+} + 4NO_3{}^- \rightarrow Pu(NO_3)_4(aq.) + 2\,F^- \tag{1.18}$$

In electrolytic dissolution methods, the enhancement in the dissolution kinetics is brought by changing the tetravalency of Pu(IV)O_2 to either hexa (oxidative) or tri (reductive) valency using suitable redox agents in dissolvent HNO_3 [227]. The Electro Oxidative Dissolution Technique (EODT) uses electro-generated Ag(II) or Ce(IV) as the oxidant [231]. Fe(II), Cr(II) or Hydroquinone are used in Electro Reductive Dissolution Technique (ERDT) [232-233].

1.9.2.3 Dissolution of Thorium Dioxide

Since, Th has only single oxidation state (IV) (**Table 1.18**), the oxidative or reductive methodologies of the dissolution in nitric acid are not feasible. The dissolution reaction of ThO_2 in HNO_3 is shown by Eq. (1.19);

$$ThO_2 + 4HNO_3(aq.) \rightarrow Th(NO_3)_4\,(aq.) + 2H_2O \qquad (1.19)$$

The non-spontaneity of dissolution in HNO_3 is evident from ΔG_{298} value +10.3 Kcal/mole for the reaction shown by Eq. (1.19). The addition of F^- as catalyst is the only practical solution for dissolution of ThO_2 in HNO_3. However, HCl / HF mixture as a dissolving media [234] and a solid state reaction method involving fusion with $(NH_4)_2SO_4$ at 360 °C [235] have also been reported in literature. The dissolution of ThO_2 and $(Th,U)O_2$ has been reported in trifluoromethanesulphonic (triflic) acid solution [236]. Another important factor in the dissolution of ThO_2 is its crystallites size. Small crystallites (< 50 Å) easily dissolve in HNO_3 whereas large crystallites (> 124 Å) do not dissolve completely even after 240 hours [237].

The dissolution of ThO_2 in HNO_3/ HF mixtures has been studied by many workers [238-241]. F^- acts as catalyst but a large excess precipitates insoluble ThF_4. The dissolution mechanism shows the ThO_2 hydrolyses by reaction between oxide and water as shown by Eq. (1.20):

$$ThO_2\,(s) + 2\,H_2O \rightarrow ThO(OH)_2 + H_2O \qquad (1.20)$$

The hydroxyl group dissociates on the oxide surface in the acidic solutions leaving surface thorium with positive charge Eq. (1.21) which promote fluoride ion adsorption Eq. (1.22) forming $ThOF^+$. The hydrolysis of $ThOF^+$ further provides positively charged thorium site and the surface reaction with fluoride goes on forming ThF_2^{2+}. The rate controlling step is desorption of thorium fluoride complex ThF_2^{2+}. The nitrate ions further replaces fluorides from the soluble ThF_2^{2+} due to higher activity in the vicinity giving rise to $Th(NO_3)_4$ and thus completing the dissolution Eq. (1.23).

$$ThO(OH)_2 + 2H^+ \rightarrow ThO^{2+} + 2H_2O \tag{1.21}$$

$$ThO^{2+} + F^- \rightarrow ThOF^+ \tag{1.22}$$

$$ThF_2{}^{2+} + 4\,NO_3{}^- \rightarrow Th(NO_3)_4\,(aq.) + 2\,F^- \tag{1.23}$$

1.9.3 Oxidation and Reduction Behavior of Nuclear Material Oxides

The oxidation and reduction to either lower or higher oxides of ThO_2 is not feasible owing to single oxidation state (**Table 1.18**). Nevertheless, it can be reduced to thorium metal by calciothermic reduction through intermediate ThF_4 [87]. However, uranium and plutonium exhibit multiple oxidation states (**Table 1.18**) thus exist in several oxide forms. Important oxides of uranium are UO_3, U_3O_8 and UO_2, whereas plutonium has Pu_2O_3 and PuO_2. Higher oxides of plutonium i.e. > Pu(IV) do not exist in the solid state contrary to uranium. However, this is reverse in case of uranium that the lower oxides of uranium i.e. < U(IV) are not found. The UO_2 and PuO_2 can also be reduced to respective metals by reduction through respective tetrafluoride intermediates [87, 242].

1.9.3.1 Oxidation of UO_2

The oxidation of UO_2 has been studied extensively over many years [108, 243], because of its relevance to disposal of used nuclear fuel [244], powder storage and some fuel-recycling processes [40]. The oxidation of UO_2 is a two-step reaction Eq. (1.24) [245-247]:

$$UO_2 \rightarrow U_3O_7\,/\,U_4O_9 \rightarrow U_3O_8 \tag{1.24}$$

The UO_2 has the FCC crystal structure. The intermediate oxidation products U_3O_7 and U_4O_9 are derivatives of this structure. Formation of U_3O_7/U_4O_9 from UO_2 involves a slight volume reduction. In contrast, U_3O_8 has a distinctly different crystal structures (orthrhombic) and a density that is 23% less than that of UO_2, which corresponds to a 36% net volume increase [248]. The air oxidation of UO_2 is complicated because the reaction Eq. (1.24) has two stages which have different reaction mechanisms and often occur concurrently. The intermediate U_3O_7/U_4O_9 forms as a discrete layer on the surface of the UO_2 and the rate of oxidation is limited by the rate of oxygen diffusion through the U_3O_7/U_4O_9 layer. The formation of U_3O_8 follows a nucleation-and-growth mechanism and thus, displays sigmoidal reaction kinetics.

1.9.3.2 Reduction of Uranium Oxides

The reduction of UO_3, U_3O_8 is carried out at temperatures in the range 300-900 °C using reductants like H_2, NH_3, CO, C, CH_4 etc. The direct reduction of UO_3 using H_2 proceeds in two stages first being the reduction of UO_3 to U_3O_8 Eq. (1.25) and secondly the reduction of U_3O_8 to UO_2 Eq. (1.26) [248-249].

$$3UO_3 + H_2 \rightarrow U_3O_8 + H_2O \qquad (1.25)$$

$$U_3O_8 + 2H_2 \rightarrow 3UO_2 + 2H_2O \qquad (1.26)$$

Thermal decomposition of UO_3 to U_3O_8 on heating is another mode of reduction Eq. (1.27) [250]. This reaction depends upon the temperature, sample size, geometry and partial pressure of oxygen in the environment.

$$3UO_3(s) \rightarrow U_3O_8(s) + 0.5\,O_2\,(g) \qquad (1.27)$$

The reduction of U_3O_8 to UO_2 by H_2 is a surface controlled gas-solid reaction which proceeds according to contracting-sphere model involving desorption of water as the rate-limiting step [211, 251]. The conversion of U_3O_8 to UO_2 proceeds through formation of reaction intermediates (U_3O_7/ U_4O_9) which are unstable at temperature > 300 °C [251]. The net chemical reaction involved in the reduction of U_3O_8 is shown by Eq. (1.26).

1.9.3.3 Reduction of PuO_2

The reduction of PuO_2 [212, 242] may be carried out by heating (> 1500 °C) PuO_2 with reductants like carbon in helium atmosphere (1800 °C), dry hydrogen or in vacuum. The reduction of PuO_2 by dry hydrogen purified over titanium turnings gives Pu_2O_3 as shown by Eq. (1.28). PuO_2 can be reduced to Pu_2O_3 by heating at high temperature (1500 °C) with Pu metal turnings or chips Eq. (1.29).

$$2PuO_2 + H_2 \rightarrow Pu_2O_3 + H_2O \qquad (1.28)$$

$$3PuO_2 + Pu \rightarrow 2Pu_2O_3 \qquad (1.29)$$

1.10 Present Research Work

Recycling of nuclear fuel rejects has gained recently more attention worldwide [34-43, 199-201, 203-205]. The preliminary research in small laboratory scale or in household microwave ovens was carried out at AFFF. The encouraging results inspired us to upscale the work on industrial level. The microwave processing systems of industrial capacities were designed, fabricated and installed inside glove-boxes to work with plutonium bearing materials. The direct installation of the commercial microwave ovens could not be adapted in view of the tedious maintenance jobs inside the glove-boxes and the processing involving acidic and corrosive chemicals. Thus, separation and isolation of electrical/ electronic control and microwave generation parts were carried out. A total of four systems of different microwave output (0.8, 3, 6 kW) were glove-box adapted. The systems could be used for variety of applications like drying, dissolution, calcination, oxidation, reduction, decomposition, denitration etc. The systems were equipped for measurement of realtime temperature and power during the processing. The off-gas system for treatment of the process off gases was installed to meet the statutory guidelines.

The use of microwave in the recycling nuclear fuel scrap or rejects has indicated a tremendous potential to be explored [11, 13, 44]. The MOX fuel scraps shared a large quantum ~25wt% of the total material throughput (**Fig. 1.1**). Thus, a systematic study was planned to establish the efficient processes for recycling of these fuel rejects. The present thesis describes the development of microwave based methods for recycling of scraps or rejects generated in the industrial production of oxide and MOX fuels. The fuel scraps studied were UO_2, $(U_{1-y}Pu_y)O_2$, ThO_2, $(Th_{1-y}U_y)O_2$ and $(Th_{1-y}Pu_y)O_2$. The processes were developed for both chemically clean (CRO) and chemically impure (DRO) scraps. The extensive experimental work carried out was immediately implemented for recycling of large quantity of $(U_{1-y}Pu_y)O_2$ rejects on the industrial scale. Oxide/ mixed oxide fuel scraps more than 3 MT was recycled by establishing the processes based on the present study.

1.10.1 Problem Identification and Objectives

The recycling of characteristically different oxides (UO_2, PuO_2, ThO_2) and their mixed oxide nuclear fuel rejects was identified as the research problem. It was planned to exclusively use microwave heating technology after looking at their cutting edge advantages over the standard or conventional methods with the following main objectives.

1. Development of efficient methods for recycling of characteristically different MOX fuel rejects.
2. Development of a wet processing method based on dissolution and direct denitration. The main driving forces are minimal liquid waste generation and standard powder equivalent properties.
3. Development of dry processing methods for UO_2 containing rejects using microwave direct oxidation with objective to shorten the conventional prolonged heat process

cycles and to improve the products comparatively. The main motivations are their high production rates and no liquid waste generation.

4. The methods preferably should use 100% recycled powder for re-fabrication of fuel bringing out the maximum scrap recycling ratio (SRR: 1) offering several advantages to the fuel fabricators. SRR indicates the wt. fraction of recycled powder added to the total wt. of fuel batch fabricated.
5. Study the effects of various parameters which influence the product properties so as to tailor the characteristics of recycled powder.

1.10.2 Motivation behind Development of Novel Methods of Recycling

The conventional methods inherently had many limitations. This necessitated the development of novel methods or major modifications in the existing methods. The conventional wet routes showed many disadvantages (**Table 1.17**) however, these consistently produced powder owing either standard equivalent or better properties as compared to the dry routes. Due to this reason, the fuel fabricators had increased interest in the wet processing routes. A wet processing method where powder properties were function of a limited number of parameters and generate negligible liquid waste was desirable. Generally, the wet processing methods generate large quantities of liquid wastes and powder properties are sensitive to number of process parameters (**Table 1.10**).

The microwave direct denitration method was capable of converting nitrate solutions into respective sinterable oxide powders. The dissolution of sintered UO_2, $(U_{1-y}Pu_y)O_2$ fuel and refractory ThO_2 based fuels could be carried out via faster microwave assisted dissolution which was time consuming via conventional heat methods. The denitration potentially had the minimum number of process steps, parameters and required the least effluent treatment thus, outweighed the gelation and precipitation methods [16, 124]. The main advantages of the denitration process were simple and fast processing and no primary liquid waste generation. In the microwave denitration, temperature was main parameter which controlled the powder characteristics. However, in the precipitation-calcination methods, several parameters need to be controlled like pH, concentration of reactant and products, temperature of precipitation, sequence of addition, mixing rate etc. This is well known that the primitive thermal denitration was unable to produce sinterable UO_2 powder [69-71]. However, among the other acceptable denitration techniques for production of sinterable powders like fluidized bed denitration [110-111], ammonium-uranium double salt denitration [109] etc.; the microwave direct denitration offered distinct merits [14, 16, 124]. Thus, microwave dissolution and direct denitration was selected for the wet recycling of sintered scrap.

Microwave based direct denitration process has been in use for a long time in reprocessing plants for metal nitrate conversion into respective oxide powder. However, extensive studies were required in recycling of characteristically different scrap using microwave denitration to tailor the powder properties. The gaps were required to be filled by conducting a systematic study supported with detailed data. The microwave direct denitration of thorium based mixed nitrate solutions; though has been reported to be technically feasible, yet need to be studied in detail. No data was reported in the literature on the recycling of thoria based MOX rejects using microwave direct denitration process.

The conventional dry routes had several advantages (**Table 1.17**) like higher production rates, no liquid waste generation etc. However, these produced recycled powders that had inferior powder properties to the standard powders. A dry route was preferable where the powder properties could be improved than that obtained through electrical resistance heating based thermo-oxidative approach. Microwave heating can quickly attain very high temperatures and thermal runaways in the UO_2 pellets resulting in their cracking

[11, 66-68]. Thus, microwave based dry recycling through oxidative pulverization was pursued.

1.10.3 Recycling Methodologies

The most important application of microwave heating with regard to the present work was the faster dissolution of difficult to dissolve Pu and Th oxides/ mixed oxides and the direct denitration of so obtained nitrate solutions to sinterable grade powders without forming the 'mastic phase'; a technical lacuna in the primitive thermal direct denitration [14-16, 70-71]. Another was the efficient direct heating of nuclear material oxides [62-68]. The quick material heating with high ramp rates and thermal runaways (considered as disadvantage) were exploited for the oxidative pulverization of UO_2 or UO_2 containing MOX matrix [11, 66-68]. The wet recycling of oxide or mixed fuel rejects was planned with microwave dissolution and microwave direct denitration technique. In the dry recycling of rejects, microwave direct oxidation methodology was employed.

1.10.4 Scope of the Present Study

The present work scoped microwave based recycling of both the chemically clean and impure rejects of UO_2, ThO_2, PuO_2 and their mixed oxides. The rejected fuels were piled-up in various MOX fuel fabrication campaigns carried out at AFFF for example MOX fuel for BWR, PFBR, FBTR and experimental irradiation (**Table 1.11, Table 1.12** and **Table 1.13**) [31-32, 144-146, 202]. The rejected fuels were stored over many years. The recycling of various MOX rejected fuels was getting difficult through the conventional methods even non-feasible in high plutonium content MOX. The conventional methods were impractical in ThO_2 based MOX. In such circumstances the microwave based recycling has emerged as a potential prospect. The $(U_{1-y}Pu_y)O_2$ MOX in the entire range of plutonium (y: 0-1) was studied. The study also included the recycling of thoria based rejects $(Th_{1-y}U_y)O_2$, (y: 0-0.3) and $(Th_{1-y}Pu_y)O_2$ ($y < 0.1$) which were produced in fuel development programme for future thorium fueled reactors (AHWR, AHWR-LEU) and for experimental irradiation.

The development of processes for recycling of impure scrap was part of research scope as they constitute ~5 wt% share (**Fig. 1.1**). The impurity analysis in the impure scrap and source identification was carried out. Both, metallic and non-metallic impurities were determined and the deviation from the allowed limits (AL) was expressed in terms of impurity factors (IFs). Since, the several scrap types were characteristically different in terms of impurities (chemical nature, content etc.), various recycling methodologies were recommended. Some of the scrap types needed dry processing treatments and some required dissolution of the impure scrap in HNO_3 for purification. Thus, the dissolution behavior of the several types of impure scrap was investigated. Since, quantitative dissolution was required, fluoride catalysed and fluorideless dissolution through solid solution formation via sintering were compared.

On the basis of the systematic study carried out, flow sheets for 100 % recycling of rejects were developed. The product and intermediates were characterized for SSA, particle size, particle morphology using SEM, phase by XRD, metallic and non-metallic impurities, O/M ratio, density etc. The recycled powder suitability for fabrication was demonstrated by fabrication of experimental fuel batches initially and then implemented at the plant scale.

The entire research work was divided in two major parts; 1) development of methods for recycling of clean rejects and 2) development of methods for recycling of impure scraps. The detailed experimental description of methods for recycling of clean $(U_{1-y}Pu_y)O_2$ fuel rejects is presented in Chapter 4. Two processes were developed; one for wet recycling scheme and other in the dry recycling scheme. The wet recycling method was based upon microwave dissolution and direct denitration and called modified microwave direct denitration (Modified-MWDD) method. In the dry recycling scheme, microwave direct oxidation (MWDO) method based upon direct heating by microwave in two stages was developed. The recycling of clean ThO_2, $(Th_{1-y}U_y)O_2$, $(Th_{1-y}Pu_y)O_2$ fuel rejects via an integrated method is presented in Chapter 5. This method included integration of three basic approaches of recycling namely comminution, thermo-oxidation and microwave dissolution-direct denitration.

Development of methods for recycling of $(U_{1-y}Pu_y)O_2$ and thoria based impure scrap is elaborated in Chapter 6. The scrap characterization and recycling methodologies for impure production scrap were described. The process developed for recovery of impure scrap was annexed with that for clean scrap after purification. The entire process was called integrated process for recycling of fuel scrap which could recycle both types of scrap chemically clean and impure. The data related to recycling of a few experimental batches was presented using the integrated method. Chapter 7 is describing the low temperature processing applications of microwave on calcination and reduction of the recycled oxide and mixed oxide materials through developed methods. The low temperature processing has improved the properties of recycled powder significantly. The overall conclusions and the future line of developments are described in Chapter 8.

Chapter 2

MICROWAVE HEATING FUNDAMENTALS AND NUCLEAR MATERIAL PROCESSING

2.1 Introduction to Microwave and other Heating Techniques

Microwaves are electromagnetic radiations having frequency in the range 300MHz-300GHz. Microwave technology came into existence during World War-II while developing communication radars for military use [5, 252]. Subsequently, its applications have grown-up tremendously. Microwave oven is now a house hold item for cooking and a powerful industrial tool of heating variety of materials. However, there is an interesting story behind the discovery of heating effect of microwaves. The discovery is accidental; P.L. Spencer was studying high power microwave sources, he noticed the melting of a chocolate bar kept in his pocket while he leaned against an open waveguide. Since these beginnings, the heating capability of microwave has been recognized by scientific community. The first microwave oven was developed by P.L. Spencer in 1952 [253].

Fig. 2.1 shows the microwave region of the electromagnetic spectrum [254]. The electromagnetic waves used for communication, radiate power into space, whereas for the electroheat (heating using microwave) the power is often generated at much higher level and must be contained in the processing equipment. Indeed, the amount of microwave leaking is controlled within the specified limits for the safety of personnel and to avoid electromagnetic interference (EMI) with communication services. Thus, particular frequencies were assigned for applications of radiofrequency (RF) and microwave other than communications under Industrial, Scientific and Medical (ISM) band by Federal Communications Commission (FCC) in 1959. Applications in these bands were limited to RF process heating, microwave ovens and medical diathermy machines. In spite of the real purpose of ISM bands, there has been a rapid growth in its use in low-power, short-range communication platforms as Bluetooth devices, cordless phones and Wi-Fi network devices. For example, the 2.54 GHz is used in microwave ovens in addition to cordless phones, radars etc. In 1985, the FCC opened the ISM bands for use in mobile communications and wireless LANs. The ISM bands are generally open frequency bands, which vary according to different regions and also called unlicensed bands. However, the 2.54 GHz is commonly accepted band for worldwide operations. ISM frequency bands for RF and microwave are listed in **Table 2.1** [255].

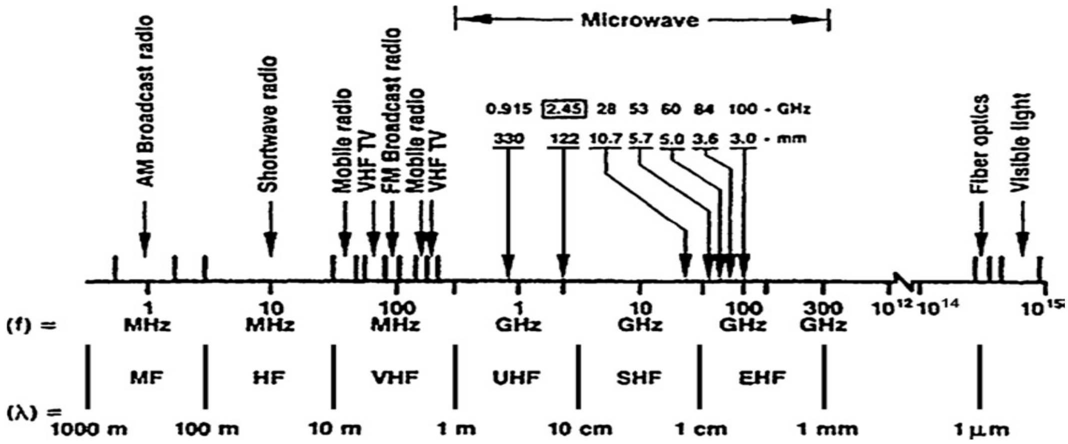

Fig. 2.1: The Electromagnetic Spectrum showing Microwave Region [254]

Table 2.1: Industrial, Scientific and Medical (ISM) Frequency Bands [255]

Frequency (MHz)	Wavelength	Frequency (MHz)	Wavelength
13.56	22.12 m	915	32.8 cm
27.12	11.06 m	2,450	12.2 cm
40.68	7.37 m	5,800	5.2 cm
		22,125	1.4 cm

2.1.1 Conduction Heating

This is the most common type of heating used worldwide. Conduction heating called resistance heating is the process by which the passage of an electric current through a conductor releases heat at the rate of I^2R according to Ohms's law, where I is current and R is electrical resistance. Conduction heating invariably uses alternating supply of 50-60 Hz [5].

2.1.2 Induction Heating

Induction heating is technique for the heating of electrical conductive materials like metals. When a conductor is placed in an alternating magnetic field, eddy current is produced due to electromagnetic induction. The eddy current heats the conductor. The induction heating generates heat within the object itself and high temperatures are achieved quickly. However, the eddy currents flow on the surface of the conductor and diminish towards centre, thereby material heats at the surface. The Induction heating uses alternating supply 50Hz-30 kHz [5].

2.1.3 Radiofrequency Heating

RF heating is eletroheating technique utilized to heat materials that are dielectric insulators [5]. When the material has high resistivity, the low frequency usually used (50-60 Hz) in conduction heating is ineffective in heat generation. This is obviated by increasing the frequency to the range 1-100 MHz, most often 27.12 MHz (**Table 2.1**). In RF heating system the RF generator creates an alternating electric field between two electrodes. The material to be heated is kept between the electrodes causing polar/ induced polar molecules in the material to continuously reorient to face opposite electrodes. Friction resulting from this molecular movement causes the material to rapidly heat volumetrically.

2.1.4 Microwave Heating

Microwave heating is an electroheating technique used for heating of dielectric insulators [5]. Commonly 915 and 2450 MHz frequencies (**Table 2.1**) are used in microwave heating in compliance with the international agreement with the principal aim of minimizing the EMI. Microwaves have electromagnetic energy that is converted into heat energy depending upon the type of interaction with the target materials. The heating of a material using microwaves depend on its dielectric and magnetic properties as the electric and magnetic field components interact with the material during irradiation [1-5].

2.2 Microwave-Material Interaction and Heating Mechanisms

Thermal effects of microwaves are basically the result of electromagnetic nature of the microwaves and dielectric properties of the materials [1-5, 45-47].

2.2.1 Dielectric Properties of Materials

The dielectric parameters of materials, their physical significance and attenuation of microwave power are described below [1-5, 45-47];

2.2.1.1 Complex Dielectric Permittivity

The degree of interaction (or absorption) of microwaves with a dielectric material is described in terms of complex dielectric permittivity or complex dielectric constant of the material as represented ε^* by Eq. (2.1). The real part of the complex dielectric permittivity is ε' called dielectric constant or relative permittivity and the imaginary part is ε'' , called dielectric loss factor.

$$\varepsilon^* = \varepsilon' - j\,\varepsilon'' \qquad (2.1)$$

where, $\varepsilon^*$is complex dielectric constant and $j = \sqrt{-1}$. The multiplication of dielectric constant of material and permittivity of free space ε_o (8.86 × 10^{-12} F/m) gives absolute permittivity of material in F/m.

2.2.1.2 Relative Permittivity or Dielectric Constant

The relative permittivity is a dimensionless number analogous to refractive index of an optical material. ε' represents the capacitive component of dielectric, hence the amount of electrical energy that can be stored within the dielectric material. The dielectric constant measures the ability of material to be polarized.

2.2.1.3 Dielectric Loss Factor

The power dissipation in the dielectric material analogous to capacitor is expressed by dielectric loss factor ε''. The power dissipation results in heating of the dielectric material. ε'' measures the ability of material to convert microwave energy into heat.

2.2.1.4 Loss Tangent Factor

The loss tangent ($\tan\delta$) indicates the ability of material to be polarized and gets heated-up under microwave field. $\tan\delta$ is expressed by Eq. (2.2) which upon rearrangement gives dielectric loss factor Eq. (2.3). The product $\varepsilon' \tan\delta$ is called loss product factor. Where δ is dielectric loss angle.

$$\tan\delta = \frac{\varepsilon''}{\varepsilon'} \tag{2.2}$$

$$\varepsilon'' = \varepsilon' \tan\delta \tag{2.3}$$

2.2.1.5 Dielectric Relaxation

Microwave heating is the result of dielectric relaxation [46]. In the dielectric materials, the charges move under the response to the electrical field of microwave (10^9 Hz). So there occurs polarization (electronic, atomic, molecular etc.), ionic conduction, dipole orientation and Maxwell-Wagner polarization. The movement of the charges and the polarization of molecules are restricted by surroundings. So there is time lag, known as relaxation time between the electric field of microwave and the constituent movement. This is called dielectric relaxation and is responsible for dissipation of energy as heat within the material. The dipolar rotation is most important mechanism for energy transfer at the molecular level.

2.2.1.6 Penetration Depth

As the microwave propagates through the material, its amplitude diminishes owing to absorption of power as heat in the material. The parameter D_p the penetration depth is defined to describe the attenuation of microwaves when these penetrate and propagate through a material. Penetration depth, D_p (m) is the distance inside the material where its electric field reduces by a factor of 1/e (0.368) of the electric field at the surface, Eq. (2.4):

$$D_p = \frac{c}{2\pi f\sqrt{2\varepsilon'}\left(\sqrt{1+\tan^2\delta}-1\right)^{\frac{1}{2}}} \tag{2.4}$$

For materials, where $\varepsilon'' \leq \varepsilon'$ or $\tan\delta \leq 1$ the above Eq. (2.4) gets simplified to Eq. (2.5):

$$D_p = \frac{\lambda\sqrt{\varepsilon'}}{2\pi\varepsilon''} = \frac{\lambda}{2\pi\sqrt{\varepsilon'}\times\tan\delta} \tag{2.5}$$

where, c is speed of light (3×10^8 ms^{-1}), λ is incident or free space wavelength of microwave (m), $\omega = 2\pi f$, ω is angular frequency (radians/ sec), f is microwave frequency (s^{-1} or Hz). The penetration distance of microwaves is negligible in reflectors like metals, infinite in transparent materials like vacuum and finite in absorbing materials like water.

2.2.1.7 Microwave Power Absorption and Attenuation

P is the power absorbed per unit volume (W/ m^3), provides the basis for heating by dielectric heating equation Eq. (2.6):

$$P = 2\pi f\varepsilon_o\varepsilon''\left|E_i\right|^2 + 2\pi f\mu_o\mu''\left|H_i\right|^2 \tag{2.6}$$

where, E_i is internal electrical field (V/m), μ_o is magnetic permeability in air (Hm^{-1}), μ'' is imaginary component of magnetic permeability and is known as magnetic loss factor. H_i is internal magnetic field (Am^{-1}). In the case of non-magnetic materials the contribution from the magnetic loss factor is negligible. Thus, Eq. (2.6) gets transformed to simple Eq. (2.7);

$$P = 2\pi f\varepsilon_o\varepsilon''\left|E_i\right|^2 = 2\pi f\varepsilon'\tan\delta\left|E_i{}^2\right| \tag{2.7}$$

P is proportional to f, ε', $\tan\delta$ and E_i and Eq. (2.7) describes the basic relationship between four parameters. The four parameters are interdependent. E_i further depends on the materials size, geometry, location, design and volume of the cavity. The ε' and $\tan\delta$ are two most widely used and measured parameters that describes the behavior of a dielectric under microwave field. During heating both increase with increasing temperature. The increase in ε' is due to increase in the polarisability caused by volumetric expansion. In contrast to ε', the $\tan\delta$ is far more affected by temperature. The rapid increase in the $\tan\delta$ is due to increase in the local electrical conductivity [2].

The microwave power attenuation follows exponential decay curve. The power P_y at a distance y from the surface of material is given by Eq. (2.8) [1].

$$P_y = P_o e^{(-2\alpha y)} \tag{2.8}$$

where, P_o is incident power at surface of material and α is called attenuation factor (dB m^{-1}).

2.2.2 Thermal Runaway in Microwave Fields

The loss tangent, $\tan\delta$, initially rises slowly with temperature upto critical point (T$_c$), beyond which it rises rapidly. This causes a condition of thermal runaway in microwave heated material. As $\tan\delta$ begins to increase rapidly, the material begins to absorb and heat more efficiently which in turn causes $\tan\delta$ to rise even faster. The net result is an exponential increase (runaway) in temperature. The temperature rise rate and the critical temperature (T$_c$) vary widely for different materials. **Fig. 2.2** is depicting thermal runaway condition for two different materials A and B at different power levels (a) and (b) [2].

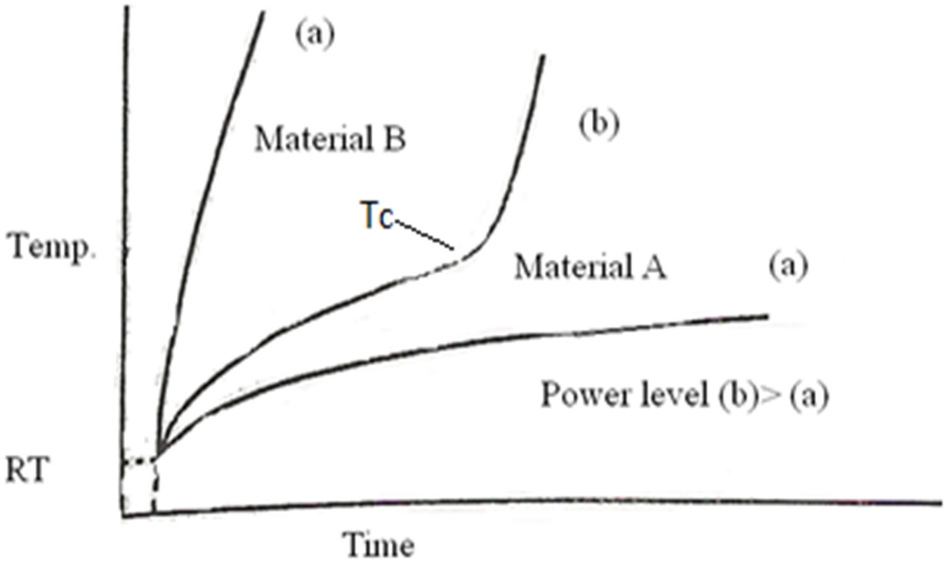

Fig. 2.2: A Depiction of Thermal Runaway in Microwave Field [2]

Thermal runaway can cause undesirable hot spots with in a material. The hot spots may also bring a condition of local melting. It can also be used to heat materials at rapid rates. The condition of the thermal runaways may be controlled by controlling or pulsing the microwave input power. The T_c are reported for room temperature microwave transparent Al_2O_3 at nearly at 800 °C [2, 256] and ZrO_2 at 600 °C [257]. For microwave absorber materials like SiC, UO_2 etc. the temperature rise is not linear rather exponential as the loss tangent increases with rise in temperature. In sintering of UO_2, the thermal runaways can cause cracking of the green compacts [11, 66-68]. **Fig. 2.3** shows the dependence of $\tan\delta$ with temperature for some room temperature microwave transparent materials [2]. The dielectric loss product factor $\varepsilon' \tan\delta$ increases with temperature in U_3O_8 [131] as shown in **Fig. 2.4**. Thus, with rise in the temperature of the material (**Fig. 2.3** and **Fig. 2.4**), the material absorbs the microwave efficiently. The increase in the microwave absorption and heating capabilities of materials with rise in the temperature is attributed to the combined effect of increase in the polarisability (the result of volumetric expansion) and in the local electrical conductivity with rise in temperature of the material.

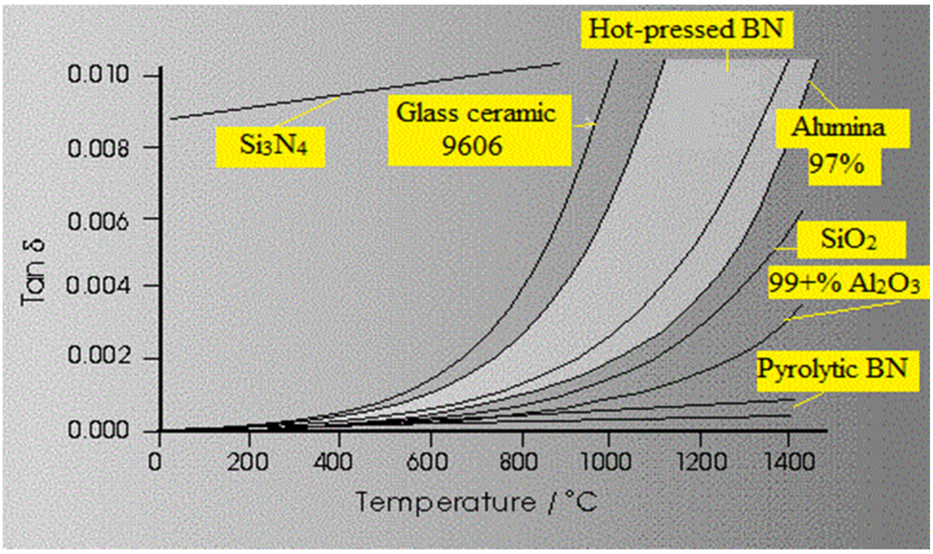

Fig. 2.3: Loss Tangent as Function of Temperature for Common Transparent Materials

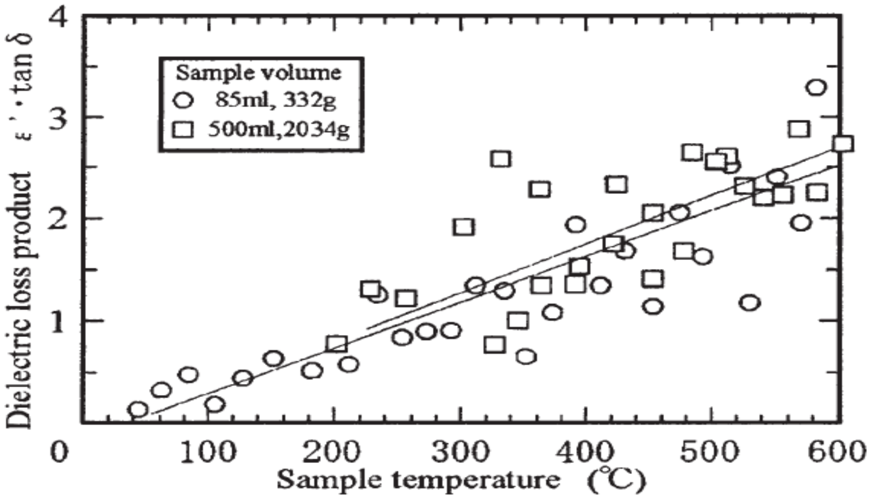

Fig. 2.4: Dielectric Loss Product Factor as Function of Temperature in U_3O_8

2.2.3 Categorisation of Materials on the basis of Interaction

Materials are categorized into three main classes on the basis of their response under microwave field as a) Reflectors, b) Absorbers and c) transparent [1-2, 5, 46]. **Fig. 2.5** shows the relationship between the dielectric loss factor and microwave power absorbed per unit volume (*P*) for some common materials [46].

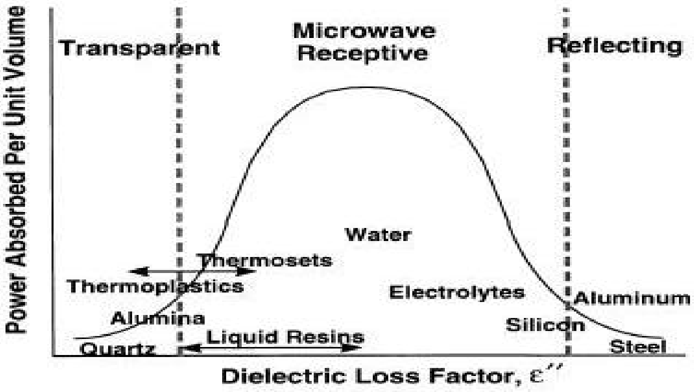

Fig. 2.5: Common Materials Catogorisation on the basis of ε'' in Microwave Field

2.2.3.1 Reflectors

The materials in which microwaves get reflected without or negligible energy absorption and exhibit negligible penetration depth are known as ‘reflectors’ or ‘opaque’. For example, metal sheets are microwave reflectors. These are also called ‘No loss’ materials.

2.2.3.2 Absorbers

The materials in which microwaves get absorbed (totally or partially) depending upon the value of the dielectric loss factor and subsequently get heated up are known as ‘microwave absorber’ or ‘microwave active’. For example, water, SiC, mineral acids, UO_2 etc. These are also called ‘high loss materials’ or ‘lossy materials’.

2.2.3.3 Transparent

The insulator materials through which microwaves pass without absorption at room temperature are termed as microwave ‘transparent’ or ‘low loss’ materials and are generally used for making of microwave processing vessels e.g. glass, Teflon, quartz and Si_3N_4.

2.2.4 Thermal Response of Important Materials in Microwave Field

2.2.4.1 Thermal Response of Common Materials

The dielectric properties of several common materials and their behavior at 2.45 GHz microwave are listed in **Table 2.2** [1, 5, 131]. Water and nitric acid can be used for hydrothermal processing using microwave. Si_3N_4, alumina, Teflon, glass and quartz glass are transparent at room temperature thus serves as microwave processing vessels. SiC being very good absorber is used as susceptor for hybrid heating of transparent materials.

Table 2.2: Dielectric Properties and Behavior of Common Materials at 2.45 GHz

Material	**Behavior**	**Temp. °C**	ε'	$\tan\delta$	$\varepsilon'\tan\delta$
Water ice	Weak absorber	-12	3.2	0.001	0.003 [5]
Water distilled	Strong absorber	25	77	0.169	13 [5]
HNO_3	Strong absorber	100	200	2.500	500 [131]
SiC	Strong absorber	20	30	0.367	11 [1, 5]
Si_3N_4	Transparent	25	7.8	$1.2\ x10^{-3}$	$9.5x10^{-3}$ [131]
Al_2O_3	Transparent	25	8.9	0.001	0.009 [5]
Bororsilicate glass	Transparent	25	4.05	0.001	0.005 [5]
Bororsilicate glass	Transparent	750	5.9	0.017	0.1 [5]
Fused quartz	Transparent	25	3.78	$2.6\ x10^{-4}$	0.001 [1, 5]
Polyvinyl chloride	Transparent	20	2.85	0.006	0.016 [5]
PTFE (Teflon)	Transparent	25	2.08	0.000	0.0003 [1, 5]
CCl_4	Transparent	25	2.17	0.004	0.0087 [5]

2.2.4.2 Thermal Response of Nuclear Materials

The oxides of U, Pu and Th respond differently in the microwave field. UO_2, U_3O_8 and PuO_2 are good microwave absorbers. UO_3, ThO_2, ZrO_2 etc. are room temperature transparent. The nitrate of Th, U and Pu are absorbing microwaves and subsequently can be decomposed into their oxides. The loss product factor, thermal response and potential heat processing applications of nuclear materials at 2.45 GHz are listed in **Table 2.3** [2, 15, 17-19, 257-259].

Table 2.3: Microwave Interaction Behavior of the Nuclear Materials at 2.45 GHz

Material	Behavior	Achievable Temp. (°C)	$\varepsilon' \tan\delta$	Heat Processing
UO_2	Strong absorber [2, 15, 17-18]	> 2600	7.46 [15]	Direct sintering, oxidation, reduction
U_3O_8	Strong absorber [2, 19]	> 2600	9.07 [15]	Direct sintering, oxidation, reduction
$UO_3.xH_2O$	Transparent [15, 258]	< 100	0.81 [15]	Need seed or temp. > 400 °C to heat
$UO_3.0.8H_2O$	Transparent [15, 258]	< 100	0.19 [15]	Require seed or temp. > 400 °C
PuO_2	Absorber [19]	>1000	---	Direct sintering, calcination etc.
ThO_2	Transparent [258-259]	<150	---	Need hybrid heating
ZrO_2	Transparent upto 600 °C [261]	< 150	---	Need hybrid heating upto 600 °C
$(NH_4)_2U_2O_7$	Absorber [258]	>400	---	Direct decomposition
AUC	Transparent [258]	< 200	---	Require seed
$UO_2(NO_3)_2$	Absorber [15]	> 400	6.85 [15]	Direct decomposition
$Pu(NO_3)_4$	Absorber [15]	>400	---	Direct decomposition
$Th(NO_3)_4$	Absorber [258- 259]	>300	---	Direct decomposition

---: Data not available

2.2.5 Microwave Heating Mechanisms in Non-Magnetic Materials

The non-magnetic materials are affected only by electric field component of the microwave. The two main mechanisms for non-magnetic materials are dipolar and conduction loss [1].

2.2.5.1 Dipolar Loss

Dipolar loss is major mechanism of heating in dielectric insulator materials like water and most of the ceramics. The material having permanent dipoles, induced dipoles or molecules with spatially separated charges when exposed to microwave field, the oscillating electric field agitates the molecular diploes. Since the microwave electric field oscillations is of the order of 10^9 Hz, the molecules have no longer time to follow it and just oscillate back and forth around a central point or start rotating. Participation of each individual molecule starts (higher D_p) and hence the phenomenon of oscillation or rotation occurs throughout the mass resulting in enormous molecular friction and instantaneous generation of heat.

2.2.5.2 Conduction Loss

Microwave causes the movement of ions of the material (ionic conduction). The charge distributions around each atom or molecule in the absorbing material and solvated ions resist this movement resulting in the generation of heat. The distilled water undergoes heating mainly via dipolar rotation. However, when salts are added, the conduction via movement of ionic charge carriers becomes significant component of heat generation. This is reflected in the increased value of ($\varepsilon' / \varepsilon''$) of distilled water and its 0.5 molal NaCl solution which are 77/13 and 68/54 respectively at 25 °C [5].

2.2.6 Microwave Heating Mechanisms in Magnetic Materials

The magnetic materials are affected by both electric and magnetic fields of microwave. The electric field imparts motion to free electrons, whereas magnetic field affects the electron spin, domain wall and their orientation [1].

2.2.6.1 Hysterisis Loss

Hysteresis loss is due to the disturbance induced by external magnetic field in the orientation of magnetic domains. The domains are oriented inside the bulk magnetic materials such that the net magnetic effect of material is zero. The domains try to align themselves in the direction of external magnetic field. In the oscillating magnetic field of microwave, the domain alignment tries to keep on oscillating. There is lag in the alignment of domains resulting in the hysteresis loss and generation of heat.

2.2.6.2 Eddy Current Loss

The eddy currents are produced in all the magnetic domains of the conductors (mainly at the surface) in oscillating magnetic field of microwave. The resultant eddy current for the bulk material may be considered as a net effect of all the eddy currents produced in the magnetic domains. Due to oscillating magnetic field of microwave, the resultant eddy current changes direction bringing energy loss in the form of heat in the bulk.

2.2.7 Types of Microwave Heating

2.2.7.1 Direct Heating

This is the most common type of heating which is used to heat the materials that couples with microwave. This kind of heating usually leads to reverse thermal gradients (inside hotter than the surface) in the bulk materials due to more heat losses from the surface. However, the heat insulation improves the temperature gradients. The reverse thermal gradients are not usually observed in direct heating of solutions due to convection currents.

2.2.7.2 Hybrid Heating

Microwave heating is used in hybrid mode to overcome the reverse thermal gradients and heating of non-microwave absorbers. The hybrid heating is completed in three steps as i) microwave absorber heating, ii) conventional heating of non-absorber via hot absorber and iii) microwave heating of the target material above T_c, A depiction of temperature gradients in conventional, microwave and microwave hybrid heating is shown in **Fig. 2.6** [260].

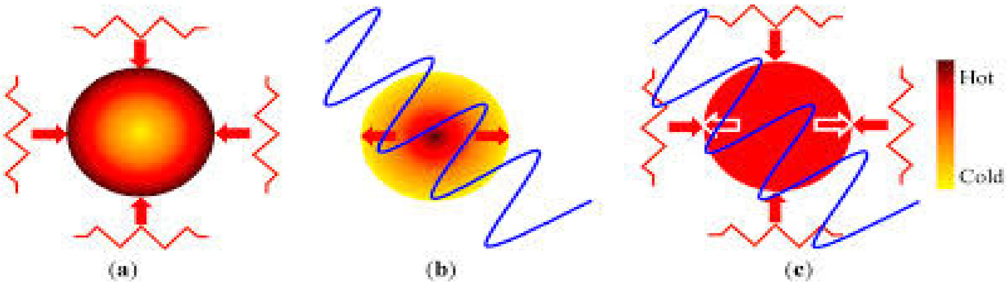

Fig. 2.6: Temperature profile within the Sample in (a) Conventional Heating, (b) Microwave Heating and (c) Microwave Hybrid Heating

2.2.8 Salient Features of Microwave Heating

Having an elaborate discussion on fundamentals viz. microwave interaction, generation, transmission and processing, the salient features of microwave heating are listed in **Table 2.4.**

Table 2.4: Salient Features of Microwave Heating and Their Description

Feature	Description
Direct material heating	Material under microwave irradiation heats-up due to direct coupling.
Non-contact heating	As microwave can travel in vacuum, air etc.; material need not be in contact with microwave generator.
Bulk heating	Microwave penetrates the materials deep inside and cause bulk heating.
Rapid heating	Heating starts instantaneously contrary to conventional where medium is required for conduction of the heat.
Quick start and stop	Can be turned on and off instantly, ability to pulse the power for precise control.
Atmosphere non-specific	The microwave heating is independent of atmosphere types corrosive, reducing, oxidizing etc. The conventional heating uses atmospheric specific heating elements and process vessels.
Clean, Environment friendly	No greenhouse gas emissions
Material selective	Microwave is not a universal heating method, only selective class of materials (absorber) is heated
Material specific heating	Each material cannot be heated to same temperature.
Thermal runaways	Can lead to unwanted hot spots; even localised melting
Reverse thermal gradients	Inside hotter than the surface of bulk solid materials

2.3 Components of Microwave Heating Systems and Microwave Measurement

2.3.1 Microwave Generator and Working Principle

The magnetrons, travelling wave tubes and klystrons are microwave generators [5, 46] of which magnetrons are most commonly used as they are mass produced at lowest cost.

2.3.1.1 Structure of Magnetron

Magnetron uses resonant structures to generate fixed frequency microwave [5]. The magnetrons used in domestic microwave ovens have power output typically 600-1200W. The laboratory scale ovens have output power in the range 600-2000W, whereas the industrial magnetrons generate > 2000W. **Fig. 2.7** shows photograph of a water cooled magnetron. **Fig. 2.8** is cutaway view of 0.8kW air cooled magnetron depicting its internal components.

The anode is a hollow cylinder with a number of anode vanes extended inwards. The open trapezoidal shaped areas between each of the vanes are called cavities. A high vacuum 10^{-6} mm of Hg is maintained. The filament (cathode) is thoriated tungsten electrode. The magnetic field is provided by permanent magnets or electromagnets.

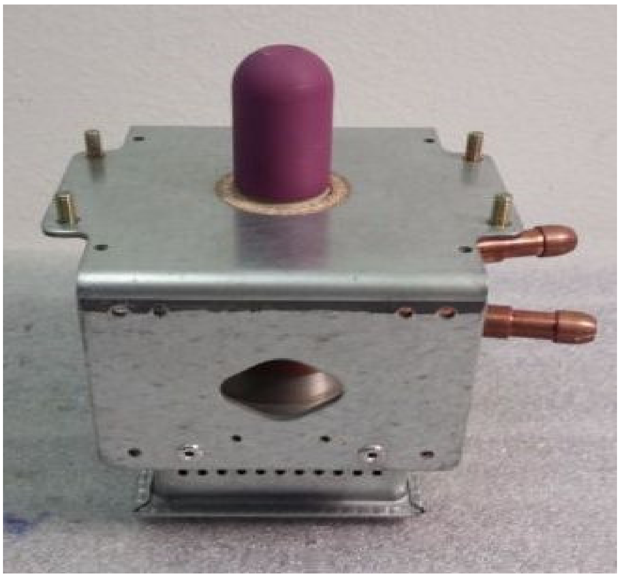

Fig. 2.7: Typical 3 kW Water Cooled Magnetron

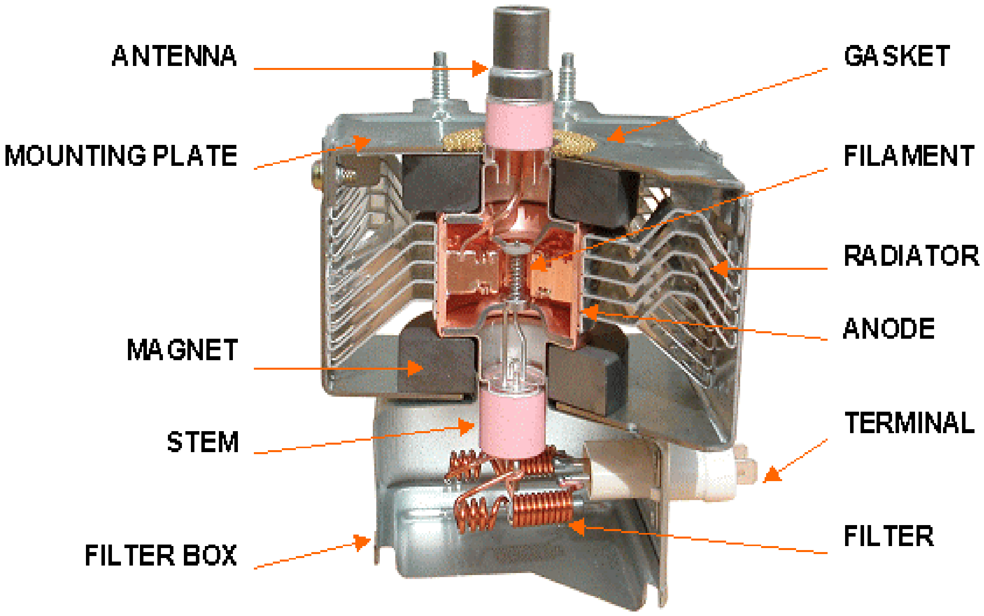

Fig. 2.8: Cutaway View of 0.8 kW Air Cooled Magnetron

2.3.1.2 Working of Magnetron

The principle of magnetron operation is based on motion of electrons under the combined influence of electric and magnetic fields [5]. The process begins with a low voltage being applied to the filament, which causes it to heat up and emit electrons by the process of thermionic emission. The electrons are repelled away from cathode by a negative 4 kV DC or above (2-20 kV) applied across the central cathode and anode. The electrons from the cathode travel straight towards the positive anode. The force (F) on the charge q in the electric field (E) is given by Eq. (2.9).

$$F=qE \tag{2.9}$$

As electrons move towards the anode, they meet the perpendicular magnetic field. The force on charge q moving with velocity v in magnetic field (B) is given by Eq. (2.10).

$$F=q(v\times B)=qvBSin\theta \tag{2.10}$$

The net effect of the two forces is such that the electron proceeds to anode in expanding circular path rather than straight (**Fig. 2.9**). This whirling cloud of electrons interacts with the anode and produces an alternating current (I) to flow in the resonant cavities (**Fig. 2.10**). As a cloud of electrons approaches an anode vane, it induces a positive charge on that segment which diminishes as the electron cloud passes away. This process repeats itself in the next segments. Each cavity behaves as an inductive-capacitive (LC) circuit and all the cavities as equivalent of a series of LC circuits having frequency (f) given by Eq. (2.11). The oscillation of charge and current at 2450 MHz starts at the antenna and electromagnetic waves called microwaves are radiated.

$$f=\frac{1}{2\pi}\sqrt{\frac{1}{LC}} \tag{2.11}$$

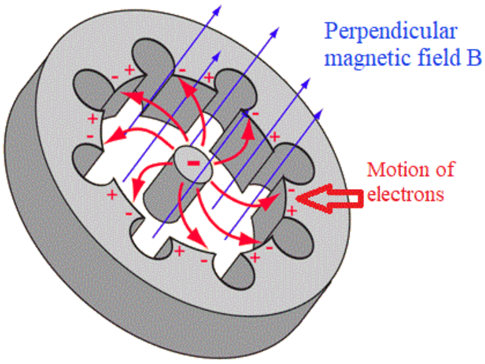

Fig. 2.9: Path of Electrons under Combined Effect of Electric and Magnetic Fields

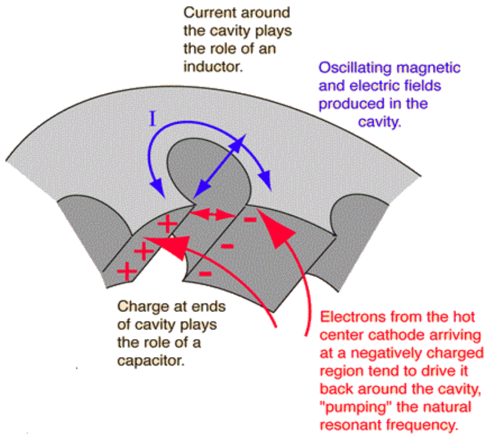

Fig. 2.10: Anode Cavity and Vane showing the Oscillating Current (I) and Charge at Resonant Frequency

2.3.1.3 Magnetron Characteristics

The frequency of microwave generated by a magnetron is most important characteristic. The frequency is used to decide the application of the microwave and is regulated internationally (**Table 2.1**). The conversion efficiency of input electrical power to the usable microwave output power is termed as tube efficiency. Generally, the magnetron has efficiency ~70-75% which goes down with time due to loss of cathode emission.

Cooling of the magnetron is an important feature essentially required for reliability and long life. The anode of the magnetron becomes hot due to bombardment of electrons from the cathode. This may lead to a situation of severe melting of the anode in absence of cooling. Thus, either air cooling (usually in lower power magnetrons) or water cooling is provided on the magnetrons during operation.

2.3.2 Components of Industrial Microwave Heating System

The magnetron is discussed in the above section (§ **2.3.1**). The other components which include the transmission components as launcher, isolator, directional coupler, tuner, waveguide etc. and the processing component called cavity or applicator are discussed hereafter [5, 46, 261-262].

2.3.2.1 Microwave Transmission Components

A launcher is a mechanical component that launches microwave generated from magnetron antenna into the waveguide. When materials are heated that are not good absorbers of microwave, a significant amount of power is reflected back to the microwave source. The magnetron must be protected from the damaging effects of reverse power. This is usually accomplished using a 3-port circulator and a dummy load (often water), often called an isolator when used together. The directional couplers are devices used to couple power from the waveguide at a reduced value to facilitate measurement of power or frequency. A multi-stub tuner (three stubs or four stubs) is a very important mechanical waveguide component used for matching of load impedance to that of magnetron, thereby reducing reflected power and maximizing the coupling of forward power to the load.

The waveguides are hollow metallic enclosures either rectangular or circular cross sections. The choice of waveguide size depends mostly on operating frequency and power rating. **Table 2.5** lists rectangular waveguides used for two ISM frequencies most commonly used for microwave heating; 2450 MHz and 915 MHz [5, 46, 262].

Table 2.5: Rectangular Cross Section Waveguides for Microwave Transmission

Inside dimensions (inches)	ISM frequency	IEC Designation	RCSC (UK) Designation	EIA (US) Designation
2.84 x 1.34	2450 MHz	R32	WG10	WR284
3.40 x 1.70	2450 MHz	R26	WG9A	WR340
4.30 x 2.15	2450 MHz	R22	WG8	WR430
9.75 x 4.875	915 MHz	R9	WG4	WR975

IEC: International Electrotechnical Commission, RCSC: Radio Components Standardization Committee and EIA: Electronic Industries Alliance

Although, the frequency range for WR284 is 2.60-3.95 GHz, this size is often the preferred choice for 2.45 GHz operation upto 6kW. WR340 waveguide is used at power levels upto 20 kW while WR430 is recommended for higher power levels.

The waveguides based transmission systems in microwave incorporate bends (usually 90^o) invariably. Bends are designated as E-plane and H-plane bends. E-plane bend involves the side smaller wall of the waveguide remaining in the same plane. The H-plane bend has broad wall of the waveguide remaining in the same plane. The integration of various components of waveguides is achieved through specified flanges.

2.3.2.2 Material Processing Applicators

The applicator or cavity is a physical metallic wall boundary for the interaction between microwave and material. The design of applicators [5, 46] is critical in microwave heating because microwave energy is transferred to materials in the applicators. The heating uniformity within the materials undergoing microwave heating is directly connected to distribution of microwave within the applicator. Two types of applicators are commonly used; single mode applicator and multimode applicator. Single mode applicator is essentially a waveguide with one resonant mode where microwave field strength is high. The cavity having several resonant modes at the same time is called multimode applicator. Consequently, these are usually much larger than single mode applicators. Multimode applicators are more versatile than single mode for batch operations and processing of large and complicated shape objects. Thus, by far multimode cavities are common processing systems used in industrial applications including the domestic microwave oven. Presence of several modes results in multiple hot spots within the processing chamber. To reduce the effects of hot spots by improving field homogeneity several techniques are employed; increasing the cavity dimensions (usually not preferable), use of turntables, use of mode stirrers and multiple microwave inputs [46].

2.3.3 Microwave Measurement

Measurement of microwave power (W) or power density (Wm^{-2}) and frequency (Hz) are required to be carried out. The microwave forward and reflected powers are process parameters thus, measured in the transmission components and in the processing applicator. Similarly, the measurement of microwave leakage from the transmission and application components is essentially required from safety point of view [5, 255, 263].

2.3.3.1 Power Output of Magnetron

The power output of magnetron experimentally can be determined by measuring the temperature rise of material large enough to absorb essentially all the energy delivered to the microwave cavity [264]. The standard practice involves measuring the rise in temperature of 1 L of water at a given power (calculated from electrical parameters) for 2 min. The power test is more accurate if the starting temperature is 20±2 °C. The power output P (in watts) is calculated using expression Eq. (2.12).

$$P\ (output\ in\ watts) = \frac{C_p K\ \Delta T\ m}{t} \qquad (2.12)$$

where, K is the conversion factor, C_p is specific heat capacity (J Kg^{-1} $^oC^{-1}$), ΔT (in ^{o}C) is rise in temperature, m is mass of material (in Kg) and t is time in seconds. For water, C_p: 4186 J Kg^{-1} $^oC^{-1}$, Density: 1Kg L^{-1}, and K is ~1, the Eq. (2.12) can be simplified to Eq. (2.13).

$$P\ (output\ in\ watts) = 35 \times \Delta T \qquad (2.13)$$

2.3.3.2 Power Measurement using Bolometers and Thermocouple

Measurement of microwave power is based on the detection of microwave by crystal diodes (comparison of power levels) or by the measurement of heat produced (absolute power levels) when a certain amount of microwave power is dissipated in a load [263].

The bolometers are used to measure absolute power. Microwave power incident on the bolometers raises its temperature. The change in the temperature causes variation in its direct current resistance. There are two general types of bolometers; a) Positive temperature coefficient type are conductors e.g. barreter and b) Negative temperature coefficient type are semiconductors e.g. thermistor. The simplest way is to place the bolometer in one arm of the Wheatstone bridge. The unbalance current is indicated by the meter which is calibrated directly in watts. A thermocouple can also be employed for absolute measurement. The tip of thermocouple can be made-up of microwave absorber, where temperature rise subsequent to interaction establishes a temperature difference between the heated and the cold junction.

2.3.3.3 Power Measurement using Crystal Diode

The diodes that are used for detection of microwave are either point contact diodes or metal semiconductor schottky barrier diodes. Output current is proportional to square of the electric field at the location of the diode. Thus, output current is direct measure of power.

2.3.3.4 Frequency Measurement

Microwave frequency can be measured by mechanical and electronic techniques. The mechanical devices commonly use circuit elements as slotted lines and resonant cavities. The electronic devices are frequency counters which compare known standard frequency with unknown microwave frequency and have considerably higher accuracy.

2.3.4 Temperature Measurement in Microwave Fields

Temperature is the most important parameter to measure in a microwave environment [254]. Inaccuracies in temperature measurement or perturbation of the microwave field by temperature sensors can lead to erroneous indications of process temperature. The temperature measurement in microwave presents several difficulties as:

1. Temperature measurement must be made directly within the sample and not in its vicinity. Microwaves heat the sample itself and not the surroundings and hence temperature probes must maintain good contact with the sample.
2. Thermal gradients developed during microwave heating make measuring sample temperature using a single probe difficult. The surface temperature may be different from the core value.

3. The presence of metallic thermocouple temperature probes in microwave environment can cause excessive localized heating (arcing), particularly at the tip.
4. Optical techniques such as pyrometers need knowledge of material emissivity.

Thermocouples and optical measurement techniques are most often used in microwave processing [254, 265]. When metallic temperature probes are used in the microwave environment, EMI problems may occur. They can locally distort the electromagnetic fields, conduct heat away from the sample and electrical discharge due to concentration of the electric field lines at the tip of the conducting probe. The concentration of electric fields at the tip is very high and leads to ionization of the air causing arcing. Alumina sheathed thermocouples have been used to reduce the effect of localized heating [266].

Optical temperature measurement techniques measure surface temperature, which may be significantly different than internal temperatures due to microwave penetration and surface heat losses. Second, the accurate knowledge of the object's emissivity and its variation with temperature and frequency is possibly the most serious source of error in optical pyrometric measurement. The optical fiber based measurement using Fiber Braggs Grating (FBG) sensor has demonstrated the accurate measurement of temperature in the intense microwave field [267].

Type-K[9] thermocouples inside the stainless steel sheath (rounded tip to avoid arcing) and inside the recrystallized alumina sheath are employed successfully in the temperature measurement. Rounding the tip of the stainless steel sheath avoids the arcing at the tip. The alumina sheathed thermocouple does not show arcing related problem in the

---

[9] Type -K thermocouple is composed of chromel (90% nickel, 10% chromium) and alumel (95% nickel, 2% aluminum, 2% manganese and 1% silicon) junction and is most common thermocouple upto temperature 1250 ºC.

microwave field [266]. The reliability in the measurement of temperature is increased by using two or more thermocouples. Further, reliability can be increased by comparing the response of thermocouples by switching the microwave power on and off. There should not be sudden large decrease in temperature as microwave power is switched off and sudden temperature surge while microwave power is projected which is attributable to voltage breakdown and subsequent arcing [254].

2.4 Adaptation of Microwave for Nuclear Material Processing in Glove-Boxes

The processing of nuclear materials demands adaptation of equipments inside special enclosures (fume-hoods, glove-boxes or hot-cells) due to their radiotoxic nature (**§1.3.3**).

2.4.1 Glove-Box and its Ventilation System

The philosophy of handling plutonium is based on the multiple redundant containment systems. The glove-box and its ventilation system are vital for handling of plutonium [100-104]. Glove-box prevents operators from inhaling radioactive particulates. The glove-box forms the primary containment for nuclear materials. Work with plutonium requires glove-boxes of high integrity typically with leakage rates <0.05% (dry powder handling) and < 0.1% (liquid handling) of glove-box volume per hour. The ventilation system of the glove-box serves as the secondary containment also called dynamic containment. The flow of air into the glove-box is once-through. The third containment is the building itself which is the last barrier between radioactive material and, the environment and public. **Fig. 2.11** shows the 3D-schematic of a typical plutonium handling glove-box and its ventilation system.

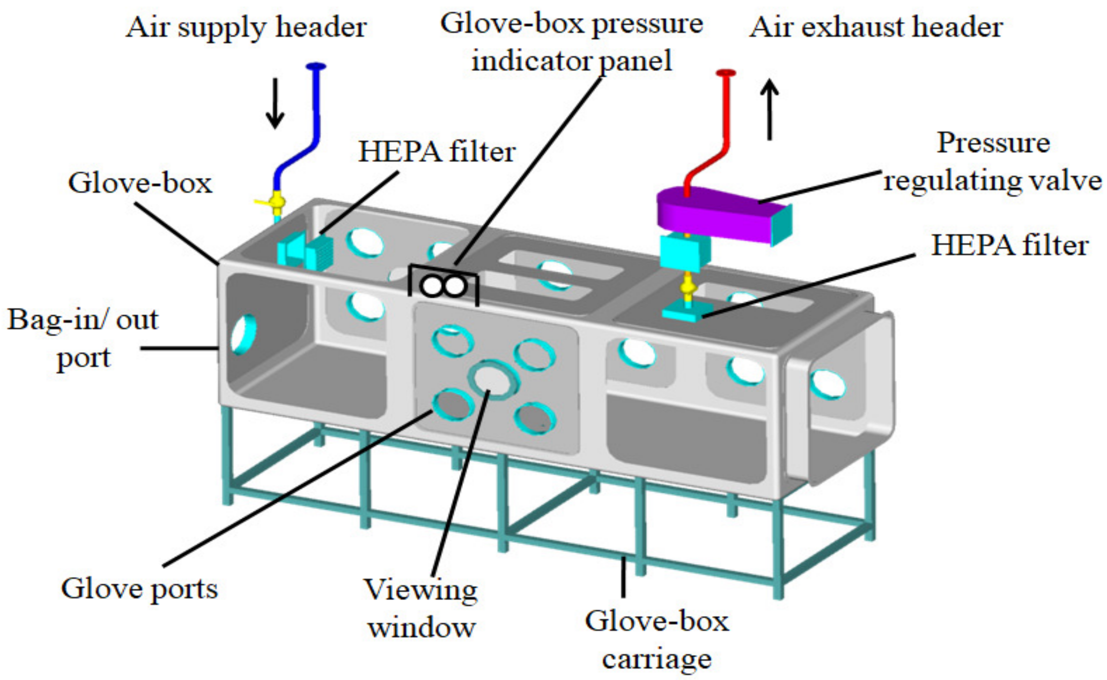

Fig. 2.11: Plutonium Handling Glove-Box and its Ventilation System

Work inside the glove-box is carried out by rubber gloves installed on the glove-ports. A glass viewing window is provided on the front panel to see inside the glove-box. The glove-boxes may also be installed with a glass front panel to improve the visibility. The operation of material entry into (and out of) the glove-box is carried out through a common Bag-in/ out port. A HEPA filter is installed in the exhaust of the glove-box. The exhausted air is sucked by air exhaust header which has negative pressure head nearly -250 mm of water gauge. The operating pressure of glove-box is maintained at -25 mm of water gauge (WG) by a pressure regulating valve. The flow of air into the glove-box is maintained so as to achieve nearly 2-3 air changes per hour of glove-box volume. The air is supplied into the glove-box by air supply header through a HEPA filter (inlet filter). Thus, HEPA filters installed on the inlet and on the exhaust of the glove-box practically retain almost all the particulate activity inside the glove-box even in case of positive pressurization or loss of ventilation. The pressure of the glove-box and the differential pressure across the exhaust HEPA filter are continuously monitored by pressure gauges (Magnhelic$^{®}$ Gauges) on the glove-box pressure indicator (GBI) panel. The air flow into the glove-box is continuously measured by flow meters (Rotameters) installed at the air inlet. The mandatory provision of emergency flow >32 m min^{-1} through a glove-port (diameter 200 mm) takes care of inadvertent condition of a glove slippage, glove cut or puncture while working.

2.4.2 Limitations of Commercial Microwave Ovens

The commercial microwave (domestic or laboratory) oven is usually a single entity where the electronic and electrical control parts are installed on the applicator. The maintenance jobs become quite difficult or sometimes impossible by installing such commercial microwave ovens inside the glove-box. The scenario turns more critical if the process involves acidic and corrosive chemical processing. The commercial ovens become useless in one or two acidic processings. Thus, stainless steel becomes choice for material of construction for microwave ovens. Since, no electronic or electrical component can withstand long in the acidic atmosphere; separation of the control parts from the applicator is essentially needed for glove-box installation.

2.4.3 Indigenous Microwave Heating Systems

Microwave ovens offer several distinct advantages for the processing of nuclear materials in glove-box and in the corrosive environments. The biggest is that the microwave generator and the control panels can be separated from the applicator. Another is that the microwaves are fed upto the applicator through air leak tight cum microwave transparent waveguide components from remote generators. The applicator is simply a box which hardly needs any maintenance. The schematic diagram of a microwave heating system and its glove-box adaptation perspectives are shown in **Fig. 2.12. Fig. 2.13** shows the photograph of an indigenously developed 6 kW (MHS-6) system at AFFF.

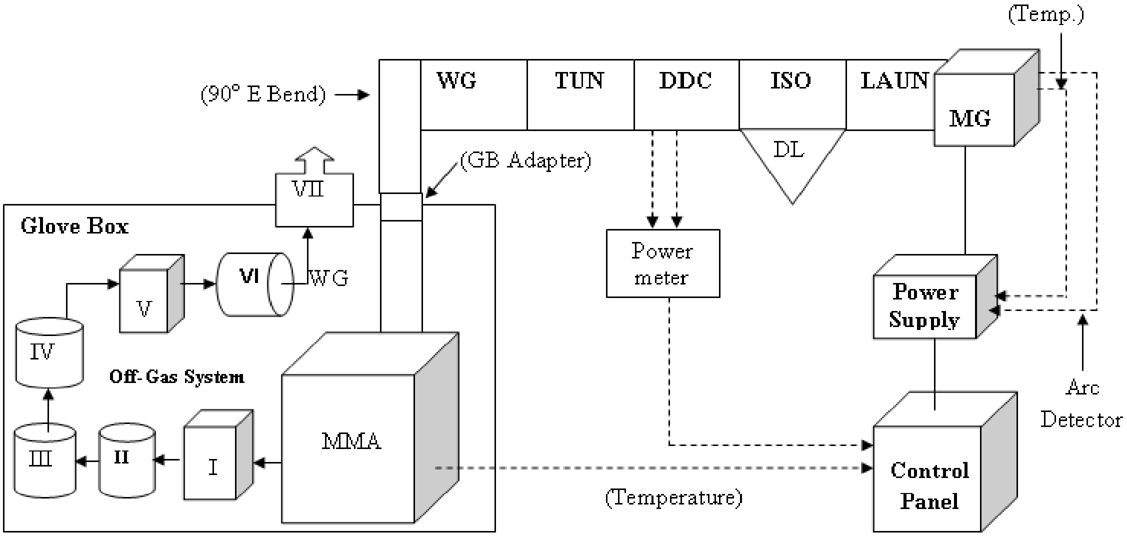

MG: Microwave Generator; **LAUN:** Launcher; **ISO:** Isolator; **DL:** Dummy Load; **DDC:** Dual Directional Coupler, **TUN:** Tuner; **WG:** Wave Guide; **MMA:** Multimode Applicator

Off-Gas System- I: Primary condensation tank; **II:** Water scrubber; **III:** Alkali scrubber; **IV:** Empty Tank; **V:** Chiller heater; **VI:** HEPA filter and **VII:** Main Exhaust line

Fig. 2.12: Schematic of Glove-box Adapted Microwave Heating System

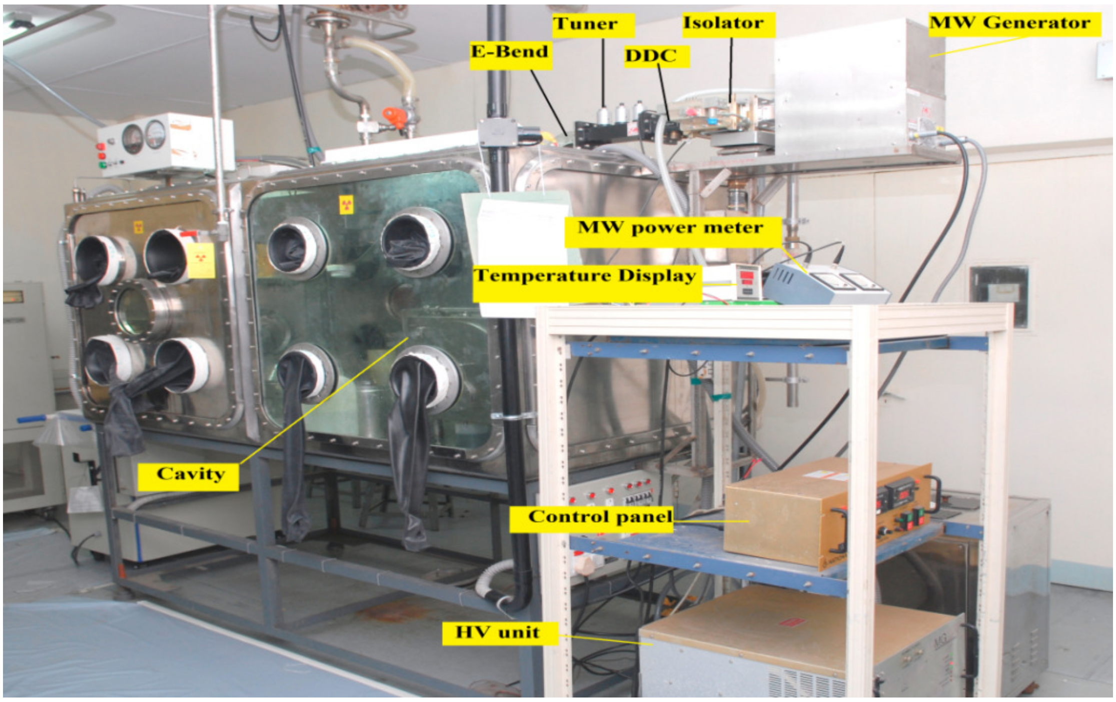

Fig. 2.13: A Glove-Box Adapted 6 kW Microwave Heating System (MHS-6)

2.4.4 Indigenous Microwave Processing Applicators

Indigenous microwave applicators made-up of stainless steel have been installed at AFFF. These are specially designed to work inside glove-boxes for variety of applications like drying, dissolution, calcination, oxidation, reduction, decomposition, denitration, sintering etc. The 3D model and photograph of typical microwave applicators used for multi processing applications involving nuclear materials are shown in **Fig. 2.14** and **Fig. 2.15** respectively.

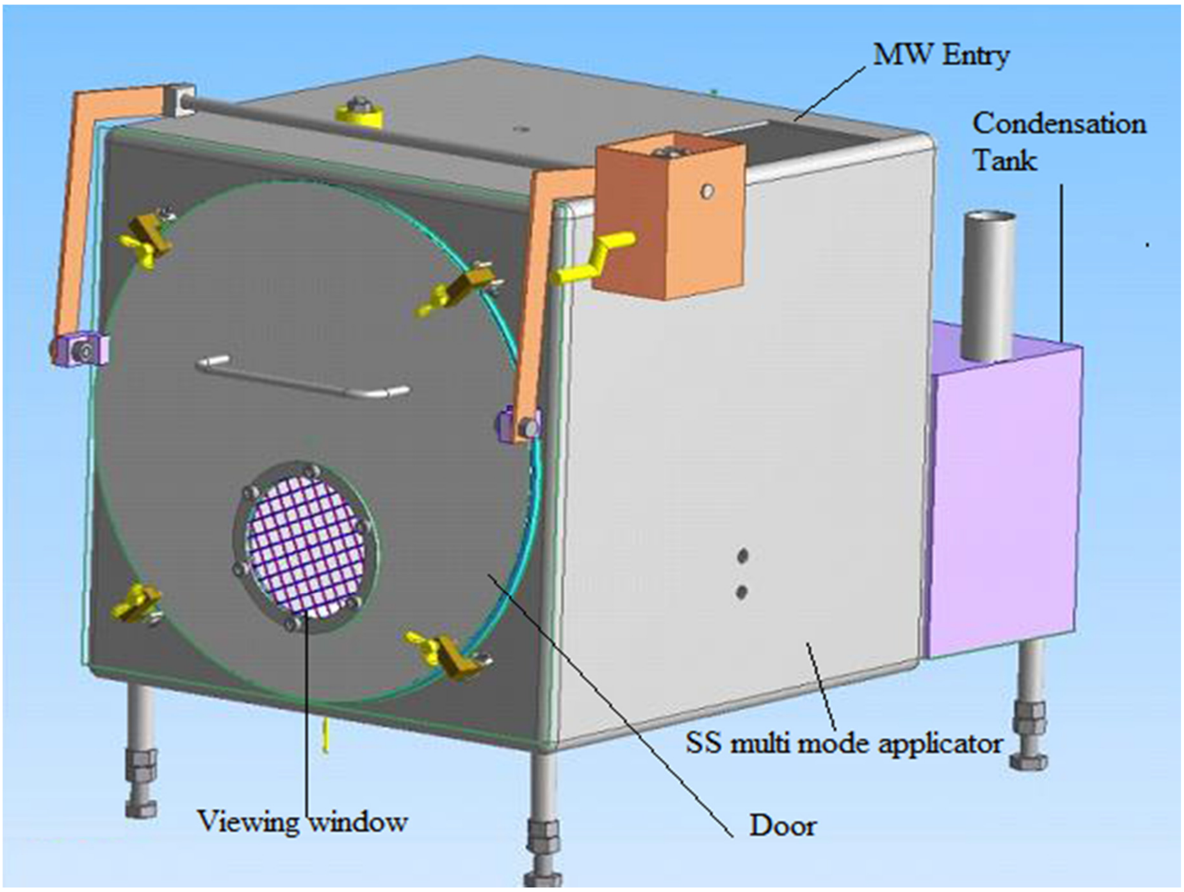

Fig. 2.14: 3D Model of a Typical Applicator for Nuclear Material Processing

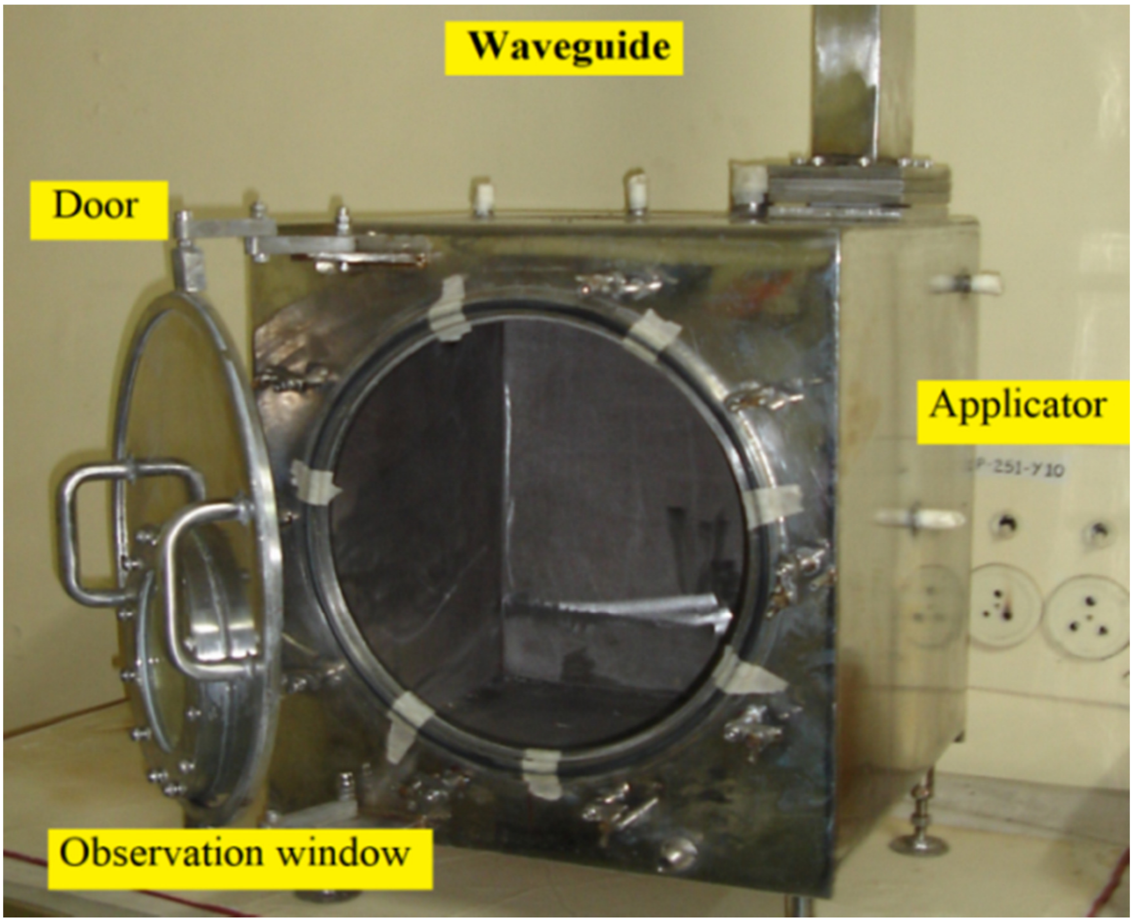

Fig. 2.15: Photograph of a Typical Indigenously Fabricated Applicator at AFFF

2.5 The Microwave Effect

Numerous observations have been reported in the literature about accelerated reaction rate (mass transport, solid-state reaction rates, synthesis rates etc.) during microwave thermal processing of a variety of ceramics, polymer materials and organic/ inorganic synthesis as compared to the conventional thermal (resistance heating, induction heating etc.) processing. These observations of kinetic enhancements in microwave processing have been broadly called the "microwave effect" [254, 268]. For example the densification rates (and therefore the rate of mass transport) in sintering of UO_2, alumina etc. are sometimes enhanced by an order of magnitude or more as compared to the conventional thermal processing [67-68, 269-

270]. Thus, the process times and temperatures are drastically reduced in microwave thermal processing. The observation of diffusion rates data of tracer $^{18}O^{2-}$ ions into the surface of sapphire single crystals heated in microwave ovens and conventional ovens indicate diffusion rate enhancements of upto two orders of magnitude [271]. The most prevalent reports of microwave effects have been about the acceleration of reaction rates. Other processes showing the microwave effect are accelerated grain growth, annealing, combustion synthesis, calcination and solid-state reactions. As a general summary, the kinetics of synthesis and sintering reactions are augmented by 2 or 3 orders of magnitude or even more when conventional heating is substituted for microwave radiation. There have also been a few reports in which no effect of the microwave radiation on the kinetics was observed [254]. The scientific community proposed two competing explanations for the apparent microwave effects; (1) that a 'non-thermal' mechanism is responsible for the enhanced reaction rates and (2) that the researchers observing these apparent reaction rate enhancements were misinterpreting their results due to incomplete or inaccurate knowledge of the thermal state (internal temperature) of the microwave-heated specimens called 'thermal' effect.

The experimental and numerical investigations were made by Booske et al. [268] on the 'non-thermal' mechanism of the microwave effect. They [268] have established the fact that the microwave electric fields induce a nonlinear ponderomotive driving force[10] for ionic mass transport near surfaces and structural interfaces (e.g., grain boundaries) in ceramic materials. This driving force can influence reaction kinetics by enhancing mass transport rates. The observation of 'microwave effect' further depends upon the fact whether microwave ponderomotive force exceeds or is smaller than other thermo-chemical driving forces. The 'non-thermal' effect of enhanced ionic motion during microwave heating in

---

[10] A ponderomotive force is a nonlinear force that a charged particle experiences in an inhomogeneous oscillating electromagnetic field at any abrupt non-uniformity in medium, such as free surfaces, grain boundaries, or amorphous-crystalline structure interfaces.

polycrystalline solids was attributable to non-thermal phonon distribution excited by the microwave field and explained the anomalous reduction of activation energy for diffusion and overall faster kinetics [272].

Zhao et al. [8], proposed both the viewpoints to interpret the microwave acceleration of the reaction rate and drastic reduction in the processing time. The first viewpoint suggests that the tremendous acceleration is due to 'non-thermal' activation under microwave field as discussed above [268]. The microwaves have 'non-thermal' interaction with reactants, which considerably decrease the activation energy of reaction [273-274]. The second viewpoint proposed by Zhao et al. [8], states that the kinetic enhancement results are due to microwave 'thermal effect [275]. The microwave 'thermal' effect advocates about the higher internal temperature causing superheating and larger local temperature during microwave heating however, showing a lower overall reaction temperature.

Therefore, there may be several processes for interaction of the reactants under microwave field; the 'non-thermal' effect which could reduce the activation energy of the reaction, the 'thermal' effect where the superheating makes the local temperature higher than the reaction conditions, the large temperature gradient generating strong thermal currents between solids and liquids assisting the large mass transport [276]. It is now widely accepted that the 'microwave effect' exists, however the satisfactory physical explanations are not in agreement.

2.6 The Economic Aspects of Microwave Heat Processing

Commercialization of the microwave technology will not only be based on the areas of applications and the properties of the materials produced but also on its economics. The evaluation of economics of microwave heating is complex since the efficiency of microwave processing varies from one material to another depending upon the dielectric and magnetic properties. The summary from the literature on the evaluation of the economics of microwave heating is briefly discussed below [5, 254]. The economic issues may be examined in terms of:

1. Cost of capital equipment by comparison with conventional equipment; microwave processing equipment is almost always more expensive.
2. Operating costs; energy requirement, replacement, maintenance etc.
3. Energy efficiency: The conversion efficiency of fuels (coal, oil etc.) to electrical energy is nearly 30%. The conversion efficiency of electrical to microwave energy is nearly 80% (magnetron efficiency) and microwave energy to heat energy depends upon coupling behavior of the load material (good absorbing loads ~ 80-90%). Hence, overall efficiency of electrical to heat energy via microwave heating method is 65-74%. With all losses in transmission, applicator design, insulation arrangement, this efficiency may go down to ~55%. The conversion efficiency of electrical to heat via conventional electrical heating is 55-65% which may go down to 40-50% considering all losses. Thus, approximately 21% and ~18% are the overall energy efficiency of microwave (good absorber) and conventional.
4. Savings in time and space and changes in yield over conventional processing.

The efficiency of heating cannot be standardized and economics of heating has to be evaluated on case to case basis. Thus, the economic benefits of microwave processing are difficult to define in a general way. In most successful industrial applications of microwaves, factors other than energy account for savings realized from microwave processing; improvements in productivity, material properties and savings in time and space are probably the best bases for selecting microwaves over conventional processes.

2.7 Safety Perspectives of RF and Microwaves

The microwave and radiowave are non-ionizing radiations (NIR). The microwaves are not sufficiently energetic to produce ionization or to break chemical bonds in matter like high energy photons of X and γ radiations. The microwave on interaction with a molecule, may affect its rotational energy levels. At present, the only confirmed effect is warming, from the conversion of electromagnetic energy to heat. Thus, microwave exposure standards are based on the ‘thermal’ effects of exposure. However, the ‘athermal’ or ‘non-thermal’ effects of microwave are also reported on induction of the physiological and genetic changes [277]. Microwave exposure to human body may cause thermal risks as human body is composed mostly of water. If body temperature goes up by 5 to 10 ^{o}C, macromolecular denaturations occur and irreversible effects take place. On the basis of normal heat dissipating capacity of human body, the microwave exposure standard of 10 mWcm^{-2} measured at 50 mm was used from 1940 onwards, since this amount of exposure would lead to the acceptable equivalent heat generation in the human body which is approximately one third of heat quantity required for sensation of warmth within human being [5, 278].

2.7.1 Measurement of Microwave Leakage

The microwave leakage meters consist of either a thermal sensor (thermistor, bolometer, thermocouple etc.) or a most commonly used diode for measuring microwave electric field. The instruments are hand held, usually have a microwave transparent foam cover (dome) surrounding the sensor dimensioned to place it at 50 mm from the outer contour. The instrument may be used in several ranges of leakages (typically 0-2, 0-10 and 0-100 mWcm^{-2}). Photograph of a microwave leakage meter is shown in **Fig. 2.16**.

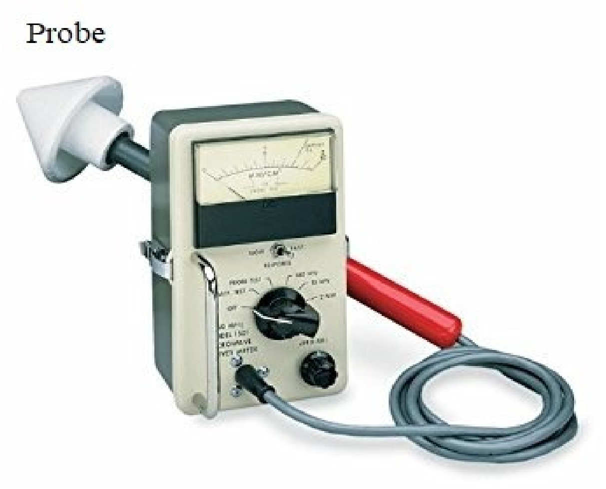

Fig. 2.16: A Commercial Diode based Microwave Oven Leakage Meter

2.7.2 Safety Guides and Standards

Recommendations for the protection of workers and members of the public from the harmful effects of RF and microwave radiation have been made by numerous international and professional organizations [5, 255, 279]. On the international level, world health organization (WHO), International labor organization (ILO) and ICNIRP have recommended exposure limits. Professional organizations such as ACGIH, Institute and Electrical and Electronics Engineers (IEEE) through American National Standard Institute (ANSI), Federal Communication Commission and OSHA have also recommended exposure limits for RF and microwave radiation. For microwave 2450 MHz, Federal Communication Commission maximum permissible exposure (MPE) limits for occupational exposure is 5 mWcm^{-2} (averaging time 6 min.) and member of public is 1 mWcm^{-2} (averaged over 30 min.). OSHA recommends limit of 10 mWcm^{-2} averaged over 0.1 h. IEEE/ANSI recommends 8.2 mWcm^{-2} (averaged over 6 min.) and 1 mWcm^{-2} (averaged over 30 min.) for an occupational worker and to a member of public respectively. ICNIRP recommends permissible exposure as 5 mWcm^{-2} and 1 mWcm^{-2} to an occupational worker and to a member of public respectively in 2 to 300 GHz range.

Chapter 3

EXPERIMENTAL MATERIALS, METHODS AND INSTRUMENTS

3.1 Introduction

This chapter describes the experimental materials, methods, techniques and instruments used for carrying out the present research work. The properties of standard materials used for comparative evaluation with the recycled materials are tabulated. The scrap materials (starting materials); sintered thoria and urania based MOX fuel pellets subjected to fuel recycling experiments are elaborated. The preparation and sources of the chemicals and reagents employed in the study are recorded. Subsequently, the processing equipments used in the study are described alongwith associated operational and technical specifications. The characterization methods are elaborated with respect to their procedure and associated measurement errors. The analysis instruments employed are detailed alongwith photographic illustrations. The methods to evaluate key parameters like impurity factor (IF), oxidation (%), reduction (%) and scrap recycling ratio (SRR) are described.

3.2 Materials

3.2.1 Standard Feed Materials for Fuel Fabrication

The sinterable nuclear grade UO_2 (ADU route derived), PuO_2 (oxalate route derived) and ThO_2 (oxalate route derived), were used as standard feed materials for fabrication of oxide or MOX fuels by powder-pellet route. Nuclear grade deeply depleted uranium dioxide ($DDUO_2$) powder was supplied by M/s Nuclear Fuel Corporation, Hyderabad, India. PuO_2 powder was obtained from the reprocessing of the spent PHWR fuels from PREFRE plant, Tarapur and KARP, Kalpakkam. ThO_2 powder was supplied by M/s Indian Rare Earths Ltd., Mumbai. Their important characteristics are listed in **Table 3.1** [163-164, 177-179]. The value in the parenthesis is the typical property value.

Table 3.1: Important Properties of Standard Sinterable Oxide Powders

Property	**ThO_2**	**UO_2**	**PuO_2**
Powder bulk density (gcm^{-3})	0.8-1.2 (0.85)	> 0.625 (1.8)	1-1.5 (1.2)
BET surface area (m^2g^{-1})	3.5-4.5 (3.6)	3.0-8.0 (3.2)	5-30 (16.05)
Average particle size (μm)	0.8-1.5	5-15	1-2
O/ M ratio (M; Th, U or Pu)	2.00	2.00-2.15	2.00
Sinterability above 90% of TD	Sinterable	Sinterable	Sinterable

3.2.2 Starting Materials for Recycling Studies

3.2.2.1 UO_2 based Mixed Oxide Sintered Scrap Pellets

UO_2 and $(U_{1-y}Pu_y)O_2$ pellets with varying plutonium content were fabricated at AFFF during several campaigns [31-32, 141, 144-146]. The rejected pellets generated during fuel production were subjected to present recycling studies. **Fig. 3.1** and **Fig. 3.2** show the photographs of PFBR sintered fuel pellets. The material identification, dimensional properties and linkage to respective fuel programme are listed in **Table 3.2.**

Fig. 3.1: Photograph of PFBR Annular MOX Fuel Pellets

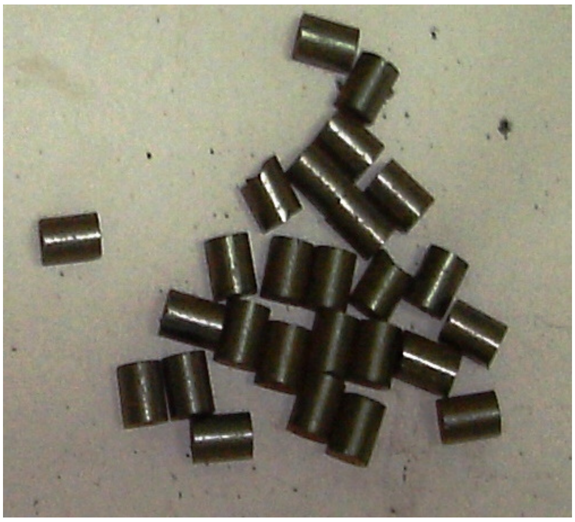

Fig. 3.2: Photograph of PFBR Axial Blanket $DDUO_2$ Pellets

Table 3.2: Identification and Other Important Properties of $(U_{1-y}Pu_y)O_2$ Pellets for Recycling Study

Starting material	Material composition and shape	Dimensions OD, ID, Ht. (mm)	Linkage to programme
B	$DDUO_2$, Solid cylindrical	5.5, __, 6-8	PFBR axial blanket
B3	$(U_{0.9675}Pu_{0.0325})O_2$, Solid cylindrical	12, __, 12-14	MOX for BWR
C	$(U_{0.79}Pu_{0.21})O_2$, Annular cylindrical	5.5, 1.6, 6-8	PFBR first core
D	$(U_{0.72}Pu_{0.28})O_2$, Annular cylindrical	5.5, 1.6, 6-8	PFBR first core
E	$(U_{0.56}Pu_{0.44})O_2$, Annular cylindrical	5.5, 1.8, 5-7	FBTR hybrid core

3.2.2.2 ThO_2 based MOX Scrap Pellets

Thoria based MOX pellets were fabricated at AFFF under different fuel campaigns [143]. **Table 3.3** records the fuel composition, dimension and their linkage to the fuel fabrication campaign/ programme. All the thoria based pellets were solid cylindrical. A photograph of ThO_2 sintered pellets is shown in **Fig. 3.3**. The $(Th_{1-y},U_y)O_2$ MOX were fabricated using $DDUO_2$ for simulating $^{233}UO_2$ and $LEUO_2$ (unless stated). The rejected fuel pellets or surplus pellets in their production were studied for their efficient recycling.

Fig. 3.3: Photograph of Sintered ThO_2 Pellets

Table 3.3: Identification of Thoria Based Sintered Pellets and Their Important Properties under Recycling Study

Starting material	**Material composition**	**Dimensions Dia., Ht. (mm)**	**Linkage to programme**
SM-A	ThO_2	9-10, 5-10	Fuel development
SM-B	$(Th_{0.9625}U_{0.0375})O_2$	9-10, 5-10	Fuel development for AHWR
SM-C	$(Th_{0.9}U_{0.1})O_2$	9-10, 5-10	Experimental irradiation (^{235}U: 1wt%)
SM-D	$(Th_{0.86}U_{0.14})O_2$	9- 10, 5-10	Fuel development AHWR-LEU
SM-E	$(Th_{0.7}U_{0.3})O_2$	10-11, 10-11	Fuel development AHWR-LEU
SM-1P	$(Th_{0.99}Pu_{0.01})O_2$	10-12. 10-12	Experimental irradiation
SM-8P	$(Th_{0.92}Pu_{0.08})O_2$	10-12, 10-12	Experimental irradiation

3.2.3 Chemicals and Reagents

Dissolvent used for dissolution and denitration experiments was concentrated (~16M) nitric acid (HNO_3) EMPARTA® (M/s Merck) having assay 68-72%. Dissolution of samples for metallic impurities determination by ICP-OES was carried out in 14M HNO_3 Suprapur® (M/s Merck-Millipore) with assay ≥65%. Hydrofluoric acid HF (M/s Sigma Aldrich) ~29M with assay 48-51% was employed as dissolution catalyst. Dilution of reagents was carried out with ultrapure water purified through Milli-Q® (Millipore Corp.).

Uranium and plutonium were extracted using 30% tri-n-butylphosphate (TBP) in n-dodecane (n-DD). The extraction of thorium was carried out by 40%TBP in n-DD. Tri-n-octyl phosphine oxide (TOPO) 0.2 M was used in last contact of extraction. TBP (M/s Sigma-Aldrich) with assay ≥99% and TOPO (M/s Sigma-Aldrich) with assay 99% were used. For back extraction of plutonium from loaded organic layer, hydrazine stabilized uranous

(150g U^{+4}+0.1M N_2H_4 in 0.5M HNO_3) was used. Poly vinyl alcohol (PVA) (M/s SDFCL, Mumbai) used as pore former was > 99% pure.

3.3 Processing Instruments

3.3.1 Jaw Crusher

A Jaw crusher BB 50 (M/s Retsch, Germany) was used for mechanical crushing of the sintered pellets into coarse powder. It consisted of a no-rebound feed hopper for feeding the sintered pellets. It had a fixed crushing arm and another movable arm by an eccentric drive shaft. The elliptical motion of the movable arm crushed the pellets (9-11 mm) into the powder < 1 mm. During crushing when sample became smaller than the discharge gap width (adjustable), it got collected into a removable collector. A vacuum based dust collection system collected the radioactive dust formed in crushing operation. **Fig. 3.4** shows the photograph of the jaw crusher.

Fig. 3.4: Photograph of the Laboratory Jaw-Crusher for Pellets

3.3.2 Attritor Mill

The attritor mill was used for mixing of the two or multi oxide powders and milling i.e. size reduction of the powders. Attritor mill consisted of a vertical positioned cylindrical vessel, the central shaft and horizontal impellers. The cylindrical vessel was made-up of stainless steel having capacity of 10 liters. The central shaft and impellers were made-up of hardened tool steel. A powerful motor rotated the shaft and thereby the impellers forced the grinding media to tumble randomly throughout the whole tank volume. The optimized size (Dia. 6 mm) hardened chrome steel balls were used as grinding media. The attritor speed was controllable in the range 100-400 rpm. For the mixing and milling of UO_2 and PuO_2, the material was charged at 100 rpm into the attritor followed by milling for 40 min at 200 rpm. The discharging of the material was carried out at 300 rpm. For efficient milling-mixing, 1/3rd attritor volume was filled with material, 1/3rd the grinding media and 1/3rd volume was kept empty. A typical attritor is shown in **Fig. 3.5**.

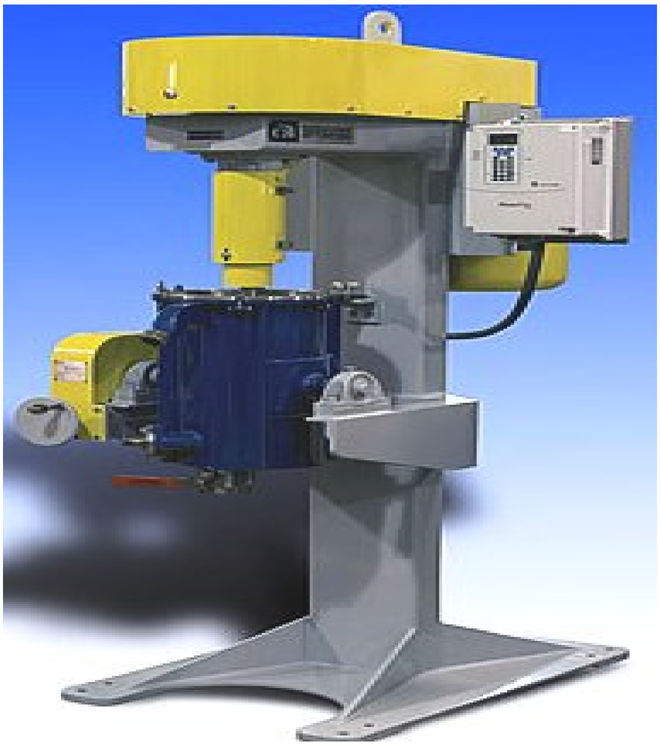

Fig. 3.5: Photograph of the Attritor for Mixing and Milling of Powders

3.3.3 Coarse Mixer-Grinder

A mixer grinder LMG-15 (M/s Lincon) was modified and adapted inside the glove-box for the coarse grinding of materials. The mixer-grinder was operable with variable speeds upto 3000 rpm and modified with hardened tool steel blades for grinding high density materials. The mixer-grinder was used to mill the oxidized pellets or granular clinkers into coarse powder (<500 μm). The photograph of the mixer-grinder is shown in **Fig. 3.5**.

Fig. 3.6: A Modified Commercial Coarse Mixer-Grinder inside a Glove-Box

3.3.4 Microwave Processing Systems

Indigenously developed microwave processing systems of different output power adapted inside glove-boxes (GB) were used. **Table 3.4** lists their key specifications and parameters. These systems were equipped with realtime temperature and power measurement during the microwave processing. The microwave forward and reflected powers were independently measured through calibrated dual directional coupler (DDC) mounted in line on the waveguide. The temperature was measured by stainless steel sheathed and re-crystallized alumina sheathed Type-K thermocouples. The stainless steel sheathed thermocouple had measurement error ±2 °C in the temperature range 0-1200 °C. The measurement error in the alumina sheathed thermocouple was ±3 °C. An optical fiber based temperature monitoring using Fiber Bragg Grating (FBG) sensor (M/s Raja Ramanna Centre for Advanced Technology, Indore) was installed inside a glove-box. The FBG sensor was designed for measurement of temperature (10-900 °C) more accurately (± 1°C) in the intense microwave fields. The reliability in temperature measurement was achieved using two thermocouples simultaneously, one placed at the surface of the material and other deep inside (upto center) the material. The temperature reported in the present study was that measured by thermocouple/ temperature sensor kept deep inside the material. The reverse temperature gradients in solid materials were kept small (< 6 °C) by keeping the bed thickness as small as possible. In case of the solutions, the reverse thermal gradients were not expected due to convection currents. The material under microwave irradiation inside the applicator could be seen through a mesh screened viewing window with the help of an illumination source. The course of the process was monitored visually through the viewing window. **Fig. 3.7** and **Fig. 3.8** show the photographs of a glove-box adapted 0.8 kW (MHS-0.8) and 3 kW (MHS-3) microwave heating systems. The 6 kW system (MHS-6) is shown in **Fig. 2.13**.

Table 3.4: Parameters and Specifications of Microwave Processing Systems

Parameter	**MHS-0.8**	**MHS-3**	**MHS-6**
Frequency	2450±50 MHz	2450±50 MHz	2450±50 MHz
Max. output Power	0.825 kW	3 kW	6 kW
Multimode Applicator	40×38×36 cm^3	39×39×39 cm^3	39×39×39 cm^3
Magnetron cooling	Air cooled	Water cooled	Water cooled
Magnetron	2M107A	NL10230	YJ1600
Incident Power	0-100 %	0-100 %	0-100 %
Power Projection	Manual/Auto	Manual/ Auto	Manual/ Auto
Magnetron position	On the applicator	Outside GB	Outside GB
Waveguides	___	WR340	WR340
Mode stirrer drive	Electrical motor	Electrical motor	Passive with suction

Fig. 3.7: Glove-Box Adapted 0.8 kW (MHS-0.8) Microwave Processing System

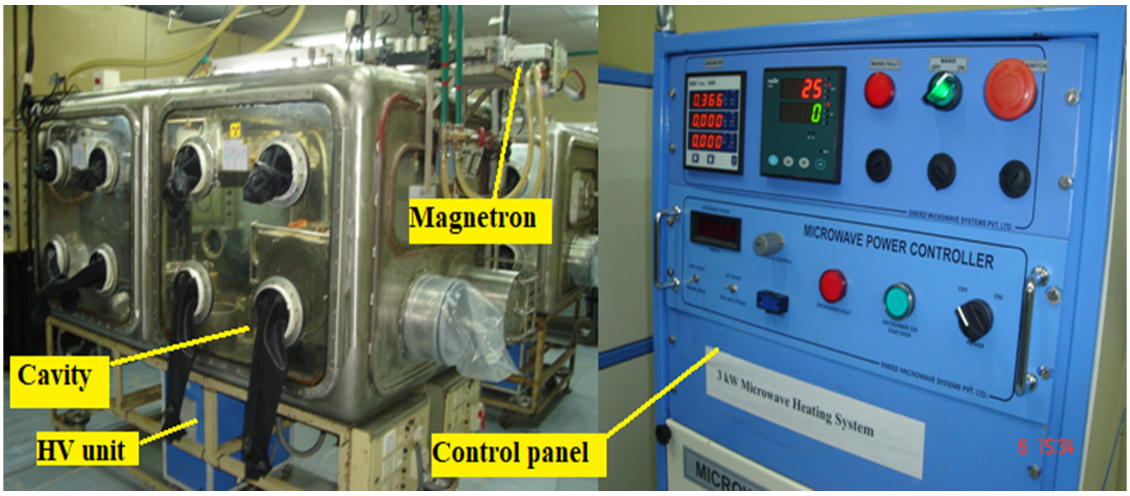

Fig. 3.8: Glove-Box Adapted 3 kW (MHS-3) Microwave Processing System

3.3.5 Treatment of the Off-Gases during Microwave Processing

The microwave dissolution and denitration produced off gases mainly containing the air sucked from the applicator, vapors of water, nitric acid, NOx gases (NO and NO_2). The off gases were routed through several scrubbers by vacuum. The vacuum was created by air ejector using compressed air line (20 Psi) which worked on the principle of venturi effect. **Fig. 3.9** shows photograph of the air ejector installed in a fume-hood. The off-gas system consisted of high efficiency cooling condensers followed by a water scrubber, alkali scrubber and HEPA filter. A schematic of the off-gas system is shown in the **Fig. 3.10.**

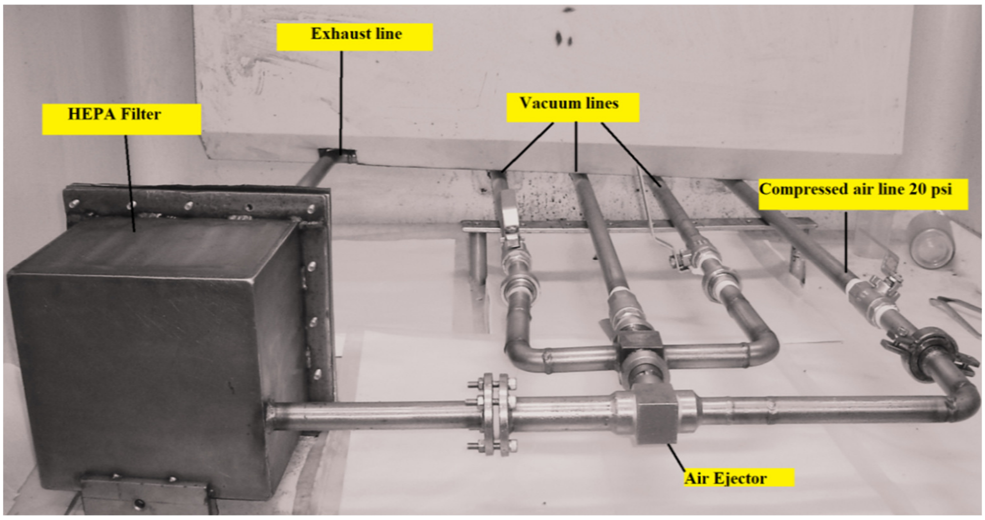

Fig. 3.9: Air Ejector for Creation of Vacuum using Compressed Air

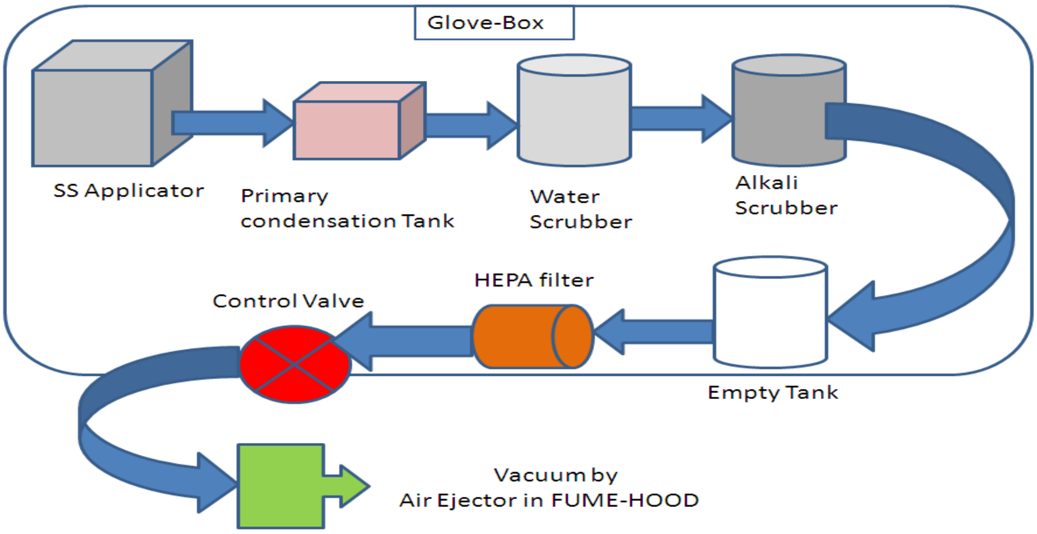

Fig. 3.10: Schematic of the Off-Gas System in Microwave Dissolution and Denitration

3.3.6 Microwave Processing Vessels

Fused quartz and alumina are transparent to microwave. Thus, quartz or recrystallized alumina made processing vessels were used for dissolution-denitration work. The quartz vessel offered added advantage over alumina being transparent to light, allowing visual monitoring of the course of the process. Different vessels (Dish, spherical, cylindrical etc.) were studied during the work and the cylindrical vessel with height (Ht.) 280-285 mm and inner diameter (ID) 74-77 mm was optimised for denitration work. **Fig. 3.11** shows photographs of quartz and alumina vessels. Microwave oxidation and calcination of materials was carried out in alumina trays. The digestion of fuel samples for bulk and trace elemental analysis was completed in perfluoroalkoxy alkane (PFA) pressure vessels (max. 120 Psi) (**Fig. 3.12**) in MHS-3.

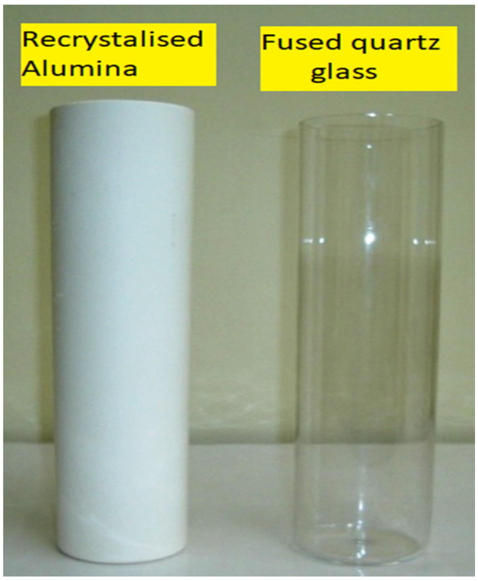

Fig. 3.11: Microwave Transparent Dissolution and Denitration Vessels

Fig. 3.12: Microwave PFA Pressure Vessel for Fuel Sample Dissolution

3.4 Physical Characterization Methods and Instruments

Physical characterization of recycled powders and fuel fabricated from the recycled powders included measurement of density (bulk and sintered density), BET surface area, particle size and shape, phase via XRD etc.

3.4.1 Density Measurement

The bulk density of the intermediate products and recycled powders (2-5 g) was measured using graduated cylinder (accuracy ±0.1 ml) and a weighing balance ER-182A (M/s Afcoset) (accuracy ± 100 µg) following the standard method [280]. The cumulative error in the measurement of bulk density was estimated using laws of uncertainty propagation which comes out to be ± 0.1 gcm^{-3}. The density of sintered pellets was measured from diameter and height of the cylindrical pellets using a micrometer (accuracy ±0.01 mm) and a weighing balance (accuracy ± 100µg) [163, 165-166]. In case of the annular cylindrical pellets, inner and outer diameters were used to calculate density. The cumulative error estimated in the measurement of sintered density of pellet (1 g) is ± 0.003 gcm^{-3}. The sintered densities were further expressed as % of theoretical density (TD). The TD of a MOX was calculated by taking wt. average of TD of the constituent oxides (**Table 1.4**). The density for a batch of fuel pellets was determined from the recommended number of randomly drawn sample pellets as specified under standard code viz. MIL STD 105D special Level-IV [281]. This recommended 13, 20 and 32 number of pellets to be randomly sampled for batch size having fuel pellets in the ranges 151- 500, 501-1000 and 1001-10000 respectively.

3.4.2 BET Surface Area Analyser

A surface area analyser SMARTSORB-93® (M/s Smart Instruments Co. Pvt. Ltd., India) adapted in a glove-box was used. This works on BET adsorption technique using carrier gas method in single point mode [182-183] at Liq. N_2 temperature (77K). The carrier gas composition used was 30% N_2-He mixture (p/p_o= 0.3). The calibration gas (N_2) used was 99.999% pure. NIST CRM 2206 with certified value 10.73±0.68 m^2g^{-1} (for single point) was used as check standard. The photograph of the BET surface area analyser adapted inside a glove-box and used in the present study is shown in **Fig. 3.13**.

Fig. 3.13: Photograph of Glove-Box Adapted BET Surface Area Analyser

The samples were a little milled using a mortar-pestle to break agglomerates (if any) and to avoid the throttling of the U-shaped sample tube. The sample tubes containing the sample (0.5-1g) were kept in regeneration unit for removal of moisture at the specified outgassing temperature and time. After cooling upto room temperature the samples were analysed for surface area. The carrier gas was allowed to flow through the U-shaped sample cell. The sample cell was immersed in liquid N_2 bath (77K). The physisorption on the sample decreased the concentration of N_2 in the carrier gas. The decrease in concentration in comparison to that in the initial gas mixture (through reference cell) was detected by thermal conductivity detector (TCD). After removal of the cooling bath, the sample cell was immersed in water bath and subsequently desorption peak was recorded. The sharper desorption peak could be better integrated and thus used for evaluation of the gas amount initially adsorbed [182]. The known volume of the calibration gas (pure nitrogen) was injected to calculate the volume of the N_2 adsorbed on the sample such that the sample desorption and the calibration peaks were of similar size [182]. The accuracy (relative error) and precision (RSD) in the measurement of specific surface area of NIST CRM 2206 in single point mode was better than 4% for 10 measurement replicates. The precision (RSD) obtained for specific surface area in natural UO_2 powder was nearly 5% for 10 measurement replicates.

3.4.3 Particle Size and Morphology Analysis

The particle size analysis of the coarse powder was carried out using standard ASTM sieves (M/s Jayant, Mumbai, M/s Retsch, Germany). Size analysis of fine powders was carried out using laser diffraction based particle size analyzer CILAS 1090 LD (M/s Cilas, France) for thorium samples and for plutonium bearing samples at Radio-metallurgy Division, BARC. The morphological properties were analysed using scanning electron microscope (SEM) model Mini-SEM SNE-4500M (M/s SEC Co. Ltd. South Korea). The instrument has high resolution; 5 nm (30 kV, SE) and 10 nm (30 kV, BSE) and magnification 20X to 100000X.

3.4.4 X-Ray Diffraction

The phase analysis in the samples was carried out by glove-box adapted X-ray diffractometers (M/s Diano Corporation, USA) at Radio-metallurgy Division, BARC and EMMA (M/s GBC Equipments, Australia) at AFFF, India. All the diffraction scans were taken on powder samples using Cu-K_α radiation (1.54 Å). The powder samples were milled and homogenized in a mortar-pestle. The X-Ray diffraction patterns were taken at scanning rate of 1^o min^{-1} over 2θ range from 20^o to 70^o. Silicon (111) was used as an external standard.

3.5 Chemical Characterization Methods and Instruments

3.5.1 O/ M Measurement

Thermogravimetric method based on gas equilibration was used for determination of O/M ratio in the raw material (standard or recycled) and sintered samples. The technique is based on measurement of weight change that occurs when an oxide or MOX is converted to stoichiometric reference state of O/M ratio of 2.000 by heating at 800 ^oC for 6h in an atmosphere with oxygen potential maintained at -100 kcal/ mole [172]. The O/M ratio is calculated using Eq. (3.1);

$$O/_{M} = 2 - \frac{(W_2 - W_1)M}{W_2 \times 16} \qquad (3.1)$$

where, W_2 is the final weight of the sample at O/M ratio 2.000, W_1 is the initial weight and M is the molecular wt. of the stoichiometric oxide or mixed oxide at O/M 2.000. For weighing of the samples (1g), a weighing balance ER-182A (M/s Afcoset) with accuracy ± 10µg was used. Considering the error only in weighing and using the laws of uncertainty propagation; the corresponding cumulative error is estimated to be ± 0.003 in O/M. The O/M values reported in the present work are average of three (n=3) measurement replicates performed on random samples drawn from a batch. The O/M of standard U_3O_8 powder was determined precisely using this method with standard deviation (s) and RSD of ±0.001 and 0.04% respectively in 3 measurement replicates.

3.5.2 Non-Destructive Methods for Heavy Metal Content Analysis

Heavy metals (U, Th and Pu) in various nuclear materials as powder blends, rejects were analysed non-destructively by a glove-box adapted XRF, Rigaku-Supermini (M/s Rigaku, Japan). The samples were prepared in diskette form by compaction in a hydraulic press after grinding in a mortar-pestle and using polyethylene glycol (PEG) as binder [282]. This instrument determined the heavy metals with accuracy (relative error) and precision (RSD) both better than ±0.5%.

Another non-destructive technique used for the estimation of plutonium in variety of MOX blends, sintered rejects and recycled powders was NWCC [151]. Isotopic composition data is a prerequisite for estimation of plutonium by NWCC. Relative error nearly 2% is obtained in estimation plutonium content in sample containing ~5g PuO_2 using NWCC. In the determination of PuO_2 content, the samples were kept in a cylindrical well for counting of neutrons by ^{3}He gas filled detectors after thermalisation by high density polyethylene (HDPE). The neutrons emitted from spontaneous fission of even-even isotopes of plutonium (^{238}Pu, ^{240}Pu, ^{242}Pu) are counted using coincidence logic to separate from background (α,n) neutrons.

3.5.3 Chemical Methods for Heavy Metal Content Analysis

The precise analysis of U, Pu and Th in the oxide or mixed oxide nuclear fuel samples required sample preparation and were dissolved in HNO_3. HF addition was required for dissolution of Th and Pu bearing samples. The sample dissolution was carried out in Pt dishes under infra-red heater method or by pressure vessel (**Fig. 3.12**) dissolution in microwave oven.

3.5.3.1 Uranium Analysis

The uranium was determined by the method known as Davies and Gray redox titrimetric [150, 154] method followed by potentiometric end point using $K_2Cr_2O_7$ as titrant. In this method, reduction of U(VI) (prevalent oxidation state in solution) was carried out using excess of Fe(II) in strong phosphoric acid medium (~10M) wherein, the redox potential values of U(VI)/U(IV) (**Table 1.19**) was reversed such that Fe(II) reduced U(VI) into U(IV). The excess unreacted Fe(II) was selectively oxidized to Fe(III) by HNO_3 in presence of molybdate catalyst and the resulting HNO_2 was destroyed with sulphamic acid. This destruction was essential to prevent the nitrite catalyzed nitric acid oxidation of Fe (II) and U(IV) during titration. The solution was then diluted with 1M H_2SO_4 containing VO^{2+}. In this step, concentration of H_3PO_4 decreased upto 3M, where the conditional redox potential value of Fe(III)/ Fe(II) was sufficiently larger than U(VI)/U(IV) couple, as a result Fe(III) ions oxidized U(IV) to U(VI) generating equivalent amount of Fe(II). The equivalent Fe(II) was titrated with standard solution of $K_2Cr_2O_7$. VO^{2+} assisted in producing a sharp end point. Since, oxidation of U(IV) as U^{4+} to U(VI) as UO_2^{2+} is kinetically slow due to involvement of oxygen bond formation, so titration was carried out in the presence of catalyst. The presence of plutonium and thorium in the sample has no effect on uranium determination [150]. The concentration of the uranium in solution was calculated using Eq. (3.2):

$$\text{Uranium concentration (mg/g)} = \frac{[W_3 \times 0.02 + W_2] \times 0.05 \times 119}{W_1} \qquad (3.2)$$

where, W_1, W_2 and W_3 were weights (g) of uranium solution sample, 0.05 meq/g and 0.001 meq/g of titrant respectively. 0.02 was dilution factor and 119 was equivalent wt. of uranium. The accuracy (relative error) and precision (RSD) better than 0.2% were achieved in the estimation of uranium in the range 3-15 mg in the aliquot for 10 replicates.

3.5.3.2 Plutonium Analysis

The method by Drummond and Grant was used for the determination of plutonium by titrating with potassium dichromate [150, 155]. In this method, the various oxidation states of plutonium (Pu exists in multi oxidation states simultaneously in the solution) were oxidized to Pu(VI) using excess AgO in 1M H_2SO_4 medium. The unreacted excess AgO was reduced with a slight excess of sulphamic acid. Now a known excess amount of standard Fe(II) was added to reduce quantitatively Pu(VI) as PuO_2^{2+} to Pu(IV) as Pu^{4+}. The unreacted Fe(II) was titrated using standard $K_2Cr_2O_7$ solution to a potentiometric end point. Th and U present in the solution did not interfere in Pu determination [150]. The concentration of the plutonium in the solution was calculated using Eq. (3.3):

$$\text{Plutonium concentration (mg/g)} = \frac{[W_F A - (W_2 + W_3 \times 0.02] \times 0.05 \times 119.6}{W_1} \quad (3.3)$$

where, W_1, W_2 and W_3 were weights (g) of plutonium solution sample, weights of concentrated and dilute dichromate solutions (0.05 meq/g and 0.001 meq/g) respectively. W_F was wt. of Fe^{2+} solution, A was wt. of dichromate solution equivalent to 1g of Fe^{2+} solution called blank value and 119.6 g was equivalent wt. of plutonium. The accuracy (relative error) and precision (RSD) better than 0.2% were obtained in the estimation of plutonium in the range 2-5 mg in the aliquot for 10 replicates.

3.5.3.3 Thorium Analysis

Ethylenediaminetetraacetate (EDTA) complexometric titration employing Xylenol Orange (XO) as the visual indicator of titration end point was used for thorium determination [150, 156-157]. The titration was carried out in a solution of pH 2 to 3. The color change from pink violet (Th-XO complex) to lemon yellow (Free indicator XO) indicated the titration end point. The thorium concentration of the sample was calculated using Eq. (3.4):

$$\text{Thorium concentration (mg/g)} = \frac{[W_3 \times 0.1 + W_2] \times 0.01 \times 232.06}{W_1} \quad (3.4)$$

where, W_1, W_2 and W_3 were weights (g) of sample, 0.01M and 0.001M titrant respectively. 0.1 was dilution factor of 0.001M EDTA and 232.06 was average atomic weight of Thorium. The accuracy (relative error) and precision (RSD) better than 0.4% were achieved in the estimation of thorium in the range 5-15 mg in the aliquot for 10 replicates.

3.5.3.4 Calculation of Heavy Metal Percentage in Fuel Sample

The concentration (mg/g) of elements (U, Th or Pu) in the solution calculated using Eq. (3.2) to Eq. (3.4) was used to calculate the percentage (%) of the element (E) in solid fuel sample using Eq. (3.5). The accuracy (relative error) and precision (RSD) nearly 0.2% for determination of U wt% and Pu wt% were obtained in the working standards. However, the relative error and RSD in determination Th% were comparatively higher (0.5%) (titration owing visual end point determination).

$$E\,(\%) = \frac{E\,(mg/g) \times Total \quad solution \quad wt.\,(g)}{Solid \quad sample \quad wt. \quad (g) \times 1000} \times 100 \qquad (3.5)$$

3.5.4 Impurity Analysis Methods

3.5.4.1 Metallic Impurity Analysis by ICP-OES

A glove-box adapted ICP-OES Horiba Ultima 2CHR® (M/s Horiba, France) was used to determine metallic impurities after removal of major matrix elements (U, Pu or Th) by solvent extraction [283]. The inter laboratory comparison exercise (ILCE) established U_3O_8 and ThO_2 standards for trace metal assay [284-286] and ICP multielement trace metal standards (M/s Reagecon, Ireland) were used for calibration. Impurities like Al, Ca, Mg, Co, Cu, Cr, Fe, Mn, Ni, Pb. Si, Sn, W and Zn were mainly determined. For the each impurity element in the range 3-1500 ppm, the precision in the measurement was < 5% (RSD). **Fig. 3.14** shows photograph of the glove-box adapted ICP-OES.

Fig. 3.14: Glove-Box Adapted ICP-OES at AFFF

3.5.4.2 Carbon Analysis

The carbon content in the samples was determined by a glove-box adapted carbon determinator CS-800 (M/s Eltra, GmbH, Germany). CS-800 was equipped with an induction furnace and four independent infrared cells. The combustion of the sample was followed by CO_2 estimation by infrared absorption technique at 2349 cm^{-1} and 770 cm^{-1} [160, 162]. The technique involved heating the sample at 1600 °C in the flowing purified oxygen gas. The gases evolved were passed through several chemical traps. MnO_2 was used to trap oxides of nitrogen and sulphur, hot copper oxide to covert CO into CO_2 and anhydrone to remove water. The stainless steel CRMs (M/s LECO) for carbon (273ppm, 1490ppm) were used as check standards. The accuracy (% error) and RSD in determination of carbon in CRMs were < 4% and ± 5% respectively.

3.5.4.3 Fluorine and Chlorine Analysis

Chloride and fluoride were determined after pyro-hydrolysis of the samples by respective ion selective electrodes (ISEs) [160, 162, 169]. The pyro-hydrolysis of the sample was performed at 900 °C under moist N_2/ Ar atmosphere. The liberated Cl and F as HCl and HF were collected in acetate buffer. Chloride was estimated by chloride-ISE (M/s Thermo Scientific) whereas fluoride was estimated by using fluoride-ISE (M/s Thermo Scientific). The ISEs were calibrated using standards of different concentration upto 25ppm. The RSD in determination of chloride and fluoride in standards was nearly 6%.

3.5.4.4 Nitrogen and Hydrogen Analysis

The nitrogen and hydrogen in the nuclear fuel materials were determined by inert gas fusion (IGF) technique following thermal conductivity measurement using TCD [162]. Nitrogen in the fuel sample was determined by a glove-box adapted nitrogen determinator O/N-2001 (M/s CIC, Vadodara). The nitrogen determination used impulse furnace for fusion of sample (~0.5g) alongwith the Fe-Ni flux at 2500 °C in a graphite crucible [160, 162, 287]. The high purity N_2 (99.995 %) and He (99.995 %) were used as calibration and carrier gases respectively. The carrier gas swept the evolved gases from the sample through various chemical traps to remove other gases (CO, H_2 etc.) except N_2. The calibration of the instrument was carried out by using volumetrically calibrated (500μL) dosing cavity method.

The calibration counts/ µg of nitrogen were calculated by peak area integrator. The counts corresponding to the purified nitrogen (from sample) were measured from sample peak area after considering the blank correction. The sample counts (area under the sample peak) were used to determine the nitrogen content using Eq. (3.6);

$$\boldsymbol{Nitrogen\ (ppm)} = \frac{\boldsymbol{Sample\ counts}}{\boldsymbol{Calibration\ counts\ (\mu g^{-1}) \times wieght\ of\ sample\ (g)}} \tag{3.6}$$

Stainless steel CRMs with nitrogen certified values in the range 30-325 ppm were used to test the measurement accuracy and precision of the system. Four (n=4) measurement replicates in a typical nitrogen CRM (M/s Elemental Microanalysis Ltd., UK) (certified value 317±8 ppm) delivered the accuracy better than 1% (relative error) and precision (RSD) ± 2.5%. Equivalent nitrate (wt%) was estimated by multiplying nitrogen content (in ppm) to its nitrate equivalent factor of 4.43×10^{-4}.

A glove-box adapted hydrogen determinator HD-2000 (M/s CIC, Vadodara) was employed for determination of hydrogen content. This used resistance heating of sample (~1 g) at high temperature (2000 ^{o}C) in a graphite crucible. High purity (99.99%) nitrogen gas was used as carrier gas. The instrument was calibrated by dosing cavity method with pure H_2 gas (>99.995 %) by dosing a cavity of size 500 µL. The calibration counts/ µg of hydrogen were calculated by peak area integrator. The liberated hydrogen was made free from other gases using a series of chemical traps before entering the TCD. The sample counts (area under the sample peak) were used to determine the hydrogen content using Eq. (3.6) for hydrogen. The analysis of stainless steel hydrogen CRMs (M/s Elemental Microanalysis Ltd., UK) (certified value 6.24 ±0.2) for five (n=5) replicates gave relative error < 3% and RSD ± 4%.

3.5.5 Fissile Homogeneity

3.5.5.1 Micro-Homogeneity through Alpha Autoradiography

The fissile homogeneity i.e. plutonium or uranium (^{235}U, ^{233}U) distribution in fuel matrix was evaluated by means of alpha-autoradiography [188-189]. The method involved the irradiation of solid state nuclear track detection (SSNTD) films (LR-115 or CN-85 etc.) by the alpha particles emitted from sample for a specified time. The differential specific alpha activity (**Table 1.2** and **Table 1.3**) of the fuel constituents (Th, Pu, U etc.) indicated their distribution in the matrix. The film was developed using chemical etchants and developers. The intensity of the etched alpha tracks and their distribution reflected about the fissile agglomerates. The surface size of the agglomerate was measured by this technique.

3.5.5.2 Bulk-Homogeneity via Dissolution Test

Dissolution test (DT) was carried out to ascertain the bulk homogeniety of the fissile plutonium in the UO_2 matrix. This test confirmed the formation of solid solution of UO_2 and PuO_2. Only solid solution of $(U_{1-y}Pu_y)O_2$ with $y < 0.35$ dissolves completely in HNO_3. The physical mixing of the UO_2 and PuO_2 without solid solution formation will result residues of PuO_2 left undissolved. Samples, one pellet for MOX and nearly 1g powder for impure scrap were taken for dissolution test. The undissolved residue left was indicative of the homogeneity. The sample was dissolved in 10 M HNO_3 for 8 h under refluxing conditions without any dissolution aid [176]. The solution was filtered through a pre-weighed sintered glass frit G-3. The crucible with the residue was dried under IR lamp to constant weight and using the weight of the empty crucible, the residue was quantified. Considering errors in the weighing (± 100μg), the cumulative error in the redidue wt% in DT was estimated to be 0.01%. The residue wt% recorded were arithmatic mean of three (n=3) replicates. The typical specification limit of residue for $(U_{1-y}Pu_y)O_2$ MOX fuel for thermal reactor and fast reactor is 0.1 wt% and 1 wt% of the sample. The residue wt% in the dissolution test was calculated using Eq. (3.7).

$$Residue\ wt.(\%) = \frac{W_R}{W_S} \times 100 \qquad (3.7)$$

where, W_R was for weight of residue and W_S was weight of the sample.

3.6 Derived Methodologies

3.6.1 Impurity Factor

The interpretation of the impurities in various scraps after their determination was carried out by defining an indicator parameter namely impurity factor (IF). The IF indicated about the impurity level, deviation from the specified limit and was expressed by Eq. (3.8).

$$Impuirty\ Factor = \frac{measured\ value}{specified\ value} \qquad (3.8)$$

where, measured value of the impurity was the arithmetic mean of the replicate measurements in representative samples. The IF was element specific or specific to a group of the elements. An IF value ≤ 1 indicated that the scrap was clean whereas a value > 1 implied the material was impure and termed as dirty or chemically impure scrap.

3.6.2 Calculation of Percentage Oxidation

The percentage (%) oxidation of an oxide or mixed oxide subsequent to oxidation was measured from the O/M ratio values. The oxidation (%) was estimated using Eq. (3.9).

$$Oxidation\ (\%) = \frac{(O/M)_f - 2.000}{Z_O} \times 100 \qquad (3.9)$$

where, $(O/M)_f$ stands for final O/M ratio (arithmetic mean of 3 samples drawn from a batch) of the oxidised powder. Z_O was theoretical increment in O/M under conditions of 100% oxidation for a given composition.

In the completely oxidised form, UO_2 transformed into U_3O_8 having O/M as 2.667. PuO_2 and ThO_2 cannot be oxidised in the solid state and thus have O/M as 2.000. For oxidation of UO_2 into U_3O_8, Z_O was 0.667 and for PuO_2, Z_O was 0. Similarly, the O/M ratio of ThO_2 is non-variable upon oxidation and Z_O value is 0. Z_O values for mixture $\{(1-y)UO_2+yPuO_2\}$ were calculated by linear interpolation where y is the weight fraction of PuO_2 and (1-y) is that of UO_2. Corresponding to measurement error of ±0.001 in O/M units, the error in calculation of oxidation (%) in UO_2 is estimated to be ±0.151wt%.

3.6.3 Calculation of Percentage Reduction

The percentage (%) reduction after reducing the oxidized powders was calculated from experimentally determined O/M values using Eq. (3.10).

$$\mathrm{Re}\,duction\ \% = \frac{(O/M)_i - (O/M)_f}{Z_R} \times 100 \qquad (3.10)$$

where, $(O/M)_i$ was initial O/U or O/(U+Pu) or O/ (Th+U) of the oxidised mixture (arithmetic mean of 3 random samples from a batch) and $(O/M)_f$ was final O/M ratio of the reduced mixture (arithmetic mean of 3 random sample from the batch). Z_R was the theoretical decrement in O/M ratio for 100% reduction upto stoichiometry. For reduction of U_3O_8 to UO_2, Z_R was 0.667, for PuO_2 and ThO_2, Z_R was 0. Z_R values for mixture $\{(1\text{-}y)U_3O_8+yPuO_2\}$ were calculated by linear interpolation where 1-y was the wt. fraction of U_3O_8 and y was that of PuO_2. The values of Z_R for (U_3O_8,21%PuO_2) and (U_3O_8,28%PuO_2) are 0.527 and 0.480 respectively. Considering the measurement error of ±0.001 in O/M units, the error in the calculation of reduction (%) in U_3O_8 is estimated to be ±0.212%.

3.6.4 Scrap Recycling Ratio

The scrap recycling ratio (SRR) indicated the weight fraction of the recycled material used in a fuel batch. This parameter was used to directly assess the suitability of the recycled powder to be used for a fuel batch. The SRR for a batch was calculated using the Eq. (3.11).

$$SRR = \frac{W_R}{W_F + W_R} \qquad (3.11)$$

where, W_R was weight of recycled powder and W_F was weight of fresh or standard powder added in fabrication of a batch. For a batch fabricated with the standard materials had 0 SRR whereas for the batch made with 100% recycled material, the SRR was maximum i.e. 1.

Chapter 4

DEVELOPMENT OF METHODS FOR RECYCLING OF (U,Pu)O_2 MOX

4.1 Introduction

The recycling of clean rejected fuel pellets produced during the fabrication of UO_2 and $(U_{1-y}Pu_y)O_2$ MOX fuel (**Table 3.2**) is described in this chapter. Two kinds of methods are developed; a wet recycling method and a dry recycling method. The experimental work is divided in two segments. Firstly, wet recycling method based on microwave dissolution and direct denitration was studied. The second half of the chapter is describing study the dry method using microwave thermo oxidation. The comparative evaluation of both the processes for recycling of $(U_{1-y}Pu_y)O_2$ MOX in the entire range of Pu (y: 0-1) was carried out. The flow sheets were developed for fabrication of MOX fuel using the recycled scrap with SRR value unity. The experimental work consisted of batch experiments, detailed influence of parameters and their optimization (time, temperature, PuO_2 content, heating mode, physical form etc.), flow sheet development, characterization of the intermediates and products and suitability assessment of recycled powder for MOX fuel fabrication. The recycled scrap and MOX fuel so fabricated were comprehensively characterized.

4.2 Microwave Direct Denitration based Recycling of Sintered $(U_{1-y}Pu_y)O_2$ MOX

Dissolution of sintered pellets of $(U_{1-y}Pu_y)O_2$ MOX in HNO_3 was carried out by microwave heating. Subsequently, microwave direct denitration was used for conversion or co-conversion of uranyl or uranyl-plutonium nitrate solutions to oxide/ mixed oxide powders. The dissolution perspectives of $(U_{1-y}Pu_y)O_2$ and factors affecting dissolution in the HNO_3 were studied. The process chemistry of the denitration and the required temperature were stated. This description was required to understand the process in-depth and to make modifications or value additions subsequently. The factors influencing the product properties were experimentally examined. The characterization of the product at the several process stages was carried out. After understanding the influence of the process parameters and factors, the denitration process was modified for improved product characteristics. The recycled powder was used for fabrication of several fuel batches. The MOX batches fabricated were characterized for fissile homogeneity by alpha auto-radiography and dissolution test. The improved sinterability was revealed by enhanced sintered density. The process was extended for recycling of the clean U, Pu scrap (solid/ solution) originated in the QC of fuel. The merits of microwave denitration process were elaborated with regard to recycling of $(U_{1-y}Pu_y)O_2$.

4.2.1 Dissolution of Clean Rejected Oxide (CRO) in Nitric Acid

The non-pulverized pellets of $(U_{1-y}Pu_y)O_2$ in batch mode were dissolved in 16M HNO_3 in the quartz or recrystallized alumina de-nitration vessels (**Fig. 3.11**) in microwave processing systems (**Fig. 2.13** and **Fig. 3.8**). The subsequent steps after dissolution like concentration, solidification, denitration and calcination were completed in the same process vessel. The main dissolution parameters examined were time, temperature, requirement of catalyst HF, PuO_2 content, physical form of rejects (intact pellets or crushed pellets) and mode of heating.

4.2.1.1 Batch Size, Dissolvent Volume and Criticality Considerations

The batch size in case of UO_2 was decided by size of the process vessel and the density of the denitrated product. For denitrated product with density < 1 gcm^{-3} in a vessel of capacity 1L (**Fig. 3.11**), 500-600 g of sintered pellets could be processed. In case of $(U_{1-y}Pu_y)O_2$ MOX, the batch size was decided by criticality calculations. The criticality safety evaluation was carried out for the microwave dissolution and denitration process at AFFF using Monte Carlo computer code MCNP-5 [288]. For 500 g $(U_{1-y}Pu_y)O_2$ MOX pellets in 700-1000 ml of HNO_3, the microwave dissolution-denitration process was safe at every stage of the process. The effective multiplication factors (K_{eff}[11]) for processing 500 g of $(U_{0.79}Pu_{0.21})O_2$ in 700 ml of nitric acid for the concentration stage (identified as most reactive process stage) are recorded in **Table 4.1**. Further, the quartz or recrystallized alumina denitration vessel used in the present work (**Fig. 3.11**) had inner diameter (ID) of 75 mm. Thus, the microwave direct denitration process was also found to be safe following single parameter subcritical limit [289] of cylinder diameter of 154 mm for aqueous solution of $^{239}Pu(NO_3)_4$. Alternatively, the batch size may be controlled below the safe mass of plutonium which is independent of concentration, shape, geometry etc. [290].

Table 4.1: K_{eff} Values in the Concentration Stage of Microwave Dissolution-Denitration Process for $(U_{0.79}Pu_{0.21})O_2$ MOX [288]

Isotopic composition of ^{239}Pu in $(U_{0.79}Pu_{0.21})O_2$	**K_{eff}**	
	Without water reflector	**With water reflector**
74 wt%	0.11	0.13
100 wt %	0.24	0.27

The dissolvent volume was estimated by several factors like concentration of nitric acid, duration of dissolution, duration of concentration, duration for crystallization etc. A lower dissolvent volume would lead to partial dissolution of sintered fuel pellets (UO_2 and MOX). Further heating the uranyl or uranyl-plutonium solution alongwith the un-dissolved pellets, the process undergoes through subsequent stages as concentration of solution, crystalisation of the uranyl nitrate or uranyl-plutonium nitrate salts , dehydration, denitration and clacination. The process of solidification involves concentration of solution followed by crystallization of respective nitrate salts. In such case residues of un-dissolved sintered pellet would be present in the denitrated product deteriorating the quality of the powder. However, a

---

[11] The effective multiplication factor (K_{eff}) is the ratio of the neutrons produced by fission in one neutron generation to the number of neutrons lost through absorption and leakage in the preceding neutron generation.
$K_{eff} < 1$; subcritical state, $K_{eff} = 1$; critical state and $K_{eff} > 1$; supercritical state.

higher dissolvent volume to batch size ratio makes the process prolonged because the solidification requires more time which is carried out after complete dissolution. Volume in the range 700-1000 mL of 16 M HNO_3 was found to be optimum for 500 g of sintered UO_2 and $(U,Pu)O_2$ fuel pellets.

4.2.1.2 Effect of Temperature and Dissolution Time

The temperature was found to significantly affect the rate of dissolution; higher the temperature, faster was the dissolution [291-292]. Thus, all dissolutions were carried out at boiling temperature of HNO_3 which was 115-120 °C.

The complete dissolution was ascertained by filtering the solution through a mesh filter (<500 μm). The dissolution completion times were different for various $(U_{1-y}Pu_y)O_2$ compositions. The dissolution UO_2 pellets (B, **Table 3.2**) was easiest among all and took ~20 min. The CRO pellets with Pu were comparatively difficult to dissolve and took more time. The dissolution time was increased as the plutonium content increased in the $(U_{1-y}Pu_y)O_2$.

4.2.1.3 Effect of PuO_2 Percentage on Dissolution

The CRO pellets of $(U_{0.9675}Pu_{0.0325})O_2$ (B3, **Table 3.2**) took slightly longer time (30 min.) than $DDUO_2$ (B). Sintered pellets of $(U_{0.79}Pu_{0.21})O_2$ (C, **Table 3.2**) and $(U_{0.72}Pu_{0.28})O_2$ (D, **Table 3.2**) were completely dissoluble within 60 and 80 min. respectively that too without HF catalyst. However, in case of $(U_{0.56}Pu_{0.44})O_2$ (E, **Table 3.2**), incomplete dissolution was observed in HNO_3. Nearly, 10-14 wt% of undissolved plutonium rich residue in the form of remains of pellets was observed. With the addition of few drops of HF complete dissolution was achievable within 80-90 minutes.

4.2.1.4 Effect of Initial Crushing of the Pellets

Mechanical crushing of the CRO pellets was found to increase the dissolution rate. However, the dissolution in case of the crushed pellets (coarse powder) was found to be vigorous and the flow-over was found from the denitration vessel. Similar observations have been observed with fresh UO_2 powder. In the case of the uncrushed pellets, the dissolution proceeds in a smooth manner from the surface causing shrinking in pellet dimensions. Though, dissolution of uncrushed pellets requires more time, but prevents material loss occurring due to flow-over. The dissolution reaction was so fast that the evolved NOx gases come out vigorously causing flow-over. One practical way to prevent flow-over is to turn off microwave power for short time duration and hence the heat input. Another way is the use of wider vessels for dissolution which provide more area to the evolved gases. The other disadvantage of the crushing is the addition of one more step in the process which is avoided to remove the radioactive dust hazard.

4.2.1.5 Effect of Initial Oxidation of the Pellets

The oxidation of UO_2 pulverized the pellets into U_3O_8 powder. The oxidative pulverization went on becoming cumbersome with increasing PuO_2 content in $(U_{1-y}Pu_y)O_2$ MOX. The powder from the surface of the pellets did not get dislodged in the pellets containing high PuO_2 content MOX (y>0.3). The oxidative pulverization of $(U_{1-y}Pu_y)O_2$ in conventional and microwave oven is discussed further (§ **4.3**). However, the dissolution was found to be faster in case of oxidatively pulverized M_3O_8 powder (M; U+/ Pu) than the intact pellets. This again increased number of process steps and may also lead to flow-over.

4.2.1.6 Comparison of Microwave versus Conventional Dissolution-Denitration

Comparison of dissolution-denitration curves for sintered UO_2 in microwave and conventional hot plate is shown in **Fig. 4.1**. However, in case of microwave the dissolution is faster than conventional heating. This was attributed to bulk heating by microwaves and interaction of microwave directly with the material to be dissolved. The direct denitration of nitrate solutions converting into mixed oxide powder employing conventional heaters yielded rock hard denitrated product which was very difficult to crush into smaller pieces. The direct denitration using microwave yielded the soft and porous product. In literature also these types of observations have been recorded by many researchers [11, 16, 69-71]. Thus, dissolution as well as denitration using microwave was carried out.

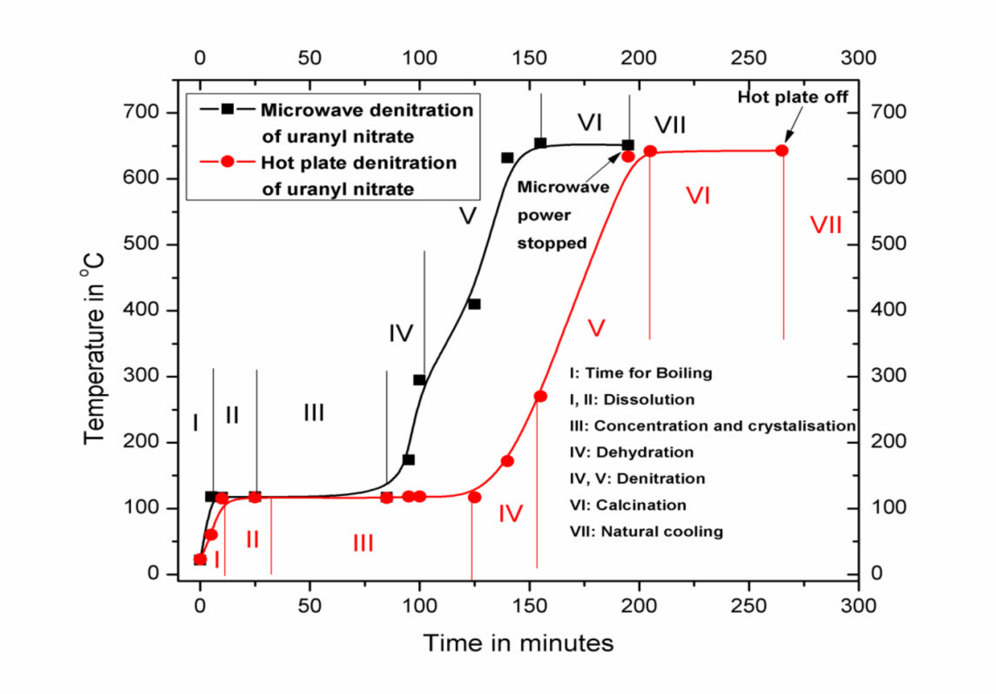

Fig. 4.1: Dissolution-Denitration of Sintered UO_2 in Microwave and Hot Plate

4.2.2 Microwave Direct Denitration Process

The pot denitration using microwave called MicroWave Direct Denitration (MWDD) process is a multistep-single vessel technique involving dissolution, concentration, de-hydration, de-nitration and calcination using microwave energy. **Fig. 4.2** shows the set-up of a denitration process vessel inside the microwave applicator.

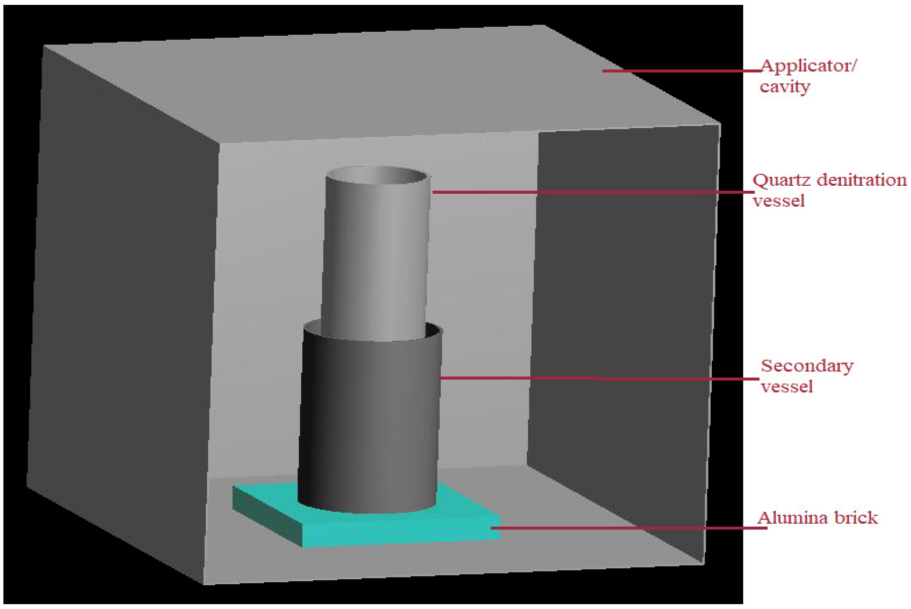

Fig. 4.2: Set-up of Denitration Process Vessel inside the Microwave Applicator

This process was extensively studied experimentally in the present work for recycling of $(U_{1-y}Pu_y)O_2$ in the entire range of PuO_2. The mechanism of the microwave denitration was studied by several researchers [14, 58, 124, 130, 132]. The chemistry of the recycling process from CRO pellets to usable reduced $(U,Pu)O_2$ powder is described below.

4.2.2.1 Dissolution, Concentration and Valance Fixation

The $(U_{1-y}Pu_y)O_2$ CRO pellets were dissolved in HNO_3 to obtain their soluble nitrates at boiling point (115-120 °C) without addition of any catalyst like HF except for $(U_{0.56}Pu_{0.44})O_2$ MOX and pure PuO_2 as represented by Eq. (4.1).

$$(U,Pu)O_2 + HNO_3 + H_2O \rightarrow UO_2(NO_3)_2(aq.) + Pu(NO_3)_4(aq.) + HNO_2 \quad (4.1)$$

The uranyl or uranyl-plutonium nitrate solution was heated at boiling point to concentrate the solution and to get crystals of nitrates by crystallization. The temperature slowly started increasing as solidification occurs (**Fig. 4.1**). The boiling fixed the oxidation state of the plutonium to Pu(VI) and brought uranium and plutonium to similar chemical form viz. MO_2^{2+} [124]. The reactions for valance fixation by boiling, and concentration and crystallization by evaporation are shown by Eq. (4.2) and Eq. (4.3) respectively.

$$Pu(NO_3)_4(aq.) \overset{\Delta}{\rightarrow} PuO_2(NO_3)_2(aq.) \quad (4.2)$$

$$UO_2(NO_3)_2(aq.) + PuO_2(NO_3)_2(aq.) + H_2O\ (Excess) + HNO_3\ (Excess) \rightarrow$$
$$UO_2(NO_3)_2.6H_2O + PuO_2(NO_3)_2.6H_2O \quad (4.3)$$

4.2.2.2 De-hydration and Denitration

In the process of dehydration, water of crystallization of nitrates was removed to get nitrates with reduced co-ordinated water at 120-300 °C as expressed by Eq. (4.4).

$$UO_2(NO_3)_2.6H_2O + PuO_2(NO_3)_2.6H_2O \rightarrow UO_2(NO_3)_2.2H_2O + PuO_2(NO_3)_2.2H_2O +$$
$$8\,H_2O \quad (4.4)$$

The denitration and dehydration occurs concurrently forming uranyl, plutonyl or uranyl-plutonyl hydroxy nitrate as represented by Eq. (4.5) to Eq. (4.7) [58];

$$UO_2(NO_3)_2.2H_2O\ (s) \rightarrow\ UO_2(OH)(NO_3)\ (s) + 1.5H_2O\ (l) + NO_2(g) + 0.25O_2(g)\ \rightarrow UO_2(OH)(NO_3)(s) + HNO_3(g) +\ H_2O(g) \tag{4.5}$$

$$PuO_2(NO_3)_2.2H_2O\ (s) \rightarrow PuO_2(OH)(NO_3)\ (s) + 1.5H_2O\ (l) + NO_2(g) + 0.25O_2(g) \rightarrow PuO_2(OH)(NO_3)\ \ (s) + HNO_3(g) +\ H_2O(g) \tag{4.6}$$

$$(U,Pu)O_2(NO_3)_2.2H_2O\ (s) \rightarrow (U,Pu)O_2(OH)(NO_3)\ \ (s) + 1.5H_2O(l) + NO_2\ (g) + 0.25O_2\ (g) \rightarrow (U,Pu)O_2(OH)(NO_3)\ (s) + HNO_3(g) +\ H_2O\ (g) \tag{4.7}$$

The hydroxy nitrates were decomposed to respective oxides on further heating above 300 °C resulting β-UO_3 and PuO_2 Eq. (4.8) to Eq. (4.9). During denitration of uranyl nitrate, the temperature was kept >400 °C. This transformed microwave transparent UO_3 into microwave absorber U_3O_8 (**Table 2.3**) simultaneously and completed the in-situ calcination. For temperature < 400 °C, the UO_3 formed after denitration did not absorb the microwave and could not be transformed into U_3O_8 by microwave calcination. In the case of uranyl-plutonium denitration, PuO_2 (being good absorber of microwave) worked as seed for absorbing microwave and subsequently the denitration product (UO_3, PuO_2) got heated above 400 °C thereby completing the calcination. Thus, temperature was critical in microwave denitration of uranyl nitrate. The temperature was increased by increasing the microwave power during denitration (**Fig. 4.1**).

$$UO_2(OH)(NO_3)\ (s) \overset{\Delta}{\rightarrow}\ \beta - UO_3(with\ adsorbed\ HNO_3) + 0.5\ H_2O(g) +\ NO_2(g) + 0.25O_2(g)\ \ \rightarrow \beta - UO_3(s) + HNO_3(g) \tag{4.8}$$

$$PuO_2(OH)(NO_3)\ (s)\ \overset{\Delta}{\rightarrow}\ PuO_2(s) + HNO_3(g) +\ 0.5O_2(g) \tag{4.9}$$

The oxidative denitration using microwave direct denitration of uranyl nitrate produces UO_3 which is shown in **Fig. 4.3**.

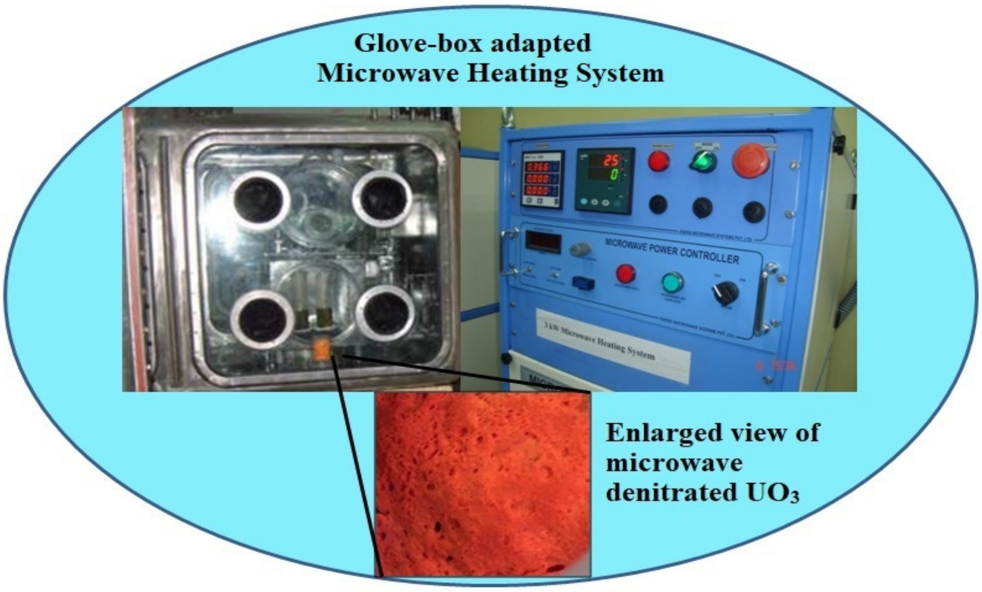

Fig. 4.3: Photograph of UO_3 formed after Microwave Denitration of Uranyl Nitrate inside a Glove-Box

4.2.2.3 Calcination and Reduction

The denitrated product which is UO_3 or (UO_3,PuO_2) was air calcined in the temperature range 400-700 °C which converted UO_3 into U_3O_8 according to Eq. (4.10). This calcination step simultaneously denitrated the residual nitrates (if any).

$$[(1-y)UO_3, yPuO_2] \rightarrow [(1-y)/3\ U_3O_8, y\mathrm{PuO_2}] + (1-y)/6\ O_2 \qquad (4.10)$$

Calcination was carried out in the same vessel. The calcined product (dried cake) was removed from the process vessel in the form of granular clinkers using a stainless steel spatula. A photograph of calcined (U_3O_8,PuO_2) clinkers is shown in **Fig. 4.4**.

The denitrated and calcined product was reduced under flowing (N_2+7%H_2) gas mixture at 500-700 °C as represented by Eq. (4.11). The temperature-power versus time profile for a batch denitration is shown in **Fig. 4.5**.

$$[(1-y)/3\ U_3O_8, y\mathrm{PuO_2}] + (1-y)/\tfrac{2}{3}\ H_2 \rightarrow [(1-y)UO_2, y\mathrm{PuO_2}] + (1-y)/\tfrac{2}{3}\ H_2O\ (g) \qquad (4.11)$$

Fig. 4.4 Photograph of Microwave Denitrated and Calcined ((U_3O_8,PuO_2)) Clinkers

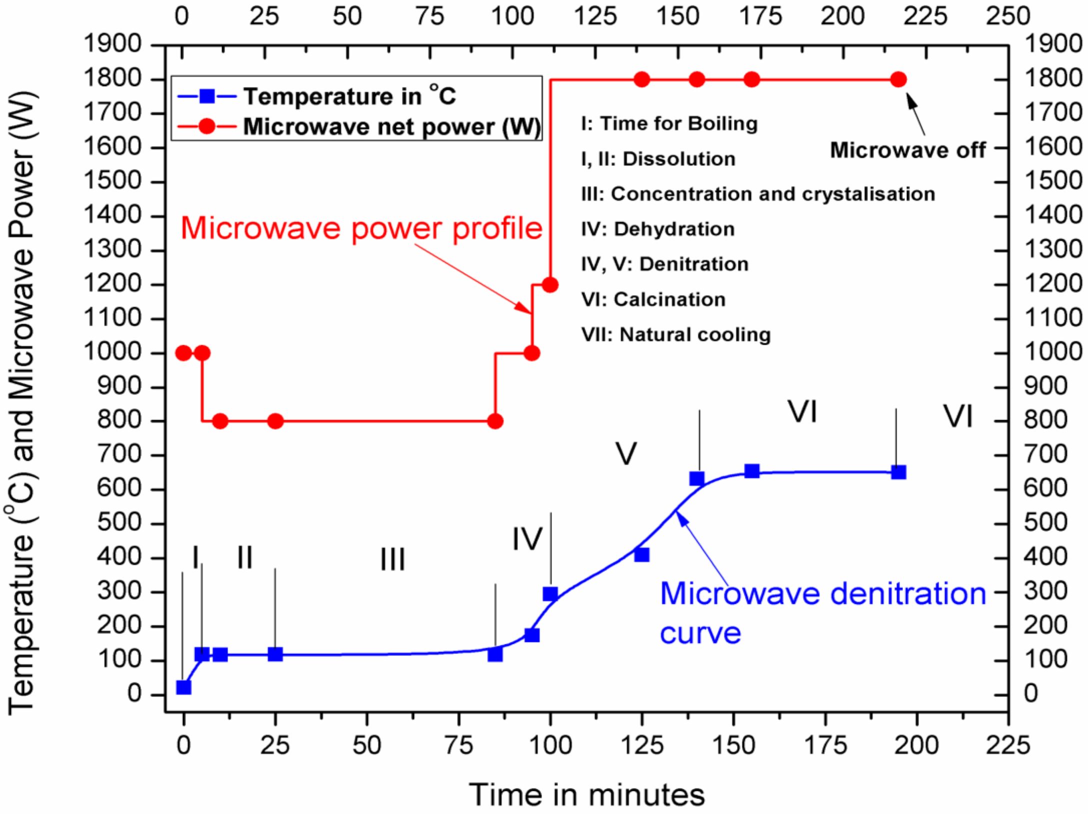

Fig. 4.5: A Typical Temperature cum Power-Time Profile of Microwave Denitration

4.2.3 Factors Influencing the Powder Characteristics in Microwave Denitration

4.2.3.1 Effect of Shape of the Denitration Vessel

The experiments carried out in round bottom flask, dish shaped and wide neck beakers showed a product which was sticky, hard and difficult to discharge from the process vessels. A quartz cylindrical vessel with height (Ht.) 285 mm and diameter (Dia.) 75 mm having aspect ratio (Ht./Dia.) of 3.8 resulted excellent product clinkers. Observations and experimental key parameters for denitration of uranyl nitrate into UO_3/U_3O_8 carried out in the several different shape process vessels are recorded in **Table 4.2**.

Table 4.2: Key Parameters in Selection of Microwave denitration Process Vessel

Shape	Dimension (mm)	Aspect ratio (Ht./Dia.)	Effervescence in transition from slurry to solidification	De-nitrated product characteristics
Round bottom flask	Dia.: 66	~1	Moderate	Relatively lesser sticky than dish and difficult to remove from vessel
Dish	Ht.: 60; Dia.:180	0.3	Insignificant	Sticky and rock hard, very difficult to remove
Broad beaker	Ht.: 140; Dia.: 120	1.17	Moderate	Slightly sticky and hard mass
Long beaker	Ht.: 285 Dia.: 76	3.8	Vigorous	Enormous gas pockets and porous. Not sticky and easy to remove

It was observed that with increasing aspect ratio (Ht./Dia.), the cake formed was more porous and easily removable from vessel. This was due to the fact that the long narrow process vessel offered small evolution area for outgoing gases/ vapors so bringing out the maximum effervescence. Since, the solidification with microwave heating occurred instantaneously while the evolution of the off gases was still continuing, the product formed consisted of enormous gas pockets and porosity. Though, the neck area was least for the round bottom flask (offering least area for outgoing gases), the product could not become more porous as its diameter was larger causing moderate effervescence during solidification. Further, it is difficult to take out the denitrated material from round bottom flask. Thus, long narrow vessel was selected for denitration work.

4.2.3.2 Effect of Stirring during Solution Stage

The effect of the stirring during solution stage on the bulk density of the denitrated dry cake (UO_3/U_3O_8, PuO_2) was examined. The solution was stirred with the help of a glass rod at the time interval of nearly 5 min. during dissolution and concentration. The intermittent stirring during the solution stages of the process delivered the denitrated mixed oxide (U_3O_8, PuO_2) with uniform bulk density 1 gcm^{-3}. Significant variation in density was found in the batches denitrated without stirring. Comparatively higher density product was observed in the bottom of the process vessel in the batches in which stirring was not carried out. The density was found to decrease while moving upward in the process vessel. Consequently, the unstirred batches delivered a higher average bulk density (~1.7 gcm^{-3}) than the batches obtained by incorporating the stirring (1 gcm^{-3}). This was attributed to the downward settlement of the material in the bottom where solution got saturated before solidification in the unstirred batches. The stirring led to elimination of such settlement and mass was uniformly mixed before solidification though solution was saturated. The solidification due to microwave heating occurred instantaneously throughout the bulk unlike the conventional heating where it proceeds from surface towards core. Thus, gas pockets or porosities were generated uniformly during the subsequent stages of the process like dehydration and de-nitration.

4.2.3.3 Effect of Addition of Pore Formers

Fig. 4.6 shows the variation of cake bulk density (CBD) and powder bulk density (PBD) in denitrated products of $(U_{1-y}Pu_y)O_2$. Both, the CBD and PBD were found to increase with PuO_2 percentage, highest being in pure PuO_2. The denitration product of uranyl nitrate is voluminous UO_3 and that of plutonium nitrate is PuO_2. Due to large difference in the densities of UO_3 (6.69-8.62 gcm^{-3}) and PuO_2 (11.46 gcm^{-3}), CBD (thus, PBD) increased with PuO_2 percentage.

A decrease in the CBD was observed by addition of small quantity (50 g in a batch) of solid polyvinyl alcohol (PVA) before solidification (**Fig. 4.6**). Aqueous solution of PVA may be added for more uniformity. During denitration, the PVA decomposed pyrolytically producing enormous gaseous products like hydrocarbons, H_2O, CO_2, CO etc. [293]. This resulted in formation of more pores in the dried cake. This could bring down the CBD below 1 gcm^{-3} in C and D, and below 1.5 gcm^{-3} in E and PuO_2 (refer **Table 3.2**). Though, the use of PVA decreased the CBD of the denitrated product in the entire range of PuO_2 in $(U_{1-y}Pu_y)O_2$, however, the effect was more evident above 20% PuO_2. For comparison, the bulk densities of the denitration products without PVA are also plotted in **Fig. 4.6**.

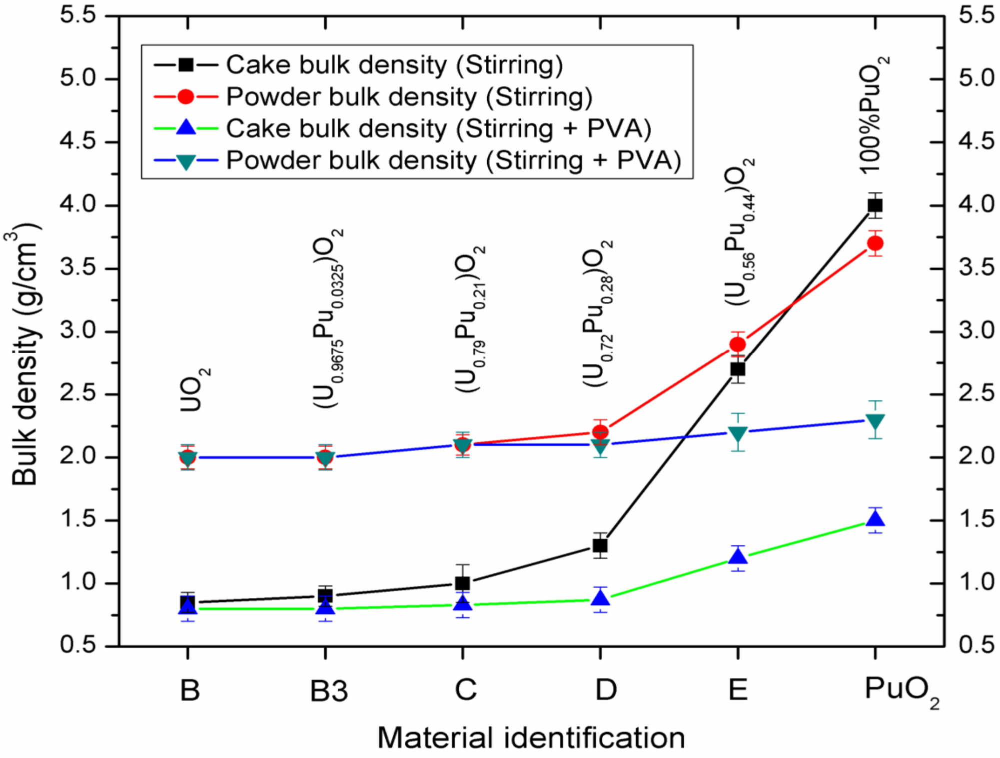

Fig. 4.6: Variation of Cake and Powder Bulk Density upon PVA Addition as function of PuO_2 Percentage in $(U_{1-y}Pu_y)O_2$

This was due to PVA decomposition which made the cake porous independent of the $(U_{1-y}Pu_y)O_2$ composition. However, a little increase in the CBD and PBD was still found above 20% PuO_2 which was attributable to higher density of PuO_2 than UO_3. It is evident from PBD trend in **Fig. 4.6** that upto 30% PuO_2, the addition of PVA is not rendering much advantage. The cake and powder bulk densities in E and PuO_2 obtained without addition of PVA are comparatively higher (**Fig. 4.6**). Denitration using PVA reduced the CBD and PBD in $(U,Pu)O_2$ MOX with y> 0.3 and brought out similar PBD (marginally higher) to that obtained without addition of PVA in MOX with y< 0.3 (A, B3, C and D). Thus, addition of PVA is required for obtaining low PBD while recycling $(U,Pu)O_2$ MOX with y> 0.3.

Fig. 4.7 shows the BET-SSA of the microwave denitrated powders with and without PVA. The typical values of standard $DDUO_2$ and PuO_2 powders are also shown (**Table 3.1**). For comparison, the SSA in mixtures of standard UO_2 and PuO_2 are plotted. The SSA in the mixtures was calculated by linear interpolation of their nominal values. The nominal value for UO_2 was 3.0 m^2g^{-1} and that for PuO_2 was 5.0 m^2g^{-1} (**Table 3.1**).

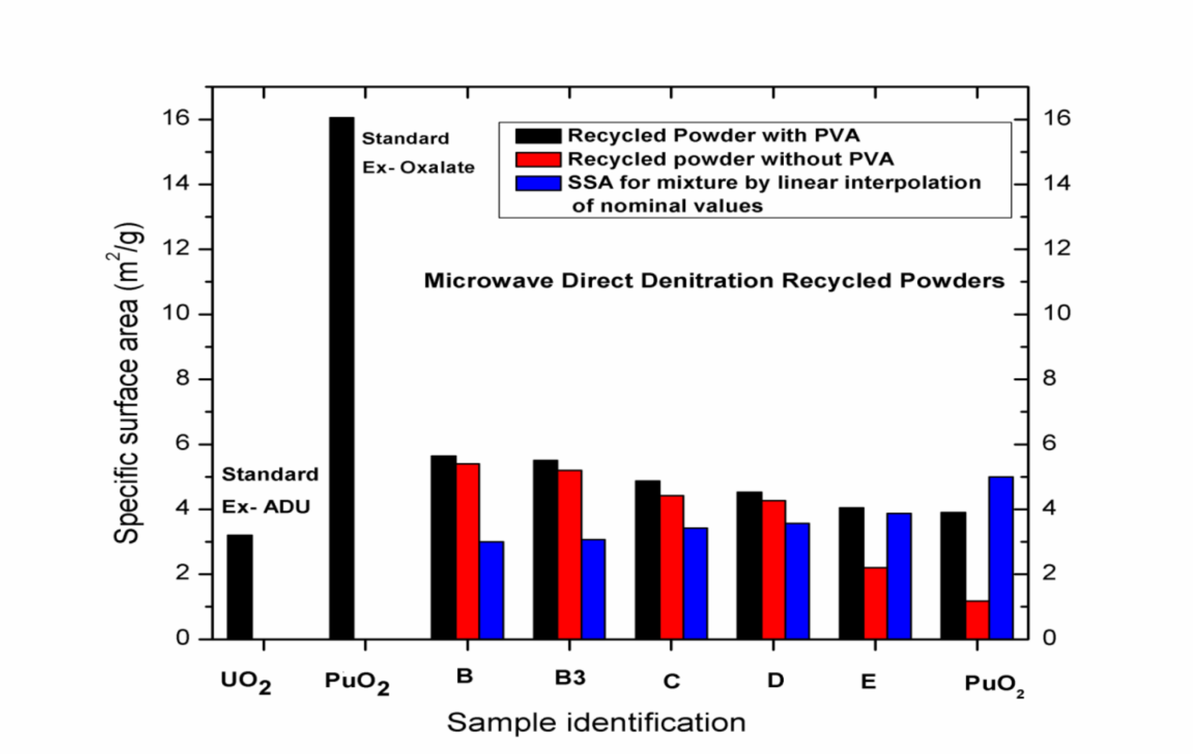

Fig. 4.7: SSA of Microwave Denitrated-Calcined Powders with PVA and without PVA

Fig. 4.7 shows that the recycled powders from B and B3 obtained by denitration with PVA and without PVA, the SSA were more than the required nominal values. In case of C and D, the SSA of powders with PVA addition and without PVA addition was comparable and was near to the mixture nominal values. However, the SSA values were significantly lower in the recycled E and PuO_2 powders denitrated without PVA addition as compared to that with PVA addition (**Fig. 4.7**). Though, the SSA in PVA added Recycled E and PuO_2 powders were not exceeding the nominal value calculated from interpolation, but these were above the nominal value for UO_2 ($3.0\ m^2g^{-1}$) which can be used for pellet fabrication. Thus, the addition of PVA during denitration was recommended for recycling $(U_{1-y}Pu_y)O_2$ with y> 0.3 (above 30% PuO_2) so as obtain higher BET-SSA in the recycled powder.

4.2.3.4 Calcination by Microwave Heating

UO_3 formed in denitration got transformed into U_3O_8 during the calcination of cake at 700 °C for 30-40 min (**Fig. 4.5**). The calcination at 700 °C for 30-40 min. during the microwave denitration process left small amounts of residual UO_3 and nitrates in the dry cake. This cake was removed from the vessel in the form of U_3O_8 or (U_3O_8,PuO_2) clinkers (**Fig. 4.4**). The clinker was milled using a coarse mixer grinder (**Fig. 3.5**) and again air calcined at 350 °C for 1h in microwave. The re-calcination of coarse milled powder conventionally was carried out at 700 °C, 4h in a resistance furnace. The air calcination of coarse milled powder at 350 °C for 1h using microwave was designated as low temperature microwave calcination (LTMC).

The re-calcination of U_3O_8 or (U_3O_8,PuO_2) powder (LTMC or conventional process) was intended to quantitatively convert the residual UO_3 into U_3O_8 and to denitrate the residual nitrates (if any) in the denitrated product. The residual UO_3 may affect the powder specified properties like O/M, density etc. whereas the residual nitrates may increase the nitrogen impurity content in the recycled powder. The milling of the clinkers opened-up the several closed pores and surfaces of the product thereby helped in achieving the quantitative calcination. A photograph of microwave calcined (U_3O_8,PuO_2) powder is shown in **Fig. 4.8**.

Fig. 4.8: Photograph of Powder obtained after Microwave Denitration and Calcination of ($U_{0.79}Pu_{0.21}$)O_2 MOX

The O/M ratio of co-denitrated (U_3O_8,21%PuO_2) was found to be 2.564 (theoretical 2.527) suggesting the partial conversion of UO_3 into U_3O_8 during the calcination step. The LTMC quantitatively converted remaining UO_3 into U_3O_8 which was confirmed by O/M ratio value of 2.521 (**Table 4.3**). A preliminary judgment can be made on colour appearance of clinkers; colour change from orange-yellow to gray-black (**Fig. 4.3** and **Fig. 4.4**) showed conversion of UO_3 into U_3O_8. The microwave calcination could also remove the residual nitrates effectively (**Table 4.3**).

The powder XRD pattern **(Fig. 4.9**) showed presence of the orthorhombic $(U,Pu)_3O_8$ (M_3O_8) and FCC $(U,Pu)O_2$ (MO_2) phases in the product obtained from microwave dissolution-denitration and calcination of ($U_{0.79}Pu_{0.21}$)O_2 MOX.

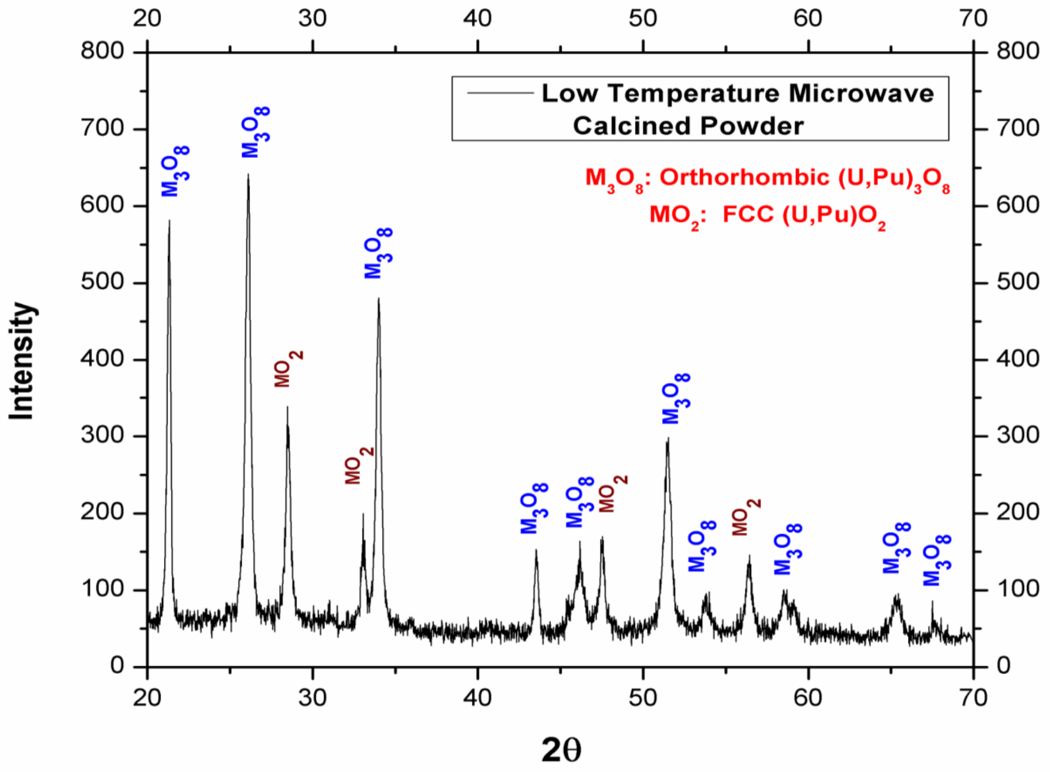

Fig. 4.9: XRD Pattern of Powder obtained after Microwave Denitration and Calcination of $(U_{0.79}Pu_{0.21})O_2$ MOX

4.2.3.5 Reduction by Microwave Heating

The reduction of the calcined powder was carried out at 550 °C for 3h in flowing N_2+7% H_2 gas mixture using microwave heating in place of conventional resistance heating assisted reduction (700°C, 4h). The reduction was called low temperature microwave reduction (LTMR). This could further enhance the powder properties in terms of SSA (**Table 4.3**). This was due fact that the reduction was carried out at a lower temperature (150 °C lower) and smaller soaking time than the conventional (700 °C, 4h). The higher temperature treatment and larger soaking time period deteriorates the powder properties [99, 112]. The reduction could be effectively carried out at lower temperature since heat is generated within the material itself using microwave. A detailed discussion on low temperature processing using microwave is described in Chapter 7. The calcined powders were reduced to slight hyper-stoichiometric mixed oxide (**Table 4.3**) rather than to complete stoichiometry (O/M: 2.000). The slight hyper-stoichiometry in the MOX powder (a small fraction in M_3O_8 phase) increases the sintering rate [44, 294], and thus assists in fabricating high density MOX pellets after sintering.

4.2.3.6 Magnetic Separation of Impurities

The reduced powder was passed through a magnetic particle separator. The magnetic foreign impurities (if any) present in the recycled powder were removed. This treatment avoided the chances of presence of unwanted metallic inclusions in the final product.

4.2.4 Modified-MWDD Process Flow Sheet

After experimentally examining the various influencing factors, the old process flow sheet called MicroWave Direct Denitration (MWDD) [44, 295] was modified. **Fig. 4.10** shows the MWDD and Modified-MWDD processes in a comparative mode for recycling of $(U_{1-y}Pu_y)O_2$ rejects. In the Modified-MWDD process, five modifications were incorporated to improve the powder properties. The modifications are distinctly marked in the **Fig. 4.10** and are as follows:

1. Intermittent stirring during the solution stage
2. PVA addition as pore former
3. Low temperature Microwave Calcination (LTMC); 350 °C, 1h
4. Low Temperature Microwave Reduction (LTMR); 550 °C, 3h
5. Magnetic separation.

Fig. 4.10 also shows the parameters like time, temperature, environment maintained during each process step. The quality control checks followed are also depicted at required process step. The well characterized recycled powder was then used for fabrication of the fuel by standard powder-pellet process.

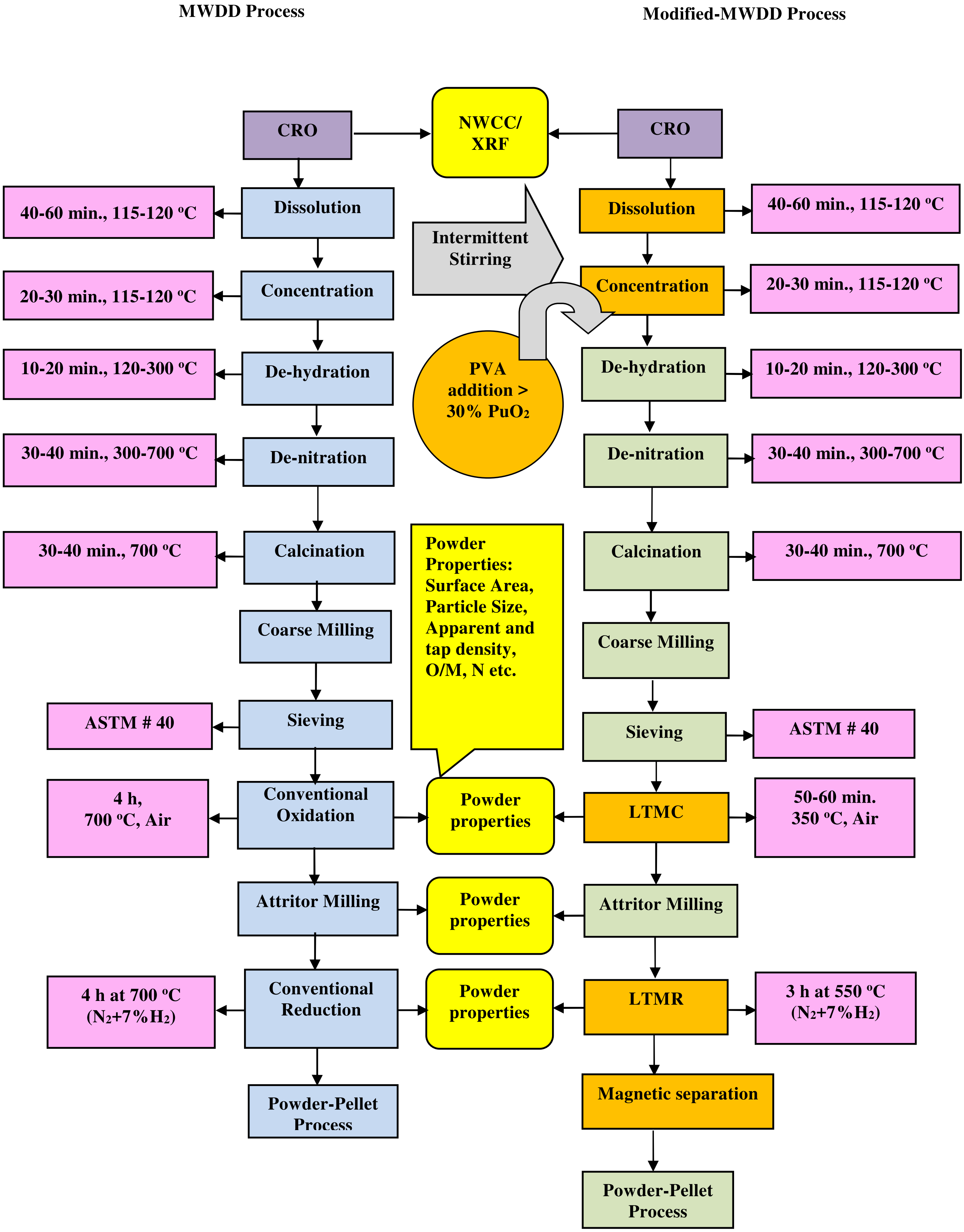

Fig. 4.10: MWDD versus Modified-MWDD Flow Sheets for Recycling $(U,Pu)O_2$ MOX

4.2.5 Powder Characterization

The bulk density, O/M ratio, specific surface area, particle size and impurity content of the powders prepared via MWDD and Modified-MWDD routes were determined and listed in **Table 4.3**. The BET surface area of microwave calcined and reduced powder were found to be improved than the conventionally processed (in MWDD) due to lower temperature processing using microwave. In the MWDD process [44], the air calcination and reduction were carried at 700 °C for 4h conventionally. The bulk densities of cake and powder in Modified-MWDD upon comparison with MWDD showed significant improvement attributable to incorporation of modifications (**Fig. 4.8**). The average particle size of the recycled powder was found slightly lower in Modified-MWDD process. This may be assigned to the modification leading to more porosity in the cake using PVA. The lower nitrate content suggested more efficient removal of nitrates during microwave calcination and reduction. The low temperature processing was advantageous as it rendered less harm to powder properties.

Table 4.3: Product and Powder Properties during Recycling of $(U_{0.79}Pu_{0.21})O_2$ by Modified-MWDD vis-à-vis MWDD

Property	**Modified-MWDD**			**MWDD**		
	Denitrated calcined cake	**LTMC powder**	**LTMR powder**	**Denitrated calcined cake**	**Conventional calcined powder**	**Conventional Reduced powder**
Chemical Form	$(UO_3/U_3O_8, PuO_2)$	(U_3O_8, PuO_2)	(UO_{2+x}, PuO_2)	$(UO_3/U_3O_8, PuO_2)$	(U_3O_8, PuO_2)	(UO_{2+x}, PuO_2)
O/M ratio ($\bar{x}$ ±1s, n=3)	2.573±0.001	2.521±0.001	2.052±0.001	2.564±0.001	2.522±0.001	2.014±0.001
Bulk density (gcm^{-3}) ($\bar{x}$ ±1s, n=3/batch, Batches= 4)	1.0±0.2	2.1±0.1	2.6±0.1	1.7±0.2	2.6±0.1	2.9±0.1
Average particle size (µm) in 3 batches	-----	1-2	1-2	----	----	1-3
SSA (m^2g^{-1}) ($\bar{x}$ ±1s, n= 3/ batch, batches = 3)	-----	5.23±0.21	4.87±0.19	----	3.12±0.14	2.71±0.12
Nitrate Equiv. (wt%) ($\bar{x}$ ±1s, n=3/ batch, batches = 2)	0.53±0.04	0.24±0.04	0.18±0.03	0.45±0.04	0.23±0.03	0.21±0.03

Every MOX fuel batch is subjected to impurity (metallic and non-metallic) analysis as per quality control plan. If batch is rejected for the reasons other than the impurities (**Table 1.16**), the rejected material is called CRO. However, if the batch is rejected for exceeding the impurity contents than the specified (**Table 1.15**), the rejected MOX is called DRO. **Table 4.4** records the individual impurities in a typical (U,Pu)O_2 CRO batch, the recycled powder from this batch via Modified-MWDD process and the MOX batch fabricated using the recycled powder in comparative mode with the standard $DDUO_2$ and PuO_2 powders. The metallic impurities were determined by ICP-OES and non-metallic by different methods (§ **3.5.4**).

Table 4.4: Impurity Analysis in a Typical $(U_{1-y}Pu_y)O_2$ CRO Batch, Recycled Powder, MOX Fuel from Recycled Powder alongwith standard Materials

Element (s)	**$DDUO_2$ powder** (ppm)	**PuO_2 Powder** (ppm)	**$(U_{1-y}Pu_y)O_2$ CRO: (a)** (ppm)	**Recycled Powder from (a) by Modified-MWDD: (b)** (ppm)	**MOX prepared using recycled powder (b): (c)** (ppm)
Al, Ag	10, <0.1	10, 0.5	130, 5	195, 8	231, 7
B, Be	0.5, 0.5	1.4, 0.6	1.3, 0.5	1.8, 0.5	2.0, < 0.5
Cd+Dy+Sm+Gd	0.1	0.2	1.5	1.7	2.5
Ca+Mg	59	211	551	523	554
Co	<10	<10	<5	<5	8
Cr	10	19	20	110	142
Cu	11	<10	35	28	45
Eu	<0.1	<0.2	0.7	0.7	0.6
Fe	45	200	471	854	1035
Mn	10	<10	<5	<10	10
Mo	<10	<10	<10	<10	10
Ni	<10	17	26	64	102
Pb	<10	10	<10	<10	10
Si	<10	10	296	204	172
W	<10	56	88	125	130
Zn	109	77	111	254	296
C	< 250	1445	133	195	65.3
H	950	350	2.85	845	2.91
Cl +F	74	50	21	56	16.74

The **Table 4.4** revealed that the impurities were least in the standard fresh materials, increased in the rejected MOX CRO batch (a), in recycled powder (b) and further in MOX fuel (c) fabricated using (b) due to process pick-ups. However, these were not exceeding the specification limits for MOX as recorded in **Table 1.15**.

4.2.6 Recycling of $(U_{1-y}Pu_y)O_2$ by Modified-MWDD Process

4.2.6.1 Recycling of UO_2 CRO

The recycling of $DDUO_2$ sintered pellets (B) via Modified-MWDD method was demonstrated. There is not much incentive in using PVA during denitration of uranyl nitrate as evident from the CBD and PBD values in **Fig. 4.6**. However, other modifications like stirring (to remove the cake density in-homogeneity), microwave calcination, microwave reduction and magnetic separation are required to be performed.

4.2.6.2 Recycling of $(U_{1-y}Pu_y)O_2$ MOX containing Lower % of PuO_2

Similarly, $(U_{0.9675}Pu_{0.0325})O_2$ (B3) was recycled by Modified-MWDD process. Recycling of B3 could be done similar to sintered $DDUO_2$ (B). However, the presence of PuO_2 has increased the dissolution time slightly as compared to $DDUO_2$. The time of dissolution of $DDUO_2$ is 20 min. and $(U_{0.9675}Pu_{0.0325})O_2$ took 30 min.

4.2.6.3 Recycling of $(U_{1-y}Pu_y)O_2$ MOX containing 20-30 % of PuO_2

The 21% and 28% PuO_2 MOX (C and D) were recycled using Modified-MWDD process. The difference in the dissolution times in $(U_{0.79}Pu_{0.21})O_2$ (60 min.) and $(U_{0.79}Pu_{0.21})O_2$ (80 min.) was attributable to higher content of PuO_2. The modifications have improved the powder properties (SSA, average particle size, nitrate content etc.) significantly (**Table 4.3**). Though, addition of PVA decreased the bulk density (**Fig. 4.6**) yet differences were not significantly large. Thus, addition of PVA may not be required on industrial scale recycling of $(U_{1-y}Pu_y)O_2$ MOX containing 20-30 % of PuO_2.

4.2.6.4 Recycling of $(U_{1-y}Pu_y)O_2$ MOX containing $PuO_2 > 35\%$

The dissolution of $(U_{1-y}Pu_y)O_2$ containing 44% PuO_2 (y: 0.44) was carried out for 80 min. using fluoride (HF) as dissolution aid. As PuO_2 content increased above 35 wt% in the MOX, the extent of dissolution decreases [291] and hence dissolution aids are required for quantitative dissolution. The addition of PVA was essential to get sinterable powder (**Fig. 4.6** and **Fig. 4.7**). All the modifications of Modified-MWDD process are required to be incorporated for recycling $(U_{1-y}Pu_y)O_2$ MOX rejected fuel containing $PuO_2 > 35\%$.

4.2.6.5 Recycling of PuO_2

100% PuO_2 pellets are hardly used in the reactors. However, it is quite possible that pellets or powder of PuO_2 or plutonium nitrate solutions get encountered. For example, PuO_2 pellets and powder are used as standards in the QC of fuels. Recycling of these may be required for the recovery. PuO_2 powder was dissolved in HNO_3 using HF in the microwave processing system and subjected to denitration similar to MOX. The bulk density of the cake was not low as in case of UO_2 and $(U_{1-y}Pu_y)O_2$, this was due to the fact that the product formed after denitration is PuO_2 rather than UO_3 or U_3O_8. As discussed earlier, UO_3 and U_3O_8 have low densities compared to PuO_2. The use of pore formers like PVA was able to reduce the bulk density (CBD, PBD) (**Fig. 4.6**). However, the SSA obtained was ~4 m^2g^{-1}, which was lower than that obtained in PuO_2 powder from oxalate route (**Fig. 4.7**). The solution combustion using aqueous solution of PVA and optimizing the ratio of PVA and HNO_3 may further improve the powder properties.

4.2.7 Fuel Fabrication using the Recycled Powder

Several batches were fabricated by powder-pellet route using recycled powders from both MWDD and after its modification. **Table 4.5** lists the batch details. A batch B-O was prepared using standard UO_2 powder (**Table 3.1**) for comparative evaluation. All the batches were prepared using SRR of 1 except the batch B-O which has SRR 0.

Table 4.5: Batch Details of Fuel Fabricated using Microwave Denitration Recycled Powders

Batch	Composition	SRR	Starting Material for Batch	Density (% TD) ($\bar{x}$ ±1s), n=32	Acceptance (%)
B-O	DDUO$_2$	0	ADU route obtained UO$_2$ powder	93±2	78
B-I	DDUO$_2$	1	MWDD processed DDUO$_2$ powder	93±1	76
B-II	DDUO$_2$	1	Modified-MWDD processed DDUO$_2$ powder	95±1	86
B-III	$(U_{0.79}Pu_{0.21})O_2$	1	Modified-MWDD processed MOX-21 powder	94±1	83
B-IV	$(U_{0.72}Pu_{0.28})O_2$	1	Modified-MWDD processed MOX-28 powder	94±1	81
M-21	$(U_{0.79}Pu_{0.21})O_2$	1	MWDD processed MOX-21 powder	93±1	80
M-28	$(U_{0.72}Pu_{0.28})O_2$	1	MWDD processed MOX-28 powder	93±1	82

It is important to note that the most of the reported recycling methods and approaches allow < 20 wt% of the recycled power in a batch due to poor powder characteristics and subsequent lower sinterability [26, 39]. Therefore, standard powders are added to enhance the sinterability. The SRR thus obtained are below 0.2. However, the materials recycled using microwave denitration methods could be used on 100% basis for fabrication of fuel batches (**Table 4.5**) bringing out maximum SRR (1). This was attributed to the standard (**Table 3.1**) comparable characteristics of microwave denitrated recycled powder (**Table 4.3**). The 100% utilization of the recycled scrap in a batch is advantageous for fuel fabricators from several reasons. First and foremost is that this practice obviates the stockpiling of the rejects and consequent exposure implications. The typical average rate of the scrap generation is nearly 25% (**Fig. 1.1**) or above. The stockpiling is eliminated when SRR is more than the fraction of scrap generation. The use of 100 % recyclable powder avoids the need of separate tooling (die, punch etc.) size for compaction of pellets. The conventionally recycled powder (if used on 100% basis) owing to poor powder properties (higher bulk density, low SSA etc.) showed lesser shrinkage after sintering. Thus, either the sintered density was lower or the pellets were oversized. Since, oxide and MOX fuels are fabricated on the sinter to size concept to avoid re-sintering (in low density pellets) and grinding (in oversized pellets) [202]. This brings consistency in the process parameters and hence in the product (fuel) consequently, the low rejection rate. The 100% usable powder also eliminates the need of adding sintering promoters.

4.2.7.1 Density of Sintered Fuel Pellets

Either similar or larger density was achieved in batches prepared from recycled powder via Modified-MWDD. The slightly higher density was observed in the batches B-II as compared to B-I and B-O. Similar trends were observed in B-III and B-IV as compared to batches M-21 and M-28. The improved densities were assignable to better powder properties in Modified-MWDD (**Table 4.3**).

The size of batch is 10 Kg which constituted more than 5500 fuel pellets. A total of 32 pellets were randomly sampled from a batch [281] and average density was measured. The average density thus determined was expressed as % of TD. The TD for MOX was calculated from the wt. average of the theoretical densities of constituents UO_2 and PuO_2 (**Table 1.4**). For example, the TD for $(U_{0.79}Pu_{0.21})O_2$ MOX is estimated to be 11.06 gcm^{-3} and sintered density achieved is 10.40 gcm^{-3} (94% of TD).

4.2.7.2 Fissile Micro-Homogeneity of the Sintered Pellets

Fig. 4.11 shows α-autoradiograph of $(U_{0.79}Pu_{0.21})O_2$ pellet fabricated from microwave denitration route. It was evident from **Fig. 4.11** that the distribution of plutonium rich islands (dark spots) in uranium matrix was uniform. The plutonium rich agglomerate > 30 µm were not present. The specified agglomerate size is ≤100 µm for $(U_{1-y}Pu_y)O_2$ MOX fuel for PFBR

(**Table 1.15**). As plutonium and uranium were mixed in solution state, MOX fabricated from microwave denitrated powder showed high plutonium homogeneity. An alpha autoradiograph of $(U_{0.79}Pu_{0.21})O_2$ MOX pellet fabricated via mechanical mixing of UO_2 and PuO_2 route is shown for comparison. **Fig. 4.12** shows the presence of a plutonium rich agglomerate of size > 100 μm.

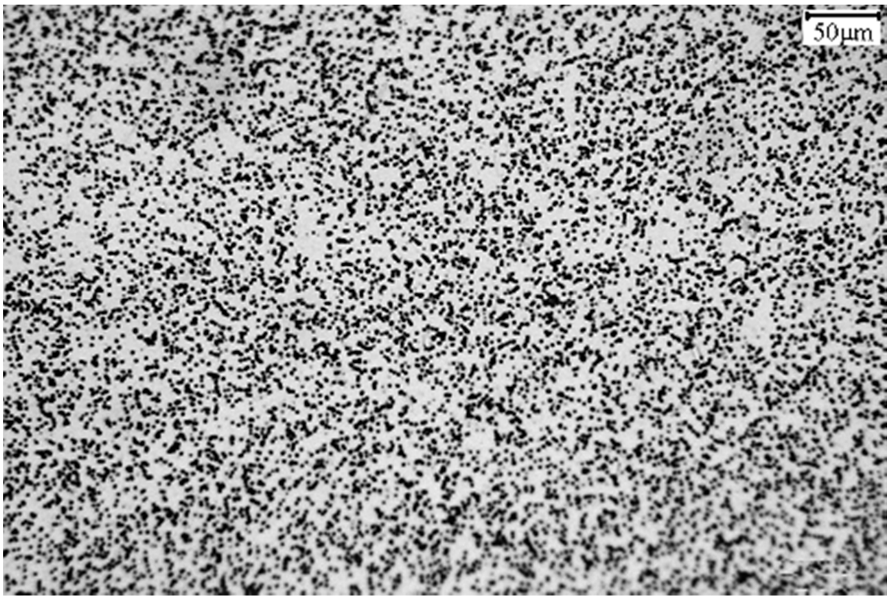

Fig. 4.11: Fissile Micro-Homogeneity via α-Autoradiograph of $(U_{0.79}Pu_{0.21})O_2$ Pellet from Microwave Denitrated Powder

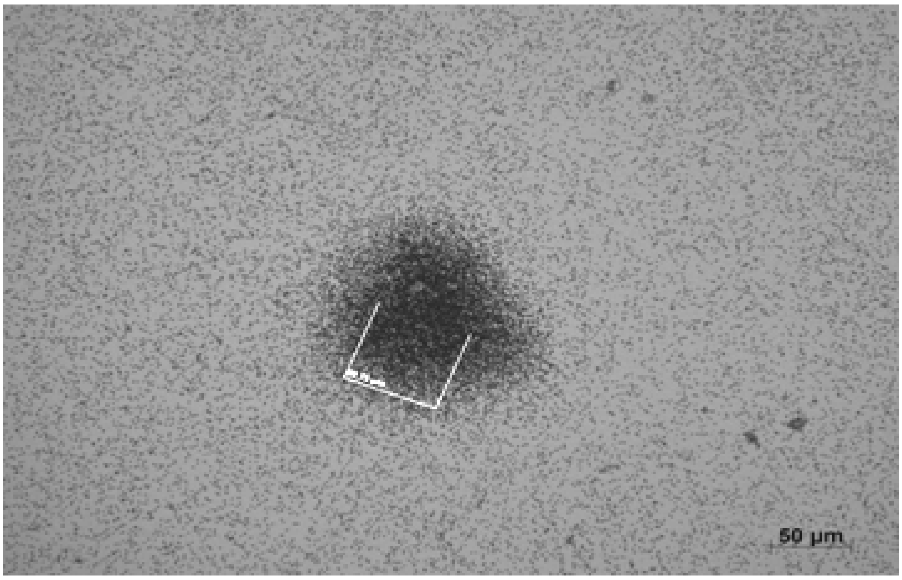

Fig. 4.12: Fissile Micro-Homogeneity via α-Autoradiograph of $(U_{0.79}Pu_{0.21})O_2$ Pellet from Mechanically Blended Powder

4.2.7.3 Bulk Homogeneity of Sintered Pellets

The bulk homogeneity of MOX pellets fabricated using powders prepared via MWDD and Modified-MWDD batches was ascertained by dissolution test (DT). The wt% of residue obtained in DT is recorded in **Table 4.6**.

Table 4.6: Residue obtained in Dissolution Test of the MOX Batches Prepared using Recycled Powders via MWDD and Modified-MWDD processes

Batch	Powder	Composition	Residue (wt. %) ($\bar{x}$ ± 1s), n=3
B-OP	Standard UO_2 and PuO_2	$(U_{0.79}Pu_{0.21})O_2$	0.83 ±0.05
B-III	Modified-MWDD processed	$(U_{0.79}Pu_{0.21})O_2$	0.11±0.02
B-IV	Modified-MWDD processed	$(U_{0.72}Pu_{0.28})O_2$	0.14±0.02
M-21	MWDD processed	$(U_{0.79}Pu_{0.21})O_2$	0.23±0.03
M-28	MWDD processed	$(U_{0.72}Pu_{0.28})O_2$	0.30±0.02

The batches prepared using Modified-MWDD powder has shown better homogeneity than batches prepared using MWDD processed powders and standard powders (B-OP). The larger residue in the batch B-OP was attributable to mechanical co-milling of the constituents which may leave some inhomogeneity than co-denitrated batches.

4.2.8 Recycling of Quality Control Generated Clean Scrap

The clean solid MOX samples (post analysis left over) in the form of pellets/ chips/ powder were getting accumulated from O/M ratio analysis using gas equilibration method [172], and from Cl and F analysis involving pyro-hydrolysis [162]. The PuO_2 content in the accumulated clean scrap was determined by NWCC technique. The material was recycled by the Modified-MWDD process (**Fig. 4.8**). Similarly, the clean dissolved fuel samples as uranyl-plutonium nitrate solution from various assays such as dissolution test (DT), bulk elemental analysis, and metallic impurities analysis (ICP-OES) were getting generated. The uranyl-plutonium solution had heavy metal (U+Pu) concentration nearly 22 gL^{-1}. Since, the heavy metal concentration in the collected solutions was lesser, a concentration step of the solution was carried out in the quartz process vessel (**Fig. 3.11**) so as to obtain ~500 g of MOX powder in a single batch of de-nitration.

4.2.9 Quantum of $(U_{1-y}Pu_y)O_2$ Scrap Recycled using Microwave Denitration Method

The microwave dissolution-denitration based recycling of oxide fuels was extensively studied and implemented to recycle large quantities of UO_2 and $(U_{1-y}Pu_y)O_2$ scrap generated at AFFF. **Table 4.7** records the data on the total quantity of the UO_2 and $(U_{1-y}Pu_y)O_2$ rejects recycled and used for fabrication of fuel on plant scale. The rejects recycled covers the PuO_2 range from 0 upto 45% (y: 0-0.45) in UO_2. The quantity as recorded in **Table 4.7** is total material recycled by MWDD and Modified-MWDD processes successfully.

Table 4.7: Quantity of UO_2 and $(U_{1-y}Pu_y)O_2$ Recycled Using Microwave Denitration Methods on Plant Scale

Material Description	Quantity (Kg)	Linkage to Programme
$DDUO_2$	400	PFBR axial blanket
$(U_{0.9675}Pu_{0.0325})O_2$	17	BWR MOX
$(U_{0.79}Pu_{0.21})O_2$	910	PFBR MOX, Enrichment-I
$(U_{0.72}Pu_{0.28})O_2$	2440	PFBR MOX, Enrichment-II
$(U_{0.56}Pu_{0.44})O_2$	9.5	FBTR MOX for Hybrid core

4.2.10 Salient Features of Microwave Denitration Technique

4.2.10.1 Powder and Product Characteristics

It is evident from **Fig. 4.6, Fig. 4.7, Table 3.1** and **Table 4.3** that the microwave recycled powders are suitable as feed powder for fuel fabrication. Sintered density (> 92%TD) of numerous fuel batches has demonstrated the excellent sinterability of powder. The fissile homogeneity through dissolution tests (DT) and alpha autoradiography were found to be better than that obtained through standard powders.

4.2.10.2 Adaptation, Automation and Maintenance Ease

The microwave denitration set-up is easy to adapt inside the glove-boxes or in hot-cells. The technology is viable and attractive from automation viewpoints. Microwave heating systems are easy to maintain compared to the conventional furnaces comprising frequently failing heating elements which are usually non-separable from the furnace hearth.

4.2.10.3 Multiprocess-Single-Vessel Technique

Microwave direct denitration which involved several processes (dissolution, concentration, dehydration, denitration calcination etc.) can be easily completed in a single vessel thus is a multiprocess single vessel technique. The losses of U/Pu during processing were negligible.

4.2.10.4 Manageable Liquid Waste

The liquid waste generation in the denitration methods is inherently lesser compared to other powder preparation methods (**Table 1.10**). The liquid waste generated was secondary waste which constituted the off-gases (NOx gases and acid/ water vapors) treatment scrub solutions (**Fig. 3.10**). Thus, the activity concentration of the liquid waste was several orders lower. The typical gross alpha activity concentration in the water scrubber unit and active washing liquid (primary waste) were 8.3×10^{-4} µCi/ml and 2.56×10^{-1} µCi/ml respectively.

4.2.10.5 Recyclable Lean Nitric Acid

Among the other advantages of the process was the reusability of the condensed nitric acid for the processing of the other batches. The assay of the nitric acid decreased with number of recycles. Typically, the 16M HNO_3 came down to ~12M in the first recycle which subsequently decreased to 7-8 M in the next recycle. This lean acid can be used either by mixing with fresh 16M nitric acid or by increasing dissolution time to achieve the complete dissolution. The prolonged dissolution retards the production rates. The lean acid after several recycles was not usable and thus declared as waste.

4.2.10.6 Proliferation Resistance

The plutonium is not separated from uranium in the process, hence is proliferation resistant inherently. Thus, process is preferred under the policy of non-proliferation due to non-diversion of special nuclear materials.

4.2.11 Summary of Microwave Direct Denitration based Recycling of $(U_{1-y}Pu_y)O_2$

Fig. 4.13 depicts the simplified pictorial representation of the wet recycling scheme for $(U_{1-y}Pu_y)O_2$ scrap.

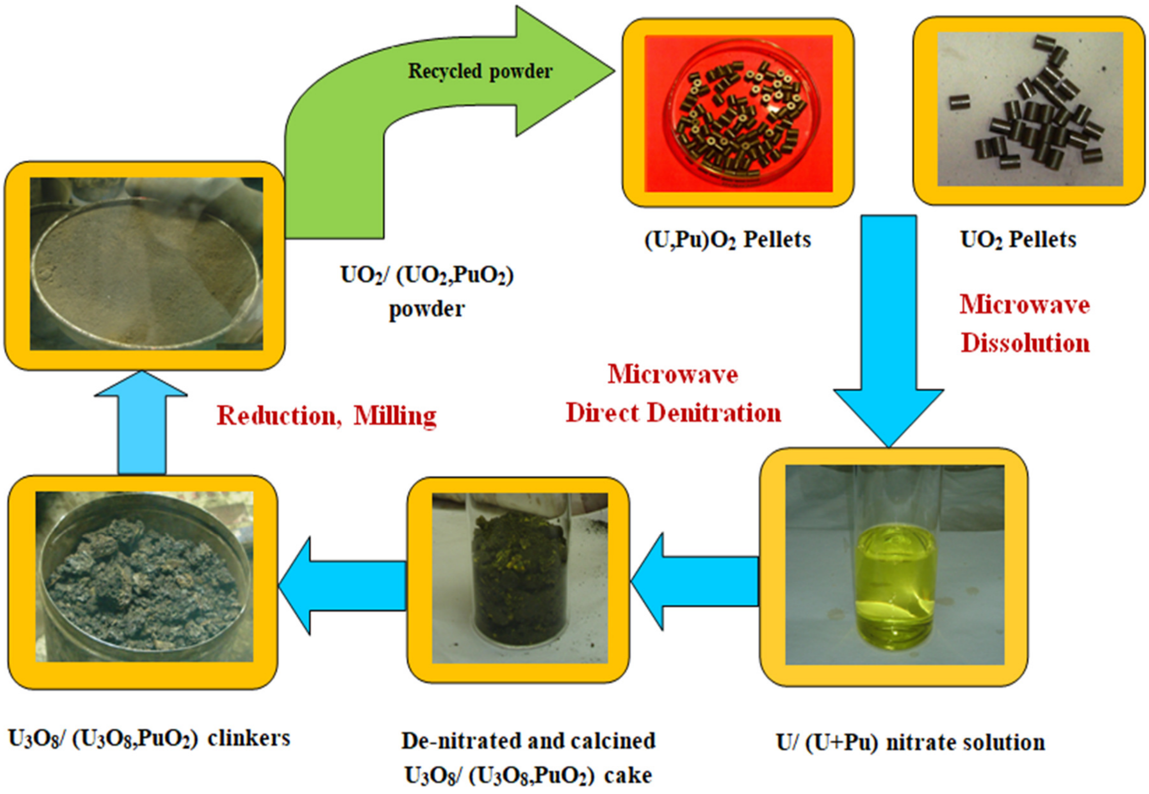

Fig. 4.13: Schematic of Wet Recycling of $(U_{1-y}Pu_y)O_2$ by Microwave Denitration

The conclusive summary of the microwave direct denitration based recycling of $(U_{1-y}Pu_y)O_2$ is as follows:

1. The microwave dissolution and denitration method was applicable in the 0-100 % range of PuO_2 in $(U_{1-y}Pu_y)O_2$ MOX.

2. As PuO_2 content increased in the MOX, the dissolution times were need to be increased for complete dissolution. The complete dissolution of the $(U_{1-y}Pu_y)O_2$ MOX with Pu > 35 wt% (y> 0.35)essentially needed fluoride addition.
3. The stirring during solution stage eliminated the density inhomogeneity in the denitrated products.
4. Solid PVA addition has tremendously improved the BET-SSA in the entire range of PuO_2 (y; 0-1) in $(U_{1-y}Pu_y)O_2$ denitrattion. The cake bulk density (hence PBD) were improved significantly especially above 20% of PuO_2 (y>0.2). The PVA addition is recommended for $(U_{1-y}Pu_y)O_2$ with PuO_2 >30 wt% (y> 0.3) for industrial recycling on 100% basis.
5. The LTMC (350 °C, 1h) was effective in quantitative calcination and removal of nitrates rendering lesser harm to the powder sinterability.
6. The reduction using microwave has improved the properties significantly. The reduced powder (PVA added) was found to have better specific surface area (4.87 m^2g^{-1}) as compared to conventionally reduced (2.71 m^2g^{-1}) with similar particle size.
7. The MWDD process was modified incorporating five major modifications namely stirring, PVA addition, LTMC, LTMR and magnetic separation. The Modified-MWDD has demonstrated better powder and product properties.
8. The better fissile homogeneity in MOX (evaluated by dissolution test) has been demonstrated in Modified-MWDD

4.3 Dry Processing Methods for Recycling of Sintered $(U_{1-y}Pu_y)O_2$ MOX Pellets

The dry recycling methods based upon oxidative or thermo-mechanical pulverisation of $(U_{1-y}Pu_y)O_2$ MOX by conventional heating were reported in literature (§ **1.12**). The oxidation of UO_2 and MOX sintered pellets containing small amounts of Pu (<3.2 wt%) showed appreciable degree of pulverisation between 400-600 °C. However, no pulverisation was observed in fast breeder reactor MOX pellets containing Pu ~30 wt% [296]. Tanaka et al. [297] observed that oxidation of $(U_{1-y}Pu_y)O_2$ containing 30 wt% Pu (y; 0.3) did not cause the disintegration of pellet however, MO_{2+x} formation was observed. $(U_{1-y}Pu_y)O_2$ MOX pellets containing PuO_2 > 20 wt% (y> 0.2) could not be pulverized into powder by conventional thermal treatment in air inspite of employing multiple oxidation-reduction steps and higher oxygen potential. Moreover, mechanical crushing was inevitable [44].

Microwaves heating caused instantaneous high rise in temperature attributable to thermal runaways in UO_2 pellets leading to development of cracks during sintering [11, 67-68]. This observation was therefore investigated for oxidative pulverisation of rejected sintered $(U_{1-y}Pu_y)O_2$ pellets using microwave heating in the present work. The direct oxidation of the off-specification pellets was carried out by microwave (2450 MHz). The process was named as MicroWave Direct Oxidation (MWDO) process and was designed to have two-stages within a single cycle process. The detailed experimental work consisted of batch oxidation experiments, characterization of materials, suitability assessment of recycled powder, flow sheet development for 100% recycling, fuel fabrication and comparative analysis.

4.3.1 Oxidation Experiments

The oxidation of sintered UO_2 and $(U_{1-y}Pu_y)O_2$ MOX pellets (**Table 3.2**) was carried out both in the conventional resistance furnace and in the microwave processing system, MHS-3 (**Fig. 3.8**) and MHS-6 (**Fig. 2.13**) for comparative evaluation of the data. Oxidation of sintered UO_2 pellets was carried out in a conventional resistance furnace at 700 °C, 4h in flowing air and in oxygen atmospheres. Similarly, the oxidation experiments were carried out in microwave ovens. The microwave assisted oxidation was performed using two stage-MWDO process. The experimental set-up of the oxidation of UO_2 and $(U_{1-y}Pu_y)O_2$ sintered pellets inside the microwave cavity is shown in **Fig. 4.14**. For oxidation in air, the cavity was not air leak-tight. The air entered the cavity mainly through two points 1) from the air/ gas entry point and 2) through the viewing window mesh (provided at the door) of the cavity. For the oxidation in oxygen atmosphere, the oxygen was fed through the gas entry point into the cavity. The cavity in this case was made leak-tight. The oxygen left the cavity through the controllable exhaust valve. The microwave entered the cavity from waveguide WR340 through air leak tight Teflon window installed at the interface of the cavity and the waveguide. The temperature was measured by two thermocouples T1 and T2 (**Fig. 4.14**). T1 was inserted upto center of the material and T2 touched its surface. The measurement of T1 was reported as the experimental temperature. Temperature gradients (T1-T2) found were less than 5 °C.

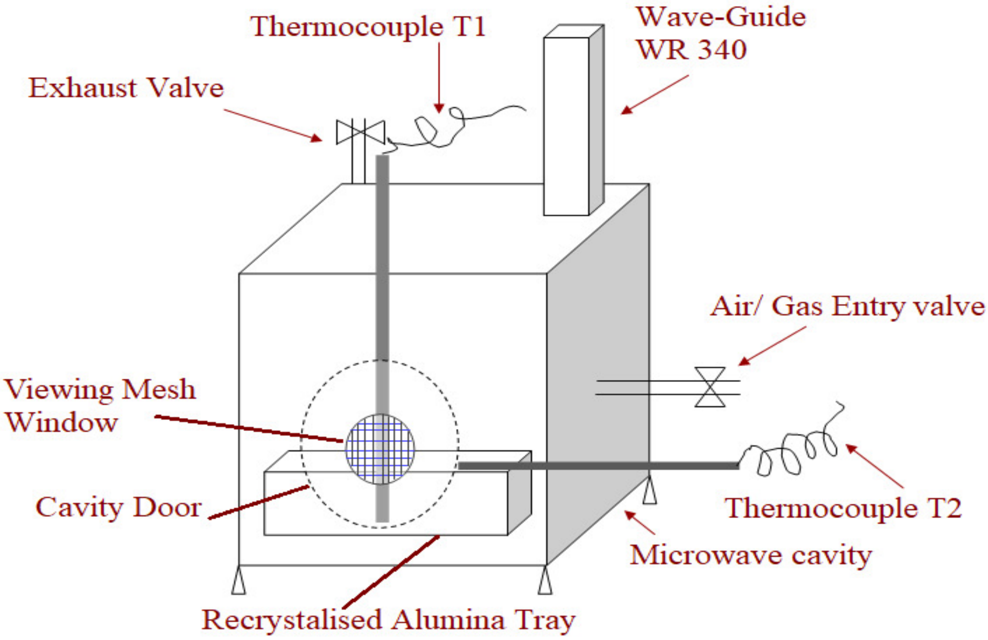

Fig. 4.14: Set-up inside the Microwave Cavity for Oxidation of $(U_{1-y}Pu_y)O_2$ Pellets

4.3.1.1 Two-Stage MicroWave Direct Oxidation Process

The off-specification high density (~10 gcm^{-3}) pellets were batch-wise (200-500 g) subjected for oxidation in flowing air and oxygen (1 m^3/h) atmospheres. The oxidation employing microwave was carried out in two distinct stages. A temperature nearly 800 °C was achieved within 10 sec. by projecting high power in the stage-I of MWDO for 5 min. Subsequently, in the stage-II, temperature of 550 °C was maintained for longer time. The microwave power, duration, other parameters and observations for oxidation are depicted in **Fig. 4.15**. The stage-I duration (5 min.) was kept constant for all the batch experiments whereas for stage-II duration was varied as shown in **Fig. 4.15**.

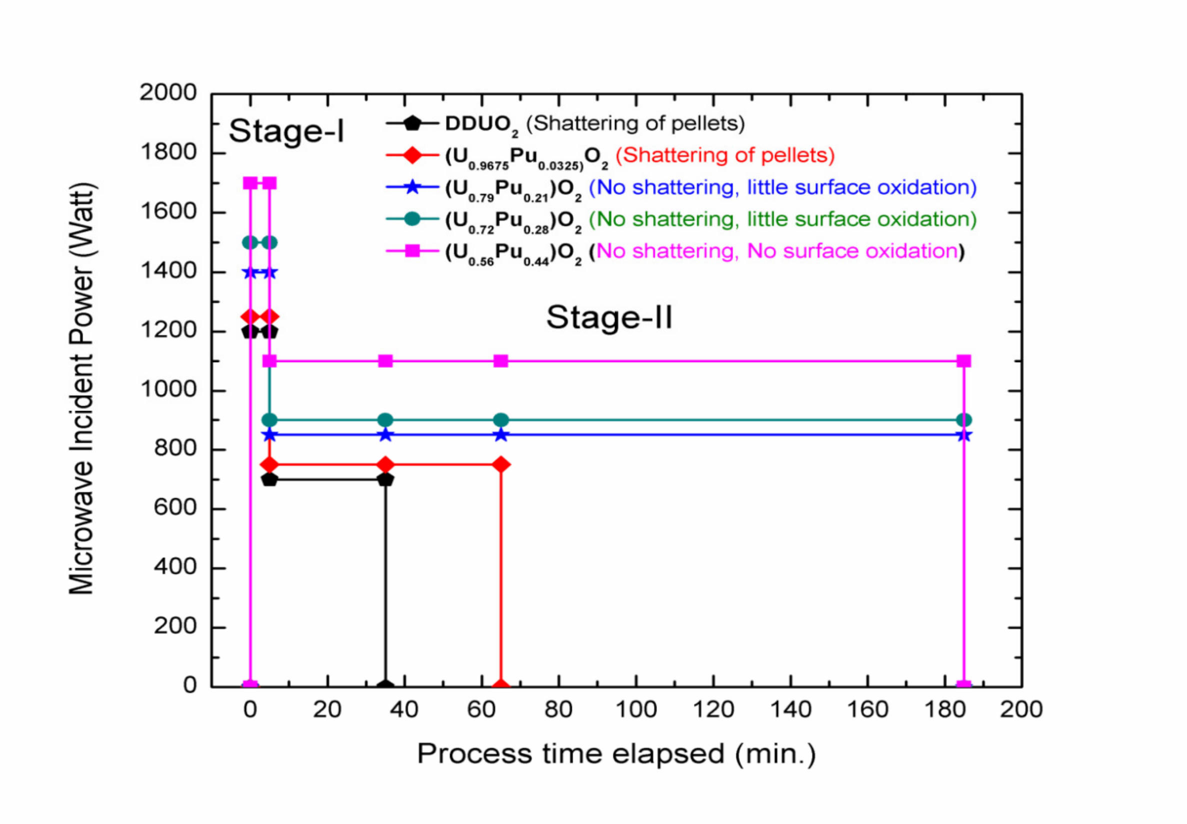

Fig. 4.15: Microwave Power Profile and Observations for MWDO Process of $(U_{1-y}Pu_y)O_2$

4.3.1.2 Conventional Oxidation of UO_2 and $((U_{1-y}Pu_y)O_2$

Similarly, oxidation batch experiments were conducted in a resistance furnace at temperature 700 °C for 4 h by conventional method. No shattering was observed in the pellets processed conventionally, however surface oxidation was observed. The oxidation from the surface of the pellets (powder dislodging from surface) was observed visually after carrying out the oxidation process as noticed by Campbell et al. [298]. Upon oxidation, the powder from the pellet surface started dislodging because oxidation started from the surfaces in contact with air. The powder formation from the surface was evident visually. The powder formation in materials B and B3 was almost complete. However, in higher Pu (> 20 wt%) MOX, the oxidation was partial. A fair judgment could also be made from the pellet initial surface finish and after the oxidation. The oxidised powder on the surface of the MOX pellet could easily be dislodged by even fingers of the hands or by a spatula contrary to the un-oxidised MOX pellets. The oxidation cycles for MWDO and conventional oxidation for $(U_{0.72}Pu_{0.28})O_2$ pellets are shown in **Fig. 4.16**.

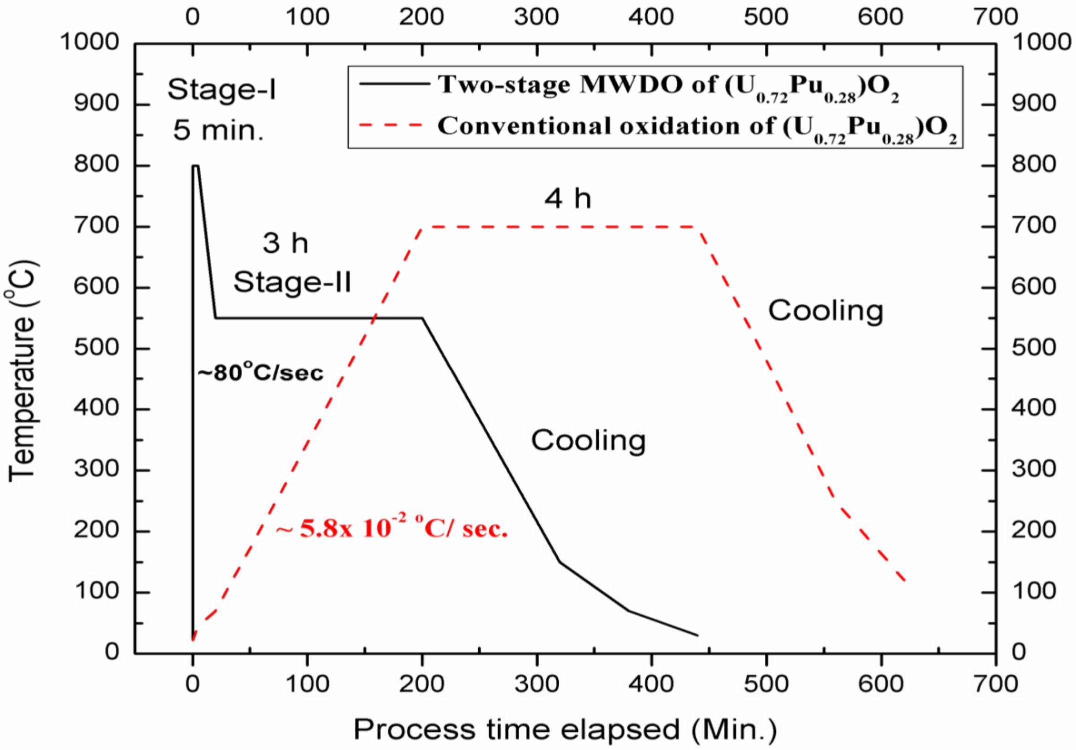

Fig. 4.16: Temperature Profiles of Two-Stage MWDO and Conventional Oxidation

The oxidised pellets were further milled in all the batch experiments using a coarse mixer-grinder (**Fig. 3.6**) and sieved through ASTM sieve # 40 (< 425 μm). The samples were then drawn for O/M ratio determination. The first MWDO cycle oxidised and micronized (using mixer grinder) material was again subjected to second and subsequent cycles to see any further improvement in the powder properties.

4.3.2 Microwave based Oxidative Pulverisation of $(U_{1-y}Pu_y)O_2$ MOX

In the stage-I of MWDO process, shattering was observed in the sintered pellets of $DDUO_2$ (B) and $(U_{0.9675}Pu_{0.0325})O_2$ (B3) whereas no shattering was observed in the MOX pellets containing 21, 28 and 44% PuO_2 (**Fig. 4.15**). Interestingly, no shattering was observed in UO_2 and MOX pellets oxidised by conventional process. However, oxidation from pellet surface was visually observable. In the oxidation of a UO_2 pellet, U_3O_8 formation started on the surfaces in contact with oxygen. The oxygen propagates along the grain boundaries and causes spallation of grains. Microwave directly interacts with the material and heat is generated internally throughout the bulk. The higher temperature rise rate (80 $^oC\ sec^{-1}$) in stage-I of MWDO as compared to conventional process of oxidation (~5.8×10^{-2} $^oC\ sec^{-1}$) **Fig. 4.16**, lead to the shattering of UO_2 and $(U_{0.9675}Pu_{0.0325})O_2$ pellets in the beginning of the process offering more surface area for oxidation reaction. Shattering of UO_2 pellets in stage-I may not be solely due to the thermal runaways caused by microwave. This might have resulted under the combined effect of thermal runaways and higher susceptibility of UO_2 towards oxidation as compared to MOX.

The stage-II processing time for $DDUO_2$ and $(U_{0.9675}Pu_{0.0325})O_2$ pellets was kept smaller, since complete oxidation was achieved within 30 min. and 60 min respectively (**Fig. 4.15**). Whereas in higher Pu MOX, stage-II processing was carried out for 3h, resulting more oxidation than the conventional process carried out for 4h at higher temperature (700 ^oC). The variation in the degree of oxidation of $(U_{1-y}Pu_y)O_2$ versus its PuO_2 content after subjecting to MWDO first cycle is shown in the **Fig. 4.17**. A total of four variations were studied for each composition of $(U_{1-y}Pu_y)O_2$ (except E, only two variations) as 1) MWDO in air, 2) MWDO in oxygen (O_2), 3) Conventional oxidation in air and 4) Conventional oxidation in O_2.

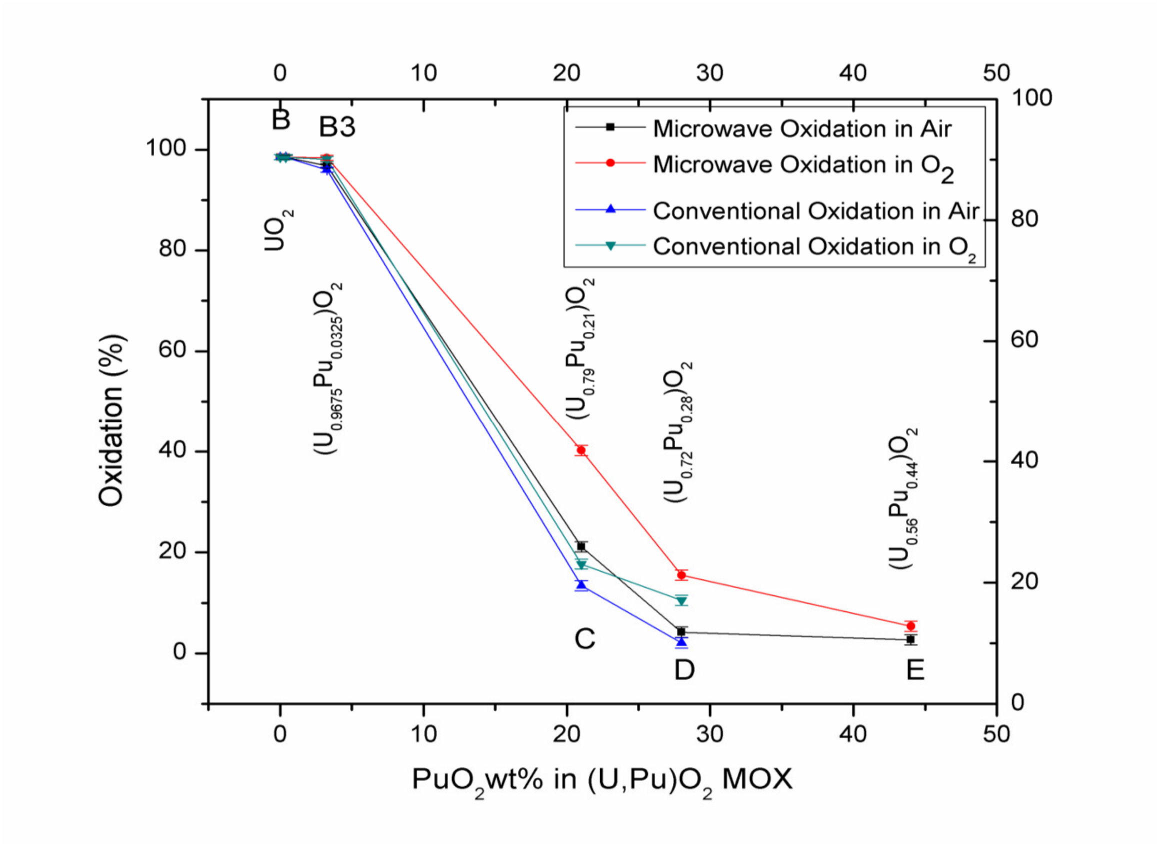

Fig. 4.17: Oxidation (%) as a function of PuO_2 (%) in MOX by MWDO and Conventional Oxidation

4.3.3 Factors Affecting MWDO Process

Several factors affect the process of oxidation of sintered UO_2 and $(U_{1-y}Pu_y)O_2$ MOX pellets. These are mainly temperature of oxidation, plutonium content, oxygen partial pressure, particle size, grain size, pellet density etc. [40, 244-246].

The temperature directly affects the rate of the oxidation. At low temperature (< 50 °C) the surface oxidation of UO_2 pellets gives UO_{2+x} forming a thin oxide layer (a few nanometers thick) of U_3O_7/ U_4O_9 (**§1.9.3.1**). The degree of oxidation below 50 °C is proportional to logarithm of time [245]. Above 100 °C, the rate of oxygen diffusion is rapid enough to cause sufficient oxidation. The bulk oxidation to orthorhombic U_3O_8 occurs at an easily measurable rate > 250 °C. The intermediates U_3O_7/ U_4O_9 are generally not observed in major quantities; instead, the bulk oxidation appears to proceed directly to U_3O_8 in temperature range 350-550 °C. Above 550 °C, the rate of U_3O_8 formation on sintered UO_2 pellets does not display Arrhenius behavior, but rather, it declines with increasing temperature. This behavior has been attributed to the increased plasticity of U_3O_8 formed above 550 °C; thus, the U_3O_8 forms a barrier to retard further oxidation [245]. The product of UO_2 oxidation remains U_3O_8 upto 1100 °C. Thus, the oxidation experiments using MWDO process were carried out at 550 °C in stage-II. The stage-I (800 °C, 5 min) of MWDO was aimed only at shattering of the pellets, to increase the surface area thereby the rate of oxidation.

The presence of plutonium increases the thermal stability of $(U_{1-y}Pu_y)O_2$ [245]. The oxidation of $(U_{1-y}Pu_y)O_2$ in air at 450-700 °C forms a mixture of orthorhombic $(U,Pu)_3O_8$ and FCC $(U,Pu)O_2$ whose composition depends upon PuO_2 content [245] and discussed in more details further **(§ 4.3.5.2**). Similarly, the presence of Th in UO_2 makes $(Th_{1-y}U_y)O_2$ more oxidation resistant than pure UO_2 [245]. The rate and the extent of UO_2 oxidation, both directly depend upon the oxygen partial pressure of the atmosphere and are strong function of particle size and hence the surface area. The sample with smaller particle size (larger surface area) reacts faster than that with large particle size or sintered pellets. For example, fine UO_2 powders react pyrophorically with oxygen, whereas UO_2 pellets reacts slowly.

Increased pellet density, results in the decreased rate of oxidation [244-245]. The low reactivity for high density UO_2 pellets is due to low open porosity in such samples. Smaller grain size usually offers higher oxidation as it facilitates the rapid diffusion of oxygen along the grain boundaries, followed by inter-granular oxidation. Indeed, it is generally difficult to separate the effects of grain size and sintered density. The O/M achievable depends upon the extent of oxidation (in %) which in turn is function of several parameters as discussed above. The theoretical O/M values corresponding to 100% oxidation are estimated based on the knowledge of higher oxides formed (**§ 3.6.2**). The following sections describe the effect of various factors influencing the oxidation of $(U_{1-y}Pu_y)O_2$ over a large range of PuO_2 (y: 0-0.44).

4.3.3.1 Effect of Mode of Heating

Fig. 4.15 reveals that a higher microwave power was needed to achieve the required temperature in both the stages of MWDO as PuO_2 content increased from nil to 44 wt% (y: 0 to 0.44) in MOX. This was assignable to increasing content of PuO_2 in the MOX. PuO_2 is comparatively a weaker microwave absorber than UO_2 and U_3O_8. The oxidation % variation in UO_2 (B, **Fig. 4.17**) and $(U_{0.9675}Pu_{0.0325})O_2$ (B3, **Fig. 4.17)** was not evident as both the compositions oxidized to same extent in the conventional and microwave oxidations. The oxidation was significantly higher using microwave heating in the high PuO_2 content $(U_{1-y}Pu_y)O_2$ (C and D, **Fig. 4.17**) as compared to the conventional. In the MOX containing 21wt% PuO_2 (C), more than two-folds higher oxidation (in %) was achievable using microwave (in O_2 atmosphere) as compared to conventional (in O_2 atmosphere). This may be attributed to internal and direct heating of material caused by microwave unlike surface heating in conventional resistance furnace. Though, visible shattering was not found in the oxidized MOX pellets. It might be due to formation of very small micro-cracks in the pellets allowing the permeation of air or oxygen through grain boundaries and hence the higher oxidation.

4.3.3.2 Effect of Atmosphere Oxygen Partial Pressure

Fig. 4.17 demonstrates that the oxidation (in %) achieved is similar in the sintered UO_2 and $(U_{0.9675}Pu_{0.0325})O_2$ pellets irrespective of atmosphere (air or O_2). The degree of oxidation however, is distinctively larger in O_2 atmosphere than in air in high Pu MOX (C, D and E). This was due to higher oxygen potential of O_2 atmosphere than air and is in agreement with the fact that the rate of oxidation is directly proportional to oxygen partial pressure [245].

4.3.3.3 Effect of MOX PuO_2 Percentage

As PuO_2 content increased in MOX, the oxidation (%) reduced due to decreased susceptibility of higher PuO_2 containing MOX towards oxidation. In the solid state, oxidation of UO_2 to U_3O_8 is thermodynamically a feasible phenomenon [245] contrary to PuO_2 which cannot be oxidised to its higher oxides [299-300]. This makes low PuO_2 content MOX susceptible for higher oxidation and vice-versa. **Fig. 4.17** shows that the oxidation of the sintered UO_2 and $(U_{0.9675}Pu_{0.0325})O_2$ was nearly 100% for all the variations studied since, the content of plutonium is lesser in $(U_{0.9675}Pu_{0.0325})O_2$ so as to retard its oxidation. Further, **Fig. 4.17** shows that the oxidation (%) was higher in $(U_{0.79}Pu_{0.21})O_2$ and least in $(U_{0.56}Pu_{0.44})O_2$ MOX. These findings are similar to those reported by Seehars et al. [296]. They [298] found a strong decrease in the degree of pulverization of MOX pellets with increasing Pu content. The plutonium lead to enhancement in the thermal stability of the MOX pellets.

4.3.3.4 Effect of Multiple Oxidation Cycles and Initial Micronisation

The high plutonium MOX pellets (C, D and E) were not completely oxidised in the first oxidation cycle (**Fig. 4.17**) therefore subjected to more number of oxidation cycles after milling. The BET-SSA and oxidation (%) after first, second and third MWDO cycles for $(U_{0.72}Pu_{0.28})O_2$ MOX are shown by bar graphs in **Fig. 4.18**. It is evident from **Fig. 4.18** that the degree of oxidation (in %) and the SSA significantly increased with number of successive oxidation cycles. The oxidation after MWDO cycle-1 (first cycle) was low (~ 5%), since the starting material comprised sintered intact pellet. The oxidation % increased upto 25% in the MWDO cycle-2 (second cycle) because the starting material was now micronised.

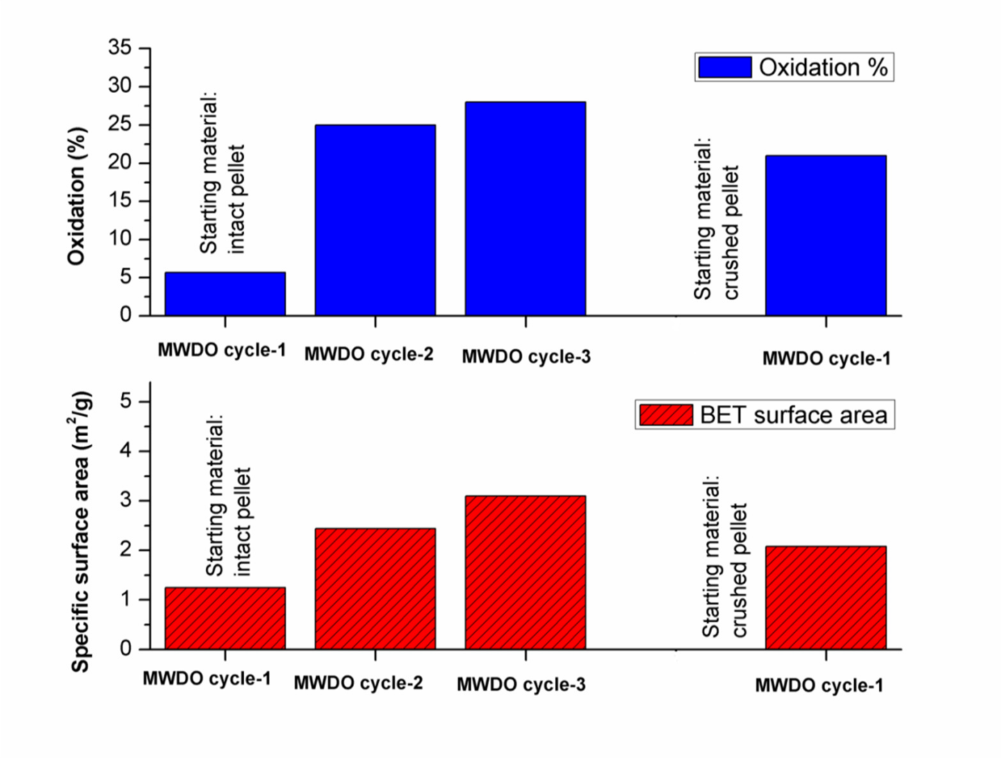

Fig. 4.18: Effect of Physical Form of the Starting Material and Multiple Oxidation Cycles on the Surface Area and Oxidation (%) in $(U_{0.72}Pu_{0.28})O_2$ MOX

This increase in oxidation may be attributed to the micronisation which has increased the SSA in contact with air and hence the extent of oxidation. As oxidation increased, the SSA was found to be increased (**Fig. 4.18**). The transformation of MO_2 into M_3O_8 is attributable for the increased SSA subsequent to multiple oxidation cycles in addition to micronisation. The effect of initial material physical form as pellet or powder has profound effect on the degree of oxidation (in %). **Fig. 4.18** shows that the micronisation of the sintered MOX after crushing tremendously increased the SSA after first MWDO cycle. Mernache et al. [35] found that the SSA of the recycled UO_2 powder increases with number of oxidation-reduction cycles.

Fig. 4.17 shows that the oxidation of the sintered UO_2 (B) and $(U_{0.9675}Pu_{0.0325})O_2$ (B3) is nearly 100% for all the variations studied hence, any of the four variations can be used for their oxidative pulverization for purpose of recycling. With increasing plutonium in MOX (C, D and E), the oxidation in O_2 atmosphere using microwave brought out highest % oxidation in all the cases. Microwave oxidation of C in air was higher than the conventional in O_2. However, in D, the conventional oxidation in O_2 was found to be more than MWDO in air. This may be attributable to the effect of oxygen partial pressure which was more predominant than the microwave heat. The MWDO in O_2 and in air atmospheres brought out comparable % oxidation (slightly higher in O_2) in $(U_{0.56}Pu_{0.44})O_2$. This was assignable to the high content of PuO_2 in E which made it sufficiently stable such that the variation in partial pressure of the atmospheres was hardly bringing any change in the oxidation achievable. Thus, MWDO in O_2 is preferable for oxidation of higher PuO_2 MOX. The oxidation can be further enhanced by incorporating the micronisation and/ or successive oxidation cycles.

4.3.4 Characterization of MWDO Process Recycled Powder

The variation of bulk density of the oxidized powders as function of PuO_2 % in MOX after first MWDO cycle is shown in **Fig. 4.19**.

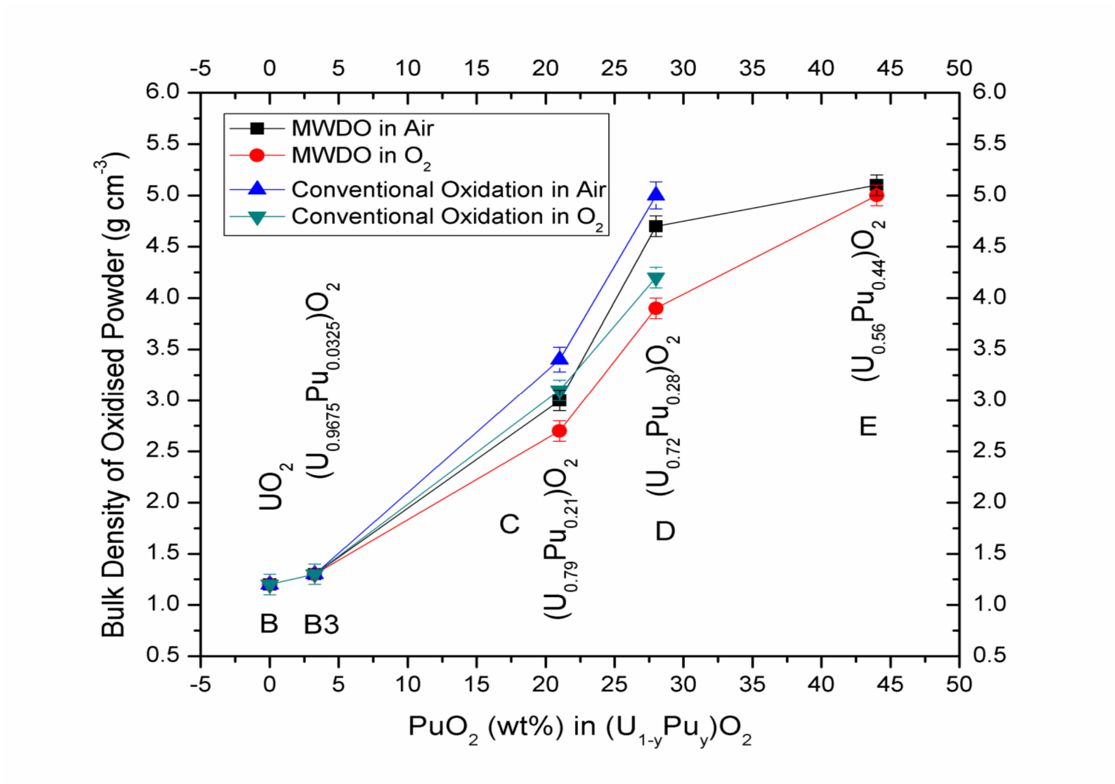

Fig. 4.19: Variation of Bulk Density in Oxidised Powders after First MWDO cycle

The SSA of various oxidized (referred Ox) powders after first MWDO cycle and that of standard UO_2 is shown by histograms in **Fig. 4.20**. The standard UO_2 powder (A) was oxidised under identical conditions for comparative evaluation. The bulk density in Ox-A was comparable to that in the Ox-B (**Fig. 4.19**). The BET-SSA was found to decrease in the oxidised samples as PuO_2 increased in MOX (**Fig. 4.20**). A slight more surface area was found in Ox-A as compared to sample A due to formation of U_3O_8.

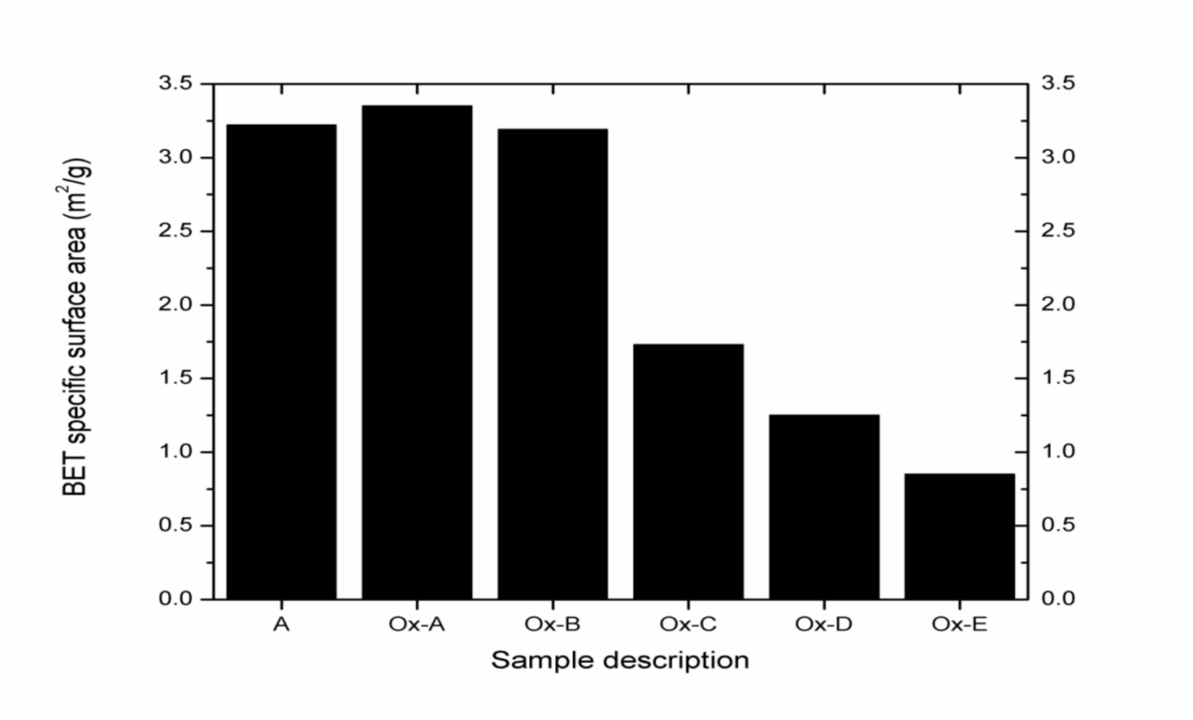

Fig. 4.20: SSA of Oxidised Powders after First MWDO Cycle versus Standard UO_2

4.3.5 Microwave Oxidation of $(U_{1-y}Pu_y)O_2$ Fuel Pellets

4.3.5.1 Oxidation of UO_2 Pellets

The conventional oxidative or thermo-mechanical pulverisation technique has been employed in recycling of defective nuclear fuel pellets for long time. A large volumetric increase (36%) arising from transformation of FCC UO_2 to orthorhombic U_3O_8 subsequent to oxidation leads to generation of internal stresses and hence pulverisation of sintered compacts [245-246]. The oxidation reaction is function of mainly surface area, particle size, grain size, density, temperature and oxygen potential [245]. The UO_2 to U_3O_8 transformation has been thoroughly studied and proceeds via formation of U_3O_7/U_4O_9. Formation of intermediates U_3O_7/U_4O_9 from UO_2 involves a slight volume reduction and follows diffusion-controlled kinetics [248]. In contrast, U_3O_8 formation from UO_2 accompanies volume increase and displays sigmoidal “nucleation-and-growth” kinetics. The U_3O_8 formed on a sintered UO_2 pellet generally spalls from the surface as a fine powder. The time required for visual observation of U_3O_8 powder is referred to as the powder formation time, t_p [298]. The t_p for UO_2 in the MWDO process was < 5 min. since powder formation was observed in the stage-I of the process.

4.3.5.2 Oxidation of $(U_{1-y}Pu_y)O_2$ MOX Pellets

The presence of PuO_2 in the MOX reduces its ability to undergo oxidation and thus making oxidative pulverisation based methods more difficult. The PuO_2 is the most stable oxide of Pu and resist its further oxidation [114, 212]. The difficulties in oxidation of MOX pellets containing PuO_2 > 20 wt% by conventional thermal treatment in air has already been discussed [11, 296-297]. The applicability of microwave based oxidative pulverisation depends upon the microwave coupling behavior of UO_2, U_3O_8 and PuO_2 and oxidation characteristics. UO_2, U_3O_8, PuO_2 are known to be strong coupling materials at microwave frequency 2450 MHz and high temperature can be achieved (**Table 2.3**). However, PuO_2 comparatively has lower dielectric loss properties as compared to UO_2. UO_2 can be easily oxidized to U_3O_8 whereas PuO_2 cannot be oxidised to its higher oxides upon heating [299-300]. PuO_2 is the stable oxide of Pu and below 2100 ^{o}C no oxides of higher oxidation are formed [114, 212]. In the $(U,Pu)O_2$, two important parameters viz. thermal response in microwave field and oxidation ease depends upon its composition. Higher the content of PuO_2 in MOX, lower was the ease of oxidation and microwave absorption.

The accuracy in the estimation of oxidation (%) depends upon the precise and accurate measurement of U, Pu contents and O/U or O/(U+Pu) ratio. The precise methods described in section § **3.5.3** were used. The % oxidation of MOX was estimated using final O/M ratio of the oxidized MOX using Eq. (3.9). The X-ray diffractogram of $(U_{0.72}Pu_{0.28})O_2$ MOX and MWDO oxidised powder is shown in **Fig. 4.21**. The oxidation of $(U_{0.72}Pu_{0.28})O_2$ showed the formation of orthorhombic $(U,Pu)_3O_8$ phase (M_3O_8) and FCC $(U,Pu)O_2$ phase (MO_2).

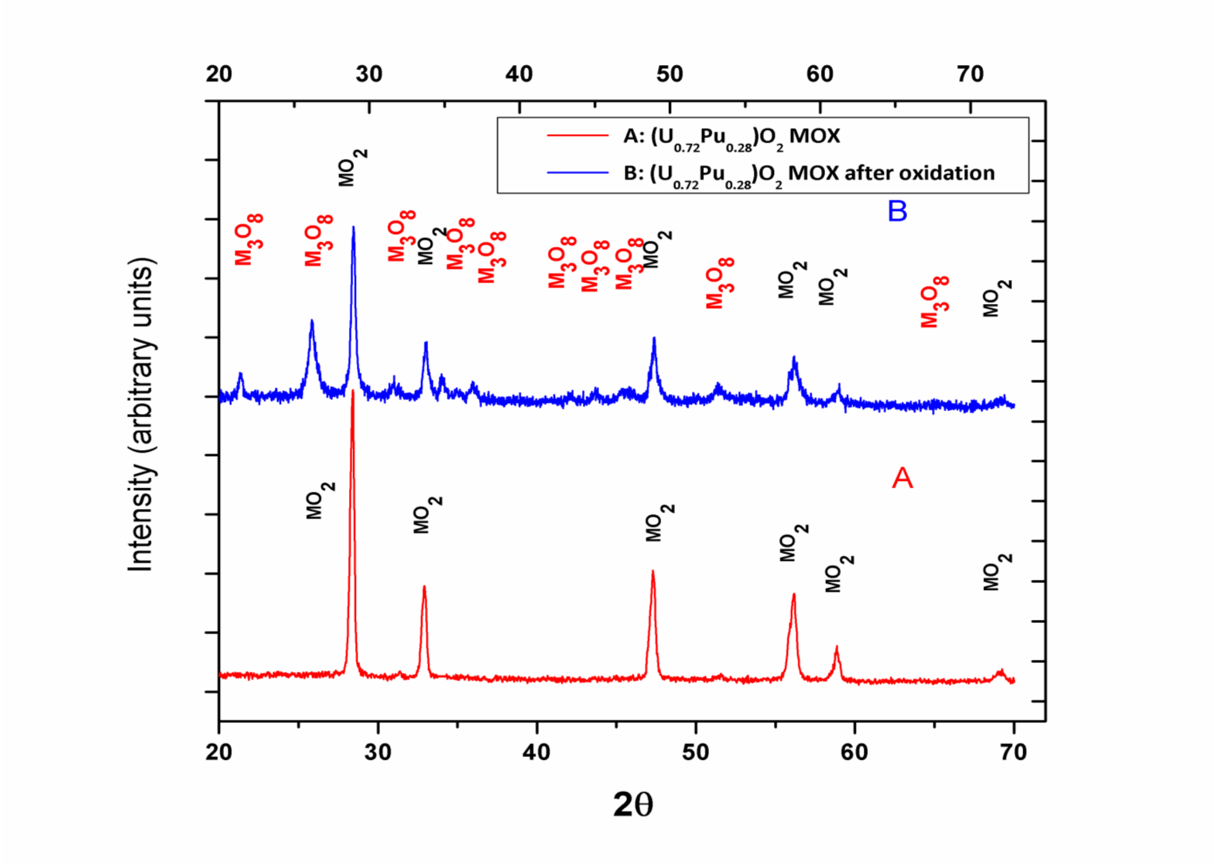

Fig. 4.21: X-Ray Diffractogram of MWDO Oxidised $(U_{0.72}Pu_{0.28})O_2$ Powder after Cycle-3

The oxidation of $(U_{1-y}Pu_y)O_2$ produces mixture of hypo-stoichiometric uranium rich orthorhombic phase $(U,Pu)_3O_{8-x}$ and/ or hyper-stoichiometric plutonium rich FCC phase $(U_{1-y}Pu_y)O_{2+x}$ whose composition depends upon Pu content in the MOX [301-304]. Here x represents the oxygen non-stoichiometry in the crystal structures. The Pu content in the MOX plays an important role in the formation of different phases formed subsequent to oxidation.

For 0-5 wt% PuO_2 in MOX, orthorhombic $(U,Pu)_3O_{8-x}$ is the only phase. The oxidation of MOX having 5-30 wt% PuO_2 (y: 0.05-0.3) gives a biphasic system containing uranium rich $(U,Pu)_3O_{8-x}$ (M_3O_8) and plutonium rich $(U_{1-y}Pu_y)O_{2+x}$ (MO_2) where orthorhombic $(U,Pu)_3O_{8-x}$ is the major phase. Above 30 wt% PuO_2, orthorhombic phase starts decreasing and FCC phase is major phase [212, 301]. However, for Pu > 50 wt%, $(U_{1-y}Pu_y)O_{2+x}$ is reported to be only single FCC phase [304-305]. The formation of orthorhombic phase accompanies volume increase and hence the pulverization occurs. This suggested that the oxidative pulverisation based recycling is difficult above Pu> 50 wt% MOX. However, this discussion principally agrees for applicability of oxidative pulverisation based methods for MOX up to 50 wt% PuO_2. As PuO_2 wt% increases in the MOX, the tendency of formation of the orthorhombic phase M_3O_8 decreases and thus, the oxidative pulverisation.

4.3.6 Reduction of Oxidised U_3O_8 and Biphasic Mixture (M_3O_8, MO_2)

The reduction of oxidized materials was carried out conventionally in resistance furnaces at 700 °C and 4h flowing (N_2+7%H_2) mixture gas. The microwave reduction has been developed for stoichiometric reduction of U_3O_8 and biphasic mixture (M_3O_8,MO_2), M: (U,Pu) powders which is a novel method (described in **Chapter 7**) in view of shorter processing cycle, lower temperature processing, improved powder properties and energy efficiency as compared to conventional reduction methods. The optimum condition for reduction of U_3O_8 and (M_3O_8,MO_2) mixture using 2.4 GHz microwave was 550 °C and 3 h.

4.3.7 Oxide and MOX Fuel Fabrication using MWDO Recycled Powder

The powder obtained after first MWDO cycle for sintered pellets (B and B3) and after three successive MWDO cycle for High Pu MOX (C, D and E) were used (after reduction) for fabrication of MOX fuel using the flow sheet as shown in **Fig. 4.22**. Experimental batches (size: 500 g) of UO_2 and $(U_{1-y}Pu_y)O_2$ fuel were fabricated using MWDO recycled powder following the standard powder-pellet route. The composition, dimensions of the pellets fabricated from the recycled powder, batch SRR and sintered densities are listed in **Table 4.8**.

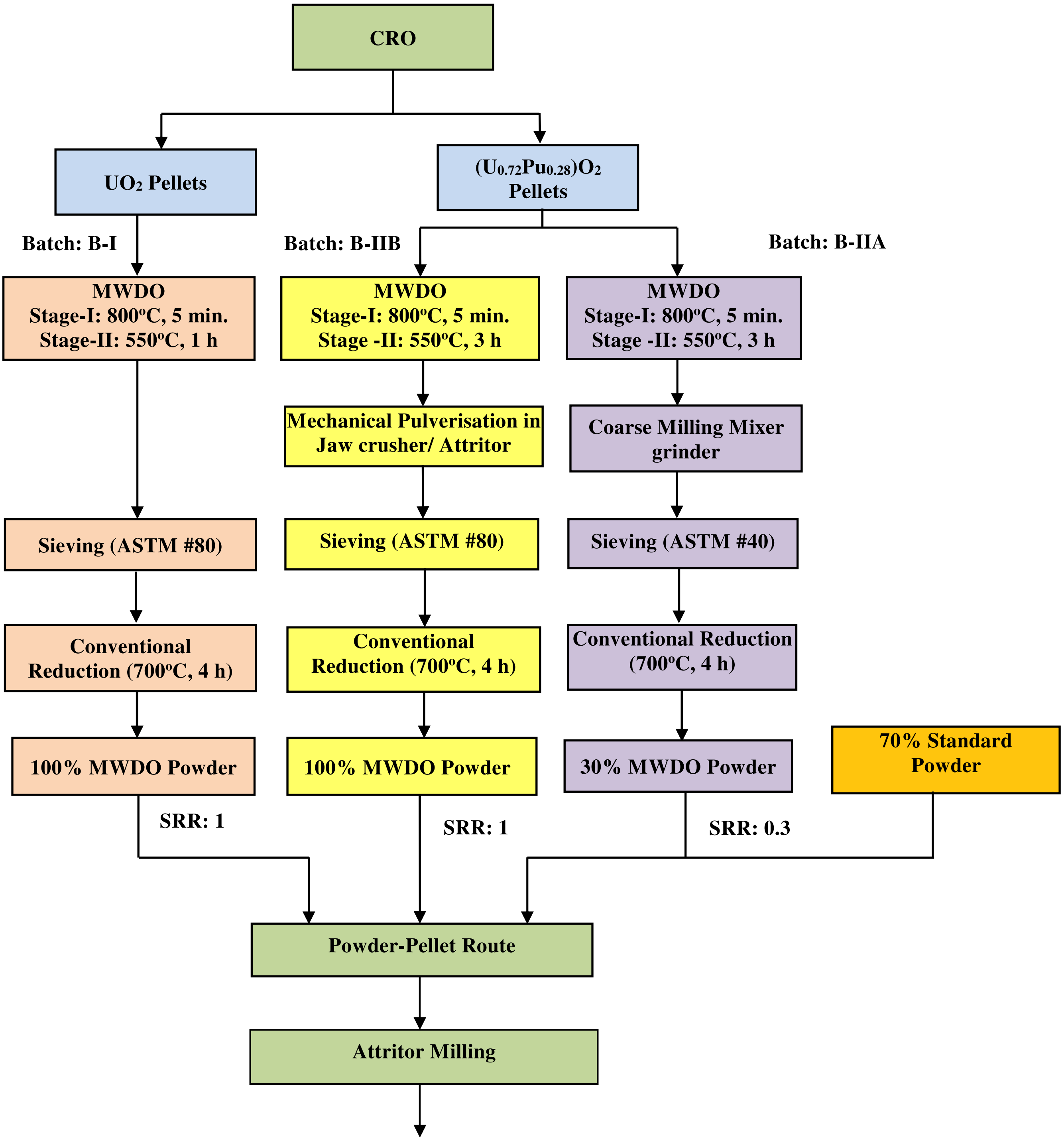

Fig. 4.22: Flow Sheet for MOX Fuel Fabrication using MWDO Process Recycled Powder

Table 4.8: Batch Details of Fuel Pellets Fabricated using MWDO Recycled Powders

Batch	Composition, dimensions OD, ID, Ht. (mm)	SRR	Starting Material for Fuel Batch	Powder recycling treatments	Sintered Density (% TD) ($\bar{x}$±1s), n=32
B-I	$DDUO_2$ (5.5, __, 6-8)	1	MWDO processed $DDUO_2$ powder	MWDO cycle-1	94±2
B-IIA	$(U_{0.72}Pu_{0.28})O_2$ (5.5, 1.8, 6-8)	0.3	30 wt% MWDO recycled+70 wt% standard powder	MWDO cycle-1 and micronisation in mixer-grinder	93±2
B-IIB	$(U_{0.72}Pu_{0.28})O_2$ (5.5, 1.8, 6-8)	1	100% MWDO recycled powder	Three successive MWDO-micronisation cycles and attritor milling	93±2

4.3.7.1 UO_2 Fuel Fabrication

The properties like bulk density (**Fig. 4.19**) and specific surface area (**Fig. 4.20**) of UO_2 powder after first MWDO cycle from sintered UO_2 pellets (**B**, **Table 3.2**) were found to be comparable to standard UO_2 powder (**Table 3.1**). The Batch, B-I (**Fig. 4.22**, **Table 4.8**) was fabricated using 100% MWDO recycled UO_2 powder (obtained after first MWDO cycle) and has shown acceptable density. Hence, UO_2 pellets could be successfully recycled using MWDO cycle-1 only, eliminating the need of successive multiple oxidation cycles.

4.3.7.2 Low Plutonium Content $(U_{1-y}Pu_y)O_2$ MOX Fuel Fabrication

The CRO containing low PuO_2 content (**B3, Table 3.2**) was recycled using MWDO cycle-1 and followed by reduction similar to UO_2. Since, the plutonium content is low, it behaves like UO_2 only. The bulk density (**Fig. 4.19**) and BET surface area (**Fig. 4.20**) shows that the values were nearly similar to that oxidized $DDUO_2$ pellets (B). Hence, cycle-1was sufficient for obtaining sinterable grade powder from **B3**.

4.3.7.3 High Plutonium Content $(U_{1-y}Pu_y)O_2$ MOX Fuel Fabrication

In case of recycled MOX powder, the bulk density was found to increase with increasing PuO_2 % in $(U,Pu)O_2$ MOX (**Fig. 4.19**). The degree of oxidation (**Fig. 4.17**) and surface area (**Fig. 4.20**) were found to decrease with increasing content of PuO_2. The MOX with high plutonium content could not be completely used for fuel fabrication after first MWDO cycle thus resulting in SRR <1. The batch B-IIA fabricated using 70 wt% standard powder has delivered SRR of 0.3 only. The SRR of 1 was achieved by subjecting the coarse milled powder to the attritor mill after three oxidation-micronisation cycles as demonstrated in batch B-IIB (**Fig. 4.22**).

4.3.8 Quantity of UO_2 and $(U_{1-y}Pu_y)O_2$ Recycled using MWDO Method

Table 4.9 records the total quantity of the UO_2 and $(U_{1-y}Pu_y)O_2$ MOX rejects recycled using the dry MWDO process (**Fig. 4.22**). After establishing the MWDO process (**Fig. 4.22**) several fuel batches (each 10 Kg) were fabricated. The acceptance of the batches sorted for correct diameter was >75%. The $DDUO_2$ and $(U_{0.9675}Pu_{0.0325})O_2$ were recycled using MWDO cycle-1 only. However, in $(U_{0.79}Pu_{0.21})O_2$ and $(U_{0.72}Pu_{0.28})O_2$, some batches were fabricated employing 100% recycled powder from multiple (3) MWDO-micronisation cycles. A few were prepared by addition of 30 wt% of the recycled powder into the standard powder using single MWDO cycle.

Table 4.9: Record of UO_2 and $(U_{1-y}Pu_y)O_2$ MOX Recycled using Dry MWDO Method

Material Description	Quantity (Kg)	Linkage to Programme
$DDUO_2$	160	PFBR axial blanket
$(U_{0.9675}Pu_{0.0325})O_2$	7	BWR MOX
$(U_{0.79}Pu_{0.21})O_2$	42	PFBR MOX, Enrichment-I
$(U_{0.72}Pu_{0.28})O_2$	25	PFBR MOX, Enrichment-II

4.3.9 Summary of Microwave based Dry Recycling Processes

Microwave based direct oxidation process was investigated for recycling of rejected sintered UO_2 and $(U_{1-y}Pu_y)O_2$ pellets. The MWDO is a dry recycling process and consists of two distinct stages where in the stage-I, temperature of 800 °C was achieved rapidly with intense temperature rise rate (80 °C sec^{-1}) aiming at cracking of pellets. A lower temperature (550 °C) for longer time (3 h) was kept in the stage-II so as to give highest oxidation and sufficient time reaction. A pictorial depiction of the MWDO process is shown in **Fig. 4.23**.

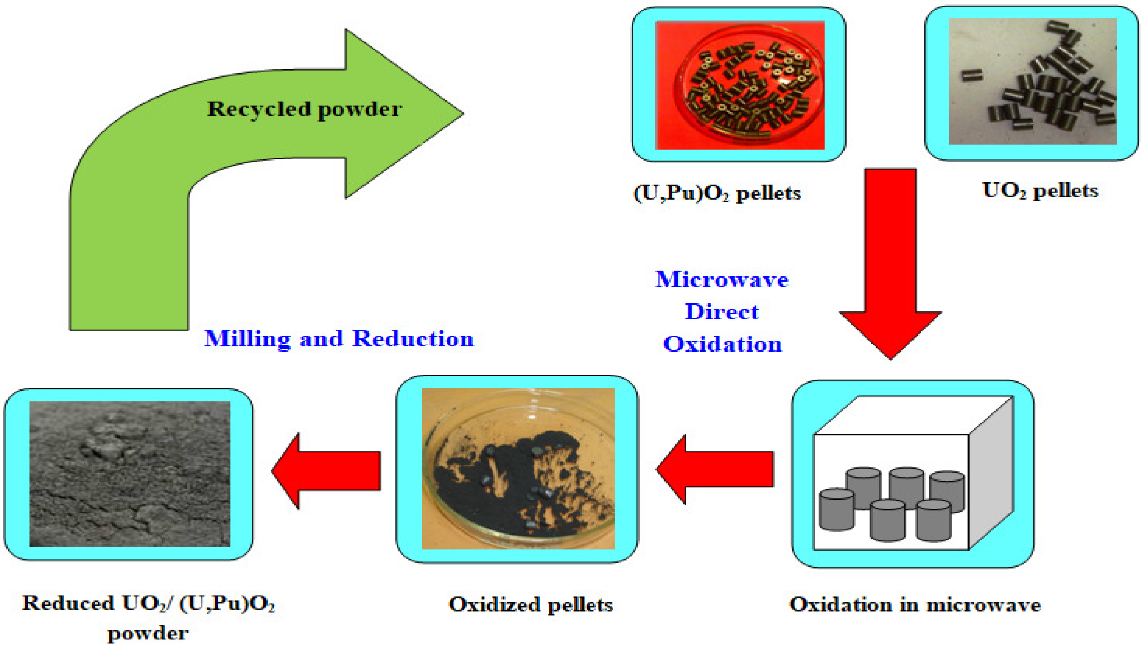

Fig. 4.23: Schematic of Microwave Direct Oxidation Process for Recycling of $(U_{1-y}Pu_y)O_2$

The summary of the detailed experimental investigations is given below:

1. The microwave based oxidation as in MWDO was superior to the conventional dry oxidation owing to smaller processing time and higher oxidation (%) achievable especially in higher Pu content (y>0. 2) $(U_{1-y}Pu_y)O_2$ MOX.
2. The shattering of UO_2 and $(U_{0.9675}Pu_{0.0325})O_2$ pellets was observed in MWDO. Notably, it could not shatter MOX pellets with PuO_2 >20 wt% (y> 0.2), however significant oxidation was found.

3. The flow sheet was developed for use of MWDO recycled powder with maximum utilization of scrap delivering SRR of 1.
4. The multiple micronisation-oxidation cycles further enhanced the oxidation (%) and surface area of recycled powder. Three successive microwave oxidation-micronisation cycles and attritor milling of $(U_{0.72}Pu_{0.28})O_2$ yielded powder having surface area more than 3 m^2g^{-1}. The initial micronisation/ crushing of the sintered pellets significantly favour the oxidation process.
5. The SSA and oxidation (%) of the MWDO recycled powder could be enhanced when microwave oxidation is carried out in an atmosphere with higher oxygen partial pressure (oxygen atmosphere).

4.4 Comparative Evaluation of Microwave based Wet and Dry Processes for Recycling of Sintered UO_2 and $(U_{1-y}Pu_y)O_2$ MOX

The wet recycling scheme using Modified-MWDD is applicable in the entire range of plutonium composition in $(U_{1-y}Pu_y)O_2$. The recycled powders can be used on 100% basis for fuel re-fabrication. The Modified-MWDD is a multiple recycling method wherein the powder properties are regenerated in every recycle.

The dry recycling scheme using MWDO process is difficult to be implemented in the entire range of Pu in $(U_{1-y}Pu_y)O_2$. The % oxidation drastically decreases with increase in the plutonium content. MWDO process is alike to the conventional dry recycling approach where the powder properties keep on deteriorating with number of recycles. Thus, after a few number of recycles the powder may not be usable on 100% basis. This is due to excessive recrystallization of the powder particles undergoing increased number of heat treatments. The bulk density of powder and the particle size goes on growing, the SSA decreasing with decreased porosity.

Chapter 5

DEVELOPMENT OF METHODS FOR RECYCLING OF ThO_2 AND ThO_2 BASED MOX

5.1 Introduction

The fuel development pragramme for AHWR and AHWR-LEU or others has piled-up variety of thoria based sintered pellets either rejected or surplus [77, 81, 85-86, 143]. These comprise, ThO_2, $(Th_{1-y}U_y)O_2$ with UO_2 range of 0-30 wt% (y; 0-0.3) and $(Th_{1-y}Pu_y)O_2$ with PuO_2 range < 10 wt% (y< 0.1). The recycling of ThO_2 based rejected sintered pellets is essential for ThO_2 fuel fabrication plants. Conventionally processed recycled powder possesses poor sinterability and thus requires addition of fresh powder [41, 208]. Thus, work was pursued for developing methods for 100% recycling of sintered ThO_2 based rejects. $^{233}UO_2$ and $LEUO_2$ were simulated with $DDUO_2$ unless stated.

The recycling of ThO_2 based MOX fuels is difficult as compared to UO_2 based fuels. ThO_2 is a stable stoichiometric compound [118] and doesn't undergo oxidation like UO_2. UO_2 undergoes oxidation to U_3O_8 causing nearly 36% crystal volume increase, thereby making feasible the oxidative pulverization of sintered rejects [245]. Similarly, the reduction of ThO_2 to lower oxides is not feasible. Therefore, the dry recycling of ThO_2 sintered pellets by oxidative or oxidative-reductive pulverization is not feasible.

However, the presence of UO_2 in $(Th_{1-y}U_y)O_2$ MOX opens an option for oxidative pulverisation of the matrix and hence, its dry recycling. Oxidation of $(Th_{1-y}Pu_y)O_2$ is not feasible as PuO_2 cannot be oxidized to higher oxidation states in solids. Further, the comminution processes, where sintered rejected pellets are mechanically crushed into powder are universally applicable.

The recycling may be carried out by dissolving sintered thoria based pellets in HNO_3 following standard oxalate precipitation-calcination processes from thorium nitrate solution [20, 99]. However, this alternative requires addition of highly corrosive fluoride for dissolution [216, 237-239, 306] and generates enormous quantities of active liquid waste.

The thoria and thoria-urania powders were successfully prepared by bulk microwave denitration [21-23]. The combustion synthesis of ThO_2 and $(Th_{1-y}U_y)O_2$ solid solutions using citric acid, glycine and PVA by microwave heating have been reported [73-75, 121, 307]. The powders so produced are highly sinterable and leave conventional methods far behind. Therefore, direct denitration of thorium nitrate or co-denitration of mixed thorium-uranyl/ plutonyl nitrate solutions using microwave was explored for recycling the thoria based rejected sintered pellets.

5.2 Development of An Integrated Process for Recycling of ThO_2 based MOX

The integrated method was developed for 100% recycling of ThO_2, $(Th_{1-y}U_y)O_2$ (y; 0-0.3) and $(Th_{1-y}Pu_y)O_2$ (y; 0-0.1) sintered pellets. The method entails conjunction of comminution processes with the microwave dissolution-denitration for recycling of ThO_2 and $(Th_{1-y}Pu_y)O_2$ fuel rejects. For $(Th_{1-y}U_y)O_2$ rejects, comminution was followed by conventional air oxidation and microwave dissolution-denitration method. The integrated method produced sinterable powder which can be 100% utilised for fuel re-fabrication. The properties of recycled powder were compared with the standard powders (**Table 3.1**). A profound effect on the powder physical properties was observed due to presence of UO_2 and by addition of PVA during microwave denitration. The experimental work consisted of batch experiments, characterization of intermediates or products, suitability assessment of recycled powder for re-fabrication of fuel, flow sheet development and comparative analysis.

5.2.1 Process Flow Sheet for Integrated Method of Recycling

The flow sheet for recycling thoria fuel rejects by integrated method is shown in **Fig. 5.1.** The sintered pellets were crushed to coarse powder using a jaw crusher (**Fig. 3.4**). The coarse powder in case of ThO_2 and $(Th_{1-y}Pu_y)O_2$ was directly attritor milled and in the case of $(Th_{1-y}U_y)O_2$, it was subjected to air oxidation at 700 °C for 4h in conventional resistance furnace (200 °C/ h) and subsequently for attritor milling. The attritor milling (40 min., 200 rpm) further resulted in micronisation of the coarse powder which was sieved through standard ASTM sieves.

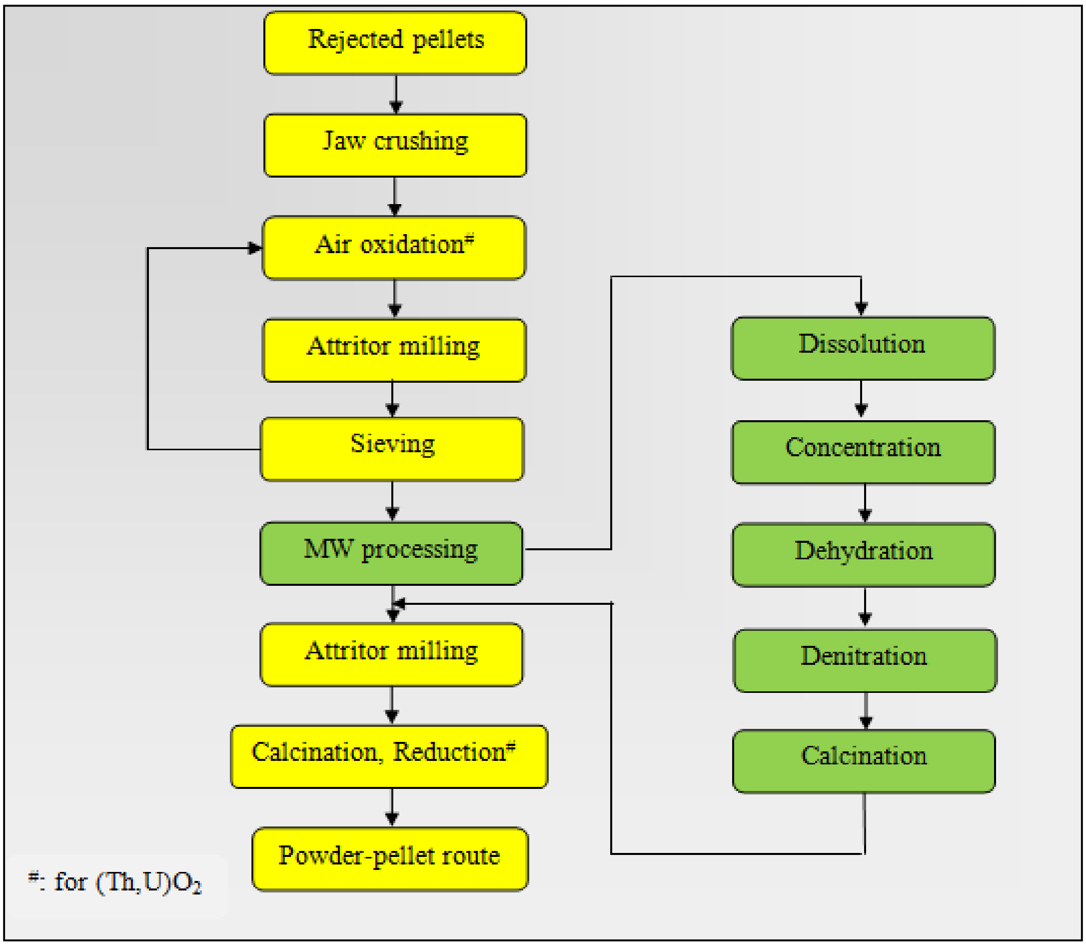

Fig. 5.1: The Integrated Process Flow Sheet for Recycling of ThO_2 based Clean Rejects

The sieved powder (in batch wise mode) was taken for aqueous processing using microwave. It was dissolved in 16M HNO_3 in quartz denitration vessels (**Fig. 3.11**) in microwave processing system. Several batches of 500 g of sieved powder in 1000 ml of HNO_3 were dissolved and denitrated. The typical temperature profile during microwave dissolution and denitration of a batch is shown in **Fig. 5.2**. **Fig. 5.2** also depicts the various stages of the process up to metal oxide conversion.

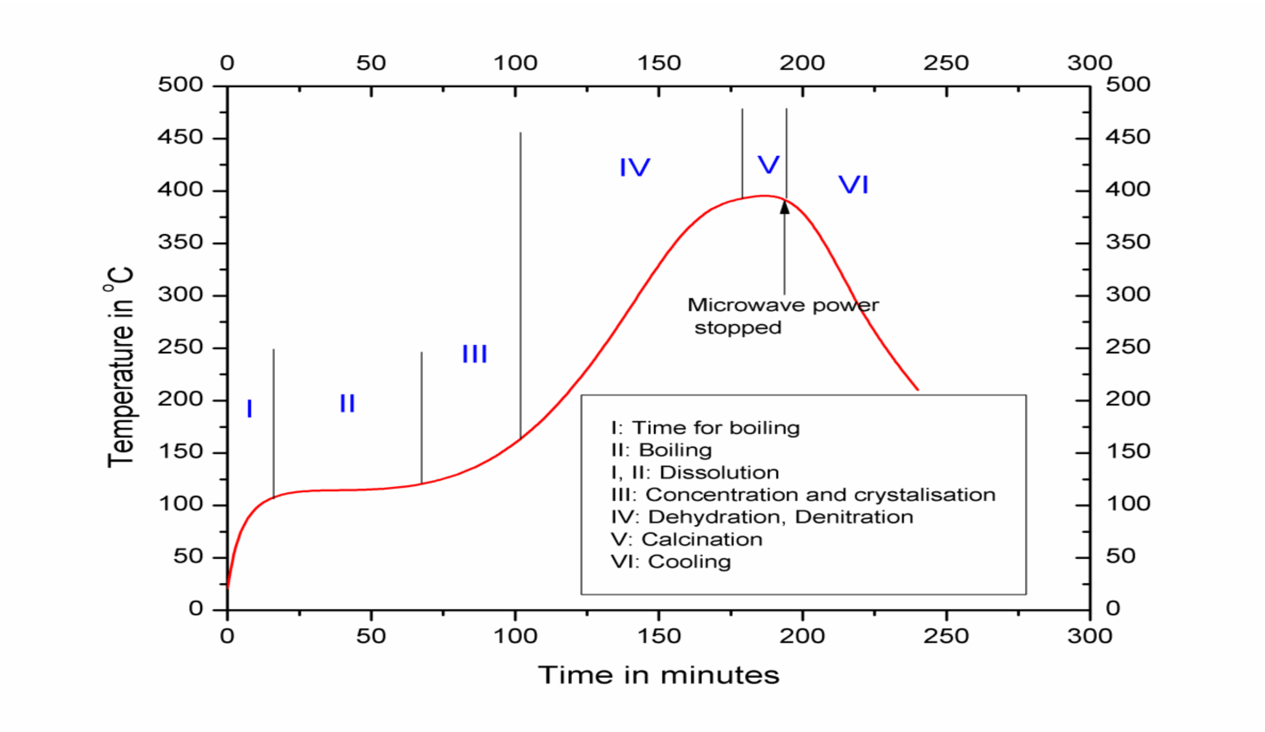

Fig. 5.2: Temperature Profile of ThO_2 Microwave Dissolution-Oxidative Denitration

The porous and dry cake of oxide or mixed oxide was obtained as product. Using spatula the dry cake in the form of clinkers was removed from the process vessel. The clinkers were attritor milled and subjected to air calcination at 700 °C, 2h for ThO_2 and $(Th_{1-y}Pu_y)O_2$. The calcination and reduction (700 °C, 4h) for (ThO_2,U_3O_8) was carried out.

5.2.2 Process Chemistry of Microwave Denitration in Integrated Process

5.2.2.1 Dissolution and Concentration

The attritor milled and sieved powder was dissolved in boiling HNO_3 to form their soluble nitrates using HF as catalyst. The dissolution of ThO_2 is shown by Eq. (1.19) [9, 216, 237-241, 306]. The dissolution of UO_2 and PuO_2 are described through Eq. (1.14) and Eq.

(1.15) respectively. The dissolved thorium nitrate solution was further heated to concentrate and crystallize or solidify by removal of excess H_2O and HNO_3. The dissolution, concentration and crystallization are depicted in I, II and III zones in **Fig. 5.2**. This resulted in formation of hydrated crystals of thorium nitrate as represented by Eq. (5.1).

$$Th(NO_3)_4\,(aq.) \rightarrow Th(NO_3)_4.5H_2O \qquad (5.1)$$

5.2.2.2 Dehydration and Denitration

In the process of dehydration, water of crystallization of nitrates was removed to get nitrates with reduced water of crystallization above 120 °C (zone IV in **Fig. 5.2**). The partially hydrated nitrates were decomposed to respective oxides or mixed oxide on further heating. The denitration reaction for thorium nitrate pentahydrate is shown by Eq. (5.2) [73-74,110].

$$Th(NO_3)_4.5H_2O \rightarrow ThO_2 + 4\,NO_2 + O_2 + 5\,H_2O \qquad (5.2)$$

The nitrogen dioxide (NO_2) combines with available H_2O and oxygen, and forms HNO_3. After partial dehydration, the uranyl nitrate dihydrate undergoes oxidative denitration to form UO_3 through formation of uranyl hydroxy nitrate compound as shown by Eq. (4.4), Eq. (4.5) and Eq. (4.8) [15, 130-132]. Plutonium (IV) nitrate upon boiling converts to plutonyl nitrate Eq. (4.2), the hexavalent oxidation state similar to uranium [124]. $PuO_2(NO_3)_2.6H_2O$ undergoes dehydration and denitration via $PuO_2(OH)NO_3$ into PuO_2 as shown by Eq. (4.4), Eq. (4.6) and Eq. (4.9).

5.2.2.3 Calcination and Reduction

The mixed oxide (ThO_2,UO_3) product obtained after denitration was further calcined in air converting UO_3 into U_3O_8 in the same process vessel as represented by Eq. (5.3). Another, calcination (700 °C, 2h) was carried out after attritor milling for removal of residual nitrates, H_2O, carboneous impurities (if any) and quantitative conversion of UO_3 into U_3O_8. The calcined material was reduced in flowing (N_2+7% H_2) atmosphere at 700 °C, 4h and the reduction reaction for (ThO_2,U_3O_8) is shown by Eq. (5.4) [249, 251]. The reduction step for calcined ThO_2 and ($Th_{1-y}Pu_y$)O_2 was not carried out.

$$[yUO_3,(1-y)ThO_2] \rightarrow \left[\frac{y}{3}\,U_3O_8,(1-y)ThO_2\right] + \frac{y}{6}O_2(g) \tag{5.3}$$

$$[y/3\,U_3O_8,(1-y)ThO_2] \rightarrow [y\,UO_2,(1-y)ThO_2) + \frac{y}{3}O_2(g) \tag{5.4}$$

Fig. 5.3 and **Fig. 5.4** shows the photographs of microwave denitrated and calcined ThO_2 and (ThO_2,U_3O_8) powders respectively.

Fig. 5.3: Microwave Denitrated and Calcined ThO_2 Powder

Fig. 5.4: Microwave Denitrated and Calcined (ThO_2,U_3O_8) Powder (SM-D)

5.3 Unit Operations, Influence of Variables and Product Characterization

5.3.1 Mechanical Micronisation

Mechanical micronisation using jaw crusher and attritor mill produced powder from the sintered pellets. The particle size and the surface area data after different stages of the integrated process (**Fig. 5.1**) are recorded in **Table 5.1** for SM-A, SM-D and SM-E. The size analysis was carried out for sieved powders using standard sieves after jaw crushing, air oxidation and attritor milling of sintered rejects. The values in the parenthesis show (**Table 5.1**) the wt. fraction of powder in the corresponding particle size range during analysis of sieved powder. The laser particle size analyser Cilas 1190 LD (M/s Cilas, France) was used for microwave denitrated and attritor milled powders and values recorded are average particle size (**Table 5.1**).

Table 5.1: Properties of ThO_2 based Recycled Powder at Different Stages of the Integrated Process

Process step	ThO_2		$(Th_{0.86}U_{0.14})O_2$		$(Th_{0.7}U_{0.3})O_2$	
	Particle size	SSA (m^2g^{-1})	Particle size	SSA (m^2g^{-1})	Particle size	SSA (m^2g^{-1})
Jaw crushing	0.9-1 mm (> 0.9)	< 1	0.9-1 mm (> 0.9)	< 1	0.9-1mm (> 0.9)	< 1
Air oxidation	---	---	0.7-0.8 mm (> 0.8)	1.12	0.5-0.7 mm (>0.8)	1.8
Attritor milling	180-250 μm (> 0.9)	1.6	125-150 μm (> 0.9)	1.7	80-100 μm (>0.9)	2.3
Microwave denitration, milling	1.7 μm	3.5	1.6 μm	5.0	1.45 μm	6.5
Microwave denitration, PVA, milling	1.5 μm	7.4	1.42 μm	7.7	1.42 μm	8.4

The powder obtained after jaw crushing operation (**Table 5.1**) was compared with the sinterable grade feed powder (**Table 3.1**). The specific surface area of jaw crushed powder was found to be lower (<1 m^2g^{-1}) than the sinterable ThO_2 powder (**Table 3.1**). Similarly, its particle size was found to be many folds larger (3 order) than the sinterable grade ThO_2. Thus, the jaw crushed powder may not be sintered to the densities required for an oxide fuel typically > 90% of TD. Further improvement in the physical properties of powders was carried out by attritor milling. Though, the powder so obtained also showed better surface area and smaller particle size as compared to the precursor jaw crushed powder (**Table 5.1**), it cannot be recommended as sinterable grade (**Table 3.1**). The extended micronisation using attritor mill may be useful however, this leads to prolonged processing cycle. More importantly, the issues of concern are the impurity pick-up due to wear of attrition media and the associated radioactive dust hazard in the extended micronisation. The dust raised frequently chokes the HEPA filters calling for their frequent replacement. High energy ball or attritor milling is useful, however, it is energy intensive. Thus, mechanically micronized powder (after attritor milling for 40 min) so obtained is not suitable as fuel feed material. Else, mechanically micronized powder can be mixed with fresh feed powders for fuel fabrication. Mishra et al. [41] reports the addition of maximum 15 wt% of the $(Th_{0.7}U_{0.3})O_2$ MOX sintered rejects recycled via mechanical micronisation process (crushed and attritor milled) for fabrication of fuel.

5.3.2 Air Oxidation

The oxidation of $(Th_{1-y}U_y)O_2$ is technically feasible since uranium is oxidisable to higher oxidation states. The extent of oxidation further is anticipated as the function of the uranium content. Thoria-urania solid solution exhibits considerable range of hyper-stoichiometry $(Th,U)O_{2+x}$ due to higher oxidation states of uranium. The range of hyper-stoichiometry shows very strong dependence on Th/(Th+U) ratio of the solid solution [206]. Anthonysamy et al. [207] have studied the kinetics of oxidation of $(Th_{1-y}U_y)O_2$ solid solutions in air over a wide range of UO_2 composition (15 -77wt%). The oxidation of low urania containing $(Th_{1-y}U_y)O_2$ solid solutions (y; 0.15 and 0.3) showed the oxidiesd product to be a single phase fluorite structure $(Th_{1-y}U_y)O_{2+x}$. However, the oxidation of high urania containing solid solutions (y; 0.72 and 0.77) produced a biphasic oxidized product. The biphasic mixture contained a fluorite phase MO_{2+x} (M; U+Th) and an orthorhombic U_3O_8 phase [207]. It is reported that ThO_2 is insoluble in U_3O_8 [207].

The hyper-stoichiometry $(Th_{1-y}Pu_y)O_2$ system is absent, however it exhibit reasonable hypo-stoichiometry. As this hypo-stoichiometry is due to the presence of lower oxidation states of plutonium, it is strongly linked to the fraction of Pu/(Th+Pu) in solid solution [206]. Thus, oxidation is not feasible whereas reduction can be carried out depending upon Pu/(Th+Pu) ratio. The oxidation of hypo-stoichiometric $(Th_{1-y}Pu_y)O_{2-x}$ may be carried out as reported by Sali et al. [308] in their study on the kinetics of oxidation of hypo-stoichiometric $(Th_{1-y}Pu_y)O_{2-x}$ (y: 0.2, 0.3, 0.7) in air upto stoichiometric $Th_{1-y}Pu_y)O_2$.

The oxidation of ThO_2 is not feasible like UO_2 [118]. However, the oxidation of UO_2 in the ThO_2 matrix has brought out hyper-stoichiometric $(Th_{1-y}U_y)O_{2+x}$. The air oxidation of powder was carried out after Jaw crushing of pellets **(Fig. 5.1)**. All the oxidation experiments for $(Th,U)O_2$ MOX were carried out in air atmosphere at 700 ^oC, 4h in a conventional resistance furnace. The air oxidation experiments were carried out keeping the temperature rise rate ~ 200 $^oC/h$, soaking at temperature 700^oC for 4h followed by natural cooling upto room temperature. The batch size (1 Kg) was kept identical for all the oxidation experiments. **Fig. 5.5** shows the experimentally obtained % oxidation in various $(Th_{1-y}U_y)O_2$ (y; 0-0.3) after air oxidation as a function of UO_2 content in $(Th,U)O_2$. The % oxidation was calculated using the experimentally measured O/M ratio of final oxidized materials using Eq. (3.9).

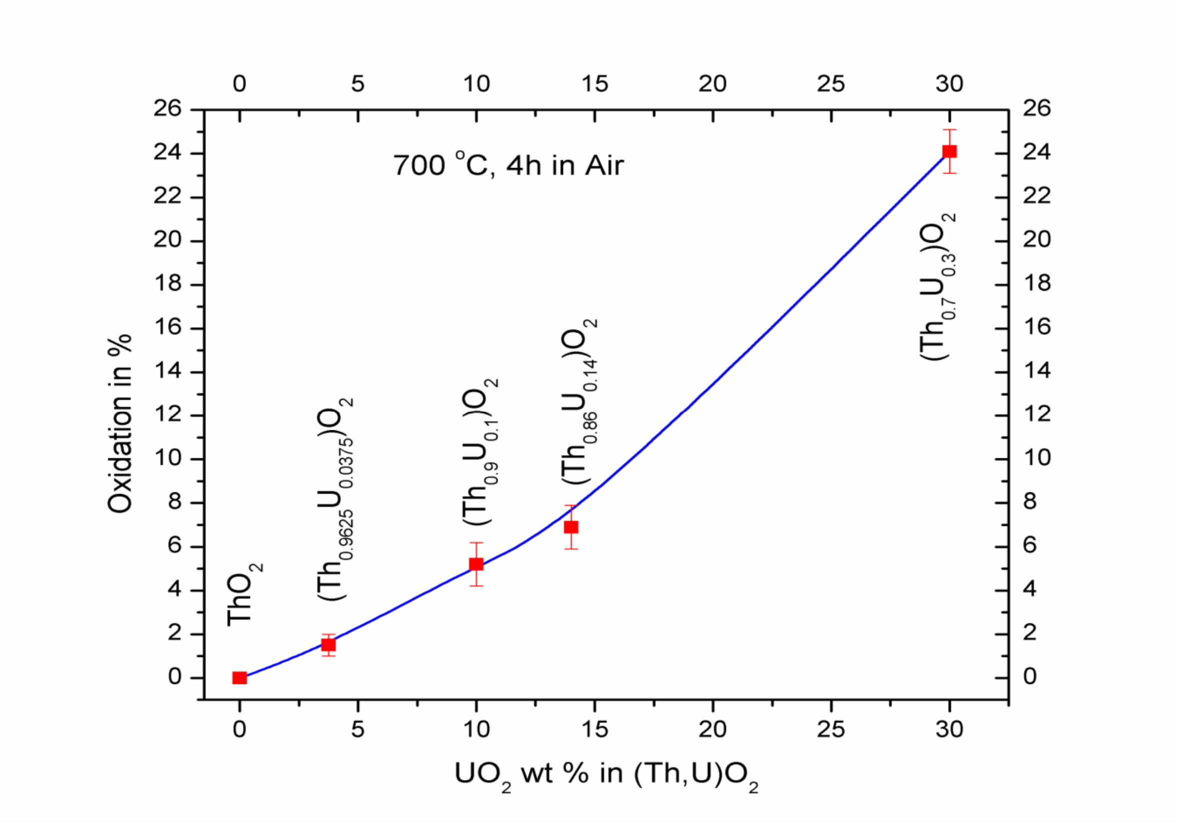

Fig. 5.5: Variation in % Oxidation as function of UO_2 % in $(Th_{1-y}U_y)O_2$

It is evident from the **Fig. 5.5** that as UO_2 content increased in the MOX, the % oxidation increased during air oxidation (after jaw crushing). The % oxidation obtained in $(Th_{0.9625}U_{0.0375})O_2$ (SM-B) was nearly 1.5% and in the $(Th_{0.7}U_{0.3})O_2$ (SM-E) nearly 24% of the theoretical oxidation possible. The increase in the experimentally obtained % oxidation was not linear function of UO_2 content. Theoretically, 100% oxidation is possible for all the cases considering oxidation of entire uranium in $(Th_{1-y}U_y)O_2$. ThO_2 is non-oxidsable as it has only single oxidation state (+4) However, the stable ThO_2 matrix inhibits the air oxidation of uranium. This effect was more predominant in low UO_2 content MOX due to higher ThO_2 content [245]. The content of UO_2, thus steered the oxidation behavior of $(Th_{1-y},U_y)O_2$ matrix. The rate of oxidation of $(Th_{1-y},U_y)O_2$ further depends upon several factors alike oxidation of

UO_2 and $(U_{1-y},Pu_y)O_2$ [245]. The surface area, particle size, grain size, density, temperature and oxygen partial pressure are key parameters governing the oxidation kinetics. The physical form of the MOX plays a crucial role in the oxidation process (**Fig. 4.18**). The powder form offers more oxidation than solid pellets. Thus, oxidation step was introduced after jaw crushing operation in the integrated process (**Fig. 5.1**) for $(Th_{1-y}U_y)O_2$ recycling. However, oxidation process was not carried out for recycling of ThO_2 and $(Th_{1-y}Pu_y)O_2$ sintered pellets in the integrated process (**Fig. 5.1**).

It is concluded from **Table 5.1** that the air oxidation of jaw crushed $(Th_{0.86},U_{0.14})O_2$ powder improved the specific surface area and reduced the particle size. The particle size and specific surface area of jaw crushed $(Th_{0.7}U_{0.3})O_2$ were 0.9-1 mm (> 0.9 wt. fraction) and < 1 m^2g^{-1} respectively and after air oxidation were 600-700 µm (> 0.8 wt. fraction) and 1.8 m^2g^{-1} respectively. This was attributed to oxidation of $(Th_{1-y}U_y)O_2$ into $(Th_{1-y}U_y)O_{2+x}$ due to presence of uranium. The oxidation of UO_2 to U_3O_8 decreases the density thereby increasing the surface area and reducing the particle size [35, 245]. The sinterability can further be increased by following multiple oxidation-reduction cycles [35].

5.3.3 Dissolution and Denitration using Microwave: Influence of Variables

The applicability of microwave dissolution and denitration was based upon the microwave coupling behavior of the precursors and compounds that were formed in the course of the process. H_2O and HNO_3 are strong couplers at microwave frequency 2450 MHz (**Table 2.2**). As discussed earlier, UO_2 and U_3O_8 are excellent microwave absorbers (**Table 2.3**) [17-18]. The UO_3 and ThO_2 are week microwave absorbers at room temperature (**Table 2.3**) [15, 75, 259]. However, the presence of other absorbing materials raises the temperature. With the increasing temperature, UO_3 got transformed into U_3O_8 which is excellent microwave absorbing material. A small amount of U_3O_8 was sufficient for transforming the entire mass of UO_3 into U_3O_8 or else a pinch of U_3O_8 was intentionally added as microwave absorbing seed (**Chapter 7**). The temperature raises the microwave dielectric loss factor (ε'') and thereby the absorption increases alongwith the temperature [2, 309]. The microwave denitration of thorium nitrate is feasible [21-23]. The mechanical micronisation and/ or air oxidation increase the surface area enhancing the dissolution of ThO_2 tremendously. Thus, micronized and/ or air oxidized powder was used for dissolution-denitration (**Fig. 5.1**). The effect of various parameters influencing the powder properties of denitrated product like cake bulk density (CBD), powder bulk density (PBD) and BET surface area was thoroughly studied. Based on the multi-parametric study, the optimized conditions were selected to deliver sinterable powder.

5.3.3.1 Effect of Method of Heating

The aqueous processing involving dissolution-denitration was carried out in microwave oven and conventional hotplate. It was found that the specific surface area in the microwave denitrated product was much higher than the hot plate processed (**Fig. 5.6**). The cake and powder bulk densities were found to be lower in microwave denitrated ThO_2. This was attributed to the direct material and bulk heating associated with microwave contrary to conventional. The solidification (**Fig. 5.2)** occurred quickly in case of microwave throughout the bulk. Thus, the evolution of gases and vapours during solidification and subsequent steps were many more times larger which formed the cake to be porous. The shape of the denitration process vessel played a key role in enhancing the cake porosity (**Table 4.2**). Long narrow neck vessel (used in the present work) offered small area for outgoing gases and vapours (nitrogen oxides called NOx, HNO_3, H_2O etc.). However, the heat conducts from the surface of the material in the hot plate. The solidification started from the surface and took longer to reach upto the core of the material. Thus, there was no quick evolution of gaseous products during solidification. Therefore, the product formed in the in hot plate denitration owed high bulk density (thus, low porosity) and low surface area. The increase in the surface area in microwave denitration was due to de-agglomeration of particles because of quick evolution of gases and vapours, which prevented the nucleation and the particle size growth. These outcomes are in line with the findings by Chandramouli et al. [75]. They found very low specific surface area of the ThO_2 powder synthesized via hot plate denitration which increased significantly when the denitration was performed using microwave. Thus, the microwave denitration was embedded in the integrated process (**Fig. 5.1**) to improve the physical properties of powder.

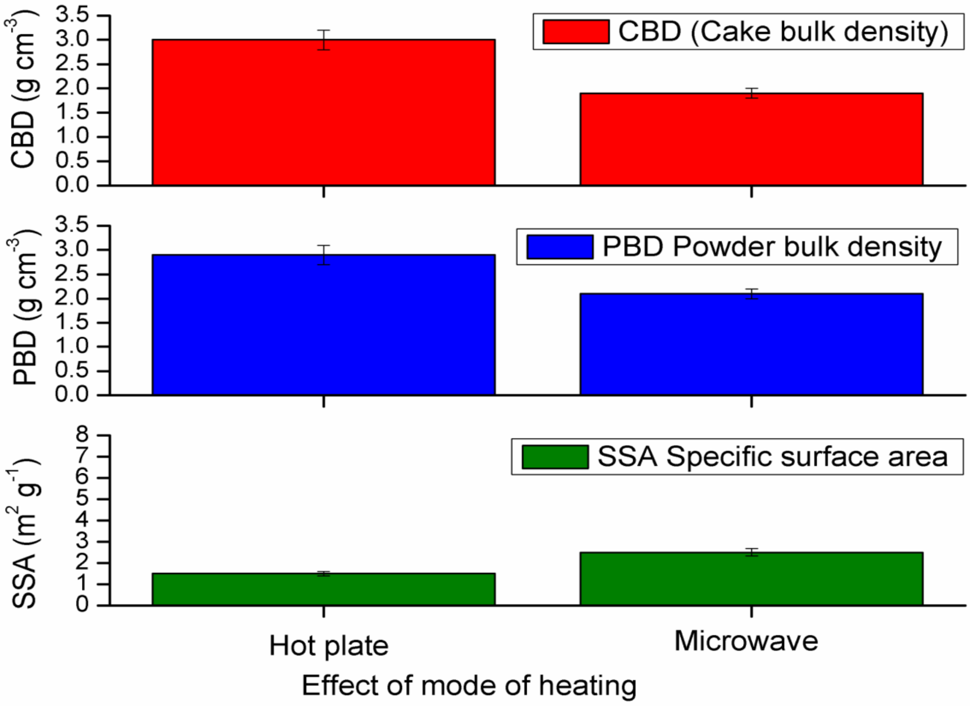

Fig. 5.6: Comparison of Microwave and Conventionally Denitrated ThO_2

5.3.3.2 Effect of HF Addition

To investigate the effect of complete dissolution of ThO_2 on the properties of microwave denitrated ThO_2 powder, the microwave dissolution of the attritor milled powder was carried out in HNO_3 in the presence and absence of HF. The HF (0.025 M) in HNO_3 was added to increase the ThO_2 dissolution. **Fig. 5.7** reveals that the dissolved ThO_2 improved the specific surface area of the microwave denitrated powder to a greater extent. The bulk densities of cake and powder were found to be lower in case of the microwave denitrated ThO_2 from completely dissolved solution. Without fluoride addition, the solution contained undissolved and sintered ThO_2 particles which subsequent to the denitration remained in the dense form. These undissolved and dense particles were responsible for poor powder properties. Thus, complete dissolution was ascertained before concentration and solidification (**Fig. 5.2**). Therefore, in all MOX batch recycling experiments using integrated method (**Fig. 5.1**), HF was added for dissolution.

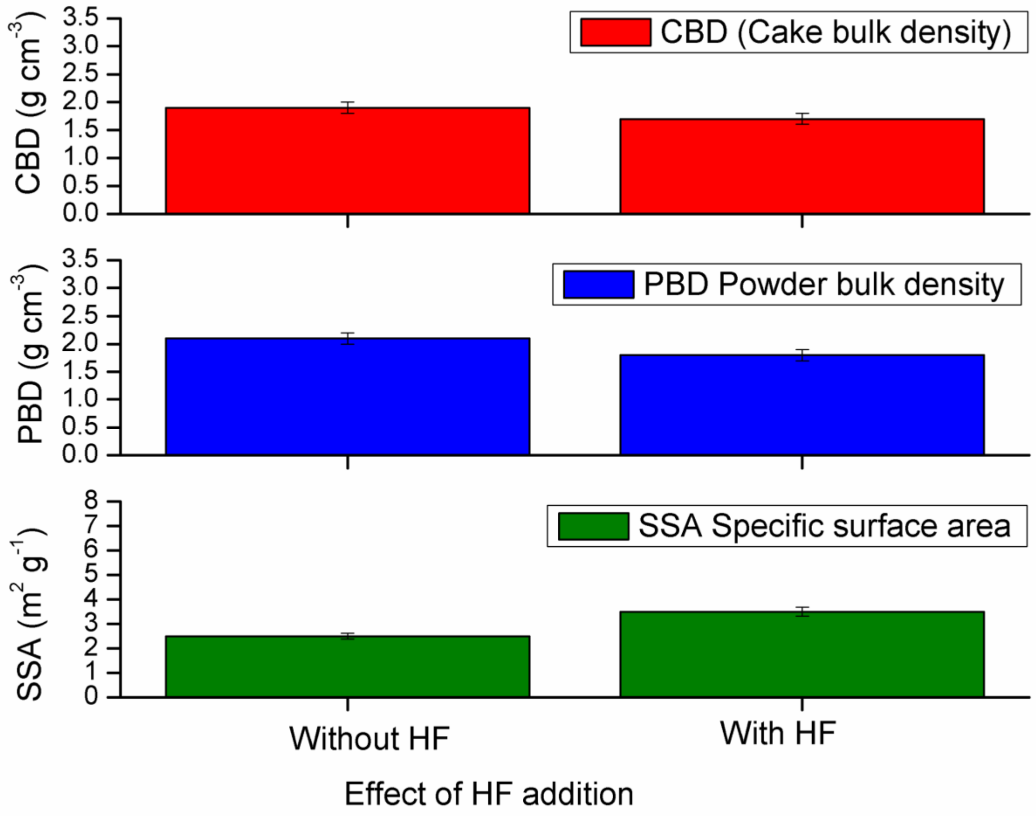

Fig. 5.7: Effect of HF Addition on Microwave Denitrated ThO_2 powder

However, it was seen that the denitrated product without HF has slightly better surface area (2.1 m^2g^{-1}) (**Fig. 5.7**) than the starting micronized ThO_2 (1.6 m^2g^{-1}) (**Table 5.2**). This may be attributed to the presence of very small crystallites of ThO_2 in micronized ThO_2 powder. The ThO_2 powder with small crystallites (<56 Å) undergoes complete dissolution without fluoride [73, 237]. More the fraction of such small crystallites in the micronized powder, higher is the extent of dissolution and hence better powder properties.

5.3.3.3 Effect of Polyvinyl Alcohol (PVA) Addition

Further improvement in the characteristics of the microwave denitrated powder was achieved by PVA addition to the completely dissolved ThO_2 (using HF). The combustion synthesis of ThO_2 from its aqueous nitrate solution using PVA has been reported [18-21]. Vigorous reaction occurs between PVA as organic fuel and HNO_3 as oxidant. The reaction was violent because of the exothermicity of the denitration and oxidation of the PVA. The product of denitration was highly porous because of the evolution of excessive gaseous products (CO_2, NOx etc.). PVA provided a surface for the denitration while preventing aggregation and sintering of particles, thereby helping the formation and stabilisation of the small crystallites of the powders. Thus, powder obtained has high surface area (> 7 m^2g^{-1}) as shown in **Fig. 5.8** and **Table 5.2**. The ratio of the organic fuel and oxidant is crucial factor in deciding the crystallite size and hence the powder properties. The aqueous solution of PVA (8-10%) was mixed with aqueous thorium nitrate solution obtained after dissolution of attritor milled ThO_2 in 1:2 volume ratio in a batch of denitration after dissolution (**Fig. 5.2**). The specific surface area and the bulk cake and powder densities of the ThO_2 so obtained are shown in **Fig. 5.8**. The large surface area of the powder obtained was in accordance with the findings by several researchers [73-75, 121, 307].

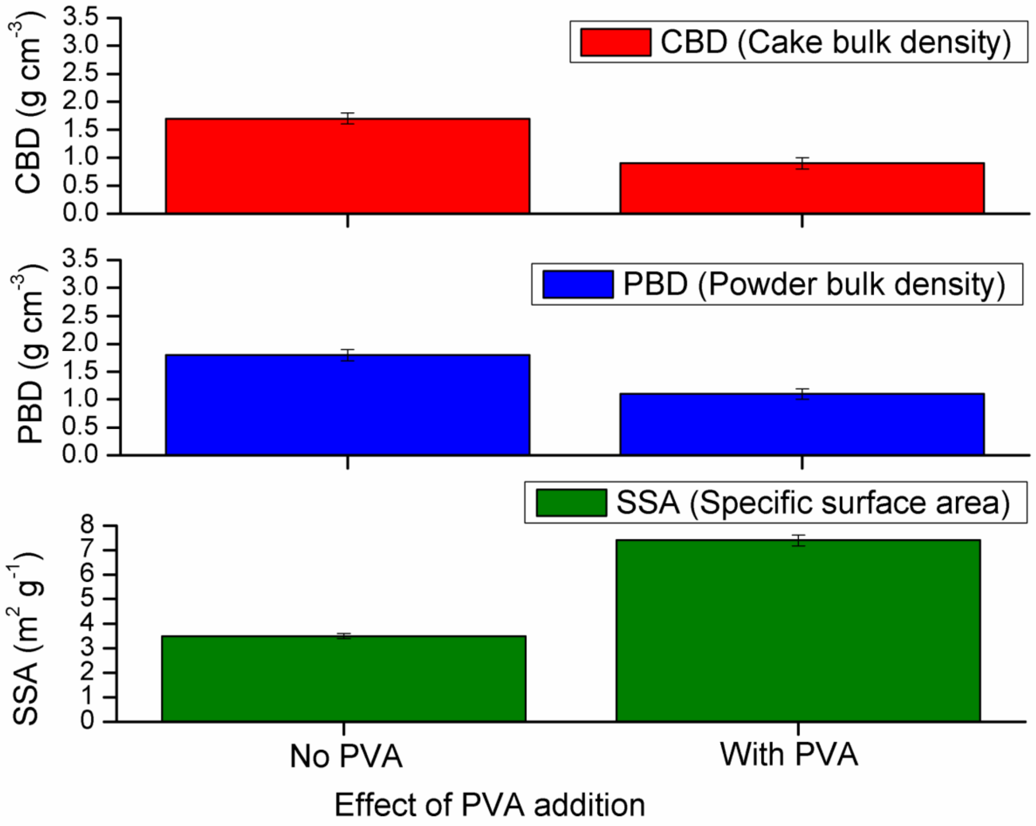

Fig. 5.8: Effect of PVA Addition on Microwave Denitrated ThO_2 powder

5.3.3.4 Effect of UO_2 Percentage in $(Th_{1-y}U_y)O_2$ MOX

A profound effect on the surface area and bulk density of the denitrated product was found due to presence of UO_2 in ThO_2 as shown in **Fig. 5.9**. This was due to the fact that the denitrated product contained UO_3. The density of UO_3 is lower (6.69 - 8.62 gcm^{-3}) [211] depending upon the allotrope formed as compared to UO_2 (10.46 gcm^{-3}) and ThO_2 (10.00 gcm^{-3}) (**Table 1.4**). It has been reported that the microwave denitration of uranyl nitrate produces β-UO_3 [15, 130-132]. The studies have shown that in the denitration of uranyl nitrate, the crystal structure of the oxide product depends upon temperature and heating rate [124]. The desired porous product is formed at faster heating rates. The calcination of UO_3 further gave voluminous U_3O_8 having density 8.326 - 8.395 gcm^{-3} [211]. The surface area and bulk density of cake and powder in the microwave denitrated $(Th_{1-y}U_y)O_2$ are shown in **Fig. 5.9**. Thus, **Fig. 5.9** reveals that with increasing UO_2 percentage in $(Th_{1-y}U_y)O_2$ the bulk density decreased and BET specific surface area increased.

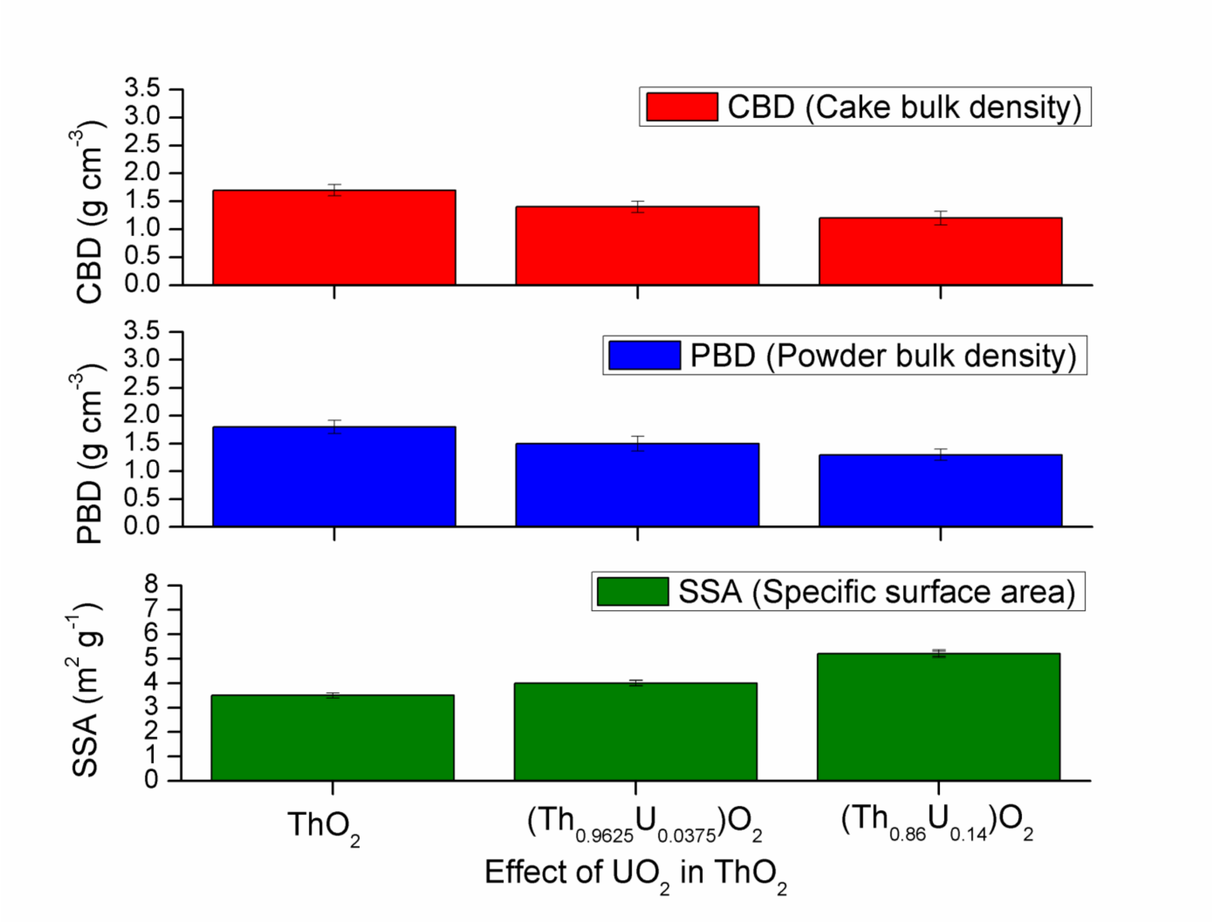

Fig. 5.9: Effect of UO_2 Content in $(Th_{1-y}U_y)O_2$ on microwave denitrated product

5.3.4 X-ray Diffraction Analysis

The X-ray diffractograms of sintered ThO_2 powder (after micronisation of ThO_2 pellets; SM-A) and microwave denitrated ThO_2 powder (dissolved using HF) are shown in **Fig. 5.10**.

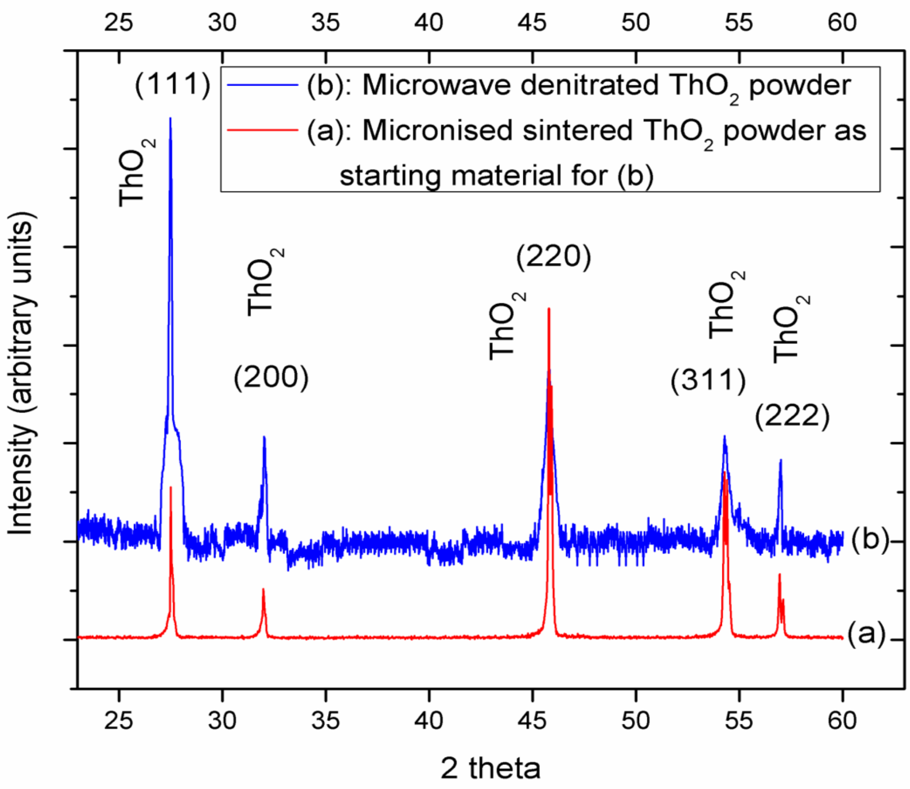

Fig. 5.10: X-Ray Diffractogram of a) Micronized Sintered ThO_2 and b) Microwave Denitrated ThO_2 Powder

The analysis of the patterns showed that the peaks were sharper for sintered ThO_2 powder **Fig. 5.10 (a)** showed more crystallinity due to sintering. The XRD pattern of denitrated ThO_2 in **Fig. 5.10 (b)** indicated that the microwave denitration of thorium nitrate give well developed crystalline thoria. However, the peaks were broader than the sintered ThO_2. The calcination was carried out after microwave denitration (**Fig. 5.1**) to remove residual volatiles (nitrate, water etc.). This further leads to the crystal growth and improves crystallinity (sharper peaks).

5.3.5 Morphological Analysis using SEM

Morphology of the microwave denitrated ThO_2 powder was compared with that of the oxalate derived ThO_2 powder. **Fig. 5.11** is the SEM microphotograph of the oxalate derived

ThO_2 which is showing the 'platelet' shapes of size in the range 1-4 μm [99]. The morphology of microwave denitrated ThO_2 powder was seen through SEM. **Fig. 5.12** is SEM microphotograph of microwave denitrated ThO_2. The shape of the particles was found to be irregular in the size range of 2-20 μm.

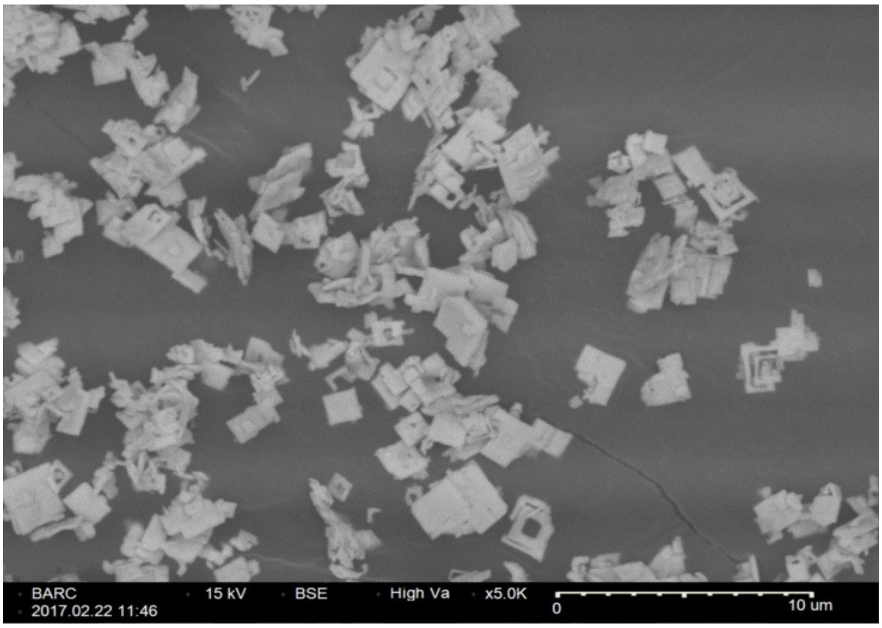

Fig. 5.11: SEM Microphotograph of Oxalate Derived ThO_2 Powder

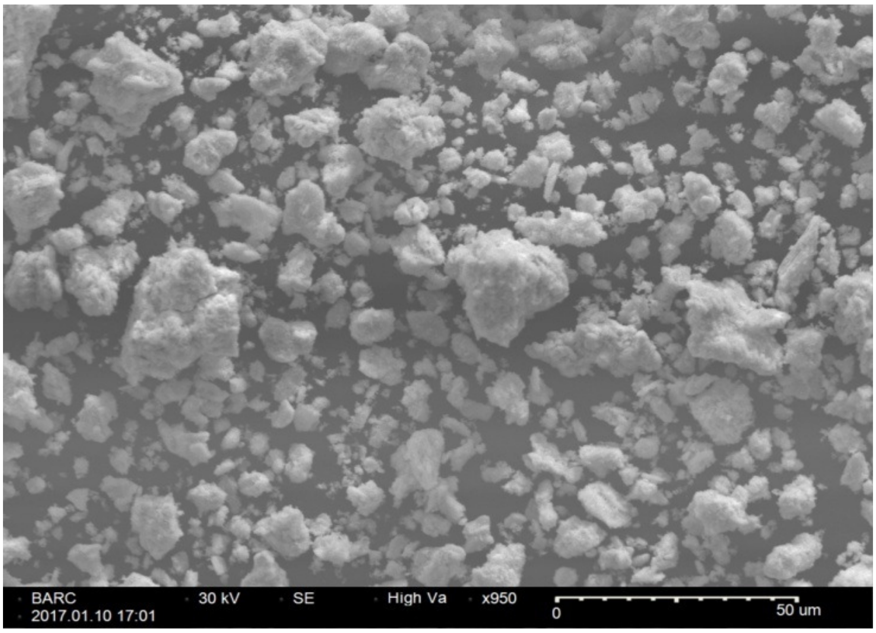

Fig. 5.12: SEM Microphotograph of Microwave Denitrated ThO_2 Powder

5.3.6 Evaluation of Suitability of the Recycled Powder

Comparison of the physical properties of the recycled ThO_2 powder (**Table 5.1**) with the standard sinterable ThO_2 (**Table 3.1**) revealed that the recycled powder obtained through the integrated process (**Fig. 5.1**) can be re-used for fuel fabrication. The recycled ThO_2 powder has specific surface area of 3.5 m^2g^{-1} (direct microwave denitration) and 7.4 m^2g^{-1} (direct microwave denitration with PVA) with average particle size of 1.0-2.0 μm. The powder properties were found to further improved due to the presence of uranium (**Table 5.1, Fig. 5.9**) in ThO_2 matrix as in case of $(Th_{1-y},U_y)O_2$. However, the presence of PuO_2 in $(Th_{1-y},Pu_y)O_2$ does not offer advantages like UO_2 (**Table 5.4**).

The powder bulk density of the as received ThO_2 powder obtained via oxalate route (**Table 3.1**) is lower (0.85 gcm^{-3}) in comparison to the recycled ThO_2 (1.7 gcm^{-3}) (**Fig. 5.7**). The microwave denitration with PVA further reduced the powder bulk density upto 0.9 gcm^{-3} (**Fig. 5.8**). This was assigned to the platelet morphology of the oxalate derived ThO_2 where packing fraction was lesser [41, 99, 208]. The attritor milling broke the platelet morphology converting into spherical shape, thereby increasing the bulk density and surface area. The ThO_2 product in integrated process (**Fig. 5.1**) was obtained as granular clinkers. The sample of granular clinker showed irregular morphology of ThO_2 (**Fig. 5.12**). However, the attritor milling of the microwave denitrated clinkers was carried out in integrated process (**Fig. 5.1**) which resulted in spherical morphology of the recycled powder and thus, higher powder bulk density (1.7 gcm^{-3}).

Table 5.2 records the impurities determined using ICP-OES (**Fig. 3.14**) and other techniques (§ **3.5.4**) in the standard ThO_2 powder, ThO_2 sintered pellet (used for recycling work) and the recycled powder via integrated method. Hydrogen, carbon, chlorine and fluorine were found to be higher in the standard thoria powder and in the recycled powder. Both the cases need the calcination step before starting the fabrication process.

Table 5.2: Impurity Analysis in Standard ThO_2 Powder, Sintered ThO_2 pellet and Recycled ThO_2 Powder via Integrated Method

Element (s)	Standard ThO_2 powder (ppm)	ThO_2 Sintered pellet (ppm)	Recycled ThO_2 Powder via Integrated Method (ppm)
Al	35	86	104
B, Be	< 0.2, < 0.1	< 0.2, < 0.1	< 0.2, < 0.2
Cd+Dy+Sm+Gd	< 0.5	< 2	< 2
Ca+Mg	245	356	364
Co	< 0.2	<0.2	<1
Cr	< 1	38	74
Cu	0.9	100	116
Fe	80.76	142	189
Mn	1.7	8.2	7.8
Mo	< 0.2	1.51	2.5
Ni	< 0.1	50	68
Pb	9.3	23	26.2
Si	55	30	53
W	2.1	<10	<10
Zn	14	35	49
C	1232	<300	635
H	600-700	<1	<800
Cl +F	40-60	13.8	30-60

Fluoride addition was essential for complete dissolution of ThO_2 in HNO_3. PVA was added for obtaining improved powder physical properties during microwave denitration (**Fig. 5.1**). The concentration of carbon and fluoride in the recycled powder was required to be measured for suitability assessment. **Table 5.3** records the values of carbon and fluoride in the recycled ThO_2 via integrated process (**Fig. 5.1**). The values for standard oxalate route derived ThO_2 are also recorded for comparative evaluation. The carbon and fluoride as impurities gets decreased to acceptable levels during the fuel fabrication operations as sintering (1600-1800 °C) and vacuum degassing (10^{-2} torr, 100 °C, 2h). However, the fluoride is required to be in controlled amount due to its corrosive nature.

Table 5.3: Carbon and Fluorine Content in the Intermediate Products and Final Recycled ThO_2 Powder

Material	Process stage	C (ppm) ($\bar{x}$ ±1s)	F (ppm) ($\bar{x}$ ±1s)
Standard ThO_2	Calcination	756±41	16±1
Recycled ThO_2 from SM-A	Mechanical micronisation	285±19	6.1±0.5
	Denitration with PVA and calcination	635±29	14±1

5.4 Recycling of Sintered $(Th_{1-y}Pu_y)O_2$ Pellets using Integrated Method

The sintered pellets of $(Th_{0.99}Pu_{0.01})O_2$ and $(Th_{0.92}Pu_{0.08})O_2$ were recycled similar to ThO_2 sintered rejects via integrated method involving mechanical micronisation of the pellets and HF catalysed microwave assisted dissolution-denitration using PVA. The CBD and PBD, SSA of the denitrated ThO_2 and $(Th_{1-y}Pu_y)O_2$ powders are recorded In **Table 5.4**.

Table 5.4: Properties of ThO_2 and $(Th,Pu)O_2$ Recycled Powders by Integrated Process

Property	ThO_2	$(Th_{0.99}Pu_{0.01})O_2$	$(Th_{0.92}Pu_{0.08})O_2$
CBD (gcm^{-3}) ($\bar{x}$ ±1s), n= 3 Batches= 2	0.8 ±0.2	0.8±0.2	0.8±0.2
PBD (gcm^{-3}) ($\bar{x}$±1s), n=3, Batches= 2	0.9 ±0.1	0.9 ±0.1	0.9 ±0.1
BET-SSA (m^2g^{-1}) ($\bar{x}$±1s), n=4, Batches= 2	7.4 ±0.3	7.3 ±0.4	7.42± 0.3
Average particle size (µm)	1.5	1.45	1.4
O/ M ratio, n>3, Batches= 2	2.000± 0.002	2.000±0.002	2.000 ±0.001

The presence of PuO_2 could not offer advantages like UO_2 since it did not form low density higher oxides. Thus, PuO_2 and ThO_2 behave similarly in the air oxidation and microwave dissolution and oxidative denitration. This was reflected by similar properties in **Table 5.4**. O/M ratio of denitration of thorium nitrate and/ plutonium nitrate product is 2.000.

5.5 Quantity of ThO_2 based Rejects Recycled using Integrated Method

Rejected or surplus ThO_2 based fuels (**Table 3.3**) were recycled at experimental scale to study the recycling feasibilities. **Table 5.5** lists the quantities recycled using the integrated method and to obtain the data pertaining to the thoria based recycling studies.

Table 5.5: Quantity of ThO_2 based Rejects Recycled using Integrated Method

Material Description	Quantity (Kg)	Recycled at Scale
ThO_2	>18	Experimental
$(Th_{1-y}U_y)O_2$; y: 0.0375, 0.1, 0.14, 0.3	23.4	Experimental
$(Th_{1-y}Pu_y)O_2$; y: 0.01 and 0.08	0.7	Experimental

5.6 Summary of Investigations on Recycling of Thoria based Fuels

A simplified pictorial overview of the integrated recycling scheme for ThO_2 based fuel scrap is shown in **Fig. 5.13**.

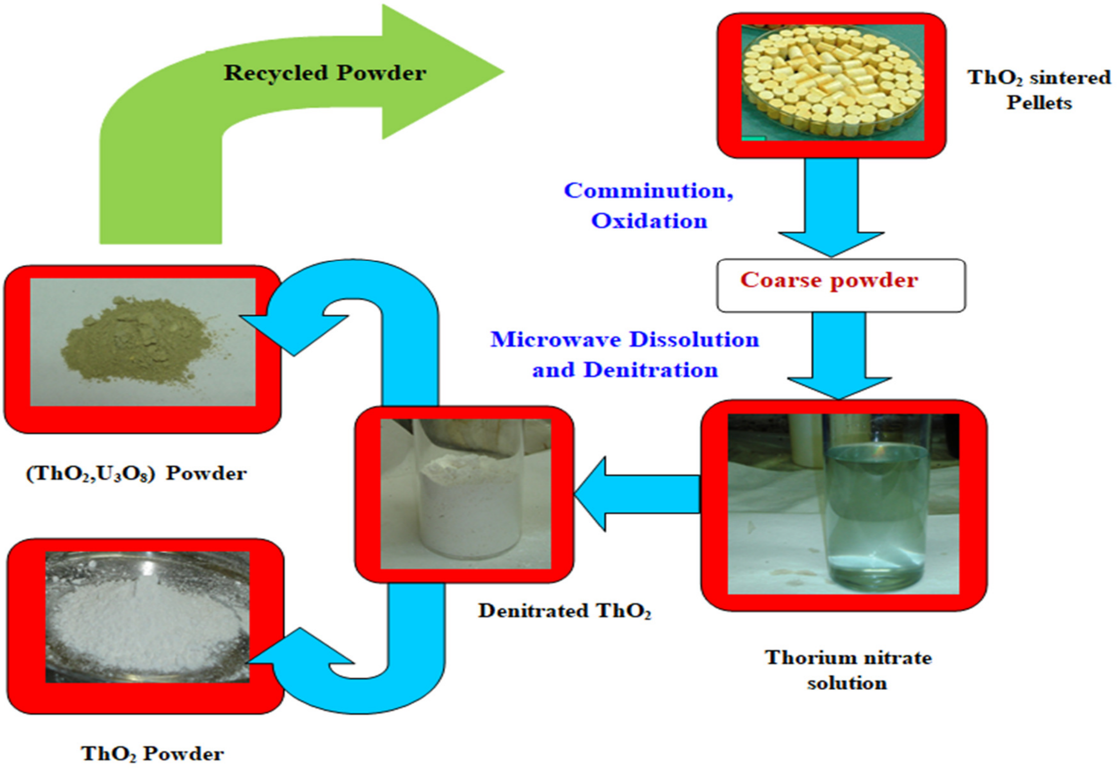

Fig. 5.13: Pictorial Representation of the Integrated Method of Recycling Thoria Rejects

Recycling of ThO_2, $(Th_{1-y}U_y)O_2$ (y; 0 to 0.3) and $(Th_{1-y}Pu_y)O_2$ (y; 0 to 0.1) sintered pellets through integrated process conclusively may be summarized as follows:

1. The mechanical micronisation using jaw crusher and attritor milling of the sintered ThO_2 pellets produced ThO_2 powder which cannot be used for re-fabrication of the fuel on 100% basis due to its low sinterability as evident from its low SSA (1.6 m^2g^{-1}) and large particle size (180-250μm).
2. In $(Th_{1-y}U_y)O_2$, air oxidation step was introduced between jaw crushing and attritor milling. $(Th_{1-y}U_y)O_2$ with y: 0.0375, 0.14 and 0.3 by this combination could not produce sinterable powder. However, multiple oxidation-reduction cycles may further improve the powder properties.
3. To enhance the physical properties of the recycled powder obtained from the combination of comminution and/ or oxidation processes, the microwave dissolution-denitration was embedded in the integrated process. Denitration using microwave improved the powder physical properties as compared to hot plate denitration.
4. The microwave dissolution-denitration using HF and PVA produced more sinterable powder which can be used 100% for fuel re-fabrication. The completely dissolved ThO_2 (using HF) resulted in better powder properties as compared to partially dissolved ThO_2. The addition of PVA during denitration increased the SSA of the denitrated ThO_2 and thoria based MOX (> 7 m^2g^{-1}).
5. The presence of UO_2 in the $(Th_{1-y}U_y)O_2$ produced recycled powder with lower bulk density and higher surface area as compared to ThO_2 as starting material.
6. The properties; CBD, PBD, SSA of denitrated ThO_2 and $(Th,Pu)O_2$ are similar.
7. The morphology analysis using SEM showed microwave denitrated ThO_2 particles to be irregular (2-20 μm) as compared to the platelet for oxalate derived ThO_2 (1-4 μm).

Chapter 6

DEVELOPMENT OF METHODS FOR RECYCLING OF IMPURE OXIDE AND MIXED OXIDE FUEL SCRAP MATERIALS

6.1 Introduction

The impure scrap constitutes nearly 5 wt% of the total material throughput as shown in **Fig. 1.1**. Though, these can be recycled, in principle, in the conventional reprocessing facilities, the inherent limitation of attaining homogeneity in mechanical mixing of constituents (ThO_2, UO_2 and PuO_2), lack of the data on impurities in the scraps and the dissolution behaviour of high plutonium content in particular are the driving force for the present study. This is noteworthy that the reprocessing facilities avoid use of the fluoride (being corrosive) for the dissolution. The mechanically blended or non-sintered (UO_2+PuO_2) mixtures cannot be dissolved quantitatively in HNO_3 alone [291-296, 310-311]. Since, the impure scrap contribute significant share of the production throughput to be declared as waste, it was planned to develop methods for recovery of valuable fissile and fertile materials by recycling. The selection of a recycling method and the development of process flow sheet require a thorough investigation of the impure scraps. The investigation entails identification of impurities and their physical/ chemical forms, analysis of impurity contents and deviations from their specified values, dissolution characteristics, the process generating the scrap and the source of the impurity. The presence of impurities in the nuclear fuel affects the in-pile behaviour of the fuel significantly. This may appear in terms of neutron economy, fuel integrity, clad failure, thermal and mechanical properties. Hence, stringent specifications are laid down for each impurity element depending upon the type of fuel, reactor etc. The standard specifications for various impurities in MOX fuel are stated in ASTM standards

[165-166], which have been adapted more conservatively by different countries. **Table 6.1** shows the specifications for various impurities in the PFBR MOX fuel [178].

Table 6.1: Specifications of Various Impurities in the PFBR MOX Fuel

Element/ Group of Elements	**Specified value (ppm)**	**Element/ Group of Elements**	**Specified value (ppm)**	**Element/ Group of Elements**	**Specified value (ppm)**
Metallic		Cr	500	W	200
Al	250	Cu	100	Zn	500
Ag	20	Fe	1500	**Non-metallic**	
B	3	Mn	200	C	300
Be	10	Mo	300	H	3
Cd+Dy+Sm+Gd	20	Ni	200	Cl	25
Ca+Mg	800	Pb	100	F	25
Co	100	Si	500	N	200

The first target was the chemical characterization which included the impurity analysis and the dissolution behaviour of the several types of impure MOX scrap generated in fabrication processes or in a few QC checks. The dissolution behaviour in HNO_3 was studied by using dissolution test [176]. The specified impurities were determined in a large variety of impure scraps. An impurity indicator parameter namely impurity factor (IF) shown in Eq. (3.8) was defined and estimated for specified impurities. Having determined the impurities and the dissolution behaviour of the impure scraps, the recycling methodologies were recommended for their efficient recycling. Several batches were recycled after developing an integrated method which comprehensively uses microwave heating.

6.2 UO_2 and $(U_{1-y}Pu_y)O_2$ MOX Impure Scrap

6.2.1 Sampling of Impure Scrap Samples

The impure scrap generated in each process was collected in 2 litre stainless steel containers. The scrap was mixed homogeneously with a Teflon spatula and ~100 g of the sample was taken from each container. The samples so withdrawn from each container were mixed with the samples of the same process. The hand-pickable foreign materials (if any) were manually removed from the samples. These further were milled using a coarse mixer grinder (< 500 µm) (**Fig. 3.6**) and sieved through a standard ASTM # 40 sieve. The mixer grinder was made-up of stainless steel AISI SS 304. The high speed steel blades having high wear and tear resistance perform the milling action.

6.2.2 Sample Preparation for Various Analyses

Solid powder samples, three in numbers (n=3) of nearly 1g each were randomly withdrawn from process representative scrap samples. These were dissolved in 40 mL of 0.05M HF in 14M suprapur® HNO_3. Samples were digested in PFA pressure vessels upto 10 bar (**Fig. 3.12**) in a glove-box adapted MHS-3 (**Fig. 3.8**). The digested samples were concentrated near to dryness and made-up to 10 mL in 4M HNO_3 repeatedly (four times) so as to remove the fluoride and acidity adjustment. The major matrix consisting uranium and plutonium was separated from above solution by solvent extraction giving three contacts with 30% TBP in n-DD (1:2 ratio) and finally one contact with 0.2M TOPO in n-DD (1:1 ratio). The aqueous phase containing the impurities was made-up to 25 mL with ultrapure water and filtered through 540 Whatman filter. The solution with acidity ~2M was analysed for metallic impurities by ICP-OES (**Fig. 3.14**).

Solid powder samples, three in numbers (n=3) of the process representative scrap samples were withdrawn for PuO_2 determination, DT and non-metallic impurities. The sample size was ~1g for estimation of each non-metallic impurity in the scrap and DT. Approximately 20 g sample was analysed for PuO_2 content of the scrap by NWCC.

6.2.3 Determination of Impurities in the $(U_{1-y}Pu_y)O_2$ Scrap Samples

The impure $(U_{1-y}Pu_y)O_2$ MOX scrap with varying content of PuO_2 was getting generated in the various fuel fabrication processes. The PuO_2 content in the various scrap was determined using NWCC. The metallic impurities were analysed by ICP-OES. The non-metallic impurities like carbon, hydrogen, nitrogen, chlorine and fluorine were determined in the solid samples using methods and procedures described (§ **3.4.8**). The values of impurity factors were determined by comparison with the specifications (**Table 6.1**).

6.2.4 Evaluation of Impurities in Fabrication Process Generated $(U_{1-y}Pu_y)O_2$ Impure Scrap

The fabrication process impure scrap was dealt under four different categories as listed in **Table 6.2**. The plutonium content in the scrap varies in the range 20 wt% to 30 wt% as determined by NWCC. The identification of $(U_{1-y}Pu_y)O_2$ impure scraps for present study and their sources of origin are recorded in **Table 6.2**.

Table 6.2: Categorization and Identification of Production Generated Impure $(U_{1-y}Pu_y)O_2$ MOX Scrap

Category	Identification	Source of origin
Glove-box floor scrap	Scrap-A (S-A)	Scrap from powder processing operations like weighing, mixing-milling, sieving etc.
	Scrap-B (S-B)	Scrap collected near the furnaces
	Scrap-C (S-C)	Scrap generated in microwave recycling operations
Scrap from furnaces	Scrap-D (S-D)	Generated from sintering, oxidation or reduction furnaces
Scrap from compaction presses	Scrap-E (S-E)	Impure scrap generated from pre and final compaction presses
Dry centreless grinder generated scrap	Scrap-F (S-F)	Impure powder/ pellets during diameteral and surface finish control

Table 6.3 and **Table 6.4** show the impurity factors for metallic and non-metallic impurities in the various impure scrap samples respectively.

Table 6.3: Impurity Factors (IF) for Metallic Impurities Determined using ICP-OES in various Process Generated $(U_{1-y}Pu_y)O_2$ Impure Scrap

Element/ Group of Elements	Wavelength (nm)	RSD %	S-A	S-B	S-C	S-D	S-E	S-F
Al	308.21	2.5	0.68	1.40	18.74	3.05	0.80	0.67
Ag	357.88	1.9	0.03	0.35	0.32	0.50	0.42	0.31
B	249.77	1.5	0.17	0.17	0.60	1.00	1.00	0.97
Be	234.86	0.8	0.05	0.05	0.05	0.05	0.05	0.05
Cd+Dy+Sm+Gd	228.80, 353.17, 359.26, 342.24	2.0	0.11	0.10	0.12	0.08	0.43	0.13
Ca+Mg	393.36, 280.27	1.2	0.38	0.24	1.69	1.30	0.36	0.30
Co	238.80	0.8	0.05	0.01	0.05	0.13	0.05	0.05
Cr	205.55	1.8	0.07	0.08	0.36	0.18	1.09	0.22
Cu	324.75	1.3	0.32	0.66	1.13	2.03	1.43	0.30
Fe	259.94	1.8	0.41	0.32	1.01	1.16	0.65	0.63
Mn	257.61	1.3	0.07	0.07	0.23	0.30	0.10	0.06
Mo	281.61	1.3	0.15	1.60	0.13	2.50	0.03	0.23
Ni	221.64	2.4	0.16	0.19	0.50	0.84	1.24	0.85
Pb	283.30	1.7	0.33	0.25	0.24	0.10	3.43	0.26
Si	288.15	4.0	0.03	0.29	2.11	0.02	1.13	0.04
W	207.91	2.8	0.11	2.04	0.56	3.05	2.99	0.05
Zn	213.85	1.6	0.10	0.28	1.39	0.84	1.37	0.20

Table 6.4: Impurity Factors (IF) for Non-Metallic Impurities in various Process Generated $(U_{1-y}Pu_y)O_2$ Impure Scrap

Element	RSD %	S-A	S-B	S-C	S-D	S-E	S-F
C	≤10	15.67	3.38	5.06	3.26	13.29	1.30
H	≤10	81.67	---	104.00	---	----	----
Cl	≤6	15.33	3.55	24.08	4.53	4.20	1.05
F	≤6	0.10	0.04	0.19	0.15	1.18	0.12
N	≤10	---	----	5.62	-----	-----	-----

----: Not Measured

6.2.5 Source of Impurities in Process Generated $(U_{1-y}Pu_y)O_2$ Scrap and Their Recyclability Aspects

The impurities present in the nuclear grade feed material originates from ore processing, reprocessing of spent fuel, due to reagents employed and wear or tear of associated equipments. Each step adds some impurity into the fuel in the subsequent steps of MOX fuel fabrication. It can be inferred from **Table 6.3** and **Table 6.4** that not all types of the process generated scraps exceed the specified limit of impurity factor (IF< 1) hence the specification values. Only Scrap-A and Scrap-F met the specifications for metallic impurities as all impurity factors <1. However, the non-metallic impurities were associated with all types of the scrap. Carbon mainly came from the carboneous materials used like organic binder (polyethyleneglycol), lubricant (oleic acid), packaging materials etc. Hydrogen in the scraps appeared from air moisture and reagents whereas chlorine and fluorine from the reagents etc. The nitrogen was estimated in impure scrap getting generated in the microwave based recycling operations wherein HNO_3 acid processing was carried out. A detailed discussion of the experimental observations of the impurities found and their sources are described in the following sub-sections.

6.2.5.1 Powder Processing Operations: Scrap-A

None of metallic impurity was found to exceed the impurity factor of 1 (**Table 6.3**). The powder processing part in the fuel fabrication consists of sieving, weighing, mixing-milling, pre-compaction and granulation (**Fig. 1.10**). Among the non-metallic impurities; C, H and Cl were found to be manifold higher than the specified (**Table 6.4**). These might come from organic binder, lubricants, pore formers added during the fuel fabrication. So a head-end treatment like roasting, air calcination or pyrohydrolysis etc. is expected to convert the impure scrap into clean material.

6.2.5.2 Near Sintering Furnace: Scrap-B

Al, Mo and W were found to exceed the unity impurity factor alongwith the non-metallic impurities like C and Cl (**Table 6.3** and **Table 6.4**). The furnace insulation lining made-up of Al_2O_3 becomes more fragile after several repeated heating and cooling cycles. After replacement of the lining or their maintenance, the Al_2O_3 powder is dislodged thereby increasing the chances of material contamination. The Mo originated from furnace boats used in the sintering which were made from TZM alloy. The TZM alloy is dispersion strengthened alloy of Mo using Ti and Zr [312]. Likewise, Mo heating elements were used for sintering in reducing atmosphere upto 1750 ^{o}C. The tungsten in the scrap might get associated from the W-Re thermocouples used for the temperature monitoring and from the tools coated with tungsten carbide for final cold compaction of the pellets prior to sintering. Since, these materials are refractory (Al, Mo and W); a head-end heat treatment for removal of C and Cl followed by a chemical purification step is required.

6.2.5.3 Microwave Recycling Operations: Scrap-C

The metallic impurities such as Al, Ca, Mg, Cu, Fe, Si and Zn and non-metallic impurities such as C, H Cl and N were exceeding the specified values (**Table 6.3** and **Table**

6.4). Microwave ovens were being used for a wide variety of applications in the MOX fuel fabrication and QC related activities. This involved mainly recycling of clean scrap, sample preparation and waste treatment for recovery of valuable nuclear materials. During these operations, a small fraction of impure scrap in solution and solid forms was generated. The solution scrap was solidified using microwave and analysed for the impurities. Several impurities were found which might get embedded in the scrap during the recycling operations of the fuel materials and various wastes. Al and Si might come from the breakage of process vessels and furnace boats made-up of alumina and quartz glass. The others might come from the equipments used like brass test sieves, mixing milling devices etc. The treatment of wastes containing many impurities may also be responsible for inclusion of impurities in Scrap-C. Thus, a chemical purification step may be adapted to recycle this kind of scrap.

6.2.5.4 Oxidation, Reduction and Sintering Furnaces: Scrap-D

Al, Ca, Mg, Cu, Fe, Mo and W were found to exceed the limits (**Table 6.3**). An aqueous purification step was required. The source of Al, Mo and W in the impure scrap from furnaces has been discussed in “Scrap-B”. The presence of higher contents of Fe and Cr in the impure scrap may be due to wear of die-plunger (tools) of the pellet compaction presses. Though, the boron was not found to exceed the specifications, its presence might be due to the boric acid powder used in the neoprene or rubber gloves. This might also come from the various packing materials used in the nuclear material inter-laboratory transfers and equipment lubricant or coolants.

6.2.5.6 Compaction Presses: Scrap-E

Impurities like Cu, Cr, Ni, Pb, Si, W and Zn were found to be higher (IF>1) (**Table 6.3**) in the impure scrap generated from the pre-compaction and final compaction presses. The compaction presses generally used are hydraulic and rotary presses. For achieving a specified dimension (depending upon the type of reactor and fuel) of the fuel pellet, green pellets were compacted (55-60 % of theoretical density) using a specified dimension die and plunger. For the annular (cylindrical pellet with central hole) MOX pellets of PFBR, a core rod was used to create the central hole in the green pellet during compaction. The compaction tools were made-up of hardened tool steel and are coated with WC. Cu, Cr and Ni may come from the wear of compaction tools. The Zn and Pb might have shown their presence from the wear from brass made feed frame used in the compaction press. The presence of Si as the impurity in the process of the compaction was not anticipated as such. But its presence might be explained as unwanted addition from glass, quartz used in several of the fabrication processes.

6.2.5.7 Dry Centreless Grinder: Scrap-F

None of metallic impurities were found to exceed the specified values in the samples obtained from the dry centreless grinder being used for diametral and surface finish control (**Table 6.3**). This was because of use of composite diamond grinding wheels showing low wear as compared to earlier used resin bonded silicon carbide grinding wheels [32, 202]. Among the non-metallic impurities, C and Cl were found exceeding the acceptable levels (**Table 6.4**). Thus, a head-end treatment like roasting, pyrohydrolysis etc. was expected to convert the impure scrap into clean material.

6.2.6 Some Quality Control Generated Impure Scrap

6.2.6.1 Impurity Analysis and U, Pu Recovery Feasibility in Graphite Crucibles

Three scrap types from QC of MOX fuel were taken into consideration and their identification is given in **Table 6.5**. The impure scrap consisted post sample analysis graphite crucibles containing MOX during the analysis of the impurities by DC-Arc-AES [313], IGF based nitrogen and hydrogen determinator [160-162, 167]. The plutonium content in the scrap was determined by NWCC and found to be in the range 2-5 wt%. The impurity contents in

QC generated impure scraps (**Table 6.5**) are shown in **Fig. 6.1**. The **Fig. 6.1** also shows the weight proportion of the $(U_{1-y}Pu_y)O_2$ MOX (sample, **Fig. 6.1**) in the QC impure scrap (QC-A, QC-B and QC-C).

Table 6.5: Source and Identification of Quality Control Generated Impure $(U_{1-y}Pu_y)O_2$ MOX Scrap

Impure scrap	Identification	Source of origin
Graphite crucibles containing MOX	QC-A	Originated in analysis of metallic impurities by DC-Arc-AES based on carrier distillation
Graphite crucibles containing MOX	QC-B	Originated in nitrogen determination based on inert gas fusion technique
Graphite crucibles containing MOX	QC-C	Originated in analysis of hydrogen in the MOX employing inert gas fusion technique

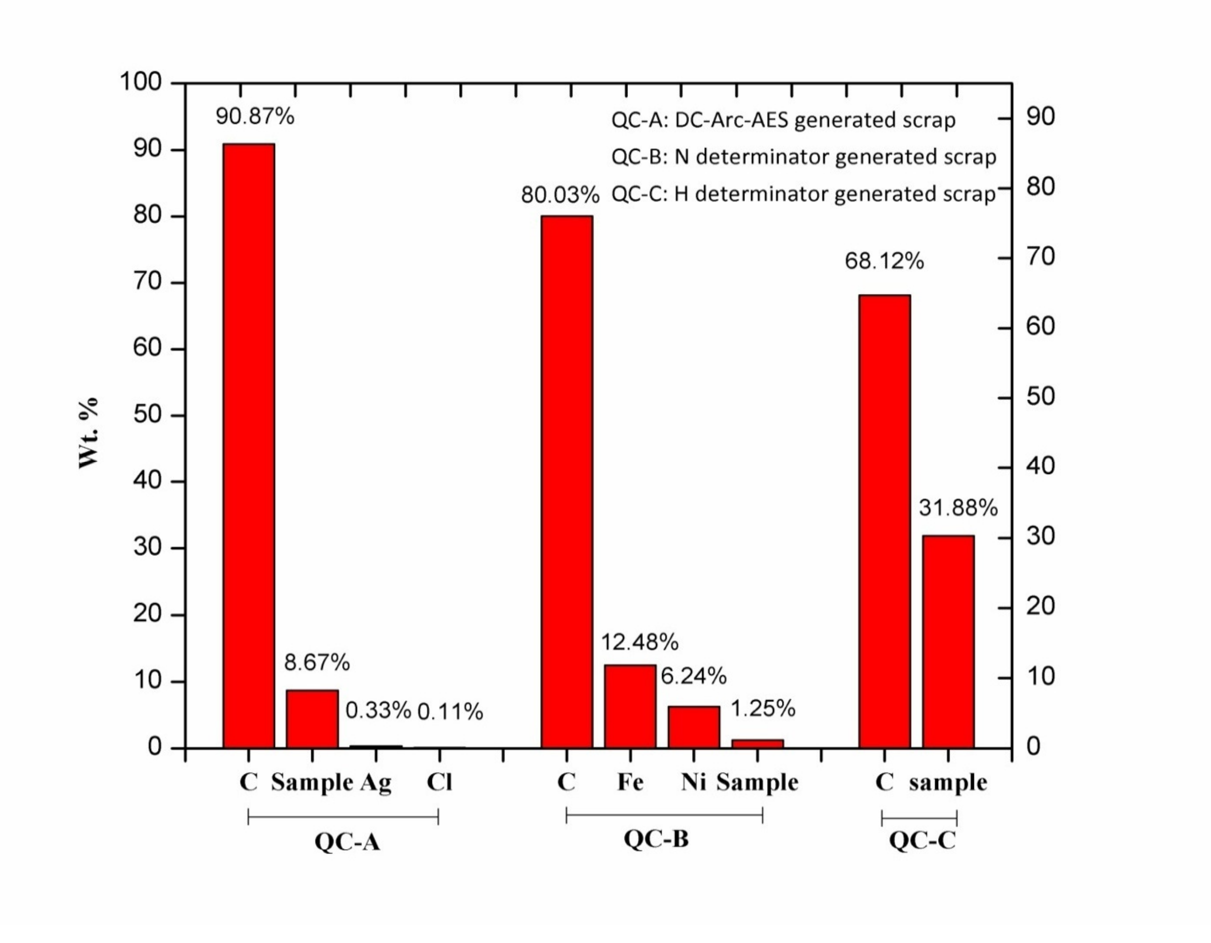

Fig. 6.1: Typical Composition of Impurities and $(U,Pu)O_2$ MOX in QC Generated Scrap

The impure scrap getting generated in a few QC activities of MOX fuel contained mainly carbon as impurity alongwith the significant amount of the sample (**Fig. 6.1**). These QC activities demand use of graphite crucibles/ electrodes for analysis to be carried out. The DC-arc-AES method for estimation of impurities using carrier distillation technique [160-161, 314] required heating of the solid sample in the graphite crucible (serves as electrode) at 3000 °C alongwith 5 wt% AgCl (as carrier) and 0.03 wt% Pd (as internal standard). The solid MOX sample was fused alongwith Fe-Ni flux at 2500 °C in the graphite crucible using induction furnace for the nitrogen estimation based on inert gas fusion (IGF) technique [160, 162, 167]. Similarly, hydrogen determination is carried out by inert gas fusion [160, 162, 167]. It used graphite crucible and involve heating the sample at 2000 °C without flux. Since, all the above techniques involved a high temperature heating of the MOX samples (with or without flux), the samples usually fuses with the graphite crucibles which are thus difficult to separate manually. The Fe-Ni added as flux during the nitrogen estimation lead to the formation of globules containing MOX. The scrap generated in the hydrogen determination (QC-C) had lesser impurities than that generated in the metallic impurity determination by DC-arc-AES (QC-A) and in determination of nitrogen (QC-B) since no flux is added in hydrogen determination.

All these types of impure scrap may be oxidized to remove the major impurity i.e. carbon (**Fig.6.1**) and subsequently the metallic impurities may be removed by chemical purification steps (e.g. solvent extraction/ ion exchange). A method was reported [10] using microwave assisted removal of carbon from the burnt graphite electrodes used in the DC-arc-AES method, however this method could not remove Ag and Pd added during the analysis. The scrap from hydrogen determination was free from metallic impurities, thus recyclable after carbon removal only. Since, carbon was the major matrix as impurity, the recycling firstly required its removal. The combustion using air or O_2 in microwave was recommended. The controlled oxidation using CO_2 is also an attractive option for removal of carbon.

6.2.6.2 Recovery for U, Pu from Graphite Crucibles

A combustion based recovery process was used for oxidation of the graphite carbon inside microwave oven (MHS-3) to recover valuable U and Pu mixed oxide. The typical schematic of the set-up for bulk oxidation of the graphite electrodes is shown in **Fig. 6.2**. The SiC susceptors were used for igniting the graphite crucibles. The air (0.5 lpm) was sucked through the quartz set-up which kept the crucibles ignited. The microwave after ignition was switched-off as air flow was sufficient to keep the ignition (fire) on. However, when the microwave was kept on during the oxidation, the process of oxidation was comparatively fast. The off-gas containing air, smoke, CO_2 and soot was passed through a water scrubber. **Table 6.6** presents the typical parameters for combustion of graphite crucibles.

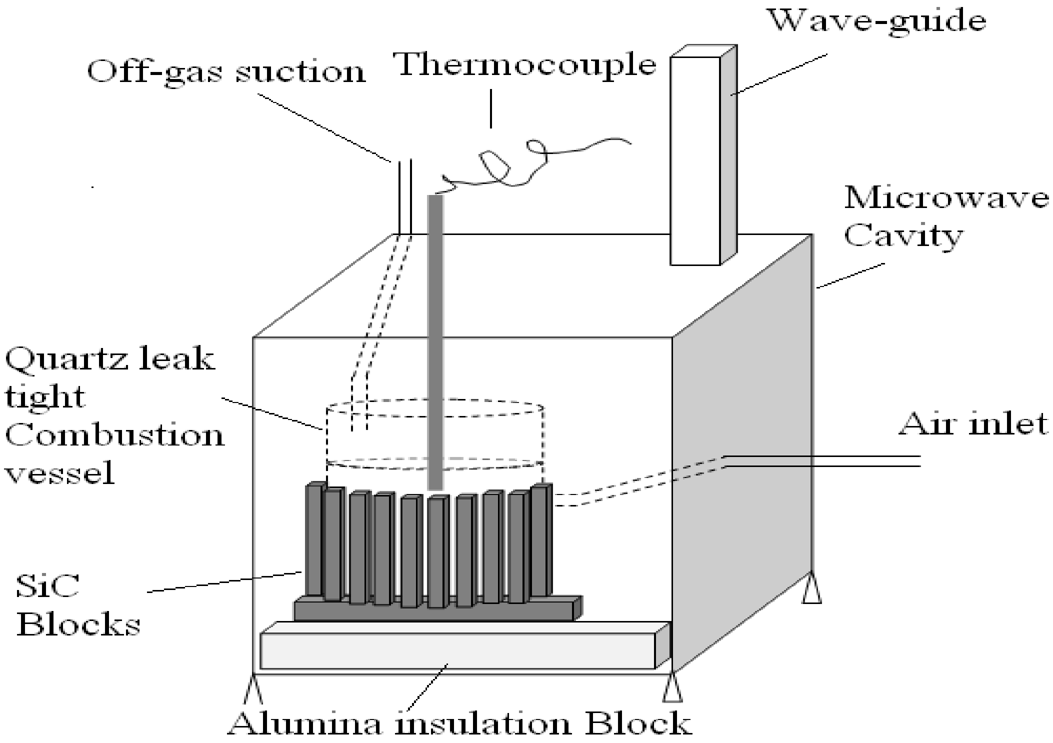

Fig. 6.2: Schematic of Set-up for Microwave Combustion of Graphite Crucibles for Recovery of U and Pu Mixed Oxide

Table 6.6: Parameters for Microwave Combustion of Graphite Crucibles (QC-C)

Wt. of Graphite Crucibles (Kg)	Microwave Power (W) and Irradiation Time (h)	Temperature (°C)	Combustion Time (h)	Wt. of the Residue (Kg)
0.5	1500 (0.5)	800-900	3	0.161
0.5	1500 (2)	800-900	2	0.147

6.2.7 Dissolution Behavior of Impure $(U_{1-y}Pu_y)O_2$ Scrap

6.2.7.1 $(U_{1-y}Pu_y)O_2$ MOX Dissolution Test

Approximately 10 g of each process representative sample was heated at 550 °C for 1 h in microwave oven to remove moisture and other volatile impurities and PuO_2 content was determined by NWCC. Sample ~1 g was drawn and dissolution test was carried out. The residue obtained was completely dissolvable in 10M HNO_3-0.03M HF under refluxing conditions for 8h. The wt% of the residue obtained in the DT of various impure scrap samples in 10M HNO_3-8 h refluxing conditions and PuO_2 content in the scrap are shown in **Table 6.7**.

Table 6.7: PuO_2 (wt%) in Various Process Generated Impure MOX Scraps Samples and Residue (wt%) obtained in the Dissolution Test

Impure scrap identification	PuO_2 (wt%) ($\bar{x}$ ±1s), n=3	DT Residue (wt%) ($\bar{x}$ ±1s), n=3
Scrap-A	21.2±0.4	18.25±0.51
Scrap-B	21.7±0.5	12.55±0.42
Scrap-C	24.3±0.5	7.01±0.25
Scrap-D	27.4±0.4	1.25±0.05
Scrap-E	22.8±0.4	10.05±0.26
Scrap-F	29.1±0.5	0.75±0.05

The prolonged dissolution of the impure (beyond standard conditions of DT) may increase the dissolution resulting in lesser residues. However, the present work was confined to compare the dissolution behavior of various scrap types under the identical conditions.

6.2.7.2 Dissolution Characteristics of Impure $(U_{1-y}Pu_y)O_2$ MOX Scrap

The presence of PuO_2 or plutonium rich regions in the MOX are detrimental to reactor operation as they are responsible for local hot spots resulting in clad failure. Such inhomogeneous MOX results in insoluble plutonium rich residues during dissolution in the reprocessing of spent fuel. $(U_{1-y}Pu_y)O_2$ solid solution has inherent characteristic for achieving adequate plutonium solubility during dissolution in HNO_3 without dissolution aids or catalyst. This is practically observable up to 35 wt% of PuO_2 in the MOX, beyond which again solid solution leave behind residue rich in plutonium [291-292, 310]. The remaining residue is due to presence of difficult to dissolve PuO_2 agglomerates or Pu rich MOX. The complete dissolution indicates formation of a true MOX solid solution and uniform distribution of plutonium. The mechanically mixed, non-sintered and partially sintered MOX when dissolved in HNO_3 under reflux boiling conditions for prolonged time, leaves behind residues. This characteristic was used as a method for assessing the formation of solid solution and bulk homogeneity [176]. The specification for the DT residue is different for fast and thermal reactor fuels which depend upon the Pu content in MOX fuel. The specifications for a typical fast reactor and a thermal reactor MOX fuel are 1 wt% and 0.1 wt% respectively (**Table 1.15**). The specified value of residue in dissolution test is 1 wt% for the both the nominal compositions of PuO_2 in MOX (21 % and 28 %) of PFBR.

From the **Table 6.7**, it can be observed that the floor scrap (**Scrap-A, Scrap-B** and **Scrap-C**) collected from the glove-box floors while cleaning and accounting campaigns left behind larger amount of residue typically 18 wt% (**Scrap-A**). This implied the presence of PuO_2 rich agglomerates with low porosity alongwith UO_2 and MOX in the floor scrap. The inhomogeneity and/ or low porosity may lead to slow dissolution resulting insoluble residues. The typical content of Pu varied from 70-85 wt% in the undissolved residue obtained in the dissolution test of PFBR MOX fuel [314]. The variation in the residue obtained in the various floor scrap (**Table 6.7**) might be due to variation in the percentage composition of the each component i.e. PuO_2, UO_2 and MOX. The residue obtained was dissolved completely using fluoride (HF).

The scrap from furnaces (**Scrap-D**) and the centreless grinding (**Scrap-F**) operations comparatively left smaller quantity of the residue (nearly 1 wt%). This was because these impure scrap were mainly sintered pellets or their powder or chips.

The **Scrap-E** left nearly 10 wt% of residue might be assignable to mechanical mixing of the constituents UO_2 and PuO_2.

6.2.7.3 Dissolution Options for $(U_{1-y}Pu_y)O_2$ Impure Scrap

If for recycling impure scrap, wet chemical processing is opted, dissolution becomes imperative. Since, the impure scrap was a three component system containing UO_2, PuO_2 and $(U,Pu)O_2$, contrary to the sintered clean scrap having solid solution $(U_{1-y}Pu_y)O_2$ only; the dissolution behavior depends upon the proportion of PuO_2 or Pu rich $(U_{1-y}Pu_y)O_2$. There are three methods which can be employed for complete dissolution [231-233, 291-292, 310]:

a. Fluoride catalysed dissolution
b. Catalysed electrolytic plutonium oxide dissolution
c. Mechanical blending, compaction and sintering

For dissolution of impure scrap, however the use of fluoride leads to corrosion of the equipments (usually not preferred). The electrolytic dissolution however, is an attractive option; need setting-up of large electrolytic cells. The last option of manufacturing the pellets of impure scrap by cold compaction followed by sintering is a method of choice. This forms the $(U_{1-y}Pu_y)O_2$ solid solution of UO_2 and PuO_2 which dissolves without fluoride ($PuO_2 < 35$ wt%), beyond which the options either a) or b) is to be followed.

6.2.8 Summary of Impurity Assessment and Dissolution Behavior of Impure $(U_{1-y}Pu_y)O_2$ Scrap

The recycling of impure scrap offered several challenges during MOX fuel fabrication contrary to the recycling of the clean scrap. This study brought the initial detailed baseline data of the impurities present and dissolution characteristics of most types of impure MOX scrap encountered. This data was fundamental to establish and assess potential recycling methodologies. From the detailed study, we arrived at the following conclusions:

1. The impure scrap contained a variety of impurities namely non-metallic and metallic, manifold higher than the specified limits.
2. The non-metallic impurities were associated with all types of the impure scrap. Hence, scrap was required to be treated by a head-end heat treatment.
3. The metallic impurities in the impure scrap were mainly refractory such as Al, W, Mo, Si etc., which essentially required chemical purification steps.
4. A few process scraps could not be dissolved in HNO_3 until fluoride was added. The impure scraps left behind larger quantities of plutonium rich residues in the dissolution test except Scrap-D and Scrap-F.
5. The recyclable scrap from QC activities involving metallic impurity assay using DC-arc-AES and nitrogen/ hydrogen determinations mainly contained carbon as impurity.
6. Based on the impurities present in the scrap it was concluded that not all types of the impure scrap need wet recycling methodology. Some of the scrap types could be purified and recycled employing dry processing methods.

6.2.9 Strategy for Recycling Various Types of Impure Scrap

Based on the impurity analysis and the dissolution behavior, recycling methodologies were explored. The recycling of impure scrap on 100% basis, firstly need removal of impurities either by physical methods involving heat treatment, sieving, magnetic separation etc. or by chemical purification techniques employing solvent extraction, ion-exchange or precipitation and subsequently converted to nuclear grade sinterable mixed oxide powder.

The dry recycling methodologies involving air calcination, roasting, controlled oxidation, pyrohydrolysis etc. are suitable alternatives for the scrap bearing the only non-metallic impurities. However, the scrap contained refractory impurities like Al, Si, W, Mo etc. and other impurity elements in addition to the non-metallic elements. Thus, a wet recycling approach essentially needs to be adapted, where dissolution was a prerequisite. Each scrap needed a head-end treatment to get rid-off non-metallic impurities prior to purification of metallic impurities. The presence of common non-metallic impurities like carbon may lead to formation of oil, organic complex, organic acids when dissolved in inorganic acids. This further may render difficulties to deploy the solvent extraction based separation of actinides. However, the organics can be removed using ozone, perchloric acid, sodium dichromate, by photochemical destruction or using Ag(II) [315-317]. The purification by solvent extraction or ion exchange steps may then be subsequently followed by microwave co-denitration or co-precipitation to deliver sinterable grade mixed powder.

It is important to make note of the fact that the sintering (a vital step in MOX fuel fabrication) at 1650 ^{o}C in (N_2+7% H_2) also reduces non-metallic impurities to a considerable extent. Finally, MOX batches undergo vacuum degassing (100 ^{o}C, 2 h, 10^{-2} torr) to remove adsorbed moisture and other volatile impurities. The degassed MOX pellets are loaded in the fuel elements, where the fuel has to meet the specifications (**Table 6.1**).

6.3 Development of Integrated Process for Recycling of $(U_{1-y}Pu_y)O_2$ Impure Scrap

A comprehensive analysis of the impurities in various impure scraps, their sources, dissolution behavior and possible recycling methodologies are discussed above. The impure scrap especially generated in fast reactor fuel fabrication contained nearly 20-30 wt% Pu and brought different issues to be thoroughly investigated. Interestingly, all the types of impure scrap did not need chemical purification step; several can be recycled either using a dry heat route or by dry heat route following microwave direct de-nitration route. Since, the impure scrap was a three component system containing UO_2, PuO_2 and $(U_{1-y}Pu_y)O_2$, their quantitative dissolution was a challenging task. It was seen that several impure scraps could not be dissolved in HNO_3 and left residues > 10 wt% (**Table 6.7**). So, wet recycling of high Pu wt% impure scrap was challenging considering their diversified behavior of impurities content, dissolution, criticality while wet processing and third phase formation while solvent extraction [318]. In this context, the recycling experience of a few small batches of impure scraps was presented. The feasibility assessment of deploying the solvent extraction based methods (using TBP-n-DD) for purification was carried out. However, the feed preparation demanded prior removal of non-metallic contaminants.

6.3.1 Dissolution of $(U_{1-y}Pu_y)O_2$ Impure Scrap by Microwave Heating

Impure scraps **S-A, S-B and S-C** (**Table 6.2**) with varying compositions of PuO_2 were taken. Microwave heating (550 °C, 2h) was carried out to remove carbon and other volatiles. Dissolution was carried out in denitration quartz vessels (Dia.; 75mm, Ht.; 280 mm) in HNO_3 which left significant amount of undissolved residue (**Table 6.8**). The complete dissolution was carried out either using 0.05M HF or by cold-pressing of the impure scrap in the form of pellets and sintering in reducing atmosphere (N_2+7% H_2) at 1500-1700 °C. After dissolution, the acidity was adjusted to 4M and solution was filtered for feed clarification. **Table 6.8** shows the wt% of residue left after dissolution in HNO_3 using HF and sintering of impure scrap in the form of pellets. The residue left were below 0.6 wt% of the batch size. The experimental details of a typical batches recycled are also presented in **Table 6.8**.

Table 6.8: Important Details of Typical ($U_{1-y}Pu_y)O_2$ Impure Scrap Batches Recycled By Microwave Dissolution and Solvent Extraction

Parameter description	Value
Batch size	150 g
PuO_2	21.69 wt%
Residue in HNO_3 dissolution	70 g
Residue in 0.05M HF+HNO_3	< 1 g
Residue in sintered impure pellets	< 1g
Plutonium conc. in 4M solution	21.9 g/L
Plutonium conc. in solution after extraction	0.26 g/L

6.3.2 Co-extraction of U and Pu and Partitioning

Uranium and plutonium were co-extracted by giving two contacts with 30%TBP in normal-dodecane (n-DD) (1:2 ratio and 1:1 ratio). The aqueous solution was analysed for plutonium concentration [155]. Pu was back extracted by partitioning from loaded organic using hydrazine stabilized uranous solution in aqueous to organic ratio of 1:2. The U was stripped from organic using 0.1 M HNO_3 or distilled water. The batch extraction was carried out in 1L beaker on the magnetic stirrer. A separating funnel was used for separation of the phases. **Fig. 6.3** shows the photograph of the typical set-up used for batch extraction.

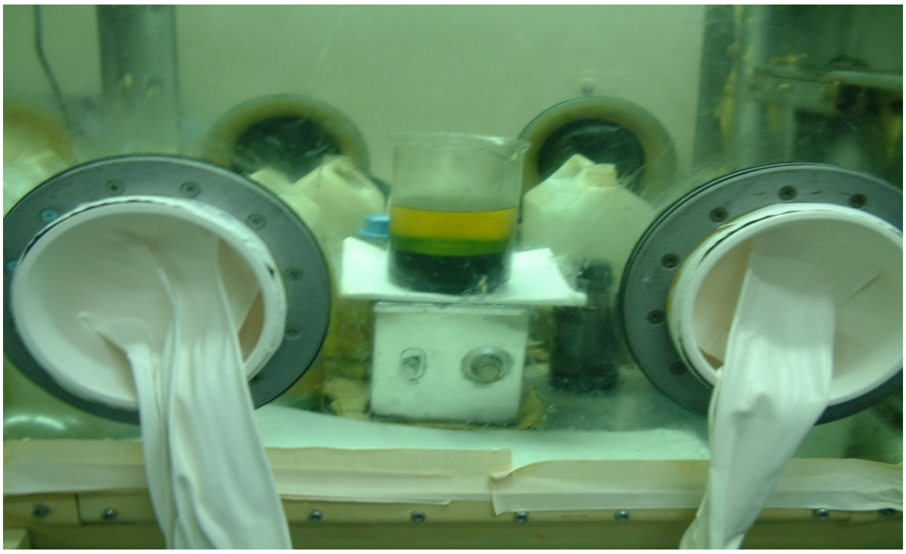

Fig. 6.3: Experimental Set-up for Batch Extraction Experiments of Impure Scrap

6.3.3 Microwave Direct Denitration of Purified U, Pu Nitrate Solution

The aqueous solution containing U and Pu was concentrated, crystallized, dehydrated and de-nitrated to get mixed oxide in denitration process vessel in MHS-6 (**Fig. 2.13**). Its further calcination delivered (M_3O_8,MO_2) porous clinkers having bulk density ~1.2 gcm^{-3}. The clinkers were milled to fine powder and reduced to (UO_2,PuO_2) using (7%H_2+N_2) atmosphere. The metallic impurities were determined by glove-box adapted ICP-OES (**Fig. 3.14**). Metallic impurities determined in the impure scrap and after wet recycling alongwith their decontamination factor (DF[12]) are listed in **Table 6.9**.

Table 6.9: Metallic Impurities in Impure ($U_{1-y}Pu_y$)O_2 Scrap and in Co-denitrated Powder alongwith Individual Decontamination Factors

Element	Impure Scrap (ppm)	Co-converted powder (ppm)	DF
Al	763	13	1.7×10^{-2}
Ca+Mg	1041	19	1.8×10^{-2}
Cr	88	10	1.14×10^{-1}
Cu	203	10	4.9×10^{-2}
Fe	1737	45	2.6×10^{-2}
Mn	59	5	8.5×10^{-2}
Ni	168	10	6.0×10^{-2}
W	609	10	1.6×10^{-2}
Zn	420	24	5.7×10^{-2}

6.3.4 Integration of Flow Sheet for Recycling of Impure Scrap with Clean Scrap

A flow sheet was developed for recycling of impure scrap based on the experimental work carried out. This was integrated with the process flow sheet for recycling of clean rejects based on microwave dissolution-denitration. The integrated flow sheet for recycling of clean and impure scrap employing microwave is shown in **Fig. 6.4**.

---

[12] Decontamination Factor is calculated as $DF = \frac{impurity\ in\ the\ product\ (ppm)}{Impurity\ in\ the\ feed\ (ppm)}$

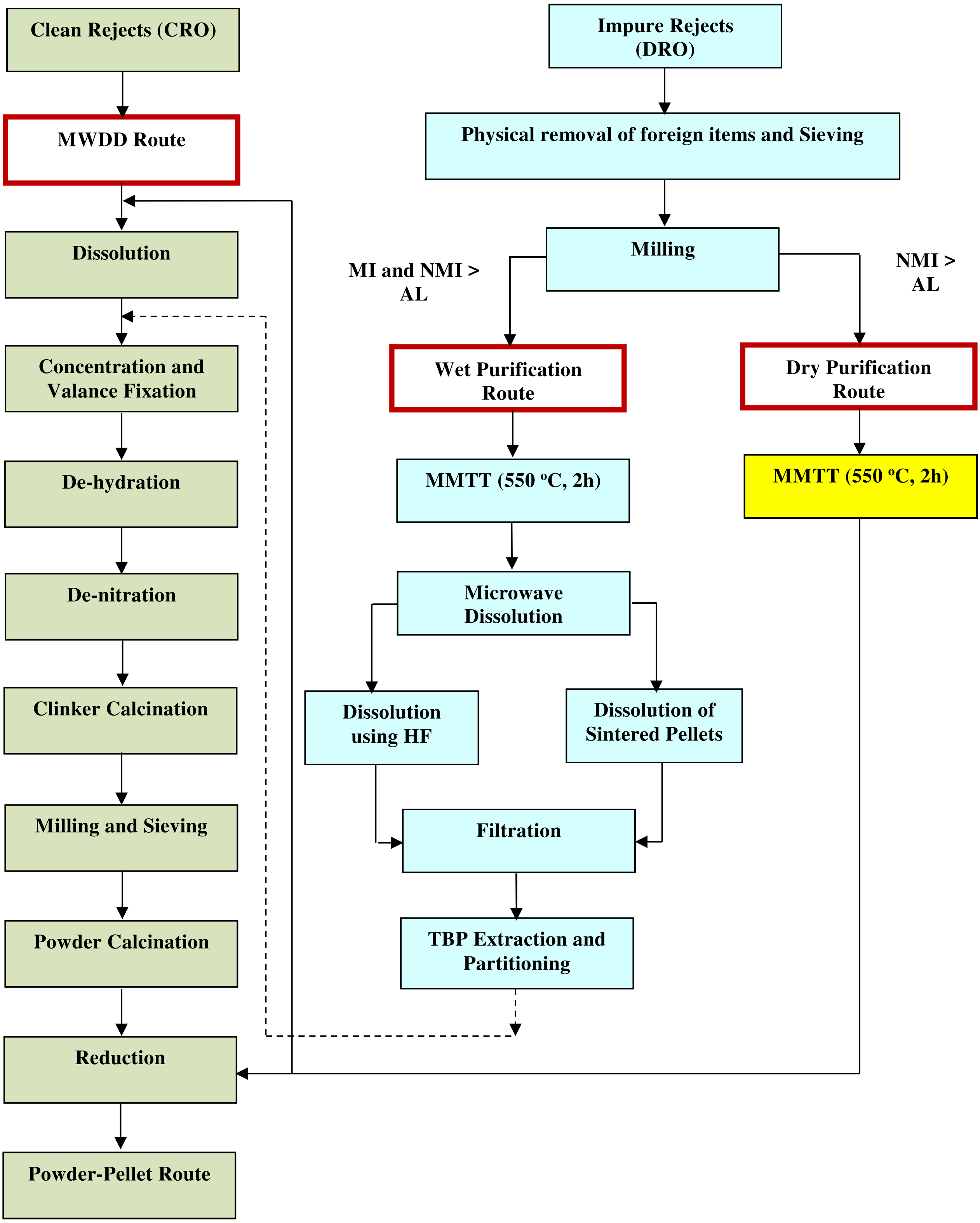

Fig. 6.4: Microwave based Integrated Flow Sheet for Recycling of various MOX Rejects

The foreign physically separable items were removed using sieving and hand-pickups. The scrap was then milled using a coarse mixer grinder/ Jaw crusher. The samples were drawn for impurity analysis. When only non-metallic impurities (NMI) were more than the allowed limits (AL), roasting using microwave moderate temperature treatment (MMTT) at 550 °C, 2h was opted. If the powder properties post MMTT were acceptable then powder directly was sent for reduction step otherwise it followed the microwave dissolution and direct denitration route to improve powder properties. In the case when both the NMI and metallic impurities (MI) were above the allowed limits, roasting using MMTT was followed by purification route comprising dissolution and solvent extraction process (**Fig. 6.4**). The U, Pu nitrate solutions were then co-converted to mixed oxides by microwave direct denitration.

The recycling of a few batches was carried out on experimental basis keeping in view the subcritical masses and limit of concentration (LOC). The material balance was not performed precisely. The losses in various process steps were significant. The aqueous phase remained after co-extraction showed high contact dose (~800 mR/h) due to ^{241}Am.

6.4 Recycling of Impure ThO_2 and ThO_2 based MOX Scrap

Recycling of impure thoria based scrap was carried out using integrated flow sheet (**Fig. 6.4**). As ThO_2 is room temperature microwave transparent material, the roasting at 550 °C, 2h was carried out using SiC as microwave susceptor or in conventional furnace. $(Th_{1-y}U_y)O_2$ and $(Th_{1-y}Pu_y)O_2$ though are microwave absorbers, but the temperature achievable depended upon the content of UO_2 and PuO_2. For $(Th_{1-y}Pu_y)O_2$ with $y<0.1$, the temperature of 550 °C could not be achieved. Similarly, $(Th_{1-y}U_y)O_2$ with low UO_2 ($y<0.2$) the temperature could not be achieved up to 550 °C. However, for $(Th_{1-y}U_y)O_2$, $y \sim 0.3$, the temperature of 550 °C was achievable. The other difference was in the dissolution in HNO_3. The dissolution was performed using fluoride (HF). The solid solution formation in $(Th_{1-y}Pu_y)O_2$ did not have any positive effect on its dissolution in HNO_3. The solid solution $(U_{1-y}Pu_y)O_2$ with $y< 0.35$ (PuO_2 < 35 wt%) dissolves completely in HNO_3 [150, 291-292, 311]. Similarly, the solid solution formation in $(Th_{1-y}U_y)O_2$ with y< 0.4 did not dissolve completely in HNO_3 [237]. Thus, fluoride was essentially required for dissolution. The recent reports on the dissolution of ThO_2 in triflic acid and ammonium sulphate based solid state reaction methods [235-236] are promising, however were not attempted in the present work. The extraction of Th and U/ or Pu was carried out using 40%TBP in n-Dodecane [92] on experimental scale. The purified thorium nitrate solution was denitrated using microwave.

6.5 Methodologies Used and Quantity of Various Types of Impure Scrap Recycled

Table 6.10 records the types and quantities of $(U_{1-y}Pu_y)O_2$ and ThO_2 impure scrap recycled. **Table 6.10** also presents the steps followed during recycling. All the process generated impure scraps were subjected to MMTT at 550 °C for 2h in air to remove the non-metallic impurities.

Table 6.10: Quantity and Related Data of Various Types of Impure Scrap Recycled

Material Description	Scrap Identification	Recycling Method Steps	Quantity (Kg)
$(U_{0.79}Pu_{0.21})O_2$	Scrap-A and Scrap-F	MMTT and microwave dissolution-denitration	28
$(U_{0.79}Pu_{0.21})O_2$	Scrap-D	HF-HNO_3 Dissolution, TBP extraction, Microwave Denitration	0.5
$(U_{0.79}Pu_{0.21})O_2$	Scrap-D	Compaction into pellets, sintering, HNO_3 Dissolution, (TBP extraction, Denitration)	2.4 (0.3)
$(U_{0.72}Pu_{0.28})O_2$	Scrap-F	MMTT and microwave dissolution-denitration	11.3
ThO_2	Impure scrap	HF-HNO_3 dissolution, 40%TBP in n-DD extraction, microwave denitration	2
Used Graphite crucibles	QC-A, QC-B and QC-C	Microwave combustion in flowing air using SiC susceptors	8.5

6.6 Summary of the Methods Developed for Recycling of Impure Scrap

The methods were developed for recycling $(U_{1-y}Pu_y)O_2$ and thoria based impure scraps. The developed methods were examined thoroughly and are conclusively summarized as follows:

1. The integrated method was successfully demonstrated for U, Pu and Th based impure oxides or mixed oxides originated in the process of fuel fabrication and in a few quality control checks.
2. A head-end treatment to get rid of common non-metallic impurities was required in all the types of the process generated impure scrap by using microwave at 550 ºC, 2h in air (MMTT).
3. The complete dissolution was achieved either by fluoride addition or by sintering the pellets of impure scrap. Of which the later is more attractive as this did not require addition of corrosive fluoride. The later method was subsequently recommended for dissolution of impure $(U_{1-y}Pu_y)O_2$ scrap for recycling by PUREX process. This method is now established for recycling of impure scrap (DRO) at the plant scale at Tarapur.
4. The recycling of thoria based impure scrap under present study by integrated process needed fluoride dissolution. Heating using microwave was embedded in the flow sheet to increase the rate of dissolution.
5. The extractant TBP could be employed for purification of impure scrap from non-volatile impurities and decontamination factors (DFs) of the order two were achieved.

Chapter 7

LOW TEMPERATURE MATERIAL PROCESSING APPLICATIONS USING MICROWAVE

7.1 Introduction

The feed material for fabrication of MOX fuel by powder-pellet route [106] with desired specifications require oxygen to metal mole ratio O/(U+Pu) either stoichiometric or slightly hyper-stoichiometric. This ratio is achieved by reduction of intermediate oxides as UO_3, U_3O_8 and mixed oxides (M_3O_8,MO_2) where, M is (U+Pu) etc. in conventional resistance furnaces at 700 to 900 °C for not less than 4 h using reductants like H_2, NH_3, CO, C, CH_4 etc. [211]. The direct use of U_3O_8 is not advisable because of the large volumetric change (~36%) accompanied from orthorhombic U_3O_8 to FCC UO_2 transformation [245-246] resulting in lower sintered density, formation of grape like pore clusters [37], low sinterability and evolution of oxygen leaving behind enormous porosities and cracks. The powder properties play utmost important role in tailoring the final characteristics of the MOX fuel. Though, sintering kinetics depends upon the heating technique, temperature profile and atmosphere, the final fate of the MOX is mainly steered by several feed material powder properties. Among these properties the specific surface area, average particle size, O/M ratio and bulk density are vital. The essential powder properties of sinterable grade UO_2, PuO_2 and ThO_2 for the fabrication of nuclear fuel are listed in **Table 3.1**.

It is reported that the recycled powder has low sinterability [35-43, 196-197, 319] compared to the standard feed powders (**Table 3.1**) prepared deploying conventional methods [106, 118, 301, 320-323]. We also have seen that the recycled powders obtained by MWDO dry recycling technique have poorer powder properties (§ **4.3, Fig. 4.18** and **Fig. 4.19**) despite of several oxidation cycles as compared to the standard powders (**Table 3.1**). However, the microwave dissolution and direct denitration based recycling process (Modified-MWDD) claimed powder properties equivalent to standard powder or even better (§ **4.2**). Thus, further improvement in the powder properties is desirable to enhance the sinterability especially where the recycled powder may not possess properties better than standard (**Table 3.1**). The improvement in the feed material properties brings down the rejection rate arising out of subsequent implications such as low density, oversize etc. in pellets, thus enhancing the productivity and reducing the fuel cost.

Direct, non-contact and homogeneous heating of the materials and in particular "microwave enhanced reaction kinetics" has shown a great deal of attraction towards the microwave technology in the nuclear industry [8]. Microwave processing has shown a large potential to improve energy economics and powder ceramic properties. The power consumption for preparation of uranium oxides powder using microwave heating was one order lesser than using conventional electric furnaces [39]. UO_2 was prepared by microwave thermal decomposition of various precursors in reducing atmosphere within 5-10 min. [13].

The present chapter is focused on to improve the properties of the recycled powder by development of processes which cause less harm to its sinterability. This was achieved by use of microwave heat process at lower temperature and/ or with a smaller process cycle as compared to conventional heating in electrical resistance furnaces. The heat processing of nuclear materials such as reduction, controlled oxidation (stabilization), air calcination were studied using microwave and optimized lower temperature and duration were recommended after extensive experimental investigations.

7.2 Potential Benefits of Lower Temperature Processing in Ceramics

It is obvious that the higher temperature treatment and prolonged duration deteriorate the sinterability and make the processing cycle large and energy-inefficient. The specific surface area of PuO_2 powder during decomposition of plutonium oxalate (400-1100 °C) decreases exponentially, or linearly as inverse function of temperature (I/T) [112]. The effect of the calcination temperature from 700 to 900 °C showed significant degradation in the MOX powder properties [14]. The BET-SSA of ThO_2 powder decreases exponentially with temperature during calcination of the precursor thorium oxalate [99]. The soaking time at peak calcination temperature of thorium oxalate beyond 5h does not have significant effect on the SSA of ThO_2 [99].

Therefore, the feed powder heat processing like air calcination, oxidation, stabilization, reduction etc. are preferred at lower temperature. However, at the same time the intent (quantitative reduction/ oxidation etc.) of the powder processing should also be served. The heat process parameters (temperature, duration) in the powder processing stage are required to be optimized so that such initial processing affects sinterability to a minimal.

7.3 Reduction of U_3O_8 and (M_3O_8,MO_2) using Microwave Heating

In view of the above mentioned advantages offered by microwave heating, the reduction of U_3O_8 and (M_3O_8,MO_2) up to stoichiometry was attempted at lower temperature. The reduction of U,Pu oxide powder was reported at 700 °C for prolonged duration in microwave ovens [11, 14]. The reduction of U_3O_8 or UO_3 to obtain UO_2 using H_2 has been reported in the literature extensively to investigate mechanistic aspects [248-249, 251], to increase U(IV) content for hydro-fluorination [324] and for many other applications at temperatures in the range 500-800 °C and a comprehensive modelling of the transformation has been proposed.

A method for stoichiometric reduction of U_3O_8 and (M_3O_8,MO_2) in H_2 atmosphere with a shorter processing cycle (550 °C, 3h) using 2.4 GHz microwave is investigated. The stoichiometric reduction is time consuming and is usually difficult [62].

7.3.1 Reduction Batch Experiments

U_3O_8 powder (as received) was obtained by heating UO_2 powder at 700 °C for 4h in air. The oxidized and milled $(U,Pu)O_2$ MOX; C and D (**Table 3.2**) from MWDO process and calcined mixed oxide powders via microwave denitration process were obtained. **Fig. 7.1** shows the schematic of experimental set-up consisting of a quartz glass reactor for reduction. The glass wool thermal insulated reactor was kept inside the microwave applicator and microwave energy was projected.

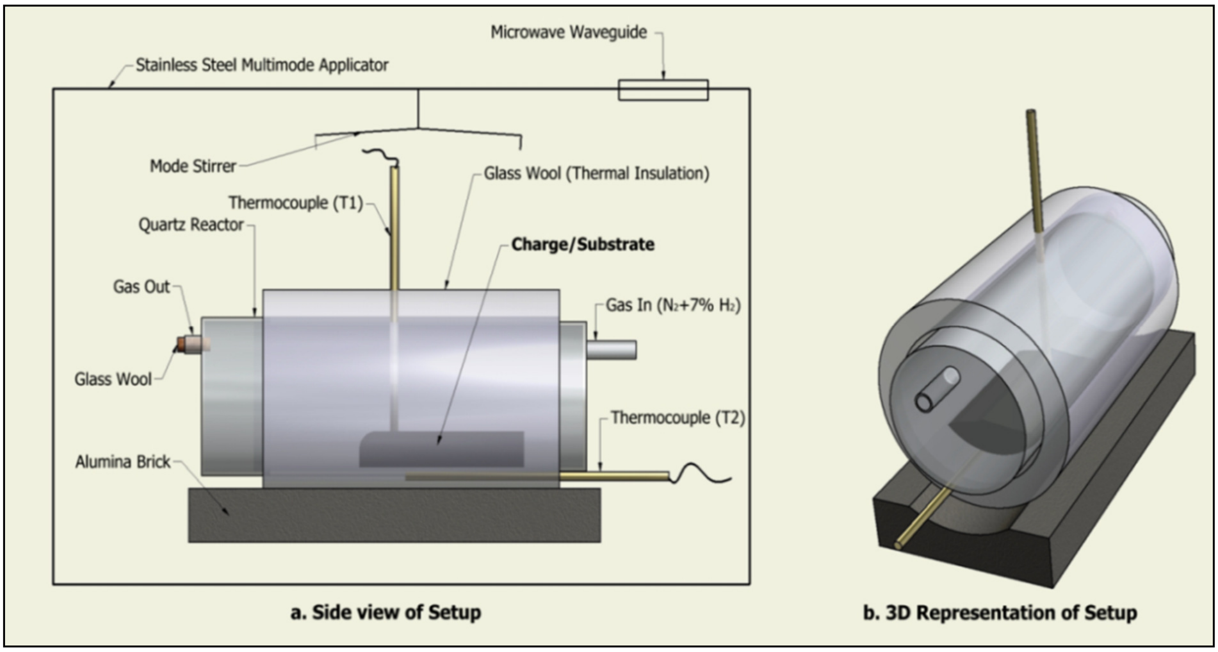

a. Side view of Setup

b. 3D Representation of Setup

Fig. 7.1: Schematic of Experimental Set-up for Reduction inside a Microwave Applicator

In order to optimize the process parameters, initially the reduction batch experiments were carried out with U_3O_8. The % reduction of U_3O_8 powder at different temperatures was calculated from measured values of O/M ratio using Eq. (3.10). The variation of the reduction % alongwith soaking time is shown in the **Fig. 7.2**. The temperature 550 °C and time 3 h were found as the optimized parameters and followed in all the subsequent batch experiments involving reduction of oxidized (U,Pu)O_2 MOX. The other experimental parameters during the microwave reduction are recorded in the **Table 7.1**.

Initial flushing of the set-up was carried out with premix (N_2+7 vol.%H_2) for 15 min. to drive out the air. A typical microwave power and temperature profile during the reduction is shown in **Fig. 7.3**. The heating rate was maintained 35 °C/ min. to achieve the soaking temperature quickly. After soaking at 550 °C for 3 h the microwave incident power was decreased (**Fig. 7.3**) slowly from 500 W down to zero power over 20 min. The corresponding temperature was reduced from 550 °C to 300 °C as depicted in the **Fig. 7.3**. The material was allowed to cool naturally which could take nearly 2h to reach up to room temperature. The atmosphere was kept reducing (N_2+7 vol.%H_2) in the full cycle to achieve completely stoichiometric mixture.

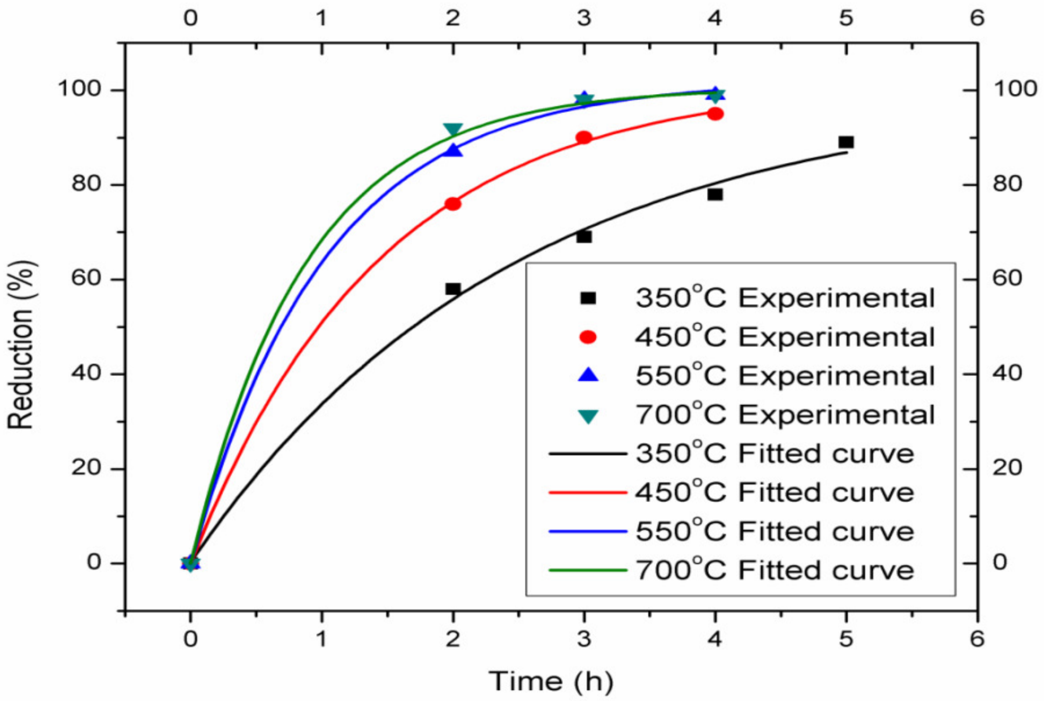

Fig. 7.2: Temporal Variation of % Reduction of U_3O_8 at different Temperatures in Microwave

Table 7.1: Experimental Parameters for Microwave Reduction of U_3O_8

Parameter	Description
Batch size	~500 g
Peak temperature	550±20 °C
Soaking at peak temperature	3 h
Reducing Gas	Premix (N_2+7%H_2), 99.99 %
Gas flow	0.5 l min^{-1}
Temperature measurement	Stainless steel sheathed, K-type thermocouple
Microwave power measurement	Calibrated dual directional coupler (DDC)

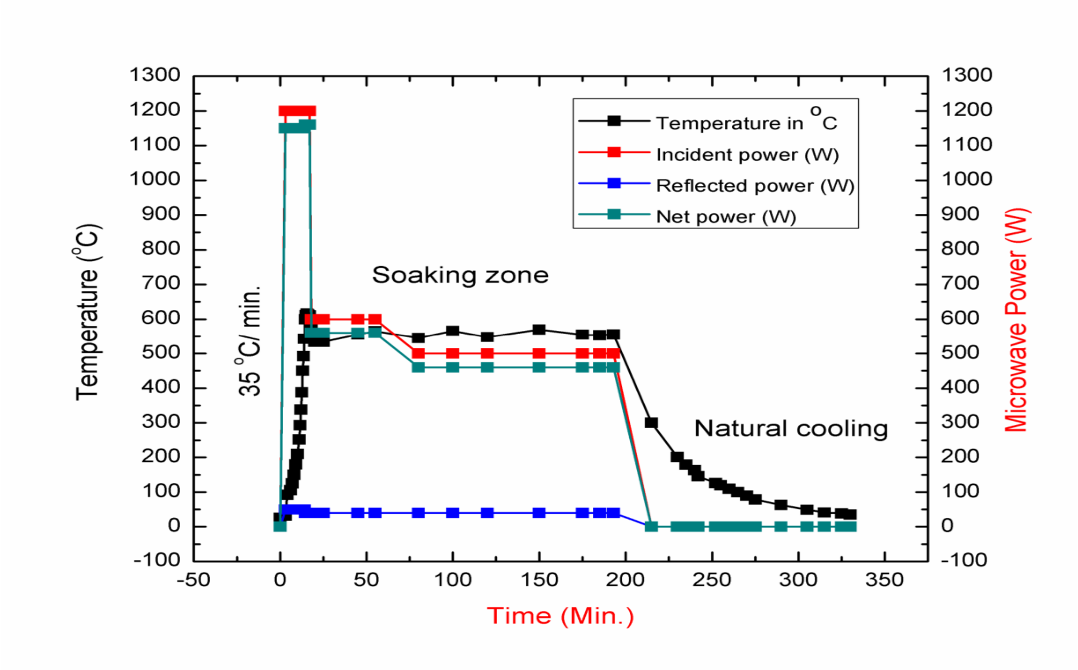

Fig. 7.3: Power-Temperature Profile for Microwave Reduction from a Cold Start

7.3.2 Temperature Measurement during Reduction

Two thermocouples; one inserted (T1) directly inside U_3O_8 powder and second (T2) was kept between insulation and the quartz reactor below the U_3O_8 powder as shown in **Fig. 7.1**. The response of thermocouples was ascertained by switching the microwave power on and off. It was observed that there was no sudden large decrease in temperature as microwave power is switched off and sudden temperature surge while microwave power is projected attributable to voltage breakdown and subsequently arcing [254]. The measurement responses of the two thermocouples were in agreement as variation in temperature in the T1 was followed by T2. The U_3O_8 powder bed thickness was below 1 cm across which the temperature gradient (reverse thermal gradient) expected was quite small to be neglected. The T2 temperature cannot be taken true representative of the powder bed surface temperature as quartz glass reactor is present between the material and the measurement device. However, T2 showed temperature which was lower (2 to 6 ºC) than T1 throughout the process.

7.3.3 Effect of Temperature on Specific Surface Area

BET-SSA was determined after reduction of as received U_3O_8 at each experimental soaking temperature for various durations. The MW-A to MW-D refer to U_3O_8 batches reduced by microwave. CR-E is conventionally reduced batch at 700 ºC. The values of BET-SSA obtained are shown in **Fig. 7.4**. SSA of as received U_3O_8 was shown for comparison.

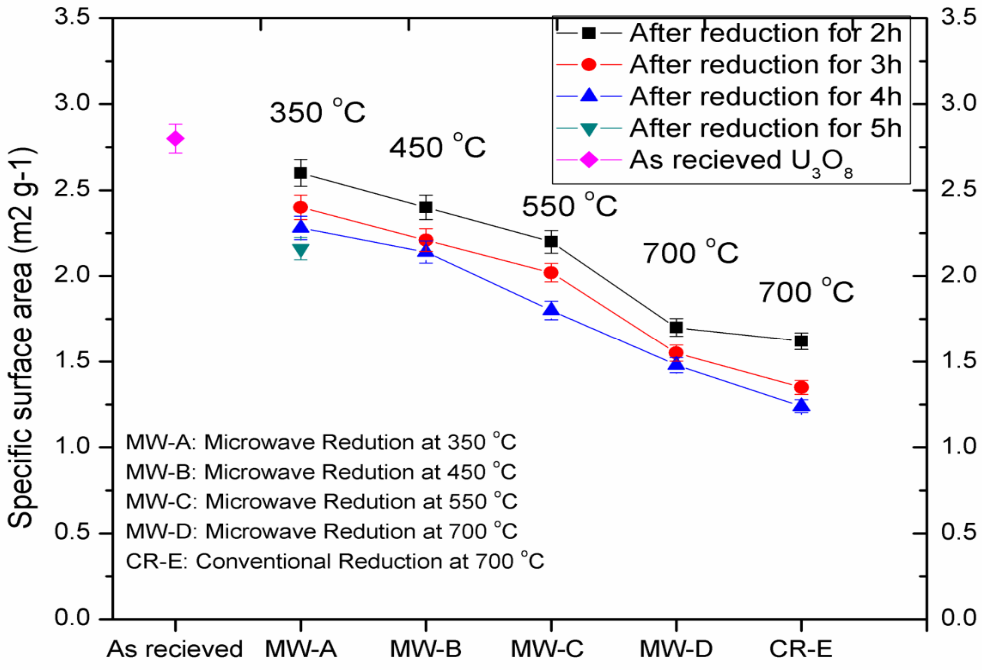

Fig. 7.4: Impact of Soaking Temperature and Duration on BET Surface Area in Microwave and Conventional Reduction of U_3O_8 to UO_{2+x}

7.3.4 Optimization of Reduction Parameters

The soaking temperature, duration and SSA were parameters which were studied. It was evident from **Fig. 7.2** that the rate of the reduction was initially high in all the cases and decreased with time. The % reduction approaches maximum asymptotically. This could be attributed to the fact that the reduction reaction of U_3O_8 to UO_2 using H_2 is a surface controlled reaction which proceeds according to contracting-sphere model [248, 251]. As the process progresses the surface sites becomes lesser available and the gas has to permeate inside the core of particles to achieve the effective reduction. It could also be seen from the **Fig. 7.2** that higher the soaking temperature higher was the rate of reduction. The higher temperature imparts more kinetic energy thereby accelerating the reduction process. A careful observation of the reduction curves (**Fig. 7.2**) at soaking temperatures 550 °C and 700 °C revealed that in both the cases the reduction (%) achieved was similar at 3h. However, the effective reduction could not be achieved at 350 °C upto 4h and at 450 °C upto 5h soaking. The prolonged soaking periods may result in stoichiometric reduction in these cases also, but would result in making process cycle longer.

The % reduction achieved in microwave reduction of U_3O_8 was more than 98% at 700 °C and 550 °C after 3 h (**Fig. 7.2**). Thus, 550 °C, 3h was selected as optimized condition for microwave reduction of U_3O_8 as it caused lesser impact on the powder surface area (**Fig. 7.4**) and was energy efficient. **Fig. 7.4** clearly showed that higher the reduction temperature, lesser was the BET surface area of the reduced UO_{2+x} powder for starting material as received U_3O_8. **Fig. 7.4** also revealed that the longer soaking at a given temperature further decreased the specific surface area of the reduced powder. No work to experimentally measure the reduction reaction rate at optimized condition was carried out. However, **Fig. 7.2** gave a fair judgment that the rate of the reduction reaction keep on decreasing with the course of reaction. The rate of reduction of UO_3 using H_2 is directly proportional to surface area, H_2 partial pressure [325] and temperature. It is to be noted that the SSA is degraded significantly in conventionally reduced batch (CR-E) than microwave reduced (MW-D) under similar conditions. This can be attributed to dielectric heating employing microwave which is principally different from conventional conductive heating. In microwave field, heat is generated autogenously from the microwave absorbing material.

7.3.5 Controlled Oxidation of Reduced UO_2 Powder

The process of reduction using microwave was further modified to incorporate a controlled amount of U_3O_8 in the reduced stoichiometric powder. During the batch reduction experiment the reducing atmosphere (N_2+7%H_2) was changed to oxidizing atmosphere (air) below temperature 100 ^oC during cooling to form a controlled amount of U_3O_8 on the surface of the reduced UO_2 powder.

This had mainly two intentions; firstly a small U_3O_8 content in UO_2 was reported to increase the sintering kinetics [44, 294]. Second was the long term storage by forming a passivation layer of U_3O_8 which further prevents the aerial oxidation of reduced UO_2 powder and changes in the O/U ratio [44, 326]. It is well known fact that the most stable form for uranium oxides is U_3O_8 for the safe long term storage [327]. Kulyako et al. [13] have recently reported that the UO_2 prepared by thermal decomposition of several precursors in reducing atmosphere using microwave becomes resistant to spontaneous oxidation in air. The handling of freshly reduced UO_2 powders is very difficult which react pyrophorically when exposed to air [243].

7.3.6 Powder Characterization

The powders were characterized before and after the microwave reduction and controlled oxidation of the reduced powder for essential properties relevant to MOX fabrication and are presented in **Table 7.2**.

Table 7.2: Powder Properties during Microwave Reduction of (M_3O_8,MO_2) and its Controlled Oxidation

Property		MWDD derived Calcined-C		MWDD derived Calcined-D	
		Initial	**Final**	**Initial**	**Final**
Bulk density (g m^{-3}) ($\bar{x}$ ±1s, n=3)		2.4±0.1	2.7±0.1	2.5±0.1	2.8±0.1
Average particle size (µm)		1.5	2.0	1.5	2.0
Surface area (m^2 g^{-1}) ($\bar{x}$ ±1s, n=3)		3.29±0.13	3.20±0.15	3.14±0.11	3.09±0.12
Microwave reduction	O:(U+Pu) ($\bar{x}$ ±1s, n=3)	2.522±0.001	2.000±0.002	2.483±0.001	2.000±0.002
	Max. U_3O_8	79 %	Nil	72 %	Nil
Microwave controlled oxidation	O:(U+Pu) ($\bar{x}$ ±1s, n=3)	2.522±0.001	2.094±0.001	2.483±0.001	2.063±0.002
	Max. U_3O_8	79 %	13.67 %	72 %	9 %

Fig. 7.5 shows the powder X-ray diffraction patterns of MWDO route recycled $(U_{0.72}Pu_{0.28})O_2$ MOX (D, refer **Table 3.2**) (a) calcined or oxidized-D, (b) after microwave reduction and (c) microwave controlled oxidized sample. The oxidised powder (a) showed presence of orthorhombic $(U,Pu)_3O_8$ (M_3O_8) and FCC $(U,Pu)O_2$ (MO_2) phases. The reduced powder (b) showed the presence $(U,Pu)O_2$ phase only. The controlled oxidized sample (c) has major MO_2 phase and minor M_3O_8 phase. The oxidation of $(U_{0.72}Pu_{0.28})O_2$ MOX produced a biphasic mixture of M_3O_8 and MO_2. Similarly, the calcination of MWDD process recycled $(U_{0.79}Pu_{0.21})O_2$ showed a biphasic mixture of M_3O_8 and MO_2 (**Fig. 4.9**).

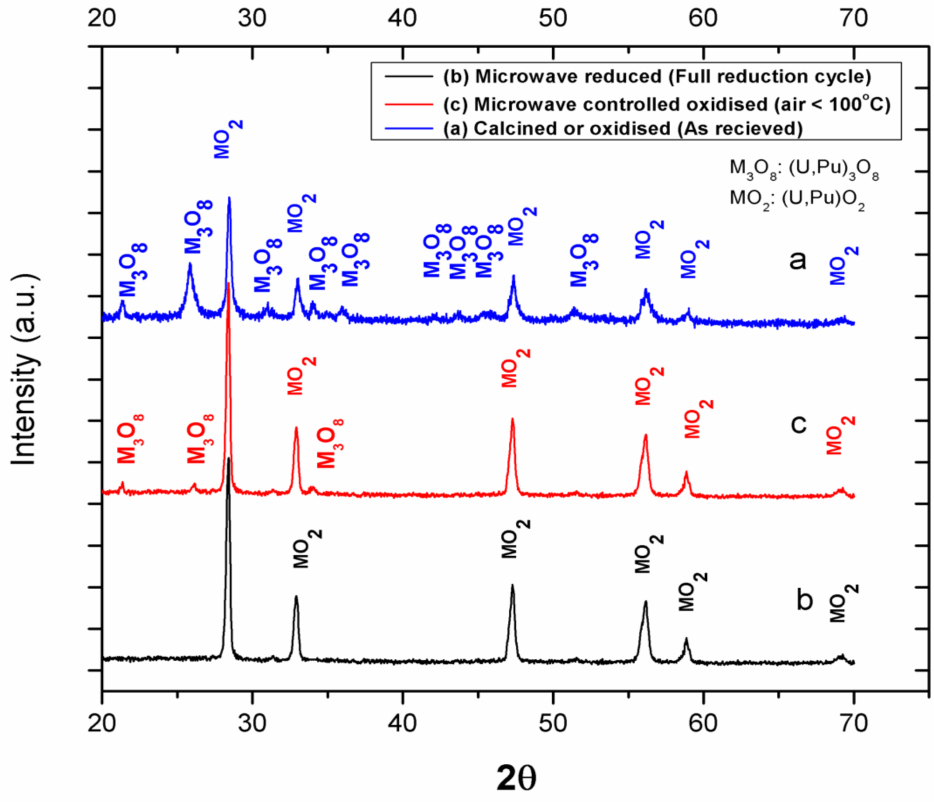

Fig. 7.5: XRD Patterns of MWDO recycled $(U_{0.72}Pu_{0.28})O_2$ (a) Oxidised, (b) Microwave Reduced and (c) Controlled Oxidised Powder

7.3.7 Microwave Reduction of Biphasic Mixture (M_3O_8,MO_2) into MO_2: Discussion

The net chemical reaction of the reduction of U_3O_8 to UO_2 by H_2 is shown by Eq. (1.31). Since, the product formed is UO_3 during the calcination of most commonly employed precursors for UO_2 production as $UO_2(NO_3)_2.6H_2O$, $(NH_4)_4UO_2(CO_3)_3$ and $(NH_4)_2U_2O_7$. The product UO_3 is further calcined to U_3O_8 at temperatures between 500 °C to 700 °C. The direct reduction of UO_3 using H_2 can also be carried out and proceeds in two stages first being the reduction of UO_3 to U_3O_8 and secondly the reduction of U_3O_8 to UO_2 [248].

As discussed earlier (§ **4.3.5.2**), the oxidation of $(U_{1-y}Pu_y)O_2$ MOX having 5-30 wt% PuO_2 (y: 0.05-0.3) forms a biphasic mixture containing uranium rich hypo-stoichiometric $(U,Pu)_3O_{8-x}$ (referred as M_3O_8) and plutonium rich hyper-stoichiometric $(U,Pu)O_{2+x}$ (referred as MO_2) where orthorhombic M_3O_8 is major phase. The reduction of (M_3O_8,MO_2) mixture obtained after calcination/ oxidation is expected to be easier than pure U_3O_8 (O/U: 2.667) as the mixture has lesser oxygen content (O/M: 2.527, **Table 7.2**) under the optimized conditions. For a mixed oxide powder (U_3O_8,PuO_2) the reduction reaction is shown by Eq. (4.11). The reduction of biphasic mixture (M_3O_8,MO_2) carried out in the flowing (N_2+7% H_2) atmosphere in the entire cycle (**Fig. 7.3**) delivered completely stoichiometric mixed oxide MO_2 with O: (U+Pu) of 2.000 (**Table 7.2**) which is difficult to achieve usually. The XRD patterns of (a) oxidized or calcined $(U_{0.72}Pu_{0.28})O_2$ MOX (D, **Table 3.2**) and (b) reduced powder are shown in **Fig. 7.5**. The peak corresponding to M_3O_8 disappeared in the reduced powder and showed single phase MO_2 or $(U,Pu)O_2$ (**Fig. 7.5b**).

Table 7.2 shows the powder properties before and after the microwave assisted reduction. The variation in the density was attributable to the phase transformation of the M_3O_8 to MO_2 upon reduction [251]. The lower bulk density in the initial mixed oxide powders (**Table 7.2**) was due to lower density orthorhombic phase M_3O_8 (orthorhombic U_3O_8 has TD 8.35 gcm^{-3}) which transformed into higher density phase MO_2 (FCC UO_2 has TD as 10.96 gcm^{-3}) [211]. The increase in the density upon reduction may also be attributed to the heat treatment during reduction leading to coarsening of particles and removal of pores. This was evidenced from the average particle size and BET surface area data (**Table 7.2**).

7.3.8 A Quick Method for Stabilization of the Reduced UO_2 or MO_2Powder

The reduction of biphasic mixture of $(U,Pu)_3O_{8-x}$ and $(U,Pu)O_{2+x}$ into $(U_{1-y}Pu_y)O_2$ as well as its controlled oxidation to get $(U_{1-y}Pu_y)O_{2+x}$ was carried out successfully. The methodology involved the reduction in flowing (N_2+7%H_2) at 550 °C, 3 h. followed by the cooling. During cooling at 100 °C the atmosphere was changed to air to get slightly hyper-stoichiometric mixture. The U_3O_8 content is usually kept below 22.7 % or O/U ratio < 2.15 in the controlled oxidation of UO_2 during the stabilization treatment [177, 294, 328]. The O/(U+Pu) of the controlled oxidized samples (**Table 7.2**) suggested the presence of hyper-stoichiometry. The presence of M_3O_8 phase along with MO_2 was further confirmed by XRD analysis as shown in **Fig. 7.5c**. Incorporation of a controlled amount of M_3O_8 phase in the reduced powder was advantageous. A small amount of U_3O_8 phase in the UO_2 powder increases the sintering kinetics [44, 294]. Thus, using controlled oxidized MO_2 powder for fuel fabrication, high density MOX pellets can be achieved or alternatively the rate of rejection due to low density can be minimized. An optimized heat treatment of the U_3O_8 and optimum content of so produced U_3O_8 seed was found to increase the grain size of the UO_2 pellets [319]. About 10 wt% of U_3O_8 powder addition into UO_2 during fuel fabrication increases the green strength of the UO_2 pellets [329].

A passivation surface layer of U_3O_8 around the UO_2 particles was intentionally formed. This prevents the permeation of air inside the particles and hence aerial oxidation of powder and subsequent changes in the O/U ratio during storage and transportation. The process of stabilization conventionally is carried out at 70 °C, 24h in air atmosphere [44, 326]. UO_2 being pyrophoric [243], undergoes aerial oxidation resulting in O/U ratio increase.

Our objective of incorporating controlled hyper-stoichiometry in the reduced UO_2 and MO_2 powders was to increase the sinterability. Lay and Carter [294] have evaluated the role of O/U ratio on sintering of UO_2 and reported that the diffusion coefficient of uranium (D^U) in the oxide at the initial stages of sintering was dependent on the O/U ratio. The D^U value having an O/U ratio of 2.02 is 10^8 times higher than that having an O/U ratio of 2.00. The O/U ratio should be between 2.00 to 2.08 for better sintering in UO_2 fuel. The quantitative estimation of $(U,Pu)_3O_{8-x}$ and $(U,Pu)O_{2+x}$ phases after oxidation were not carried out in the present work. Similarly, the solubility investigation of Pu in the U_3O_8 was not attempted.

However, the plutonium has shown low solubility (~5%) in M_3O_8 phase [330]. The air oxidation of $(U_{0.7}Pu_{0.3})O_2$ has resulted in biphasic mixture of orthorhombic $(U_{0.95}Pu_{0.05})_3O_{8-x}$ and cubic $(U_{0.65}Pu_{0.35})O_{2+x}$ [330].

7.4 Calcination of Nuclear Material Oxides by Microwave Heating

Air calcination of various oxides or mixed oxide of nuclear materials serves several intents. The calcination of UO_3 and UO_2 in the temperature 500-800 ^{o}C gives thermodynamically most stable U_3O_8. The calcination of these oxides is carried out in several stages of the feed material preparation. The calcination thermally decomposes the ADU to U_3O_8 through UO_3 [185, 331]. Air calcination of oxalates of plutonium and thorium produces respective oxides [112, 118-120]. Calcination of these powders is carried out to remove the residual carbon, nitrate, moisture which subsequently may affect the fabrication of fuel pellets and storage of the powder in U_3O_8 form. The calcination temperature and duration are most important parameters, which directly affects the powder physical properties. The BET surface area shows exponential decrease with temperature in the calcination of Pu or Th oxalate and ADU [99, 112]. Thus, lower temperature and shorter cycles are preferred in calcination.

7.4.1 Microwave Air Calcination of Uranium Oxides and U, Pu Mixed Oxides

The dielectric properties make UO_3 as transparent to microwave whereas the U_3O_8 and UO_2 as strong microwave absorbers (**Table 2.3**). The calcination of UO_2, U_3O_8 and UO_3 was been carried out in microwave ovens MHS-3 (**Fig. 3.8**) and MHS-6 (**Fig. 2.13**). The temperature profile for microwave calcination is shown in **Fig. 7.6** and the experimental parameters are recorded in **Table 7.3**.

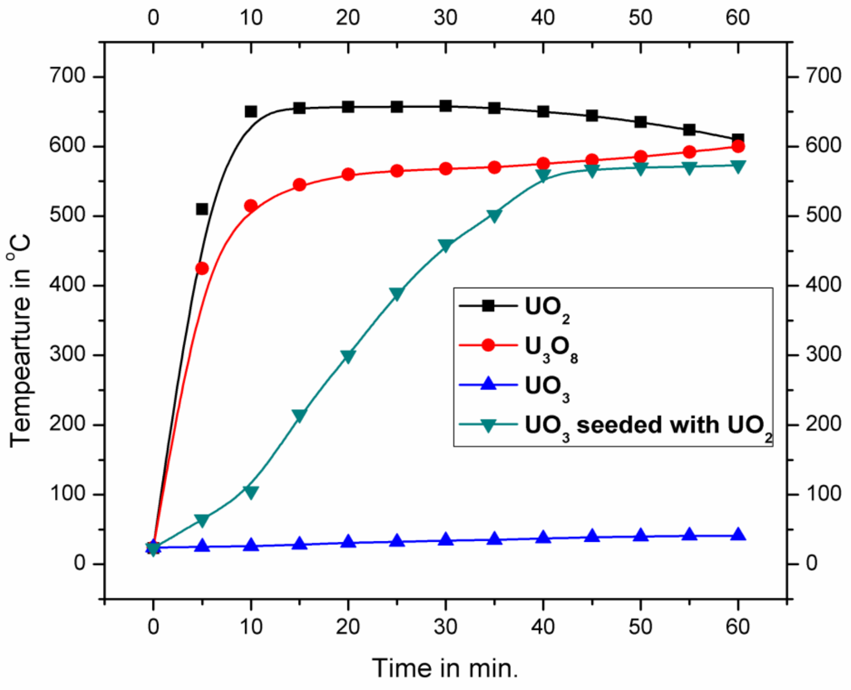

Fig. 7.6: Temperature Profile for Microwave Calcination of various Uranium Oxides

Table 7.3: Typical Experimental Parameters during Microwave Calcination

Parameter	**Description**
Charge size	450 g
MW incident power	600 W
Temperature	550 °C
UO_2 as Seed	5 g

Since, UO_3 is room temperature microwave transparent, thus seeded with UO_2. The UO_2 upon microwave absorption got heated-up, thereby converting the adjacent UO_3 into U_3O_8. Formation of U_3O_8 further enhanced the microwave absorption until entire UO_3 (orange yellow) got converted into U_3O_8 (black) and became incandescent mass. The materials were further characterized for quantitative calcination. The temperature (**Fig. 7.6**) became nearly similar in the calcination of UO_2, U_3O_8 and UO_3 (with seed UO_2) because all oxides were converted to U_3O_8 as evident from the final O/M ratio values in **Table 7.4**. The calcination using microwave on the bulk scale was carried out in the set-up used for oxidation experiments (**Fig. 4.14**). The typical batch size was 4-5 Kg. **Table 7.4** records O/U values of uranium oxides before and after microwave calcination.

Table 7.4: O/M Ratio of the Uranium Oxides during Microwave Calcination

Uranium Oxide	**Initial O/M** ($\bar{x}$ ±1s, n=3)	**Final O/M** ($\bar{x}$ ±1s, n=3)
UO_2	2.034±0.002	2.653±0.002
UO_2	2.053±0.001	2.659±0.002
UO_2	2.021±0.001	2.656±0.001
UO_2	2.007±0.001	2.653±0.001
UO_3	2.973±0.001	2.645±0.002
UO_3	2.985±0.002	2.656±0.001
UO_3	2.987±0.001	2.649±0.002
UO_3	2.986±0.002	2.648±0.002
U_3O_8	2.653±0.001	2.657±0.001
U_3O_8	2.657±0.001	2.656±0.001
U_3O_8	2.658±0.001	2.657±0.001
U_3O_8	2.652±0.001	2.655±0.001

PuO_2 is also good microwave absorber (**Table 2.3**). The calcination of PuO_2 powder may also be carried in microwave ovens. The product after denitration was (UO_3,PuO_2) where the presence of PuO_2 acted as seed for microwave absorption, thus converting the whole mass into incandescent (U_3O_8,PuO_2).

7.4.2 Microwave Calcination of Thoria based Mixed Oxides

ThO_2 is room temperature microwave transparent. The presence of UO_2, U_3O_8, PuO_2 raised the temperature of mixed oxides. However, the temperature achievable depended upon the content of UO_2 and PuO_2.

7.4.3 Microwave Calcination in Denitration Process

Post microwave denitration, the calcination of UO_3 or U,Pu mixed oxide was carried out for 650-700 °C, 40-50 min (**Fig. 4.10**). This transformed the entire mass into U_3O_8 or (M_3O_8,MO_2). In case of uranyl nitrate, the denitration temperature should be above 400 °C (**Fig. 4.5**). This was due to the fact that at temperature higher than 400 °C, the UO_3 decomposed into U_3O_8 which subsequently absorbed microwave. However, in the case of (UO_3,PuO_2), PuO_2 served as seed for microwave absorption.

The dry calcined cake was removed from the vessels. The milled U_3O_8 or (M_3O_8,MO_2) clinkers were again microwave calcined at 350 °C, 1h (called LTMC) in the Modified-MWDD process (**Fig. 4.10**). This was carried out in addition to the microwave calcination at 700 °C, 40-50 min. of the cake in the vessel after denitration. The purpose of the LTMC was to thermally decompose the residual nitrates and to convert the residual UO_3 into U_3O_8 after milling the clinkers. The milling of the clinkers opened-up several closed pores and surfaces for achieving effective calcination.

7.5 Lower Temperature Processing using Microwave

U_3O_8, UO_2 and PuO_2 are strong microwave absorbers (**Table 2.3**); their interaction with microwave heats the material volumetrically. The reduction near to stoichiometry using microwave was carried out at 550 °C, 3h as compared to the conventional heat treatment (700 °C, 4h) thereby lowering the temperature ~150 °C. The "microwave enhanced reaction kinetics" or "Microwave effect" (**§ 2.5**) may be attributable for effective reduction at a lower temperature. Two different views have been put forward in the literature lacking mutual agreement in the physical explanations [8]. Firstly the "non-thermal activation" where the microwave non-thermally interacts with the reactants thereby considerably decreasing the apparent activation energy [8, 268, 273]. According to second viewpoint, the enhanced reaction rates using microwave are due to different mode of heating called thermal "thermal effects" causing superheating at molecular level leading to higher local temperature than the bulk reaction conditions [275-276]. No effort in the present study was oriented to see the cause of the enhancement as it was beyond the scope of the work. However, the low temperature processing comprising reduction or calcination have again advocated the existence of the microwave effect.

7.6 Scale-up of Microwave based Reduction

After experimental investigations and the optimization of the parameters of the reduction using microwave, the process was used for plant scale work. **Fig. 7.7** shows the schematic of the microwave reduction furnace for reduction of the oxidized feed materials. Two thermocouples (T1 and T2) were used for temperature monitoring. T1 measures the material temperature at the center and the T2 that of the material surface.

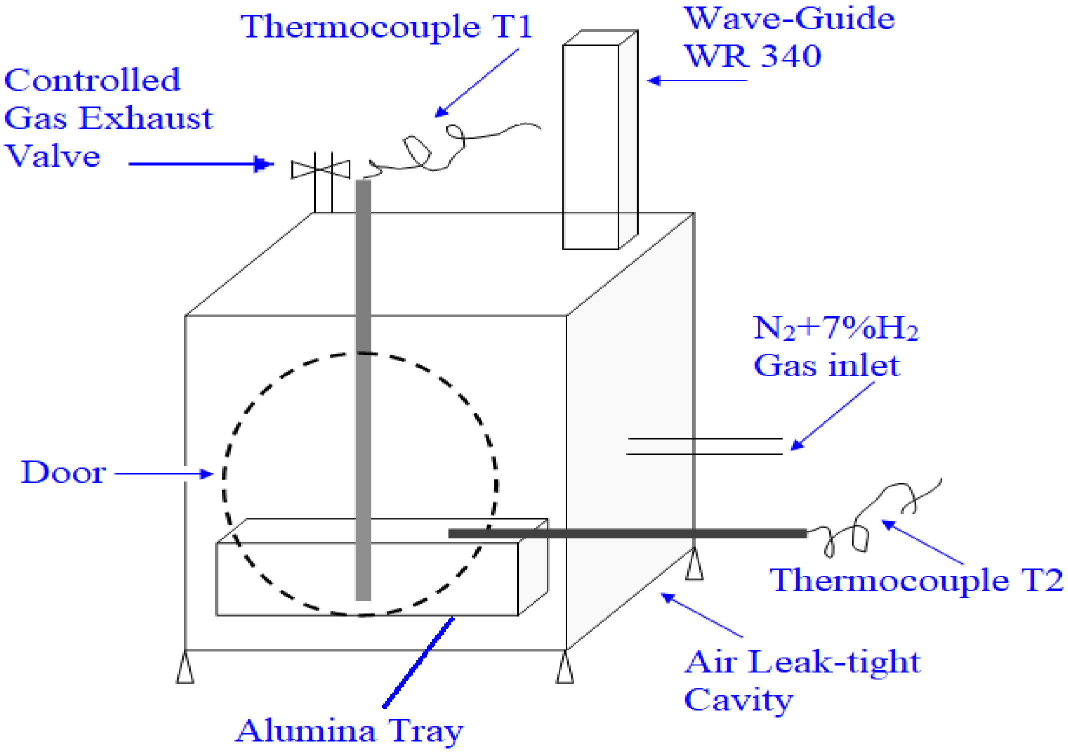

Fig. 7.7: Set-up for Bulk Microwave Reduction of U_3O_8 and (M_3O_8,MO_2)

The microwave cavity was made leak-tight for reduction with controllable exhaust from the cavity. **Table 7.5** records the parameters for the bulk reduction of U_3O_8 and biphasic mixture (M_3O_8,MO_2). The atmosphere was changed to air below temperature of 100 °C during cooling for achieving controlled oxidation of the reduced powder. **Table 7.6** presents the O/M ratio before and after reduction of a few batches.

Table 7.5: Parameters for Bulk Reduction of U_3O_8 and Biphasic Mixture (M_3O_8,MO_2) using Microwave

Parameter	**Parameter value**
Charge size	4-5 Kg
Reducing gas	N_2+7%H_2 mixture
Gas flow rate	2 m^3h^{-1}
Cavity pressure	>45 mbar
Flushing time	15 min.
Peak Temperature (T_p) and Soak time at T_p	550 °C, 3.5 h

Table 7.6: O/M Ratio of a Few Batches before and after Microwave Reduction and controlled oxidation

Starting material	**Starting Oxide/ Mixed oxide**	**Initial O/M Ratio** ($\bar{x}$ ±1s, n=3)	**Final O/M Ratio** ($\bar{x}$ ±1s, n=3)
Oxidised UO_2 pellet	U_3O_8	2.657±0.001	2.084±0.001
Oxidised UO_2 pellet	U_3O_8	2.656±0.001	2.034±0.001
Oxidised UO_2 pellet	U_3O_8	2.656±0.001	2.025±0.001
Oxidised MOX-C	(M_3O_8, MO_2)	2.465±0.001	2.045±0.001
Oxidised MOX-C	(M_3O_8, MO_2)	2.434±0.001	2.053±0.001
Oxidised MOX-D	(M_3O_8, MO_2)	2.365±0.001	2.043±0.001
Oxidised MOX-D	(M_3O_8, MO_2)	2.332±0.001	2.061±0.001
Oxidised MOX-D	(M_3O_8, MO_2)	2.351±0.001	2.032±0.001

7.7 Summary of the Work on Low Temperature Material Processing

Microwave heat processing was found to be beneficial considering the lower temperature, shorter process cycle, better powder properties in the several applications involving nuclear materials. The following points may be summarized from the detailed investigations:

1. The optimum condition for the reduction of U_3O_8 and biphasic mixture (M_3O_8,MO_2) is 550 ^oC, 3h. The reduction up to stoichiometry was successfully carried out.
2. Deterioration to the BET surface area and powder properties have been mitigated to a great extent by adapting microwave based lower temperature reduction.
3. A quick method for getting controlled hyper-stoichiometry in the reduced powder was successfully demonstrated. This served two purposes; improvement in the sinterability and the M_3O_8 passivated stabilization of $(U_{1-y}Pu_y)O_2$ powder for long term storage.
4. The microwave calcination of uranium oxides was carried out at 550 ^oC, 2h than conventional 700 ^oC, 2-4h.
5. Microwave calcination of UO_3 needed addition of microwave absorber seed as UO_2, U_3O_8 or PuO_2.

Chapter 8

CONCLUSIVE SUMMARY AND FUTURE SCOPE

The present thesis describes a systematic study carried out using microwave as a versatile heating technique to efficiently recover and reuse the nuclear oxide and MOX fuel scraps generated during the industrial production of nuclear fuels via powder-pellet route. The quick (preferably online) recycling of plutonium bearing scrap becomes indispensable because total fissile content (TFC) gets reduced with passage of time. The quick recycling alleviates the personnel exposure associated with the long term in-house storage of Pu and ^{233}U bearing scraps. The recycling schemes have been developed for both the types of scrap; CRO and DRO which jointly shares nearly 25 wt% of the total material throughput for fuel fabrication. The thesis encompasses the recycling of UO_2, PuO_2, ThO_2 and their mixed oxides. The recycling schemes exclusively employ microwave heating technology which offered several advantages over the traditional or more conventional processes as well as improved properties of the recycled materials. Since, the scrap types were characteristically different depending upon the constituents (Th, U and Pu), impurity content, dissolution behavior, microwave absorption behavior etc.; different recycling schemes were developed.

Four methods have been developed for recycling of the different scrap types. For UO_2 and $(U_{1-y}Pu_y)O_2$ two methods have been developed; 1) Modified-MWDD based on the microwave dissolution of rejects and direct denitration methodology and 2) MWDO process based on microwave thermo-oxidative pulverization approach. On the basis of the systematic study carried out, flow sheets for 100 % recycling of $(U_{1-y}Pu_y)O_2$ rejects were presented. The product and intermediates were characterized for powder properties like BET-SSA, particle size, phase, metallic and non-metallic impurities, O/M ratio, bulk density etc. The recycled powder suitability for re-fabrication was demonstrated by fabrication of several experimental fuel batches and subsequently implemented at the plant scale. The fabricated $(U_{1-y}Pu_y)O_2$ fuel was characterized for sintered density and fissile homogeneity.

The third process was developed for recycling of the ThO_2 based fuel rejects. This was an integrated method which combined the three basic approaches of recycling viz. comminution, thermo-oxidation (in UO_2 bearing rejects) and microwave dissolution and direct denitration. The recycled powders were characterized for bulk density, SSA, particle size, particle morphology using SEM, phase by XRD, O/M ratio and compared with the standard sinterable grade powders for evaluating their suitability for fabrication of fuel. The powder so synthesized has demonstrated their suitability for 100% recycling in a batch.

The fourth process was developed for recycling the impure scraps. This scheme called integrated method for recycling of impure scrap was basically integration of two schemes. One of them was purification scheme of impure scrap and the other was the microwave direct denitration of the purified solutions. The purification of the impure scrap was further of two types depending upon type of impurities present. The scrap having only non-metallic impurities like C, N, H, Cl and F could be purified by microwave moderate temperature treatment (MMTT). The impure scrap containing both the types of impurities (metallic and non-impurities) needed dissolution followed by liquid-liquid extraction for purification. The dissolution behavior of the impure scrap in HNO_3 was studied using dissolution test and significantly large quantities (> 10 wt%) of the plutonium rich residue was observed. Thus, for quantitative dissolution of impure $(U_{1-y}Pu_y)O_2$ scrap, fluoride catalysed dissolution and fluorideless dissolution through solid solution formation via sintering were investigated. The fluorideless dissolution was selected for the industrial recycling of impure $(U_{1-y}Pu_y)O_2$ due to enhanced corrosion related problems associated with use of fluoride. However, the fluoride was necessarily added to dissolve the thoria based scrap considered under present study.

The stimulation from the ‘microwave effect’ led us to carry out the lower temperature microwave processing viz. calcination and reduction of the recycled powders (obtained via developed methods) in order to improve upon the physical properties of the recycled powders (SSA, particle size etc.) and also time economize the process of recycling. The calcination and reduction were successfully demonstrated at lower temperature and/ or time than the conventional using microwave heating.

8.1 Conclusive Summary

The development of microwave based efficient wet and dry methods for recycling various kinds of rejected MOX fuel from nuclear fuel fabrication plants are systematically presented. The study carried out has filled the potential gaps and brought out scientific value addition in the area of industrial recycling of oxide and mixed oxide nuclear fuel rejects. The recycling of the fuel rejects by the developed methods which exclusively use novel microwave heating technique was practically implemented at AFFF. The systematic study and the characterization of intermediate/ products at each step have provided the in-depth knowledge of the process and subsequently used for tailoring the product properties. The technologically attractive features like direct material bulk heating, high temperature ramp-ups, non-contact heating make this more attractive and implementable for the nuclear material processing.

8.1.1 Methods for Recycling of Clean UO_2 and $(U_{1-y}Pu_y)O_2$ Scrap

Two different methods have been developed; 1) a wet process (Modified-MWDD) based on microwave dissolution and direct denitration and 2) A dry process (MWDO) based on microwave direct oxidation for $(U_{1-y}Pu_y)O_2$ sintered rejects. Rejected sintered UO_2 and

$(U_{1-y}Pu_y)O_2$ (y: 0-1) could be recycled by microwave dissolution and subsequently direct denitration technique. However, the $(U_{1-y}Pu_y)O_2$ with PuO_2> 35 wt% (y> 0.35) essentially needed fluoride for complete dissolution and addition of pore formers to achieve desired powder bulk density. The recycled $(U_{1-y}Pu_y)O_2$ powder have shown high sinterablilty (sintered density >92% TD) and fissile homogeneity. The recycled powder have BET surface area > 3 m^2g^{-1} and average particle size in the range 1-4 µm. More than 3.5 MT of rejected $(U_{1-y}Pu_y)O_2$ MOX was successfully recycled using the MWDD and Modified-MWDD.

The microwave based thermo oxidative process viz. MWDO was extensively investigated. The MWDO was found to be superior to the conventional oxidation method of recycling owing to smaller processing time and higher oxidation (%) achievable hence improved powder properties. Effect of several variables like heating method, oxygen partial pressure, MOX PuO_2 % on the oxidation of was studied. The multiple micronisation-oxidation cycles further enhanced the oxidation (%) and surface area of recycled powder. After establishing the process nearly 240 Kg of the UO_2 and $(U_{1-y}Pu_y)O_2$ MOX rejects were recycled.

8.1.2 Method for Recycling of Clean ThO_2 and Thoria based MOX

The integrated method was demonstrated for recycling of sintered ThO_2, $(Th_{1-y}U_y)O_2$ (y; 0-0.3) and $(Th_{1-y}Pu_y)O_2$ (y; 0-0.1) pellets. The addition of PVA during denitration tremendously increased the SSA of the denitrated ThO_2 > 7 m^2g^{-1}. The presence of UO_2 in ThO_2 improved the powder properties (bulk density, SSA particle size etc.) whereas that of PuO_2 could not. The denitrated ThO_2 was found to have irregular morphology than standard ThO_2 owing platelet removing the need of extensive pre-milling to break platelets. The experimental investigations were concluded by recycling ~40 Kg of ThO_2 based pellets.

8.1.3 Development of Methods for Recycling Impure MOX Scrap

Detailed study was carried out to characterize the impure scrap from various processes (fuel fabrication and quality control) and their dissolution behavior. Flow sheet was developed for recycling impure scraps which exclusively used microwave processing. The impure scrap contained a variety of impurities manifold higher than the allowed limits. The non-metallic impurities were associated with all types of the impure scrap studied; hence needed a head-end heat treatment. The presence of metallic impurities required chemical purification steps for recycling. The dissolution behavior of most of the $(U_{1-y}Pu_y)O_2$ impure scraps have left large plutonium rich residues either needing fluoride or sintering to form solid solution for complete dissolution. The compaction of $(U_{1-y}Pu_y)O_2$ impure scrap into pellets and reductive sintering (1500-1600 ^oC) followed by fluorideless dissolution preferably in microwave was recommended for industrial recycling to eliminate the corrosive fluoride. The thoria based impure scrap essentially needed fluoride for complete dissolution. The integrated flow sheet developed has demonstrated the complete recycling of impure scrap.

8.1.4 Lower Temperature Calcination and Reduction of Recycled Powders using Microwave Heating

The optimum condition for reduction of U_3O_8 and biphasic mixture (M_3O_8,MO_2) up to stoichiometry using microwave was found to be 550 ^oC, 3h compared to the prolonged conventional process (700 ^oC, 4h). A quick method for getting controlled hyper-stoichiometry in the reduced powder was successfully demonstrated for the improved sinterability and M_3O_8 passivated stabilization of $(U_{1-y}Pu_y)O_2$ powder for long term storage. The microwave calcination of various uranium oxides was demonstrated at 550 ^oC, 1h than the conventional calcination at 700 ^oC, 2-4h. After establishing the optimum parameters on the basis of experimental studies, the bulk reduction and calcination of the recycled powders was carried out on the plant scale.

8.2 Future Scope

The microwave processing in the recycling of scrap has a large potential yet to be unleashed. The recycling processes further can be time and energy economized hence the process of nuclear fuel fabrication. The recycling methods developed were batch-type methods where batch sizes were limited by the criticality calculation, by the size of vessels or the microwave generator output. However, to further enhance the production demands the continuous microwave processing may be adopted.

The dry cake clinkers after microwave denitration were presently milled and further calcined and reduced. The powder due to its non-flowability needs pre-compaction and granulation before final compaction into pellets. The granular clinkers are comparatively more flowable and thus direct final compaction of the clinkers is an attractive option which further may be investigated. This may remove several radiotoxic dust generating steps as milling, sieving, pre-compaction, granulation etc. and time economise the process of recycling.

The microwave denitration of uranyl nitrate and uranium containing mixed metal nitrate solutions was carried out in oxidative atmosphere (air) in the present work. The denitration may be studied in the reductive atmosphere. This may eliminate the reduction step ($U_3O_8 \rightarrow UO_2$) thereby making the process smaller.

The higher oxidation % achieved (~2 folds more) in the oxidation of $(U_{1-y}Pu_y)O_2$ having PuO_2 > 20 wt% (y> 0.2) using microwave heating in the MWDO process was attributable to the formation of very small micro-cracks in the oxidized pellets. The oxygen was thought to be permeating through these cracks upto internal grain boundaries bringing out higher oxidation. However, no work was carried out to see their presence experimentally. The future work may be directed towards understanding the enhanced oxidation kinetics in microwave fields.

The air oxidation of $(U_{1-y}Pu_y)O_2$ MOX lead to biphasic mixture of hypo-stoichiometric $(U,Pu)_3O_{8-x}$ and hyper-stoichiometric $(U,Pu)O_{2+x}$. The quantitative estimation of $(U,Pu)_3O_{8-x}$ and $(U,Pu)O_{2+x}$ phases after oxidation was not carried out. The future work may be focused to delineate these aspects.

The addition of PVA (solid or solution) during denitration of metal nitrate solutions resulted in improving the SSA and the particle size by serving as pore former. The increased porosity was indicated by lower dry cake bulk densities. However, a study is required for measurement of the pore volume. Further, influence of the metal nitrate concentration, nitric acid molarity and concentration of pore former may be fine tuned by conducting an elaborate study.

The determination of microwave absorption critical temperature (T_c) for room temperature transparent ThO_2 may further be studied which opens alternatives for the microwave sintering of ThO_2.

The recycling of fuel rejects such as carbide and mixed carbide may also be studied using microwave oxidation methodology.

REFERENCES

[1] R. R. Mishra and A. K. Sharma (2016), “Microwave-material interaction phenomena: Heating mechanisms, challenges and opportunities in material processing” Composites: Part A (81): 78-97.

[2] W. H. Sutton (1989), “Microwave Processing of Ceramic Materials” Am. Ceram. Soc., Bull. 68(2): 376-386.

[3] D. E. Clark, Diane C. Folz, Jon K. West (2000) “Processing materials with microwave energy” Mater. Sci. Eng. A287: 153–158.

[4] D. E. Clark, W. H. Sutton (1996) “Microwave processing of materials” Annu. Rev. Mater. Sci. 26: 299-331.

[5] Roger Meredith (Ed.) (1998) “Engineers handbook of Industrial microwave heating”, The Institution of Electrical Engineers, UK.

[6] D. Aggarwal (2006) “Microwave sintering of ceramics, composites, metallic materials and melting of glasses” Trans. Indian Ceram. Soc. 65(3): 129-144.

[7] G.G. Wicks, R. L. Schulz, D. E Clark (2000) “Microwave Remediation of Hazardous and Radioactive Waste” WSRC-MS-99-00762.

[8] Y. Zhao, J. Chen (2008) “Applications of microwaves in nuclear chemistry and engineering” Prog. Nucl. Energy, 50: 1-6.

[9] G. Singh, G. Singh, R. K. Singhal, R. K. Malav, A. Fulzele, A. Prakash, Md. Afzal and J. P. Panakkal (2011), “A comparative study on dissolution rate of sintered (Th–U)O_2 pellets in nitric acid by microwave and conventional heating” Anal. Methods 3: 622–627.

[10] R. K. Malav, Neeta D. Save, Amrit Prakash, Md. Afzal, J. P. Panakkal (2013), “Use of indigenous microwave system for dissolution and treatment of waste from nuclear materials” J. Radioanal. Nucl. Chem. 295 (1): 425-430.

[11] G. K. Mallik, R. K. Malav, J. P. Panakkal and H. S. Kamath (2005), “Microwave processing in MOX fuel cycle” Int. J. Nucl. Energy Sci. Technol. 1(2/3): 184-190.

[12] N. N. Mirashi, Satyajeet Chaudhury, S. K. Aggarwal (2010) “Dissolution of sintered thorium dioxide in phosphoric acid using autoclave and microwave methods with detection by gamma spectrometry” Microchemical Journal, 94(1): 24-27.

[13] Y. M. Kulyako (2011) "Use of microwave radiation for preparing uranium oxides from its compounds" Radiochemistry 53(6): 604-607.

[14] M. Koizumi, K.Ohtsuka, H. Oshima, H. Isagawa, H. Akiyama, A. Todokoro and K Naruki (1983), "Development of a Process for Co-conversion of Pu-U Nitrate Mixed Solutions to Mixed Oxide Powder Using Microwave Heating Method" J. Nucl. Sci. Technol. 20 (7): 529–536.

[15] W. Bao, C. Song (1998), "Research on the Conversion of Highly Enriched Uranium (HEU) Nitrate by Using the Microwave Denitration" China Nucl. Sci. Technol., Report CNIC-01272 TSHUNE-0083.

[16] E. D. Collins (2015), "Advanced thermal denitration conversion processes for aqueous based reprocessing and recycling of spent nuclear fuels" in "Reprocessing and recycling of spent nuclear fuels", by Robin Taylor (Ed.), WP Publishers, Elsevier: 313-323.

[17] C. E. Holocombe (1983), "New Microwave Coupler Material" Am. Ceram. Soc. Bull. 62: 1388.

[18] P. A. Hass (1979), "Heating of Uranium Oxides in a Microwave Oven" Am. Ceram. Soc. Bull. 58: 873.

[19] E. F. Strucken (1991), "Microwave enhanced pyrochemical reactions of PuO_2, UO_2 and U_3O_8 (U)" Report WSRC-MS-90-330.

[20] Nuclear Energy Agency (NEA) (2015), "Introduction of Thorium in Nuclear Fuel Cycle", NEA No.-7224, Organization for Economic Co-operation and Development (OECD)-2015.

[21] B. J. F. Palmer, L. E. Bahen, A. Celli (1984), "Thoria-urania powders prepared via bulk microwave denitration" Am. Ceram. Soc. Bull. 63(8): 1030-1034.

[22] I. N. Toumanov (Ed.) (2003), "Plasma and High Frequency Processes for Obtaining and Processing Materials in the Nuclear Fuel Cycle", Nova Science Publishers Inc., New York: 192-193.

[23] G. K. Mallik (2013) "Microwave processing in thorium fuel cycle" BARC News Letter, 331: 26-30.

[24] International Atomic Energy Agency (IAEA) (1999), "Minimization of wastes from uranium purification, enrichment and fuel fabrication" TECDOC-1115.

[25] Donald Skea, Philip Cartwright (1997), “Recovery of Uranium from manufacturing scraps and blending of Recycled MTR uranium” Proc. of 1st Int. Topical meeting on “Research Reactor Fuel Management” organized by European Nuclear Society (ENS-RRFM), CH04AO007: 15-20. http://www.iaea.org/inis/collection/NCLCollectionStore/_Public/35/068/35068308.pdf

[26] K. W. Song, K. S Kim, J. H Kim, Y. H. Jung (1999) “Method for recycling fuel scrap into manufacture of nuclear fuel pellets”, US patent USOO5882552A.

[27] Rajesh V. Pai P. K. Mollick, Ashok Kumar, J. Banerjee, J. Radhakrishna J. K. Chakravartty (2016) “Recovery and recycling of uranium from rejected coated particles for compact high temperature reactors” J. Nucl. Mater. 473: 229-236.

[28] Sudhir Mishra, Amrit Prakash, K. B. Khan and Vivek Bhasin (2017) “Challenges in the Fabrication and Recycling of Mixed Carbide Fuel”, FR 17-060, IAEA-CN245-060: 1-9.

[29] K. W. Kim, E. H. Lee, D. Y. Chung, H. B. Yang, K. W. Lee, S. H. Na, K. C. Song, J. W. Lee, J. W. Lee, K. H. Kang, G. I. Park (2011) “Method for preparation of uranium oxide powder for nuclear fuel pellet fabrication from uranium oxide scraps” Canadian Patent, CA2741076C.

[30] M. J. Maurice, J. Fischer, G. N. Cramer (1969), “Recovery of plutonium from non□irradiated refractory plutonium and uranium□plutonium oxides, nitrides and carbides” J. Applied Chemistry Banner, 19 (1): 15-17.

[31] H. S. Kamath and Arun Kumar (2002), “Fast Reactor Fuel Fabrication” IANCAS Bull. I (4): 26-34.

[32] H. S. Kamath, K. Anantharaman and D.S.C. Puroshattam (1999), “MOX fuel for Indian Nuclear Power Programme” IAEA-SM-358/13: 190–199.

[33] “Description of a Reference Mixed Oxide Fuel Fabrication Plant (MOFFP)” Synthesis Report (1978), Commission of the European Communities, Luxembourg, EUR 6162 EN: 5-6.

[34] Saga of Atomic Energy in India (2005) http://dae.nic.in

[35] Fateh Mernache, Naima Boutarek, Toufik Bouchemaa, Abderrahmane Kaim and Said Hadji (2016), “Recycling process of defective aged uranium dioxide pellets” J. Nucl. Sci. Technol. 53 (6): 790-796.

[36] R. I. Larson and J. W. Sammey (2002) “Dry recycle process for recovering UO_2 scrap material” United State Patent US2002/0005597A1.

[37] J. H. Yang, K. W. Kang, K. S. Kim, Y. W. Rhee and K. W. Song (2010), “Recycling Process for Sinter-Active U_3O_8 Powders” J. Nucl. Sci. Technol. 47 (6): 538-541.

[38] K.W. Kang, J. H. Yang, J. H. Kim, Y. W. Rhee, D. J. Kim, K. S. Kim and K. W. Song (2008), “Improvement of UO_2 Pellet Properties by Controlling the Powder Morphology of Recycled U_3O_8 Powder” J. Nucl. Sci. Technol. 45 (11): 1150-1154.

[39] Yu. M. Kulyako, T. I. Trofimov, M. D. Samsonov, S. E. Vinokurov, and B. F. Myasoedov (2015), “Preparation of powdered uranium oxides by microwave heating of substandard ceramic pellets of oxide nuclear fuels” Radiochemistry, 57(2): 127-130.

[40] K. K. Bae, B.G. Kim, Y.W. Lee, M.S. Yang, H.S. Park (1994) “Oxidation behavior of unirradiated UO_2 pellets” J. Nucl. Mater. 209: 274-279.

[41] S. Mishra, K. Ghoshal, J. Banerjee, Amrit Prakash, K. B. Khan, Arun Kumar (2015), “(Th-U)O_2 MOX fuel fabrication and dry recycling of the sintered rejects” Thorium Energy Conference, ThEC15, India: 637-643.

[42] I. Schwartz, M. H. Mintz, Z. Hadari (1979), “Dry recovery of ceramic uranium dioxide waste material” J. Nucl. Mater. 82: 54-59.

[43] A. Vandergheynst, J. V. Vliet, E. Pelckmans (2004), “Method for Dry Process Recycling of Mixed (U,Pu)O_2 Oxide Nuclear Fuel Waste”, United State Patent, US6783706B1.

[44] P. M. Khot, G. Singh, B. K. Shelke, B. Surendra, M. K. Yadav, A. K. Mishra, Mohd. Afzal and J. P. Panakkal (2014), “Development of recycling processes for clean rejected MOX fuel pellets” Nucl. Eng. Des. 270: 227–237.

[45] David A. Copson (1975) “Microwave Heating”, AVI Publishing Co.

[46] E. T. Thostenson and T. W. Chou (1999) “Microwave processing: Fundamental and Applications” Composites: Part A, 30: 1055-1071.

[47] D. E. Clark, W. H. Sutton, D. A. Lewis (Eds.) (1997) “Microwave: Theory and Application in Materials Processing IV”, Ceramic Transactions, vol-80: 41-91.

[48] Y, Zhao, J. Chen (2008) “Comparative studies on the dissolution of ceramic UO_2 pellets in nitric acid by microwave and conventional heating” Radiochimca Acta 96: 467-471.

[49] Y, Zhao, J. Chen (2008) "Studies on the dissolution kinetics of ceramic uranium dioxide particles in nitric acid by microwave heating" J. Nucl. Mater. 373: 53-58.

[50] J. Mellado, M. Llauradó G. Rauret (2001) "Determination of Pu, Am, U, Th and Sr in marine sediments by extraction chromatography" Analytica Chimica Acta 443: 81-90.

[51] D. Zheng, R. Zheng, H. LIU (2002), "Applications of microwave irradiation in extracting of Gold, Uranium and Environmental Protection" Hydrometallurgy of China (2): 62-65.

[52] J. Zhou, J. You (2003) "Application study on microwave digestion technique in analysis of uranium mining and metallurgy" Uranium mining and Metallurgy 22: 194-198.

[53] J. G. Sen and N. B. Bertrand (1995) "Direct ICP-MS determination of trace and ultra trace elements in geological materials after decomposition in microwave oven I. Quantitation of Y, Th, U and the lanthanides", Talanta 42: 1595-1607.

[54] R. K. Malav, A. K. Fulzele, Amrit Prakash, Mohd. Afzal, J. P Panakkal (2011) "Quantitative Dissolution of $(U,Pu)O_2$ MOX (0.4% to 44% PuO_2) by Microwave Heating" Proc. of Nucl. Radiochem. Symp. (NUCAR-2011), Vishakhapattanam 22-26 Feb: 256-257.

[55] G. Singh, R.K. Malav, R.B. Bhong, A. Name, A. Pandey, D.K. Das, P.G. Behere and Mohd. Afzal (2014) "Recent Advances in Microwave Heating Assisted Sample Preparation Methodologies in Chemical Quality Control of ThO_2 based MOX Fuels " Proc. of Symp. on Nuclear Analytical Chemistry (NAC-V), Mumbai, 20-24 Jan: 553-554.

[56] G. K. Mallik, R. K. Malav, K. Raju, H.S. Kamath (2001) "Microwave dissolution studies on Sintered ThO_2 Pellets" Proc. of Nucl. Radiochem. Symp. (NUCAR-2001), 7-10 Feb, Pune: 260-261.

[57] D. Annie, V. Chandramouli, S. Anthonysamy, Chanchal Ghosh, R. Divakar (2017) "Freeze drying vs microwave drying- methods for synthesis of sinteractive thoria powders" J. Nucl. Mater. 484: 51-58.

[58] H. Oshima (1989), "Development of Microwave Heating Method for Co-conversion of Plutonium-Uranium Nitrate to MOX Powder" J. Nucl. Sci. Technol. 26(1): 161-166.

[59] Y. Takahashi (1996) "Continuous denitration apparatus" US patent, US005589140A.

[60] T. L. White, W. D. Bostick, C. T. Wilson and C. R. Schaich (1996), "Design of Microwave vitrification systems for Radioactive wastes" Proc. of Mater. Res. Soc. Symp., 430 "Microwave Processing of Materials-V", CONF-960401--14: 541-548.

[61] K. Miyata, H. Miyazaki, H. Miyo, K. Ohstsuka (1982). "Solidification of plutonium contaminated wastes using a microwave melter", preprint 1981 Fall meeting of At. Energy Soc. Jpn., (in Japanese) G27.

[62] M. S. Ioffe (2000) "Method for preparing uranium dioxide powder" World Intellectual Property Organization (WIPO) under Patent Cooperation Treaty (PCT), (WO/00517), Patent No. WO2000032517A1.

[63] T. A. Thornton and V. D. Holaday Jr. (1983) "Sintering UO_2 and oxidation of UO_2 with microwave radiation" US patent 4389355.

[64] T. A. Thornton and V. D. Holaday Jr. (1985) "Nuclear fuel preparation and scrap recycle", Canadian Patent, CA1192734A.

[65] J. D. Ford (1967) "High temperature chemical processing via microwave absorption" J. Microwave Power, 2(2): 61-64.

[66] G. K. Mallik, R. K. Malav, A. P. Karande, V. K. Bhargava and H. S. Kamath (1997), "Studies involving direct heating of uranium and plutonium oxides by microwaves" Proc. of Nucl. Radiochem. Symp. (NUCAR-1997), 21-24 Jan, SINP Calcutta: 135-136.

[67] T. Subramanian, P. Venkatesh, K. Nagarajan, P. R. Vasudeva Rao (2000) "A novel method of sintering UO_2 pellets by microwave heating" Mater. Lett. 46: 120-124.

[68] J. H. Yang, K.W. Song, Y.W. Lee, J.H. Kim, K.W. Kang, K.S. Kim, Y.H. Jung (2004) "Microwave process for sintering of uranium dioxide", J. Nucl. Mater. 325: 210-216.

[69] Y. M. Kulyako, T. I. Trofimov, S. A. Perevalov, D. A. Malikov, S. E. Vinokurov, M. D. Samsonov, B. F. Myasoedov, S. S. Travnikov, K. N. Dvoeglazov,

and A. Yu. Shadrin (2015), "Preparation of Uranium Oxides by Reductive Denitration of Uranyl Nitrate under Microwave Heating", Radiochemistry, 57(3): 251-254.

[70] P. A. Hass, R. D Arthur, W B Stines (1981) "Development of Thermal Denitration to Prepare Uranium Oxide and Mixed Oxides for Nuclear Fuel Fabrication", ORNL-5737.

[71] P. A. Hass (1988) "A comparison of processes for the conversion of uranyl nitrate into ceramic grade UO_2", Nucl. Technol. 81(3): 393-406.

[72] D. S. Kumar, K. Ananthasivan, R. V. Krishnan, S. Amirthapandian, Arup Dasgupta (2016) "Bulk synthesis of nanocrystalline urania powders by citrate gel-combustion method" J. Nucl. Mater. 468: 178-193.

[73] V. Chandramouli, S. Anthonysamy, P. R. Vasudeva Rao (1999), "Combustion synthesis of thoria- A feasibility study" J. Nucl. Mater. 265: 255-261.

[74] V. Chandramouli, S. Anthonysamy, P. R. Vasudeva Rao, R. Divakar, D. Sundararaman (1998), "Microwave synthesis of solid solutions of urania and thoria: A comparative study" J. Nucl. Mater. 254: 55-64.

[75] V. Chandramouli, S. Anthonysamy, P. R. Vasudeva Rao, R. Divakar, D. Sundararaman (1996), "PVA aided microwave synthesis: A novel route for production of nanocrystalline thoria powder" J. Nucl. Mater. 231: 213-220.

[76] The World Nuclear Industry Status Report (WNISR), (2017).

[77] S. A. Bhardwaj (2013) "Indian nuclear power programme – Past, present and future", Sadhana Vol. 38, Part 5, Oct: 775–794.

[78] S. P. Sukhatme (2011) "Meeting India's future needs of electricity through renewable energy sources" Current Sci., 101: 624-630.

[79] R. K. Singhal (2000) "World thorium resources", Proc. of Indian Nuclear Society Annual Conference (INSAC-2000), Mumbai: 3-5.

[80] S. M. Lee, S. Govindrajan, R. Indira, T. M. John, P. Mohanakrishnana, R. Shankar Singh, S. B. Bhoje "Conceptual Design of PFBR Core" IAEA XA9643091: 83-99.

[81] R. K. Sinha, Anil Kakodkar (2006), "Design and development of the AHWR-the Indian thorium fuelled innovative nuclear reactor" Nucl. Eng. Des. 236: 683-700.

[82] K. Sasidharan, D.C. Khatri, Kanchhi Singh, A. P. Srivastav (2006) “Refurbishment and core conversion of the Apsara reactor” Nucl. Eng. Des. 236: 784-795.

[83] S.C. Katiyar, S.S. Bajaj (2006), “Tarapur Atomic Power Station Units-1 and 2: Design features, operating experience and license renewal” Nucl. Eng. Des. 236: 881-893.

[84] S.S. Bajaj, A.R. Gore (2006), “The Indian PHWR” Nucl. Eng. Des. 236: 701-722.

[85] Department of Atomic Energy (DAE), “AHWR300-LEU, Advanced Heavy Water Reactor with LEU-Th MOX fuel”, http://dae.nic.in/writereaddata/.pdf_31

[86] Neelima Prasad, Anek Kumar, Umasankri Kannan, Arvind Kumar, P. D. Krishnani, R. K. Sinha (2010) “Advanced Heavy Water Reactor-LEU (AHWR-LEU): A Reactor Safeguard by Design”, IAEA-CN-184/207.

[87] D. D. Sood (1996) “Nuclear Materials” Indian Association of Nuclear Chemists and Allied Scientists (IANCAS).

[88] B. R. Leonard Jr. (1980) “Properties of Plutonium Isotopes” in O.J. Wick (Ed.), “Plutonium Handbook- A Guide to the Technology” Vol. I & II, Am. Nucl. Soc. La Grange Park: 1-8.

[89] JANIS (Java-based Nuclear Data Information Software); The JEFF-3.1.1 Nuclear Data Library, OECD, Nuclear Energy Agency (NEA).

[90] International Atomic Energy Agency (IAEA) (2005) “Thorium fuel cycle-Potential benefits and challenges” TECDOC-1450.

[91] S. B. Roy (2005), “Benefaction and refining of U/Th” IANCAS Bull. IV(3): 174-183.

[92] P. V. Achuthan and A. Ramanujam (2013) “Aqueous Reprocessing by THOREX Process” in D. Das and S. R. Bharadwaj (Eds.), “Thoria-based Nuclear Fuels”, Springer-Verlag London: 279-333.

[93] R. B. Holden (1966) “Ceramic Fuel Elements” Gordon and Breach Science Publishing Inc., New-York.

[94] S. Majumdar (2002) “Nuclear Reactor Fuel Fabrication” IANCAS Bull. I(1): 33-40.

[95] A. K. Sengupta (2009), "Metallic Fuels for Fast Reactors" IANCAS Bull. (III) (2): 157-167.

[96] Jayshree Sriram, K. Ananthraman, U. Basak (2009) "Thorium Fuel-An overview" in "Advanced Nuclear Fuels", Arun Kumar (Ed.) IANCAS Bull. VIII (2):124-136.

[97] Sudhir Mishra (2002) "Non-oxide Fuel for Fast Reactors", IANCAS Bull. VIII(2): 151-156.

[98] International Atomic Energy Agency (IAEA), (2009) "Use of Reprocessed uranium" IAEA-TECDOC-CD-1630.

[99] S. K. Mukherjee, T. R. G. Kutty, N. Kumar, R. V. Pai, Arun Kumar (2013) "Fabrication Technologies for Thoria-based fuel" in D. Das and S. R. Bharadwaj (Eds.), "Thoria-based Nuclear Fuels", Springer-Verlag London: 205-278.

[100] Pushparaja, and D. P. Rath (2006) "Plutonium-Its Toxicity and Safe Handling" Internal Report, BARC/2006/I/013

[101] J. M. Haschke, J. L. Stakebake (2006), "Handling, Storage and Disposition of plutonium and uranium", in L.R. Morss, N. M. Edelstein, J. Fuger, J. J. Katz (Eds.), "The Chemistry of the Actinide and Transactinide Elements", Springer 3rd Edition, Dordrecht: 3199-3272.

[102] R. C. Thompson (1980) "Biological Factors" in O.J. Wick (Ed.), "Plutonium Handbook- A Guide to the Technology" Vol. I & II, Am. Nucl. Soc. La Grange Park: 785-829.

[103] Annual Book of ASTM standards (2011), "Standard Guide for Design criteria for Plutonium Glove-boxes", Vol. 12.01 Nuclear Energy (I), ASTM International, West Conshohocken, PA, C852-09: 226-230.

[104] Guidelines for Glove-Boxes, AGS-G005-2003, American Glove Box Society.

[105] International Atomic Energy Agency (IAEA), (1996), "International basic safety standards for protection against Ionising radiations and for safety of radiation sources" Safety Series No. 115.

[106] International Atomic Energy Agency (IAEA), (2012) "Experiences and Trends of Manufacturing Technology of Advanced Nuclear Fuels" IAEA-TECDOC-1686.

[107] V. N. Vaidya (2008) "Status of sol-gel process for nuclear fuels", J. Sol-Gel Sci. Technol. 46(3): 369-381.

[108] J. Belle (Ed.), (1961), “Uranium dioxide: Properties and Nuclear Applications”, Vol. 7, USAEC.

[109] F. G. Kittis (1994) “Pilot-Scale Demonstration of the Modified Direct Denitration Process to Prepare Uranium Oxide for Fuel Fabrication Evaluation,” ORNL/TM-12726, Oak Ridge National Laboratory, Oak Ridge, Tenn.

[110] A. A. Jonke, E. J. Petkus, J. W. Loeding, and S. Lawroski (1957) “The Use of Fluidized Beds for the Continuous Drying and Calcination of Dissolved Nitrate Solids” Nucl. Sci. Eng.: 303-319.

[111] Neetu A. Baveja, C.P. Shringi, Gaurav Varshney, Deepa Thomas, Sandip Bhowmick, N.K. Dandekar, M.Y. Walke and Hanmanth Rao (2012) “Development of Fluidized Bed Thermal Denitration”, BARC News Letter, 326 (312): 22-29.

[112] R. M. Orr, H. E. Sims, R. J. Taylor (2015) “A review of plutonium oxalate decomposition reactions and effects of decomposition temperature on the surface area of the plutonium dioxide product”, J. Nucl. Mater. 465:756-773.

[113] C. S. Garner (1959) “Method of making plutonium dioxide”, United States Patent 2,868,620.

[114] J. M. Cleveland (1980) “Compounds of plutonium”, in O. J. Wick (Ed.), “Plutonium Handbook-A Guide to the Technology” Vol. I & II, Am. Nucl. Soc. La Grange Park: 335-402.

[115] M. J. Sarsfield (2015) “The co-precipitation and conversion of mixed actinide oxalates for aqueous based reprocessing of spent nuclear fuels” in “Reprocessing and recycling of spent nuclear fuels” by Robin Taylor (Ed.), WP Publishers, Elsevier: 325-351.

[116] X. Machuron-Mandard, C. Madic (1996), “Plutonium dioxide particle properties as a function of calcination temperature”, J. Alloys Comp. 235 (2): 216-224.

[117] Gordon Jarvenin (2010), “Precipitation and Crystallization Processes” Los Alamos National Laboratory (LANL), http://www.cresp.org/NuclearChemCourse/monographs/09_Jarvinen_FuelCycleSep%20CrystPrec12-08fin_3_2_09.pdf

[118] J. Belle, R. M. Berman (1984) “Thorium dioxide: properties and nuclear applications”, Naval Reactors Office, US-DOE, Washington DC.

[119] G. D. White, L. A. Bray, P. E. Hart (1980), “Optimization of thorium oxalate precipitation conditions relative to thorium oxide sinterability” PNL-3263.

[120] K. Ananthasivan, S. Anthonysamy, A. Singh, P. R. Vasudeva Rao (2002), “De-agglomeration of thorium oxalate-a method for the synthesis of sinteractive thoria” J. Nucl. Mater. 306:1–9.

[121] R. D. Purohit, S. Saha, A. K. Tyagi (2001), “Nanocrystalline thoria powders via Glycine–Nitrate combustion”, J. Nucl. Mater. 288:7–10.

[122] B. Palmer, L. Bahen, A. Gin, J. Winegar, A. Celli (1986) “Preparation of thoria based powders via decomposition from nitrate solution” Journal de Physique Colloques, 47 (C1): C1-49 to C1-54.

[123] H. Roepenack, V. Schneider, W. G. Druckenbrodt (1984), “Experience with the AUPuC-conversion process for mixed oxide fuel fabrication”, Am. Ceram. Soc. Bull. 63(8).

[124] E. D. Collins (2011) “Evaluation of co-precipitation processes for the synthesis of mixed oxide fuel feedstock materials”, ORNL, Milestone Report.

[125] K. Notz and P. Hass (1981) “Properties and thermal decomposition of double salts of uranyl nitrate-ammonium nitrate” ORNL/TM-7820.

[126] E.H.P. Cordufunke (1969) “The chemistry of uranium” Elsevier Publishing Co. Amsterdam: 122-123.

[127] A. J. Bakel and G. F. Vandegrift (2013), “Equipment and Method Choices for Concentration and Denitration of the Uranium Product from UREX” Argonne National Laboratory, ANL/CSE-13/1.

[128] L. R. Morss (1991) “Synthesis of actinide oxides” in G. Meyer and L. R. Morss (Eds.) “Synthesis of Lanthanide and Actinide Compounds”, published by springer science and business media, BV: 237-258.

[129] R. Romano (1986) “NITROX Process- A process developed by COMURHEX of continuous denitration” Proc. of IAEA technical committee meeting on, “Advances in uranium refining and conversion”, IAEA TECDOC-420, Vienna, Austria: 223-230.

[130] Japan Atomic Energy Agency (JAEA), (2006), “Study on denitration process of uranyl nitrate solution by microwave heating-uranium powder production process from uranium nitrate solution” JAEA R&D Review, 8-3: 111.

[131] Y. Kato, T. Kurita, T. Abe, (2004) "Dielectric Properties of Uranium and Plutonium Nitrate Solution and the Oxide Compounds Formed in the De-nitration Process by the Microwave Heating Method" J. Nucl. Sci. Technol. 41(8): 857-862.

[132] Y. Kato, T. Kurita, T. Abe (2005) (in Japanese), "Reaction Mechanism of denitration of $UO_2(NO_3)_2$ by microwave heating" Nihon-Genshiryoku-Gakkai Shi (J. At. Energy Soc. Jpn.), 4 (1): 77-83.

[133] J. W. Hobbs and P. Parkes (2000) "Production of MOX pellets from plutonia and mixed oxide powders prepared by direct thermal denitration" International conference on "Scientific research on the back-end of the fuel cycle for the 21 century" ATLANTE-2000, 24-26 Oct, Avignon, France, FR0104337, P2-19: 1-4.

[134] L. K. Felker, R. J. Vedder, E. A. Walker, E. D. Collins (2008) "Product Conversion: The Link between Separations and Fuel Fabrication", ATLANTE-2008, 19-22 May, Montpellier, France, O1-03:1-5.

[135] T.R.G. Kutty, M. R Nair, P. Sengupta, U Basak, Arun Kumar, H. S. Kamath (2008), "Characterization of $(Th,U)O_2$ fuel pellets made by impregnation technique" J. Nucl. Mater. 374 (1-2): 9-19.

[136] T.R.G. Kutty, K.B. Khan, P. S. Somayajulu, A. K. Sengupta, J. P. Panakkal, Arun Kumar, H.S. Kamath (2008) "Development of CAP process for fabrication of ThO_2-UO_2 fuels Part I: Fabrication and densification behaviour" J. Nucl. Mater. 373: 299-308.

[137] T. R. G. Kutty P. S. Somayajulu, K. B. Khan, Arun Kumar, H. S. Kamath (2009), "Characterization of $(Th,U)O_2$ pellets made by advanced CAP process" J. Nucl. Mater. 384(3): 303-310.

[138] T. R .G. Kutty, K. B. Khan, P. V. Achuthan, P. S. Dhami, A. Dakshinamoorthy, P. S. Somayajulu, J. P. Panakkal, Arun Kumar, H. S. Kamath (2009) "Characterization of ThO_2–UO_2 pellets made by co-precipitation process" J. Nucl. Mater. 389: 351-358.

[139] P. M. Khot, Y. G. Nehete, A. K. Fulzele, Chetan Baghra, A. K. Mishra, Mohd. Afzal, J. P. Panakkal, H. S. Kamath (2012) "Development of Impregnated Agglomerate Pelletization (IAP) process for fabrication of $(Th,U)O_2$ mixed oxide pellets" J. Nucl. Mater. 420: 1-8.

[140] H. Bairiot, J. V. Vliet, G. Chiarelli, J. Edwards, S.H. Nagai, F. Reshetnikov (1999) "Overview of MOX fuel fabrication achievements", Proc. of Symp. on "MOX

Fuel Cycle Technologies for Medium and Long Term Deployment" IAEA-SM-358/VII, IAEA, Vienna: 81–101.

[141] R. B. Bhatt, Aniruddha Kumar, Amit Kulshreshtha, Mohd. Afzal. Arun Kumar, G. J. Prasad (2013) "Technological developments in safe and efficient fabrication of fast reactor fuel elements" Proc. Int. Conf. on Fast Reactors and Related Fuel Cycles (FR13), March 4–7, (Paris) France, Paper No. 113: 1-9.

[142] P. Balakrishna, B. P. Varma, T. S. Krishnan, T. R. R. Mohan, P. Ramakrishnan (1988), "Thorium oxide: calcination, compaction and sintering", J. Nucl. Mater. 160: 88-94.

[143] Arun Kumar (2015) "Indian Experience in Manufacture of Thorium based Fuels" Thorium Energy Conference, ThEC-15, 12-15 Oct., Mumbai, India http://www.thoriumenergyworld.com/uploads/6/9/8/7/69878937/indian_experience_in_manufacture_of_thorium_based_fuels_by_arun_kumar_thec15_about.pdf

[144] A. Kumar (2013) "Development, Fabrication and Characterization of Fuels for Indian Fast Reactor Programme" Proc. Int. Conf. on Fast Reactors and Related Fuel Cycles: (FR13), Vol. 2, March 4–7, (Paris) France: 17-32.

[145] H. S. Kamath and Arun Kumar (2005) "Development of Plutonium fuel for Thermal and Fast reactors" IANCAS Bull. (IV)3: 213-225.

[146] J. P. Panakkal, M. Afzal. R. B. Bhatt, A Prakash, A. K Mishra, S Kumar, H. S Kamath (2012) "Fabrication of (U-Pu) Mixed-Oxide Fuel for Pressurized Heavy Water Reactors" Nucl. Technol. 179 (2): 189-195.

[147] A. K. Sengupta, K. B Khan, J. P. Panakkal, H. S. Kamath, S. Banerjee (2009) "Evaluation of high plutonia (44% PuO_2) MOX as a fuel for fast breeder test reactor" J. Nucl. Mater. 385(1):173-177.

[148] International Atomic Energy Agency (IAEA) (1970), "Standardization of radioactive wastes" Technical reports series No. 101, Vienna.

[149] K. Raj, K. K. Prasad, N. K. Bansal (2006) "Radioactive waste management practices in India" Nucl. Eng. Des. 236: 914-930.

[150] N. Gopinath (2008), "Methodologies for the determination of thorium, uranium and plutonium in Nuclear Fuels" in "Chemical Characterization of Nuclear Fuels", IANCAS Bull. VII (3):156-168.

[151] Pradeep Kumar, K. L. Ramakumar (2008) “Application of neutron well coincidence counting for plutonium determination in mixed oxide fuel fabrication plant” J. Radioanal. Nucl. Chem.., 277 (2): 419-428.

[152] S. Muralidhar (2008), “Non-destructive Assay of Nuclear Fuels” in “Chemical Characterization of Nuclear Fuels”, IANCAS Bull. VII (3): 218-227.

[153] K. B. Khan (2008), “Chemical Quality Control of FBTR Fuel” in “Chemical Characterization of Nuclear Fuels” IANCAS Bull. VII (3): 200-207.

[154] W. Davies and W. Gray (1964) “A rapid and specific titrimetric method for the precise determination of uranium using iron (II) sulphate as reductant” Talanta 11(8): 1203- 1211.

[155] J. L. Drummond and R. A. Grant (1966) “Potentiometric determination of plutonium by argentic oxidation, ferrous reduction and dichromate titration” Talanta 13 (3): 477-488.

[156] L. F. Walker, D. J. Temer (1979), “Determination of Thorium in Plutonium-Thorium Oxides and Carbides”, LA-7958.

[157] J. Mendham, R. C. Denney, J. D. Barnes, M. Thomas, B. Sivasankar (2000), “Vogel’s Textbook of Quantitative Chemical Analysis”, 6th Edition, Pearson Education Ltd. India: 292-397.

[158] S. K Aggarwal (2008), “Mass Spectrometry for determining isotopic composition of Actinides in Nuclear Fuels” in “Chemical Characterization of Nuclear Fuels” IANCAS Bull.VII (3): 208-217.

[159] K. V. Vrinda Devi, D. B. Sathe., T. Soreng (2017) “Fissile worth of MOX fuel: A non-destructive study, Nucl. Eng. Des. 325: 124-128.

[160] M. V. Ramaniah (1982) “Analytical chemistry of fast reactor fuels- A review” Pure & Applied Chemistry 54 (4): 889-908.

[161] S. V. Godbole (2008), “Trace Metal Assay of Nuclear Materials” in “Chemical Characterization of Nuclear Fuels”, IANCAS Bull. VII (3):169-179.

[162] Y. S. Sayi, K. L. Ramakumar, V. Venugopal (2008), “Determination of Non-metallic impurities in Nuclear Fuels” in “Chemical Characterization of Nuclear Fuels”, IANCAS Bull. VII (3): 180-189.

[163] Annual Book of ASTM standards (2011), "Standard specification for Nuclear-Grade, Sinterable Uranium Dioxide Powder", Vol. 12.01 Nuclear Energy (I), ASTM International, West Conshohocken, PA, C 753-99 (2008).

[164] Annual Book of ASTM standards (2011), "Standard specification for Nuclear-Grade, Plutonium Dioxide Powder", Vol. 12.01 Nuclear Energy (I), ASTM International, West Conshohocken, PA, C 757-90 (2008).

[165] Annual Book of ASTM standards (2011), "Standard specifications for sintered (uranium-plutonium) dioxide pellets-Fast Reactor fuel", Vol. 12.01 Nuclear Energy (I), ASTM International, West Conshohocken, PA, C1008-99 (2008).

[166] Annual Book of ASTM standards (2011), "Standard specifications for sintered (uranium-plutonium) dioxide pellets", Vol. 12.01 Nuclear Energy (I), ASTM International, West Conshohocken, PA, C833-01(2008).

[167] K. V. Chetty, J. Radhakrishna, Y. S. Sayi, N. Balachander, P. Venkataramana, P. R Natrajan (1983), "Inert gas fusion for the determination of hydrogen, nitrogen and oxygen in UO_2, UC and UN" Radiochem. Radioanal. Lett. 58(3): 161-167.

[168] Poonam Verma, R. K. Rastogi and K. L. Ramakumar (2003), "Determination of trace amount of nitrogen in Uranium alloy samples using ion chromatography" Proc. of Nucl. Radiochem. Symp. (NUCAR-2003) Mumbai, India Feb 10-13: 407-408.

[169] M. A. Mahajan, M. V. R Prasad, H. R. Mhatre, R. M. Sawant, R. K. Rastogi, G. H. Rizvi, N. K. Chaudhury (1991) "Modified pyrohydrolysis apparatus for the separation of fluorine and chlorine trace impurities from nuclear fuel samples for quality control analysis" J. Radioanal. Nucl. Chem. Articles 148 (1): 93-100.

[170] Annual Book of ASTM standards (2015), "Standard Practice for Determining Equivalent Boron Contents of Nuclear Materials", ASTM International, West Conshohocken, PA, C1233-15.

[171] C. E. Johnson, I. Johnson, P. E Blackburn and C. E. Crouthamel, (1972), "Effect of oxygen concentration on properties of fast reactor mixed oxide fuel" Reactor Technology 15(4): 303.

[172] S. K. Sali (2008), "Oxygen to Metal Ratio in Oxide Nuclear Fuels" in "Chemical Characterization of Nuclear Fuels" IANCAS Bull. VII (3): 190-199.

[173] J. Rubin, K. Chidester and M. Thompson (2000) "O/M ratio measurement in pure and mixed oxide fuels- where are we now?" Report LA-UR-00-5805.

[174] C. E. Mcneilly and T. D. Chikalla (1971) "Determination of oxygen/metal ratios for uranium, plutonium and (U,Pu) mixed oxides" J. Nucl. Mater. 39: 77-83.

[175] International Atomic Energy Agency (IAEA) (2003), "Status and Advances in MOX Technology", Technical Report Series no. 415., Vienna: 37–41

[176] C. Ganguly (2002), "Fabrication, Characterization and Quality Control of Nuclear Fuels for Power Reactors in India", Proc. Int. Conf. on "Characterization and Quality Control of Nuclear Fuels" (CQCNF-2002), Hyderabad, Allied Publishers, New Delhi, India: 37-64.

[177] Government of India, DAE, IGCAR (2007) "Specification for Depleted/ Deeply Depleted UO_2 Powder for Fabrication of Fuel and Blanket Pellets" PFBR/31100/SP/1028/R-O: 1-2.

[178] Government of India, DAE, IGCAR (2007) "Specifications for Procurement of PuO_2 Powder for fabrication of $(U,Pu)O_2$ Fuel" PFBR/31100/SP/1030/R-O : 1-2

[179] R. N. Patra, and S. Sivasubramanian, (2000), "Production of Nuclear Grade Thorium oxide" Proc. of Annual conference of Indian Nuclear Society (INSAC-2000) Vol. 1, June 1-2, Mumbai, India: 6-12.

[180] Terrence Allen (Ed.) (1999), "Particle Size Measurement-Powder sampling and particle size measurement" Vol. 1, 5th Edition, Kluwer Academic Publishers.

[181] David Wayane and Carl Mrtinee (2008), "Actinide Research Quarterly", LANL: 18-27.

[182] International standard (2010), "Determination of the specific surface area of solids by gas adsorption- BET method" ISO 9277-2010 (E).

[183] International standard (2003), "Nuclear fuel technology- Guide to the measurement of the specific surface area of uranium oxide powders by the BET method" ISO 12800:2003 (E).

[184] P. Balakrishna, C. K. Asnani, R. M. Kartha, K. Ramachandran, K. Sarat Babu, V. Ravichandran, B. N. Murty and C. Ganguly (1999), "Uranium Dioxide Powder Preparation, Pressing, and Sintering for Optimum Yield" Nucl. Technol. 127(3): 375-381.

[185] Shubhankar Manna (2016) "Studies on reactive precipitation: Morphology of ammonium diuranate" A thesis submitted to Homi Bhabha National Institute, India.

[186] P. C. Doto, C. M. Peabody (1975) “Production of Ceramic-grade Plutonium Dioxide”, ARH-SA-213, Richland: 1-16.

[187] Government of India, DAE, IGCAR (2007) “Specification for Mixed Oxide Fuel Pin” PFBR/31100/SP/1027/R-O: 1-6.

[188] T. M. Kegley Jr. (1972). “Use of cellulose nitrate for alpha autoradiography” Metallography 5(2): 113–123.

[189] Chetan Baghra, D.B. Sathe, Jitender Sharma, Hema Vetal, Amrit Prakash, Mohd Afzal and J.P. Panakkal (2011) “Estimation of Micro-homogeniety of Plutnoium in sintered (U-Pu)O_2 Mixed Oxide Pellets using LR-115 Alpha Radiuography films” Proc. of National Seminar & Exhibition on Non-Destructive Evaluation, NDE -2011, Dec, 8-10, India: 342-345.

[190] T. S. Rao, V. D Pandey, S. Mazumdar (2005) “Microstructural evaluation of thermal and fast reactor fuels” Proc. of seminar on advances in metallography and microstructure, Mumbai, 1-2 December: 44.

[191] J. P. Panakkal (2014) “Techniques for Assuring the Integrity of Fuel Pins for Fast Reactors” Procedia Engineering 86: 452-460.

[192] E. R. Merz, C. E. Walter, G. M. Pshakin (Eds.), (1995) “Mixed Oxide Fuel (MOX) Exploitation and Destruction in Power Reactors”, Vol. 2, Springer: 177.

[193] International Atomic Energy Agency (IAEA) (2000), “Recycle and reuse of materials and components from waste streams of nuclear fuel cycle facilities” TECDOC-1130.

[194] M. Lung (1997), “A present review of the thorium nuclear fuel cycles”, European Commission Report EUR-17771, Luxembourg.

[195] H. Assmann and H. Barriot (1983) “Guidebook on quality control of water reactor fuels” IAEA, Tech Report series 221, Vienna.

[196] R. K. Welty (1971) “Scrap nuclear Fuel material recovery process”, United States patent 3578419.

[197] M. S. Dias, F. S. Lameiras, A.M.M. dos Santos (1991) “Recycling of nuclear fuel swarf at the fabrication of UO_2 pellets and its influence on the irradiation behavior” Proc. of the 35 Brazilian Congress on Ceramic; 3. Iberian American Congress of Ceramic, Glasses and Refractories, vol. 1, 26-29 May, Belo Horizonte, MG (Brazil): 339-345.

[198] International Atomic Energy Agency (IAEA) (1995) “Minimization of Radioactive Waste from Nuclear Power Plants and the Back End of the Nuclear Fuel Cycle”, Technical Reports Series No. 377.

[199] C. Tanaka, T. Yazama, Y. Miyajima, M. Kashiwa, H. Sugai (1990), “Method of processing Nuclear Fuel Scraps” United States Patent, 4891163.

[200] K. W. Kim, J. W. Lee, D.Y. Chung, E. H. Lee, K. H. Kang, K. W. Lee, K. C. Song, M. J. Yoo, G. I. Park, J. K. Moon (2012) “Preparation of uranium oxide powder for nuclear fuel pellet fabrication with uranium peroxide recovered from uranium oxide scraps by using a carbonate–hydrogen peroxide solution” J. Radioanal. Nucl. Chem. 292(2): 909-916.

[201] K. W. Kim, J. T. Hyun, E. H. Lee, G. I. Park, K. W. Lee, M. J. Yoo, K. C. Song, J. K. Moon (2011) “Recovery of uranium from (U,Gd)O_2 nuclear fuel scrap using dissolution and precipitation in carbonate media” J. Nucl. Mater. 418 (1-3): 93-97.

[202] H. S. Kamath, S. Majumdar, D. S. C. Purushotham (1996) “Developments in MOX fuel pellet fabrication technology: Indian experience” IAEA TECDOC-1036: 103-112.

[203] P. S. Somayajulu, S. K. Shrotriya, Y.G. Nehete, B. K. Shelke, A. K. Mishra, J. P. Panakkal and H.S. Kamath (1996) Proc. of Powder Met. Assn. India (PMAI) Conf., Banglore (India):34.

[204] B Surendra, M. K. Yadav, A. K Mishra, Mohd. Afzal, J. P Panakkal (2009), “Dry recycling of Rejected MOX fuel pellets in MOX fuel fabrication for PFBR” Trans. Powder Met. Assn. India (PMAI) 35: 44-46.

[205] S. Cagno, L Gijsemans, V. Tyrpekl. T. Cardinaels, M. Verwerft, K. Binnemans (2017), “Use of Triflic Acid in the Recycling of Thoria from Nuclear Fuel Production Scrap” J. Sustain. Metall. 3 (3): 659-667.

[206] R. Aggarwal and S. C. Parida (2013) “Phase diagrams and Thermodynamic properties of Thoria, Thoria-Urania and Thoria-Plutonia” in D. Das and S. R. Bharadwaj (Eds.), “Thoria-based Nuclear Fuels”, Springer-Verlag London: 71-106.

[207] S. Anthonysamy, K. Joseph, T. Gnanasekaran, P. R. Vasudeva Rao (2000) “Studies on the kinetics of oxidation of urania-thoria solid solutions in air” J. Nucl. Mater. 280: 25-32.

[208] P. M. Khot, S. K. Shrotriya, K. Subbarayal, N. Kumar, B. Singh, B. Surendra, A. K. Mishra, P. G. Behere, Mohd. Afzal (2016), "Development of dry recycling process for $(Th,U)O_2$ clean rejected oxide sintered pellets" Trans. Powder Met. Assn. India (PMAI) 42(2): 116-121.

[209] G. T. Seaborg and D. E Hobbart (1996) "Summary of the properties of the lanthanide and actinide elements" in D. D. Sood, A.V.R. Reddy and P. K. Pujari (Eds.) "Frontiers in Nuclear Chemistry" IANCAS: 69-94.

[210] Rudy J. M. Konings, Lester R. Morss, and Jean Fuger (2008) "Thermodynamic properties of actinides and actinide compounds" in L.R. Morss, N. M. Edelstein, J. Fuger, J. J. Katz (Eds.), "The Chemistry of the Actinide and Transactinide Elements", Springer 3rd Edition, Dordrecht: 2113-2224.

[211] Ingmar Grenthe, Janusz Droz˙dz˙yn´ ski, Takeo Fujino, Edgar C. Buck, Thomas E. Albrecht-Schmitt, and Stephen F. Wolf (2008) "Uranium" in L.R. Morss, N. M. Edelstein, J. Fuger, J. J. Katz (Eds.), "The Chemistry of the Actinide and Transactinide Elements", Springer 3rd Edition, Dordrecht: 253-698.

[212] David L. Clark, Siegfried S. Hecker, Gordon D. Jarvinen, and Mary P. Neu (2008) "Plutonium" in L.R. Morss, N. M. Edelstein, J. Fuger, J. J. Katz (Eds.), "The Chemistry of the Actinide and Transactinide Elements", Springer 3rd Edition, Dordrecht: 813-1264.

[213] N. N. Krot, and A. D. Gel'man (1967), "Preparation of Neptunium and Plutonium in the 7-Valent State", Dokl. Akad Nauk SSSR, 177: 124-126.

[214] R. E. Connick (1949) , "Mechanism of the Disproportionation of Plutonium (V)" J. Am. Chem. Soc., 71: 1528–1533.

[215] Mathias S. Wickleder, Blandine Fourest, and Peter K. Dorhout (2008) "Thorium" in L.R. Morss, N. M. Edelstein, J. Fuger, J. J. Katz (Eds.), "The Chemistry of the Actinide and Transactinide Elements", Springer 3rd Edition, Dordrecht: 52-160.

[216] H. D. Greiling and K. H. Lieser (1984) "Properties of ThO_2, UO_2 and PuO_2 as a function of pretreatment and their dissolution in HNO_3" Radiochimica Acta 36: 79-89.

[217] M. H. Rand and O. Kubaschewski (Eds.), (1963) "The thermochemical properties of uranium compounds", published by Oliver and Byod, Edinburg, London.

[218] F. Taylor, E. W. Sharratt, L. E. M. De Chazal, D. H. Logsdail (1963), “Dissolution rates of uranium dioxide sintered pellets in nitric acid systems” J. Applied Chemistry, 13(1): 32-40.

[219] M. Shabbir and R. G. Robins (1968), “Kinetics of dissolution of UO_2 in nitric acid-I” J. Applied Chemistry, 18(5):129-134.

[220] M. Shabbir and R. G. Robins (1969) “Kinetics of dissolution of UO_2 in nitric acid-II”, J. Applied Chemistry, 19(2): 52-56.

[221] A. Inoue (1986) “Mechanism of oxidative dissolution of UO_2 in HNO_3 solution” J. Nucl. Mater. 138: 152-154.

[222] T. Fukuswa and Y. Ozawa (1986); “Relationship between dissolution rate of UO_2 in nitric acid solutions and their porosity” J. Radioanal. Nucl. Chem. Letters, 106: 345-356.

[223] T. Fukasawa, Y. Ozawa, F. Kawamura (1991) “Generation and decomposition behavior of nitrous acid during dissolution of UO_2 pellets by nitric acid” Nucl. Technol. 94: 108-113.

[224] Jordi Bruno (1988) “Kinetics of dissolution of UO_2 under reducing conditions” Radiochimica Acta, 44/45: 11-16.

[225] Y. Ikeda (1995) “Kinetic study on dissolution of UO_2 powders in nitric acid” J. Nucl. Mater. 224: 266-272.

[226] J. L. Ryan and L.A. Bray (1980) “Dissolution of plutonium dioxide-A critical review” in “Actinide Separations” James D. Navratil, Wallace W. Schulz (Eds.) ACS symposium series, (117): 499-514

[227] J. L. Ryan, L. A. Bray, A. L. Boldt (1987) “Dissolution of PuO_2 or NpO_2 using electrolytically regenerated reagents”, US Patent: 4686019.

[228] J. M. Cleevland (1980) “The solution chemistry of Plutonium”, in O.J. Wick (Ed.), “Plutonium Handbook- A Guide to the Technology” Vol. I & II, Am. Nucl. Soc. La Grange Park: 403-520.

[229] S. Bagwade, V. V. Ramkrashna, S. K. Patil (1976) “Complexing of tetravalent plutonium in aqueous solutions” J. Inorg. Nucl. Chem. 38: 1339- 1345.

[230] G. Scott Barney (1977), “The kinetics of PuO_2 dissolution on Nitric-HF Acid Mixture”, J. Inorg. Nucl. Chem. 39 (9):1665-1669.

[231] Y. Zundelevich (1992), “The mediated electrochemical dissolution of PuO_2: Kinetics and mechanism” J. Alloys Comp. 182(1): 115-130

[232] Dhanpat Rai, Y. A. Gorby, J. K. Fredrickson, D. A. Moore, M. Yui (2002) “Reductive Dissolution of PuO_2(am): The Effect of Fe(II) and Hydroquinone”, J. Solution Chemistry 31(6): 433-453.

[233] K. Dhamodharan, Anitha Pius, Pradeep Kumar Sharma, S. Pugazhendi and V. Vijayakumar (2014) “Electro reductive dissolution of plutonium oxide- A preliminary study”, Int. J. Chem. Sci. Appl. 5(2): 68-75.

[234] E. Kluge and K. H. Lieser (1981), “Dissolution of ThO_2 in HCl/ HF mixtures”. Radiochimica Acta 26: 167-168.

[235] Satyajeet Chaudhury, Meera Keskar, Abhay V. Patil, K. D. Singh Mudher, V. Venugopal (2006) “Studies on the dissolution behaviour of ThO_2 and $(U,Th)O_2$ by a solid state reaction method” Radiochimica Acta 94(6): 357-361.

[236] E. Bulemela, A. Bergeron, T. Stoddard (2016) “Dissolution study of thorium-uranium oxides in aqueous triflic acid solutions” Procedia Chemistry 21: 239-246.

[237] Erich Zimmer and Erich Merz (1984) “Dissolution of thorium –uranium mixed oxides in concentrated HNO_3” J. Nucl. Mater. 124: 64-67.

[238] M. H. Shying and T. M. Fluorence (1970) “Oxide dissolution mechanism I” J. Inorg. Nucl. Chem. 32: 3493-3508.

[239] M. H. Shying and T. M. Fluorence (1972) “Oxide dissolution mechanism II”; J. Inorg. Nucl. Chem. 34: 213-220.

[240] Takechi Takfuchi (1971) “Kinetics and mechanism of the dissolution of the thorium oxide in HF and HNO_3 mixtures” J. Inorg. Nucl. Chem. 33: 1089-1098.

[241] Takechi Takfuchi (1972) “The kinetic study of the reaction of the thorium oxide in HF” J. Inorg. Nucl. Chem. 34: 2497-2503.

[242] J. M. Cleevland (1980) “Compounds of Plutonium” in O.J. Wick (Ed.), “Plutonium Handbook- A Guide to the Technology” Vol. I & II, Am. Nucl. Soc. La Grange Park: 335-401.

[243] M. J. Bannister (1968) “The storage behaviour of uranium dioxide powders-review article” J. Nucl. Mater. 26(2): 174-184.

[244] P. Taylor, D. D. Wood, A. M. Duclos (1992) "The early stages of U_3O_8 formation on unirradiated CANDU UO_2 fuel oxidized in air at 200–300 ºC" J. Nucl. Mater.189 (1): 116-123.

[245] R.J. McEachern, P. Taylor (1998) "A review of the oxidation of uranium dioxide at temperatures below 400 ºC" J. Nucl. Mater. 254: 87-121.

[246] G. Rousseau, L. Desgranges, F. Charlot, N. Millot, J. C. Niepce, M. Pijolat, F. Valdivieso, G. Baldinozzi, J. F. Be´rar (2006) "Detailed study of UO_2 to U_3O_8 oxidation phases and the associated rate-limiting steps" J. Nucl. Mater. 355: 10-20.

[247] P. Taylor, D.D. Wood, A.M. Duclos, D.G. Owen (1989) "Formation of uranium trioxide hydrates on UO_2 fuel in air-steam mixtures near 200°C "J. Nucl. Mater. 168 (1-2): 70-75.

[248] C. Brun, M. Pijolat, F. Valdivieso, M. Soustelle (1999), "Reduction by hydrogen of U_3O_8 into UO_2: Nucleation and growth, influence of hydration" Phys. Chem. Chem. Phys. 1: 471-477.

[249] P. O. Alfaro, J. H. Torres, F. P. Thiele (2015) "Reduction Kinetics of Uranium Trioxide to Uranium Dioxide Using Hydrogen" World J. Nucl. Sci. Technol. 5: 149-156.

[250] S.A. El-Fekey, M.A. Khilla and N.H. Rofail (1984) "Thermal decomposition of ammonium uranate; X-ray study" Radiochimica Acta 37 (3): 153-158.

[251] M. Pijolat, C. Brun, F. Valdivieso and M. Soustelle (1997), "Reduction of uranium oxide U_3O_8 to UO_2 by hydrogen" Solid State Ionics, 101-103: 931-935.

[252] Didier Stuerga (2006), "Microwave–Material Interactions and Dielectric Properties, Key Ingredients for Mastery of Chemical Microwave Processes", A. Loupy (Ed.) "Microwaves in Organic Synthesis", 2nd Edition. WILEY-VCH Verlag GmbH & Co. KGaA, Weinheim: 1-61.

[253] P.L. Spencer (1952) "High Frequency Apparatus" US patent No. 2,593,067.

[254] National Academy Press (1994) "Microwave processing of materials" Washington DC: 101-102.

[255] H. Cember and T. E Johnson (Eds.) (2009) "Introduction to Health Physics" 4th Edition McGraw Hill: 721-802.

[256] Morteza Oghbaei and Omid Mirzaee (2010), “Microwave versus conventional sintering: A review of fundamentals, advantages and applications” J. Alloys Comp. 494 (1-2):175-189.

[257] R. R. Menezes, P. M. Souto, Ruth H.G.A. Kiminami (2012), “Microwave Fast Sintering of Ceramic Materials” in “Sintering of Ceramics-New Emerging Techniques” Arunachalam Lakshmanan (Ed.) Published by In Tech: 3-26.

[258] G. K. Mallik (1998) “Studies on Applications of Microwave Heating in the Processing of Nuclear Materials” A thesis submitted to B. R. A. Bihar University, Muzaffarpur.

[259] V, Chandramouli (1999), “Study of the feasibility of the combustion synthesis for the preparation of thorium dioxide” A Thesis submitted to university of Madras.

[260] Wai Leong, Eugene Wong, Manoj Gupta (2015) “Using Microwave Energy to Synthesize Light Weight/Energy Saving Magnesium Based Materials: A Review”, Technologies, 3(1): 1-18.

[261] L. A. Belov, S. M. Smolskiy, V. N. Kochemasov (2012) “Handbook of RF, Microwave, and Millimeter-wave Components” Artech House, 1st Edition: 66.

[262] J. F. Gerling (2000) “Waveguide components and configurations for optimal performance in Microwave heating”, Gerling Applied Engineering, Inc.:1-8.

[263] K. C. Gupta (2005) “Microwaves” New Age International (P) Ltd.:106-121.

[264] E. D. Neas, M. J. Collins (1988) “Microwave Heating-Theoretical concepts and Equipment design” in “Introduction to Microwave Sample Preparation- Theory and Practice” by H. M. Kingston, L. B. Jassie (Eds.) Am. Chem. Soc.: 7-32.

[265] E. Pert, Y. Carmel, A. Birnboim, T. Olorunyolemi, D. Gershon, J. Calame Isabel K. Lloyd, Otto C. Wilson (2001) “Temperature Measurements during Microwave Processing: The Significance of Thermocouple Effects”, J. Am. Ceram. Soc. 84(9): 1981-1986.

[266] M. A. Janney, H. D. Kimrey, M. A. Schmidt, and J. O. Kiggans (1991), “Alumina Grain Growth in a Microwave Field” J. Am. Ceram. Soc. 74(7):1675-1681.

[267] A. Akbarnezhad, K. C. G. Ong, K. S. C. Kuang (2011), “Temperature sensing in microwave heating of concrete using fiber Bragg grating sensors” Magazine of Concrete Research, 63 (4): 275-285

[268] John H. Booske, Reid F. Cooper, Samuel A. Freeman (1997), "Microwave enhanced reaction kinetics in ceramics" Mater. Res. Innovat. 1:77–84.

[269] Jiping Cheng, Dinesh Agrawal, Yunjin Zhang, Rustum Roy (2002) "Microwave sintering of transparent alumina", Mater. Lett. 56: 587– 592;

[270] Christopher J. Bonifas, Amy Marconnet, John Perry, John H. Booske, Reid F. Cooper (2008) "Microwave-induced mass transport in nano-porous aluminium oxide membranes" J. Microwave Power & Electromagnetic Energy, 42(1):13-22.

[271] M. A. Janney, H. D. Kimrey (1990), "Diffusion-Controlled Processes in Microwave-Fired Oxide Ceramics" Proc. of Mater. Res. Soc. Symp. on "Microwave Processing of Materials II" 189: 215. https://doi.org/10.1557/PROC-189-215

[272] J. H. Booske, R. F. Cooper, I. Dobson (1992) "Mechanisms of non-thermal effects on ionic mobility during microwave processing of crystalline solids", J. Mater. Res. 7(2): 495-501.

[273] S. A. Galema (1997) "Microwave chemistry" Chem. Soc. Rev. 26: 233-238.

[274] Antonio de la Hoz, A´ngel Dı´az-Ortiz and Andre´s Moreno (2005) "Microwaves in organic synthesis: Thermal and non-thermal microwave effects", Chem. Soc. Rev. 34: 164–178.

[275] M. Al-Harahsheh, S. Kingman, S. Bradshaw (2006) "The reality of non-thermal effects in microwave assisted leaching systems?" Hydrometallurgy 84: 1-13.

[276] M. Al-Harahsheh, S. W. Kingman (2004) "Microwave-assisted leaching- A review" Hydrometallurgy 73: 189-203.

[277] S. Banik, S. Bandhyopadhyay, S. Ganguly (2003) "Bioeffects of microwave – A brief review", Bioresource Technology 87: 155–159.

[278] E. C. Okress (Ed.) (1968), "Microwave Power Engineering" 1st Edition, Vol-2, Published by Academic Press.

[279] J. A. Leavy (2009) "RF and Microwave Safety Manual"

[280] International Standard (2004), "Uranium dioxide powder- Determination of apparent density and tap density", ISO 9161:2004

[281] Military Standard (1963) "Sampling procedures and tables for inspection by attributes" MIL-STD-05D.

[282] F. A. Khan, A. Pandey, D. K. Das, P. G. Behere and Mohd. Afzal (2015) "Non Destructive estimation of plutonium in MOX fuel samples" Proc. of Chemistry in Nuclear Technology, (CHEMNUT -2015), July 30-3, IGCAR, Kalpakkam, India: 27.

[283] N. Save, S. Ghosh, R. Jaiswal, A. Prakash, G. K. Mallik, J. P. Panakkal (2005), "Extension of Nodal Method for the Determination of Metallic Impurities in Mixed oxide Fuel for PFBR by ICP-AES" Proc. of Nucl. Radiochem. Symp. (NUCAR-2005), Amritsar India: 457-458.

[284] V. K. Manchanda (2012) "Radiochemistry in India: A saga of five decades" Radiochimica Acta 100: 541-554.

[285] Bhabha Atomic Research Centre (BARC) (2001) "DAE-Inter-Laboratory Comparison Experiment (ILCE) for Trace Metal Assay of Uranium and Development of Certified U_3O_8 Reference Materials", Internal Document compiled by Radiochemistry Division and Product Development Division, BARC, Mumbai, India.

[286] Bhabha Atomic Research Centre (BARC) (2006), "Inter-Laboratory Comparison Experiment (ILCE) for the Determination of Trace Metals in Thorium oxide" Internal Document, compiled by Radiochemistry Division, BARC and Control Laboratory, Nuclear Fuel Complex, Hyderbad India.

[287] R. Gaikwad, B. N. Mahanty, C. D. Karekar, V. R. Sonar, Seema Raul, R. K. Pandey, D. K. Das, P. G. Behere and Mohd. Afzal (2015), "Determination of Residual Nitrogen in Microwave processed UO_2, PuO_2 powder by indigenously developed Nitrogen-Oxygen Determinator" Proc. of Nucl. Radiochem. Symp. (NUCAR-2015), Mumbai India: 335-336.

[288] Arti S. Mhatre, Guneshwor L. Singh, Kapil Deo Singh, G. Ganesh, R.G. Purohit and R.M. Tripathi, D.K. Das, Gitender Singh, P.G. Behere and Mohd Afzal (2013) "Criticality Safety Analysis of Wet Recycling of PFBR MOX CRO by Microwave Direct Denitration Process at AFFF", Internal Report-HDP/RMT/2013/1206.

[289] Ronald Allen Knief (1986) "Nuclear Criticality Safety-Theory and Practice" Am. Nucl. Soc. Illinois, USA.

[290] E. D. Clayton and W. A. Reardon (1980) "Nuclear Safety and Criticality of Plutonium" in O.J. Wick (Ed.), "Plutonium Handbook- A Guide to the Technology" Vol. I & II, Am. Nucl. Soc. La Grange Park: 875-919.

[291] M. J. Carrott, P.M.A. Cook, O. D. Fox, C. J. Maher, S.L.M. Schroeder (2012), "The chemistry of (U,Pu)O_2 dissolution in nitric acid" Procedia Chemistry, 7: 92 – 97.

[292] N. Desigan, Nirav P. Bhatt, N. K. Pandey, U. Kamachi Mudali, R. Natarajan and J. B. Joshi (2015) "Dissolution kinetics of Indian PHWR natural UO_2 fuel pellets in nitric acid – Effect of initial acidity and temperature" Prog. Nucl. Energy, 83: 52-58.

[293] Je-Lueng Shie, Yi-Hung Chen, Ching-Yuan Chang, Jyh-Ping Lin, Duu-Jong Lee, and Chao-Hsiung Wu (2002), "Thermal Pyrolysis of Polyvinyl alcohol and Its Major Products", Energy Fuels 16(1) :109-118.

[294] K. W. Lay and R. E. Carter (1969), "Role of the O/U ratio on the sintering of UO_2" J. Nucl. Mater. 30: 74-87.

[295] D. K. Das, G. Singh, P. M. Khot, S. Kumar, A. K. Mihsra, P. G. Behere, Mohd. Afzal, Arun Kumar (2014) "Technological advances in (U,Pu)O_2 CRO recycling using microwave heating" Proc. of European Nuclear Conference (ENC-2014), Marseille, France: 232-241.

[296] D. Seehars and D. Hochrainer (1989), "Oxidation and pulverisation of UO_2 and MOX pellets" J. Nucl. Mater. 166: 214–217.

[297] K. Tanaka, H. Yoshimochi, H. Obayashi and S. Koyama (2015), "Oxidation behavior of Am-containing MOX fuel pellets in air" Energy Procedia, 71: 282-292.

[298] T. K. Campbell, E. R. Gilbert, G. D. White, G. F. Piepel, B. J. Wrona (1989) "Oxidation Behavior of Nonirradiated UO_2" Nucl. Technol. 85(2): 160-171.

[299] H. A. Wriedt (1990) "The O-Pu (Oxygen-Plutonium) system" Bull. Alloy Phase Diagr. 11(2): 184-202.

[300] T. M. Besmann (1987), "Phase equilibria and thermodynamics of the Pu-O system: 1400 K to 1610 K" J. Nucl. Mater. 144(1-2): 141-150.

[301] International Atomic Energy Agency (IAEA) (1967), "The Plutonium-Oxygen and Uranium-Plutonium-Oxygen Systems: A Thermochemical Assessment", Technical Reports Series No. 79, STI/DOC/10/79.

[302] C. Guéneau, M. Baichi,D. Labroche, C. Chatillon, B. Sundman (2002) , "Thermodynamic assessment of the uranium–oxygen system" J. Nucl. Mater. 304 (2-3): 161-175.

[303] M. Strach, R. C. Belin, J. C. Richaud and J. Rogez (2015), "Biphasic MO_{2+x}–M_3O_{8-z} Domain of the U–Pu–O Phase Diagram" Inorg. Chem. 54(18): 9105–9114.

[304] S. K. Sali, N. K. Kulkarni, Rohan Phatak, Renu Agarwal (2016) "Oxidation behaviour of plutonium rich (U, Pu)C and (U, Pu)O_2" J. Nucl. Mater. 479: 623-632.

[305] T. L. Markin, R.S. Street (1967) "The uranium-plutonium-oxygen ternary phase diagram" J. Inorg. Nucl. Chem. 29 (9): 2265-2280.

[306] W. D. Bond (1958), "Dissolution of sintered thorium-uranium oxide fuel in nitric acid-fluoride solutions" Oak Ridge National Laboratory, ORNL-2519.

[307] V. Chandramouli, K. Ananthasivan, S. Anthonysamy, P. R. Vasudeva Rao (2000) "Novel methods for the preparation of thorium dioxide" Annual conference of Indian Nuclear Society (INSAC-2000), Vol. 1, June 1-2, Mumbai, India: 175.

[308] S. K. Sali, S. Sampath, V. Venugopal (1998), "Studies on the kinetics of oxidation of $Pu_yTh_{1-y}O_{2-x}$ (y= 0.2, 0.3 and 0.7) in air" J. Nucl. Mater. 252:131-134.

[309] Jun Tateno, Keiji Naito (1969), "On the Dielectric Properties of U_4O_9 and UO_2"Solid State Communications, 7(11): 807-810.

[310] D. Vollath, H. Wedemeyer, H. Elbel and E. Günther (1985), "On the Dissolution of (U,Pu)O_2 Solid Solutions with Different Plutonium Contents in Boiling Nitric Acid" Nucl. Technol. 71(1): 240-245.

[311] A. L. Mills, L. R. Weatherley and J. A. Crofts (1982), "Method for dissolving plutonium-containing nuclear fuels" United State Patent 4,333,912.

[312] S. P. Chakraborty and N. Krishnamurthy (2014) "Fabrication of a Mo based high temperature TZM alloy by non-consumable arc melting technique" Proc. of XXVI Int. Symp. on "Discharges and Electrical Insulation in Vacuum" Mumbai, India :749-752.

[313] Annual Book of ASTM standards (2011), "Standard Test Method for Determination of Metallic Impurities in Uranium Metal or Compounds by DC-Arc Emission Spectroscopy", Vol. 12.01 Nuclear Energy (I), ASTM International, West Conshohocken, PA, C1517 – 09.

[314] Y. S. Kapoor, M. Singh, S. Pable, A. Kelkar, A. Pandey, A. Fulzele, R. K. Jaiswal, N. D. Save, N. Kumar, S. Ghosh, D. K. Das, P. G. Behere and Mohd. Afzal (2015), "Characterization of undissolved residue obtained from macro-homogeneity

test of PFBR MOX fuel" Proc. of DAE-BRNS symposium NUFUC-2015, Tarapur, India: 72-73.

[315] S. K. Nayak, T. G. Srinivasan, P. R. Vasudeva Rao and C. K. Mathews (1988) "Photochemical Destruction of Organic Compounds Formed During Dissolution of Uranium Carbide in Nitric Acid" Sep. Sci. Technol. 23 (12-13): 1551-1561.

[316] V. Chandramouli, N. L. Sreenivasan and R. B. Yadav (1990) "Chemical head-end steps for aqueous reprocessing of carbide fuels" Radiochimica Acta 51(1): 23-26.

[317] K. Sini, S. Mishra, F. Lawre, C. Mallika, S. B. Kogant (2011) "Destruction of soluble organics generated during the dissolution of sintered uranium carbide by mediated electrochemical oxidation process" Radiochimica Acta 99 (1): 23-30.

[318] P. R. Vasudeva Rao and Z. Kalarik (1996), "A Review on third phase formation in extraction of actinides by neutral organophosphorus extractants" Solvent Extr. Ion Exch. 14 (6): 955-993.

[319] K. W. Song, K.S. Kim, K. W Kang and Y. H. Jung (2002), "Large-grained UO_2 pellets without impurity additives" Proc. Int. Conf. on "Characterization and Quality Control of Nuclear Fuels" (CQCNF-2002), Hyderabad, Allied Publishers, New Delhi, India: 247-257.

[320] J. Janov, P. G. Alfredson and V. K. Vilkaitis (1972), "The influence of precipitation conditions on the properties of ammonium diuranate and uranium dioxide powders" J. Nucl. Mater. 44(2): 161-174.

[321] Y. M. Pan, C. B. Ma and N. N. Hsu (1981), "The conversion of UO_2 via ammonium uranyl carbonate: Study of precipitation, chemical variation and Powder properties" J. Nucl. Mater. 99: 135-147.

[322] L. W. Gray, K. S. Holliday, A. Murray, M. Thompson, D. T. Thorp, S. Yarbro and T. J. Venetz (2015), "Separation of Plutonium from Irradiated Fuels and Targets" LLNL-TR-677668.

[323] V. W. Schnieder and W. G. Druckenbrodt (1982) "Recent operating experience with the AUPuC-coconversion process", Trans. Am. Nucl. Soc. United States (40) CONF-820420.

[324] E. V. Sidorov and V. L. Sofronov (2011), "Investigation of the Kinetics of U_3O_8 Reduction by Hydrogen and Ammonia under Non-Isothermal Conditions" Chemistry for Sustainable Development, 19: 315-319.

[325] A. Shiela, Morrow, S. Graves and L. Tomlinson (1961), "Hydrogen reduction of low-surface area uranium trioxide" Trans. Faraday Soc., 57: 1400-1409.

[326] P. S. Somayajulu, A. K. Mishra, Y. G. Nehete, B. K. Shelke, S. K. Shrotirya, Arun Kumar, J. P. Panakkal and H. S. Kamath (2002), "PFBR Fuel Pellet Fabrication for Experimental Irradiation" " Proc. Int. Conf. on "Characterization and Quality Control of Nuclear Fuels" (CQCNF-2002), Hyderabad, Allied Publishers, New Delhi, India: 318-326.

[327] S. M. Thein and P. J. Beleolos (2000), "Thermal stabilization of $^{233}UO_2$, $^{233}UO_3$ and $^{233}U_3O_8$" ORNL/ TM-2000/82.

[328] R. N. Jayaraj (2005) "Processing of Uranium from MDU to UO_2 Pellets" IANCAS Bull. IV(3):184-190.

[329] H. Yoo, S. Lee, J. Kim and K. Song (2003), "Effect of UO_{2+x} Powders Produced at Different Oxidation Temperatures on the Properties of Pellet" J. Korean Ceram. Soc. 40(5): 410-414.

[330] N.C. Jayadevan, R.G. Hadap and D.M. Chackraburtty (1979), "The oxidation behavior of 30 wt% PuO-UO_2 solid solution" J. Nucl. Mater. 82: 195-198.

[331] S. Manna, S. B. Roy and J. B. Joshi (2013), "Crystal growth and Morphological study of ADU and its calcined product" BARC News Letter Founders Day Special Issue, Oct: 162-166.